

**INVESTIGATING MOLECULAR
MECHANISMS UNDERLYING RESISTANCE
TO NOTCH INHIBITORS IN BREAST AND
OVARIAN CANCER**

Kübra TELLİ

İzmir Institute of Technology

November, 2022

**INVESTIGATING MOLECULAR MECHANISMS
UNDERLYING RESISTANCE TO NOTCH
INHIBITORS IN BREAST AND OVARIAN
CANCER**

**A Thesis Submitted to
the Graduate School of Engineering and Sciences of
İzmir Institute of Technology
in Partial Fulfilment of the Requirements for the Degree of**

DOCTOR OF PHILOSOPHY

in Molecular Biology and Genetics

**by
Kübra TELLİ**

**November 2022
İZMİR**

ACKNOWLEDGEMENTS

Foremost, I would like to express my deepest gratitude to my supervisor Assoc. Prof. Dr. Özden Yalçın Özuysal for her continuous understanding, support, and guidance throughout my PhD journey.

I am thankful to my dissertation committee members, Assoc. Prof. Dr. Gülistan Meşe Özçivici and Prof. Dr. Gülşah Şanlı Mohamed for their questions, positive comments, and motivations. I appreciate Assis. Prof. Yavuz Oktay and Assoc. Prof. Şerif Şentürk and Prof. Dr Bünyamin Akgül's suggestions and motivations during my thesis defence.

I am thankful to ÖYÖ research members; Aslı, Burcu, Eda, Elif, Hülya, Perge, Mahnoor, Oğuzhan, Selin and Sena for their friendships and supports. Special thanks to Arda İlpars, without him I wouldn't be able to pass a year as I always miss one important document to submit.

I appreciate Dr. Pádraig D'Arcy for his patience, kindness, motivation, enthusiasm, and immense knowledge. He let me use almost all the laboratory stocks and never mentioned a word other than high quality jokes. He would always first analyse my mental state before suggesting an idea so that I never feel uncomfortable. I own deepest thanks to my beloved D'Arcy Lab friends, Johannes, Karthik, Linda, Laura and Fahima. Without them I would not be able to handle and conclude this project. I am also thankful to Prof. Dr. Stig Linder for forwarding my application email and always treating me as one of his group members. I wish he lives 200 years.

I owe earnest thankfulness to Buket, Narin, Vaishali, Hanna, Anna, Nicole, Marcus, Simon, Matthew, Evin, Therani, Furkan, İsmail, Birgül, Asya, Aras, Yunus, Hüseyin, Elif and Zeynep for being there for me whenever I needed them. I dedicate any of my success to them. I express my very profound gratitude to my family for providing me with unfailing support and continuous encouragement. Any of my accomplishments would not have been possible without them.

Finally, I would like to specially thank to TÜBİTAK for supporting this study with 2214A project (Application No:1059B142000543) and YÖK for 100/2000 scholarships.

ABSTRACT

INVESTIGATING MOLECULAR MECHANISMS UNDERLYING RESISTANCE TO NOTCH INHIBITORS IN BREAST AND OVARIAN CANCER

Breast and ovarian cancers remain highly malignant among women with more than 11% overall of incidence rates worldwide. Traditional treatment strategies including chemotherapy, radiotherapy and hormone therapies continues to be successful yet for the long-term, cancer recurrence and drug resistance remains to be the main issue. In addition to the altering common cell fate regulations, cancer cells modify signaling pathways to overcome cytotoxicity. Notch signalling pathway is a conserved ligand-receptor pathway that necessarily plays role in survival homeostasis, yet it is dysregulated in various cancers. Currently, novel treatment strategies are targeting this pathway through Gamma Secretase Inhibitors (GSI) DAPT, R04929097 and MK0752 that are use both as a single agent and in combinations with Docetaxel or Cisplatin. The clinical success of these inhibitors requires further examination of potential intrinsic or acquired resistance profiles. In this study, we generated breast cancer cells (MDA-MB-231 and MCF-7) resistant to DAPT or R04929097 and ovarian cancer cells (IGROV-1, BG-1, SKOV-3 and A2780) resistant to MK0752 by gradual treatments of increasing doses based on drugs' IC₅₀ values. Morphological changes, growth rates, migration alterations, mRNA expressions of Notch pathway components and epithelial mesenchymal transition markers, 3D setups for acidosis responses and protein expressions for c-myc and oxidative stress response markers were analyzed. Furthermore, proteomic analysis was carried out with the ovarian cancer cell line IGROV-1. The response of the cells to different drug treatments and dysregulated protein families exposed in resistance mechanisms behind DAPT, R04929097 and MK0752 for both breast and ovarian cancer cells are reported. Overall, this study reveals possible resistance mechanisms against GSIs and emphasizes potential targets through well-known hallmarks of cancer drug resistance.

ÖZET

MEME VE YUMURTALIK KANSERLERİNDE NOTCH BASKILAYICILARINA KARŞI OLUŞAN MOLEKÜLER DİRENÇ MEKANİZMALARININ ARAŞTIRILMASI

Meme ve yumurtalık kanserleri dünyada yaygın olarak %11' den fazla insidans oranı ile kadınlarda en yüksek maligniteye sahiptir. Geleneksel tedavi stratejileri, kemoterapi, radyoterapi ve hormon tedavileri başarılı olmaya devam etse de uzun vadede kanserin yeniden nüks etmesi ve ilaç direnci ana sorun olmaya devam etmektedir. Hücre kaderini belirlemede yapılan değişimlere ek olarak kanser hücreleri sinyal yollarını da modifiye ederek sitotoksisteye karşı gelmektedir. Notch, korunmuş, hücrenin yaşamsal homeostazını koruyan lüzumlu bir sinyal yolağı olmak ile birlikte farklı kanser türlerinde düzensiz ifade edilmektedir. Yeni tedavi stratejilerinde biri olan gama sekretaz inhibitörleri, DAPT, R04929097 ve MK0752 günümüzde tek ya da anti-kanser ajanları, Docetaxel veya Cisplatin ile kombinasyonel terapötik stratejisi olarak Notch'u hedeflemek için kullanılmaktadır. Bu inhibitörlerin klinik başarılarının devamlılığı için öncü veya sonradan direnç mekanizmalarının profil edilebilmesi için ek çalışmalar gerekmektedir. Bu projede, MDA-MB-231 ve MCF-7 meme kanseri hücreleri DAPT veya R04929097'e dirençli, IGROV-1, BG-1, SKOV-3 ve A2780 yumurtalık kanseri hücreleri ise MK0752'ya ilaçların dereceli IC₅₀ artışına maruz kalması yöntemi ile dirençli hale getirilip, kombinasyonel sinerji skorları bilinen Docetaxel veya Cisplatin ile combine edilmiştir. Meme ve yumurtalık kanserinde morfolojik değişimler, proliferasyon oranları, migrasyon değişimleri, EMD RNA ekspresyon markerları, 3D asidoz yanıt deneyleri ve protein c-Myc ve oksidatif stress yanıt markerları, proteomic deneyler ile desteklenerek düzensiz regüle olan protein ailelerinin DAPT, R04929097 ve MK0752 direnç mekanizmalarını ortaya çıkarmıştır. Sonuç olarak bu proje gama sekretaz baskılayıcılarının potansiyel ilaç direnç hedef mekanizmaları hakkında geniş spektrumlu araştırmayı, bilinen kanser ilaç direnci buluşları ile vurgulamaktadır.

Dedicated to my family...

TABLE OF CONTENTS

LIST OF FIGURES.....	xi
LIST OF TABLES.....	xx
CHAPTER 1. INTRODUCTION.....	1
1.1. Cancer.....	1
1.1.1. Breast Cancer.....	2
1.1.2. Ovarian Cancer.....	3
1.2. Traditional Chemotherapy.....	3
1.2.1. Cisplatin.....	4
1.2.2. Docetaxel.....	5
1.3. Drug Resistance.....	6
1.3.1. Hallmarks of Drug Resistance.....	7
1.4. Notch Signalling Pathway in Cancer.....	11
1.4.1. Notch signalling pathway.....	12
1.4.2. Role of Notch Signalling Pathway in Breast and Ovarian Cancers...18	
1.5. Inhibition Of Notch Signalling as A Therapeutic Approach in Cancer...19	
1.5.1. Gamma secretase inhibitor; Dual Antiplatelet Therapy (DAPT).....20	
1.5.2. Gamma secretase inhibitor; R04929097.....22	
1.5.3. Gamma secretase inhibitor; MK0752.....22	

CHAPTER 2. AIMS AND OBJECTIVES OF THE PROJECT.....	24
CHAPTER 3. MATERIALS AND METHODS.....	25
3.1. Cell lines and Cell Culture Conditions.....	25
3.2. Measuring Half-Maximal Inhibitory Concentrations (IC50).....	25
3.2.1. Measuring Drug Synergies.....	26
3.3. Proliferation Assay and Multidrug treatment strategies.....	26
3.4. Generating Intrinsic and Acquired resistance.....	27
3.5. Quantitative Real Time-PCR.....	28
3.6. Wound Healing Assay.....	29
3.7. Circularity analysis.....	30
3.8. Spheroid formation and Area Measurement.....	30
3.8.1 Acid Phosphatase Assay.....	30
3.9. Protein extraction and Western Blotting.....	31
3.10. LC-MS/MS and Label-Free Quantification.....	32
CHAPTER 4. RESULTS.....	33
4.1. DAPT Resistance In MDA-MB-231 Triple-Negative Breast Cancer Cell	33
4.1.1. DAPT-resistant MDA-MB-231 cells alter Notch receptors, Notch target genes and Epithelial Mesenchymal Transition markers mRNA expression levels.....	36
4.1.2. DAPT resistant MDA-MB-231 cells exhibit increased migration.....	37
4.1.3. Docetaxel and Cisplatin’s synergistic activities with DAPT in MDA-MB-231 cells.....	38

4.1.4. DAPT Combinations with Cisplatin and Docetaxel in MDA-MB-231 spheroids.....	43
4.2. DAPT Resistance In ER/PR ⁺ MCF-7 Breast Cancer Cells.....	46
4.2.1. DAPT resistant MCF-7 cells alter Notch receptors, Notch target genes and Epithelial-Mesenchymal Transition markers expression levels.....	49
4.2.2. DAPT resistant-MCF-7 cells exhibit increased migration.....	50
4.2.3. Docetaxel and Cisplatin’s synergistic activities with DAPT in MCF-7 Cells.....	51
4.2.4. DAPT Combinations with Cisplatin and Docetaxel in MCF-7 spheroids.....	56
4.3. R04929097 Resistance In MDA-MB-231 Triple Negative Breast Cancer Cells.....	59
4.3.1. R04929097 resistant MDA-MB-231 cells alter Notch receptors Notch target genes and Epithelial-Mesenchymal Transition markers expression levels.....	62
4.3.2. R04929097 resistant MDA-MB-231 cells display accelerated migration.....	63
4.4. R04929097 Resistance In ER/PR ⁺ MCF-7 Breast Cancer Cells.....	64
4.4.1. R04929097 resistant MCF-7 cells alter Notch receptors, Notch target genes and Epithelial-Mesenchymal Transition marker’s expression levels.....	67
4.4.2. R04929097 resistant MCF-7 cells exhibits no change in the migration potential.....	68
4.5. Intrinsic MK0752 Resistance and Docetaxel And Cisplatin’s	

Synergistic Activities with MK0752 In MDA-MB-231 Cells.....	69
4.5.1. MK0752 Combinations with Cisplatin and Docetaxel in MDA-MB-231 spheroids.....	74
4.6. Intrinsic MK0752 Resistance and Docetaxel and Cisplatin's Synergistic Activities with MK0752 In MCF-7 Cells.....	77
4.6.1. MK0752 Combinations with Cisplatin and Docetaxel in MCF-7 spheroids.....	81
4.7. MK0752 Resistance In Ovarian Cancer Cells.....	84
4.7.1. Intrinsic MK0752 resistance and Docetaxel, Cisplatin synergistic effects in Ovarian Cancer Cells.....	84
4.7.2. Acquired MK0752 resistance in Ovarian Cancer Cells.....	101
4.7.2.1. MK0752, Cisplatin and Docetaxel treatments in 2D and 3D cultures in parental and MK0752 resistant ovarian cancer cells...	105
4.7.2.2. MK0752 resistant ovarian cancer cells regulates C-Myc Protein expression levels.....	121
4.7.2.3. MK0752 resistant Ovarian cancer cells regulates Oxidative stress markers protein expression levels.....	127
4.7.2.4. Proteomic profiling and comparison of IGROV-1CisR and IGROV-1MK0752R cells.....	138
 CHAPTER 5. DISCUSSION AND CONCLUSIONS.....	 152
5.1. GSI Resistance in Breast Cancer.....	152
5.2. GSI Resistance in Ovarian Cancer.....	157

SUPPLEMENTARY FIGURES (CONCLUSIVE).....166

REFERENCES.....171

LIST OF FIGURES

<u>Figure</u>	<u>Page</u>
Figure 1. Schematic representation of hallmarks of intrinsic and acquired drug resistance in cancers.....	7
Figure 3. Key events of Notch signalling pathway discovery	12
Figure 4. Schematic structures of Notch receptors and ligands.....	14
Figure 5. Cleavage locations required for activation of Notch signaling	15
Figure 6. Illustration of Gamma secretase complex assembly and clinically available inhibitors; DAPT/MK0752 and R04929097.....	16
Figure 7. Overall schematic representation of Notch signaling pathway	17
Figure 8. Treatment strategies.	27
Figure 9. The schematic explanation of the protocol used to generate R04929097, DAPT and MK0752 resistant cells is shown.	28
Figure 10. Spheroid assays and Spheroid formations.....	31
Figure 11. IC ₅₀ curves of DAPT, Docetaxel, and Cisplatin treatments for MDA-MB-231 breast cancer cell line.....	34
Figure 12. MDA-MB-231-R breast cancer cells reach confluency in the presence of DAPT.	35
Figure 13. DAPT-resistant MDA-MB-231 cells exhibit increased viability than the MDA-MB-231-C cells.....	35
Figure 14. Circularity analysis of DAPT resistant- and control MDA-MB-231 cells....	36
Figure 15. mRNA expression analysis of Notch receptors, downstream targets and EMT markers for DAPT resistant-MDA-MB-231 cells.....	37
Figure 16. DAPT resistance increases migration in MDA-MB-231 breast cancer cells Migration phenotype was evaluated by wound healing assay.....	38
Figure 17. DAPT and Cisplatin have synergistic effects for MDA-MB-231 cells.....	40
Figure 18. DAPT and Docetaxel have synergistic effects for MDA-MB-231 cells.....	41
Figure 19. Decreased viability percentages of MDA-MB-231 cells in response to DAPT, Docetaxel and Cisplatin treatments.....	43

<u>Figure</u>	<u>Page</u>
Figure 20. Decreased viability percentages of MDA-MB-231 cells in response to sequential DAPT, Docetaxel and Cisplatin treatments.....	43
Figure 21. DAPT, Docetaxel and Cisplatin's both single agent and combinational treatments decrease MDA-MB-231 sphere size.	45
Figure 22. DAPT, Docetaxel and Cisplatin reduces MDA-MB-231 sphere size.	46
Figure 23. Decreased viability of MDA-MB-231 spheroids in response to DAPT, Docetaxel and Cisplatin treatments and their combinations.....	46
Figure 24. IC ₅₀ curves of MCF-7 breast cancer cell line to DAPT, Docetaxel, and Cisplatin treatments.	47
Figure 25. MCF-7-R breast cancer cells reach confluency in the presence of DAPT....	48
Figure 26. DAPT resistant MCF-7 cells exhibits increased viability than the MCF-7-C cells.	49
Figure 27. Circularity analysis of DAPT resistant- and control MCF-7 cells.	49
Figure 28. Expression analysis of Notch pathway components and EMT markers for DAPT resistant-MCF-7 cells.	51
Figure 29. DAPT resistance increases migration in MCF-7 breast cancer cells.	52
Figure 30. DAPT's combination with Docetaxel results in synergistic effect for MCF-7 cells.	53
Figure 31. DAPT's combination with Cisplatin results in synergistic effect for MCF-7 cells.....	54
Figure 32. Decreased viability ratios of MCF-7 cells in response to DAPT, Docetaxel and Cisplatin treatments.	55
Figure 33. Decreased viability ratios of MCF-7 cells in response to sequential DAPT, Docetaxel and Cisplatin treatments.	56
Figure 34. DAPT, Docetaxel and Cisplatin's both single agent and combinational treatments decreases MCF-7 sphere size.	58
Figure 35. DAPT, Docetaxel and Cisplatin their combinations reduce MCF-7 sphere size. Normalized Area of measured from spheroid images were graphed. ...	59
Figure 36. Decreased viability of MCF-7 spheroids in response to DAPT, Docetaxel and Cisplatin treatments and their combinations.....	59
Figure 37. IC ₅₀ curves of MDA-MB-231 breast cancer cell line to R04929097 treatments.....	61

<u>Figure</u>	<u>Page</u>
Figure 38. MDA-MB-231-R breast cancer cells reach confluency in the presence of R04929097.....	61
Figure 39. R04929097 resistant MDA-MB-231 cells exhibit no changes in viability... 62	62
Figure 40. Circularity analysis of R04929097 resistant- and control MDA-MB-231 cells.	62
Figure 41. Expression analysis of Notch pathway components and EMT markers for R04929097 resistant-MDA-MB-231 cells.....	64
Figure 42. R04929097 resistance delays migration rate in MDA-MB-231 breast cancer cells.....	65
Figure 43. IC ₅₀ curves of MCF-7 breast cancer cell line to R04929097 treatments.....	66
Figure 44. MCF-7-R breast cancer cells reach confluency in the presence of R04929097.....	66
Figure 45. R04929097 resistant MCF-7 cells exhibits no changes in viability.....	67
Figure 46. Circularity analysis of R04929097 resistant MCF-7 and control cells.	67
Figure 47. Expression analysis of Notch pathway components and EMT markers for R04929097 resistant-MCF-7 cells.....	69
Figure 48. R04929097 resistance shows no change in the migration rate for MCF-7 breast cancer cells.	70
Figure 49. IC ₅₀ curves of MDA-MB-231 breast cancer cell line to MK0752 treatments.	70
Figure 50. MK0752's combination with Docetaxel results in additive effect for MDA-MB-231 cells.	72
Figure 51. MK0752's combination with Cisplatin results in additive effect for MDA-MB-231 cells.	73
Figure 52. Decreased viability ratios of MDA-MB-231 cells in response to MK0752, Docetaxel and Cisplatin treatments.	74
Figure 53. Decreased viability ratios of MDA-MB-231 cells in response to sequential MK0752, Docetaxel and Cisplatin treatments.	74
Figure 54. MK0752, Docetaxel and Cisplatin's both single agent and combinational treatments decreases MDA-MB-231 sphere size.	76
Figure 55. MK0752, Docetaxel, Cisplatin and their combinations reduces MDA-MB-231 sphere size.....	77

<u>Figure</u>	<u>Page</u>
Figure 56. Decreased viability of MDA-MB-231 spheroids in response to MK0752, Docetaxel and Cisplatin treatments and their combinations.....	77
Figure 57. IC ₅₀ curves of MCF-7 cell lines to MK0752 treatments.	78
Figure 58. MK0752's combination with Docetaxel results in synergistic effect for IMCF-7 cells.	79
Figure 59. MK0752's combination with Cisplatin results in additive effect for MCF-7 cells.....	80
Figure 60. Decreased viability ratios of MCF-7 cells in response to MK0752, Docetaxel and Cisplatin treatments.	81
Figure 61. Decreased viability ratios of MCF-7 cells in response to sequential MK0752, Docetaxel and Cisplatin treatments.....	81
Figure 62. MK0752, Docetaxel and Cisplatin's both single agent and combinational treatments decreases MCF-7 sphere size.	83
Figure 63. MK0752, Docetaxel, Cisplatin and their combinations reduces MCF-7 sphere size.....	84
Figure 64. Decreased viability of MCF-7 spheroids in response to MK0752, Docetaxel and Cisplatin treatments and their combinations.	84
Figure 65. IC ₅₀ curves of IGROV-1, SKOV3, A2780 and BG-1 cell lines to MK0752, Docetaxel, and Cisplatin treatments.	86
Figure 66. MK0752's combination with Docetaxel results in additive effect for IGROV- 1 cells.....	87
Figure 67. MK0752's combination with Cisplatin results in additive effect for IGROV-1 cells.....	88
Figure 68. MK0752's combination with Docetaxel results in additive effect for IGROV-1 ^{CisR} cells.....	89
Figure 69. MK0752's combination with Cisplatin results in additive effect for IGROV-1 ^{CisR} cells.....	90
Figure 70. Decreased viability ratios of IGROV-1 and IGROV-1 ^{CisR} cells in response to MK0752, Docetaxel and Cisplatin treatments.	91
Figure 71. Decreased viability ratios of IGROV-1 and IGROV-1 ^{CisR} cells in response to sequential MK0752, Docetaxel and Cisplatin treatments....	91

<u>Figure</u>	<u>Page</u>
Figure 72. MK0752's combination with Docetaxel results in additive effect for A2780 cells.....	93
Figure 73. MK0752's combination with Cisplatin results in additive effect for A2780 cells.....	94
Figure 74. Decreased viability ratios of A2780 cells in response to MK0752, Docetaxel and Cisplatin treatments.	95
Figure 75. Decreased viability ratios of A2780 cells in response to sequential MK0752, Docetaxel and Cisplatin treatments.....	95
Figure 76. MK0752's combination with Docetaxel results in additive effect for BG-1 cells.	96
Figure 77. MK0752's combination with Cisplatin results in additive effect for BG-1 cells.	97
Figure 78. Decreased viability ratios of BG-1 cells in response to MK0752, Docetaxel and Cisplatin treatments.	98
Figure 79. Decreased viability ratios of BG-1 cells in response to sequential MK0752, Docetaxel and Cisplatin treatments.	98
Figure 80. MK0752's combination with Docetaxel results in additive effect for SKOV-3 cells.....	99
Figure 81. MK0752's combination with Cisplatin results in additive effect for SKOV-3 cells.	100
Figure 82. Decreased viability ratios of SKOV-3 cells in response to MK0752, Docetaxel and Cisplatin treatments.	101
Figure 83. Decreased viability ratios of SKOV-3 cells in response to sequential MK0752, Docetaxel and Cisplatin treatments.....	101
Figure 84. IC ₅₀ curves of parental and MK0752 resistant IGROV-1, A2780, BG-1 and SKOV-3 cell lines.....	102
Figure 85. Morphological changes of parental and MK0752 resistant A2780, BG-1, SKOV-3, and IGROV-1 ovarian cancer cell lines.....	103
Figure 86. A2780 ^{MK0752R} cells exhibits increased viability when compared to A2780.	104
Figure 87. BG-1 ^{MK0752R} cells exhibits increased viability when compared to BG-1...	104
Figure 88. IGROV-1 ^{CisR} cells exhibits increased viability when compared to IGROV-1 ^{MK0752R}	105

<u>Figure</u>	<u>Page</u>
Figure 89. SKOV-3 ^{MK0752R} cells exhibits increased viability when compared to SKOV-3.....	105
Figure 90. MK0752, Docetaxel and Cisplatin's both single agent and combinational treatments decreases IGROV-1 sphere size.....	106
Figure 91. MK0752, Docetaxel, Cisplatin and their combinations reduce IGROV-1 sphere size. Normalized Area of measured from spheroid images were graphed.....	107
Figure 92. MK0752, Docetaxel and Cisplatin's both single agent and combinational treatments decreases IGROV-1 ^{CisR} sphere size.	109
Figure 93. MK0752, Docetaxel, Cisplatin and their combinations reduces IGROV-1 ^{CisR} sphere size.	109
Figure 94. MK0752, Docetaxel and Cisplatin's both single agent and combinational treatments decreases IGROV-1 ^{MK0752R} sphere size.	110
Figure 95. MK0752, Docetaxel, Cisplatin and their combinations reduces IGROV-1 ^{MK0752R} sphere size.	110
Figure 96. MK0752, Docetaxel and Cisplatin's both single agent and combinational treatments decreases BG-1 sphere size.....	112
Figure 97. MK0752, Docetaxel, Cisplatin and their combinations reduce BG-1 sphere size. Normalized Area of measured from spheroid images were graphed.....	112
Figure 98. MK0752, Docetaxel and Cisplatin's both single agent and combinational treatments decreases BG-1 ^{MK0752R} sphere size.	113
Figure 99. MK0752, Docetaxel, Cisplatin and their combinations reduces BG-1 ^{MK0752R} sphere size.	113
Figure 100. MK0752, Docetaxel and Cisplatin's both single agent and combinational treatments decreases SKOV-3 sphere size.....	114
Figure 101. MK0752, Docetaxel, Cisplatin and their combinations reduces SKOV-3 sphere size.....	114
Figure 102. MK0752, Docetaxel and Cisplatin's both single agent and combinational treatments decreases SKOV-3 ^{MK0752R} sphere size.	115
Figure 103. MK0752, Docetaxel, Cisplatin and their combinations reduces SKOV-3 ^{MK0752R} sphere size.	115

<u>Figure</u>	<u>Page</u>
Figure 104. MK0752, Docetaxel and Cisplatin's both single agent and combinational treatments decreases A2780 sphere size.	116
Figure 105. MK0752, Docetaxel, Cisplatin and their combinations reduces A2780 sphere size.....	116
Figure 106. MK0752, Docetaxel and Cisplatin's both single agent and combinational treatments decreases A2780 ^{MK0752R} sphere size.....	117
Figure 107. MK0752, Docetaxel, Cisplatin and their combinations reduces A2780 ^{MK0752R} sphere size.	117
Figure 108. Decreased viability of A2780 and A2780 ^{MK0752R} spheroids in response to MK0752, Docetaxel and Cisplatin treatments and their combinations.....	120
Figure 109. Decreased viability ratios of BG-1 and BG-1 ^{MK0752R} spheroids in response to MK0752, Docetaxel and Cisplatin treatments and their combinations.	120
Figure 110. Decreased viability ratios of SKOV-3 and SKOV-3 ^{MK0752R} spheroids in response to MK0752, Docetaxel and Cisplatin treatments and their combinations.	121
Figure 111. Decreased viability ratios of IGROV-1 and IGROV-1 ^{MK0752R} , and IGROV-1 ^{CisR} spheroids in response to MK0752, Docetaxel and Cisplatin treatments and their combinations.	121
Figure 112. BG-1 and BG-1 ^{MK0752R} cells c-myc protein expressions.....	123
Figure 113. A2780 and A2780 ^{MK0752R} cells c-myc protein expressions.....	123
Figure 114. SKOV-3 and SKOV-3 ^{MK0752R} cells c-myc protein expressions with	124
Figure 115. IGROV-1, IGROV-1 ^{MK0752R} and IGROV-1 ^{CisR} cells c-myc protein expressions.....	124
Figure 116. SKOV-3 and SKOV-3 ^{MK0752R} cells c-myc protein expressions with 2D and 3D conditions.....	126
Figure 117. BG-1 and BG-1 ^{MK0752R} cells c-myc protein expressions with 2D and 3D conditions.....	126
Figure 118. A2780 and A2780 ^{MK0752R} cells c-myc protein expressions with 2D and 3D conditions.	127

<u>Figure</u>	<u>Page</u>
Figure 119. IGROV-1 and IGROV-1 ^{MK0752R} cells c-myc protein expressions with 2D and 3D conditions.	127
Figure 120. BG-1 and BG-1 ^{MK0752R} cells Catalase, Smooth muscle actin, SOD1 and Thioredoxin protein expressions with MK0752, Docetaxel and Cisplatin single agent and combinational treatments.....	129
Figure 121. A2780 and A2780 ^{MK0752R} cells Catalase, Smooth muscle actin, SOD1 and Thioredoxin protein expressions with MK0752, Docetaxel and Cisplatin single agent and combinational treatments.	131
Figure 122. SKOV-3 and SKOV-3 ^{MK0752R} cells Catalase, Smooth muscle actin, SOD1 and Thioredoxin protein expressions with MK0752, Docetaxel and Cisplatin single agent and combinational treatments..	132
Figure 123. IGROV-1, IGROV-1 ^{MK0752R} and IGROV-1 ^{CisR} cells Catalase, Smooth muscle actin, SOD1 and Thioredoxin protein expressions with MK0752, Docetaxel and Cisplatin single agent and combinational treatments.....	134
Figure 124. IGROV-1 and IGROV-1 ^{MK0752R} cells Catalase, Smooth muscle actin, SOD1 and Thioredoxin protein expressions with 2D and 3D conditions.	135
Figure 125. SKOV-3 and SKOV-3 ^{MK0752R} cells Catalase, Smooth muscle actin, SOD1 and Thioredoxin protein expressions with 2D and 3D conditions.	136
Figure 126. A2780 and A2780 ^{MK0752R} cells Catalase, Smooth muscle actin, SOD1 and Thioredoxin protein expressions with 2D and 3D conditions.....	137
Figure 127. BG-1 and BG-1 ^{MK0752R} cells Catalase, Smooth muscle actin, SOD1 and Thioredoxin protein expressions with 2D and 3D conditions. ..	138
Figure 128. Proteomics data interpretation and visualization of IGROV-1 ^{MK0752R} and IGROV-1 ^{CisR} cells.	141
Figure 129. Pie charts showing the proteome distribution on molecular function, cellular component, and biological processes.	142
Figure 130. Pie charts showing the proteome distribution on protein class categories and pathways.	143
Figure 131. Functional gene network analysis of genes dysregulated in IGROV-1 ^{CisR} cells.	144

<u>Figure</u>	<u>Page</u>
Figure 132. Functional gene network analysis of genes dysregulated in IGROV-1 ^{MK0752R} cells.....	145
Figure 133. Collective functional gene network analysis of genes dysregulated in IGROV-1 ^{CisR} and IGROV-1 ^{MK0752R} cells.	146
Figure 134. Proteomic signatures of IGROV-1, IGROV-1 ^{MK0752R} and IGROV-1 ^{CisR} cells in cell proliferation.....	147
Figure 135. Proteomic signatures of IGROV-1, IGROV-1 ^{MK0752R} and IGROV-1 ^{CisR} cells in cell metabolism.	148
Figure 136. Proteomic signatures of IGROV-1, IGROV-1 ^{MK0752R} and IGROV-1 ^{CisR} cells in cell growth.....	149
Figure 137. Proteomic signatures of IGROV-1, IGROV-1 ^{MK0752R} and IGROV-1 ^{CisR} cells in membrane transport.....	150
Figure 138. Proteomic signatures of IGROV-1, IGROV-1 ^{MK0752R} and IGROV-1 ^{CisR} cells in exocytosis.....	150
Figure 139. Proteomic signatures of IGROV-1, IGROV-1 ^{MK0752R} and IGROV-1 ^{CisR} cells in the cell cytoskeleton.....	151
Figure 140. Proteomic signatures of IGROV-1, IGROV-1 ^{MK0752R} and IGROV-1 ^{CisR} cells in carcinogenesis.	152
Figure 141. Overall illustration of GSI drug resistance hallmarks for GSI treatments in breast and ovarian cancer cells.....	166
Figure 142. Summary of DAPT or R04929097 resistant MDA-MB-231 and MCF-7 breast cancer cell line’s results obtained from this project.....	167
Figure 143. Summary of DAPT or MK0752’s Docetaxel and Cisplatin combination results for MDA-MB-231 and MCF-7 breast cancer cell lines.	168
Figure 144. Summary of MK0752’s Docetaxel and Cisplatin combination results for IGROV-1, IGROV-1 ^{CisR} , A2780, SKOV-3 and BG-1 ovarian cancer cell lines.....	169
Figure 145. Summary of MK0752, Docetaxel and Cisplatin single agent treatment results for IGROV-1, IGROV-1 ^{CisR} , A2780, SKOV-3 and BG-1 ovarian cancer cell lines.	170
Figure 146. Summary of MK0752 resistance results for IGROV-1, IGROV-1 ^{CisR} , A2780, SKOV-3 and BG-1 ovarian cancer cell lines.....	171

LIST OF TABLES

<u>Table</u>	<u>Page</u>
Table 1. List of primers used for quantitative real-time PCR (Q-RT-PCR).....	29
Table 2. IC ₅₀ values of MK0752 resistant ovarian cancer cell lines.....	103
Table 3. Proteins downregulated in IGROV-1 ^{MK0752R} cells.....	139
Table 4. Proteins upregulated in IGROV-1 ^{CisR} and IGROV-1 ^{MK0752R} cells.	139
Table 5. Proteins dysregulated in IGROV-1 ^{CisR} and IGROV-1 ^{MK0752R} cells.	140

CHAPTER 1

INTRODUCTION

1.1. Cancer

Cancer is collection of diverse, dynamic, and complex neoplastic diseases that remains to be causing highest mortality worldwide. Such diversity is associated with the origin of the tissue, genetic regulators, epigenetic switches, and cell signalling pathways. The archetype cells merged in eight hallmarks and two enabling characteristics listed by Hanahan and Weinberg for a better understanding of cancers biological machinery (2000; 2011). Hallmarks categorize cancer cells routine as; growth without contact inhibition, evading cell cycle checkpoint inhibitions, and becoming replicable immortal, uncontrolled proliferating signalling's, escaping destructive immune response, tumour-associated inflammatory response, angiogenesis, genomic instability, and accumulation of mutations, evading cell death, unbalanced cellular metabolism, invasive and metastatic behaviour (Hanahan and Weinberg, 2011). Altered homeostatic stages in progenitor cells endure remodelled intra/intercellular mechanisms which results in malignancy (McGranahan and Swanton, 2017). Chemotherapy, hormone therapies, surgery and radiotherapy are reductionist treatment strategies used over decades (Zugazagoitia et al., 2022). Metastatic and invasive behaviour of malignant cells and inclusion of cumulative genetic modifications complicate traditional cancer treatments (Sarkar et al., 2013). Main hindrance for successful and long-term cancer treatments remains to be the resistance against therapy followed by recurrence. Highest therapy resistance and recurrence rates lingers among ovarian and breast cancers (Garzon et al., 2020; Riggio et al., 2021). Modern and personalized treatments are currently designed to target specific molecules or pathways to overcome recurrence conundrum in the clinic (Harbeck et al., 2019).

1.1.1. Breast Cancer

Breast cancer is highly malignant among woman remains 11.7% of overall incidence rate and 6.9% mortality rate worldwide (Sung et al., 2021). Breast malignancies originates from mammary gland, from either the basal tissue (myoepithelial) or luminal tissue near lumen area (epithelial cellular phenotype) (Yates et al., 2017; Mollen et al., 2018; Giuoli et al., 2019). Breast cancer can be classified into histological and molecular subtypes. Histological characterization classifies breast cancer as, in situ carcinoma (lobular or ductal), invasive carcinoma (lobular and/or ductal or both), invasive carcinoma type specific (papillary, medullary, apocrine, mucinous, tubular, cribriform, clear cell, and Paget disease), and Miscellaneous (anaplastic, metaplastic, malignant phyllodes tumour and pleomorphic sarcoma). Molecular characterization classifies breast cancer as, Luminal A (estrogen receptor (ER) +, progesterone receptor (PR) +, HER2-), Luminal B (ER+, PR+/-, HER2+/-), Triple Negative (ER-, PR-, HER2-) and HER2 (HER2+). (Mollen et al., 2018 and Waks and Winer, 2019). Breast cancer screening and detection are done via mammography, ultrasound, and magnetic resonance imaging (Wang, 2017). Oestrogen, progesterone hormone receptors and HER2 expressions, cell cycle proteins and Ki67 cancer cell proliferation markers are determined by immunohistochemical staining assay to define the stage as well as treatment strategy (Waks and Winer, 2019). ER/PR⁺ breast cancers are sequentially treated with hormone therapy (tamoxifen and fulvestrant), chemotherapy (paclitaxel, cisplatin, doxorubicin, docetaxel, vincristine, erlotinib and pertuzumab) after surgical operations. HER2 targeted therapies applied for HER2⁺ subtype. Triple negative breast cancer is treated with chemotherapy as they are not responsive to available hormone or targeted therapies. Anthracycline-based therapies (doxorubicin, cisplatin, paclitaxel, taxane, eribulin and vinorelbine) and taxane based therapies (capecitabine) are used as a single/multiple chemo-treatments or in combination with radiotherapy (Moo et al., 2018).

1.1.2. Ovarian Cancer

Ovarian cancer (OC) is main gynaecologic malignancy among woman worldwide (Waks and Winer., 2019). OC originates from surface epithelial-stromal cells, germ cells, sex cord-stroma and further metastasize to ovaries accordingly to staging (Hirst et al., 2018). Histological subtypes of epithelial OC are serous, endometrioid, clear cell, mucinous and malignant Brenner whereas germ cells are subtyped as teratoma, dysgerminoma, endodermal sinus tumor, choriocarcinoma. Sex cord-stroma histological subtyping consists of fibroma, Granulos-theca cell tumor, Sertoli-Leydig cell tumor accordingly to the diagnosis frequency (Flaum et al., 2020). Molecular biomarkers of serous ovarian cancers consist of low expressions of BRCA1, BRCA2 and p53 additional to, increased KRAS, BRAF, and PI3KCA expressions. Low-grade serous, mucinous, clear cell and endometrioid carcinoma, expresses dysregulations in Ras, BRAF, PIK3CA and PTEN biomarkers (Guo et al., 2021). Surgery and chemotherapy are the main treatment strategies for OC's. Traditional chemotherapeutics as paclitaxel, gemcitabine, topotecan, vinorelbine, cisplatin, docetaxel is used to treat OC's. Recurrence in short time and drug resistance against platinum-based treatments shortens therapeutic options. Bevacizumab is an angiogenic inhibitor used to treat platinum resistant OC's as well as PARP inhibitor Olaparib supported with immunotherapies. Estrogen and progesterone receptors stimulate aberrant cell cycle and OC progression (Matulonis et al., 2016). OC diagnosis involves pelvic exam, transvaginal ultrasound, CT scan of abdomen and pelvis, MRI, PET scan, biopsy, and genetic testing of BRCA1/2, PTEN, RAS family proteins, BRAF, PI3KCA and p53. Chemoresistance, non-efficient hormone therapy outcome and recurrence remains to be the main hinder for breast and ovarian cancer treatments (Waks and Winer, 2019 and Anouk et al., 2020).

1.2. Traditional Chemotherapy

Chemical agents used to induce anti-neoplastic outcome is termed as chemotherapy. Traditional chemotherapeutics induces cell death in rapidly dividing cells via structural DNA modifications or inhibition of cell division whereas millennial

treatments are aiming to target pathway specific abnormalities to overcome cancer response in long term. Commonly, chemotherapeutics is derived from herbal, bacterial and synthetic combinations (Mallat, Tanios and Itani, 2013). Alkylating agents, anthracyclines, antibiotics, taxanes and antimetabolites are some of the typical chemotherapy categories. Effectiveness of these agents counteracts with the fact of drug resistance and cancer recurrence. Homeostasis of dysregulated pathways through target specific drugs gives new aspect outcome overcoming such cancer dilemma. Cisplatin and docetaxel are the most common chemotherapeutics used both as a single agent and in combination with novel drugs in the clinic in treating breast and ovarian cancers. Their combinations with millennial therapies are magnified in both preclinical and clinical studies (Prica, Chan and Cheung, 2014).

1.2.1. Cisplatin

Cisplatin is an antineoplastic platinum-based DNA alkylating-like agent mostly used for cancer treatment (Goodsell, 2006). Discovery of cisplatin in 1844 by M. Peyrone raised platinum-based therapies in demand use for various types of cancer treatments. Supportively, preclinical, and clinical trials have widened the knowledge about the benefits of metal-based (platinum and palladium etc.) medicines in cancer therapy (Muggia et al., 2015). Cisplatin mostly used for solid tumors such as soft tissue sarcoma, lymphomas, ovarian, breast and small cell lung cancer (Siddik, 2003). Mechanism of action starts by cisplatin entering the cell by passive diffusion and Cl^- in the structure exchanged by H_2O molecule to create a bond and swap the bond between platinum and Guanine at N^7 position to start crosslinking the DNA. Cisplatin induced lesion stimulates repair mechanisms such as nucleotide excision repair and homologous repair to activate DNA repair, sidewise, if damage remains under continuous treatments DNA replicates lesion area via translesion synthesis and induces cells to undergo apoptosis (Cerón-Carrasco and Jacquemin, 2015; Rocha, Silva, Quinet, Cabral-Neto & Menck, 2018). Cisplatin, carboplatin and oxaliplatin are the most widely used platinum-based chemotherapeutic drugs (Wang, Lin, Liu & He, 2013).

Cisplatin is approved worldwide and the one with the least adverse effects in treating cancers like breast, ovarian and sarcoma's (Killari et al., 2016). Cisplatin is only affective in high doses and severely toxic to organs (induces cardiotoxicity, ototoxicity,

and kidney failure) which is creating dilemma that remains unsolved as contrarily optimum/low dose induces intrinsic or acquired drug resistance (Wang et al., 2014). Platinum-based drug resistance is one of the main restrictions in the usage of cisplatin for both short- and long-term cancer treatments. High levels of DNA damage after three-six months of chemotherapy with cisplatin urges drug resistance then tumors relapse (Callejo et al., 2015). Such resistance can be induced through multiple pathways; dysfunctioning drug influx-efflux mechanisms (imbalance in the expression of transporters), DNA repair sufficiency (increased repair machinery) and drug detoxification (increased expression of Glutathione S-transferase). Cisplatin is transported inside the cell via CTR1 (chloride transport receptor 1), and decreased influx induces resistant behavior (Dasari & Bernard Tchounwou, 2014; Rocha, Silva, Quinet, Cabral-Neto & Menck, 2018). On the other hand, increased efflux property of transporter family MRP-1 (multidrug resistance-associated protein 1) also decreases the toxicity of cisplatin. Dysregulation in ATP-dependent glutathione S-conjugate export pump (GS-X pump) also leads resistant cell behavior for cisplatin treatment (Dasari & Bernard Tchounwou, 2014; Zhu et al., 2016).

1.2.2. Docetaxel

Docetaxel (Taxotere) is member of a taxane family, an anti-microtubule agent, which binds to β subunits of tubulin and inhibits depolymerization, blocking cell division by causing mitotic catastrophe and induces cell death through Smac-DIABLO pathway. Docetaxel is commonly used as first line chemotherapeutic treating breast and ovarian cancers (Magadoux, et al., 2014). Its efficacy and tolerability (side effects such as neutropenia) are proven to be better when compared to the doxorubicin and paclitaxel monotherapies. Docetaxel is also used as secondary option after a prior chemotherapeutic strategy that proves its usability in drug resistance-cancer relapse models (Williamson and Fenton, 2005). Docetaxel is pumped out of the cell slower than paclitaxel and such mechanism is stimulated by P-glycoprotein pumps on the cell surface. On the other hand, docetaxel induces β tubulin mutations which then leads to survival pathways causing drug resistance. The mechanism of resistance remains unknown in metastatic breast cancer cells and ovarian cancers (Magadoux, et al., 2014). Docetaxel is used both as a single and combinational treatments in the clinics for treating

various cancers including breast cancer and to this date, there are over hundred clinical studies conducted (National Cancer Institute, 2020).

1.3. Drug Resistance

Toxic stimuli adaptation is defined as resistance and cancer cells mimic such adaptive behaviours against anti-neoplastic drug treatments such as chemotherapy (Bizzarri, Cucina and Proietti, 2014). Chemotherapy is one of the most powerful efficient treatments, used for over 60 years to treat many types of cancer (Luqmani, 2008 and Alfarouk et al., 2015). Resistance to chemotherapy limits the effectiveness of anti-cancer drug treatment and it causes treatment failure in over 90% of patients with metastatic cancers. Such response commonly induces cells become cross-resistant to other drugs with known or unknown mechanisms of action (Sh et al., 2019 and Wang and Guo, 2013).

Drug resistance can be divided into either intrinsic or acquired based on the innate or continuous response against the drug. Intrinsic resistance refers to innate lack of response against the therapeutic agent at clinically admissible dose. Heterogenic tumour populations with diverse sensitivity patterns and mutations can also become the cause of intrinsic resistance. Cancer stem cells evade from the traditional chemotherapies that results in rampant toxicity and cancer recurrence (Wang, Zhang, and Chen, 2019).

Contrariwise, acquired resistance indicates the lack of response that develops after initial successful therapy. Acquired resistance can depend on accordingly to the therapeutic agent used, dose and treatment schedule. Acquired resistance can induce novel mutations that might trigger the recurrence and cancer cell longevity due to the usage of traditional chemotherapeutic drugs (Nussinov et al., 2021). For instance, acute myeloid leukaemia patients with tumour recurrence after chemotherapy proved transversion mutations results in further DNA damage that might be caused by chemotoxicity (Ding et al., 2012). Intrinsic and acquired resistance can co-exist and induce single or multiple drug resistance responsible for cancer recurrence (Moulder, 2010 and Cree and Charlton, 2017). Common networks for intrinsic and acquired resistance can be represented as hallmarks of drug resistance as increased drug efflux, epigenetic modifications, changes in tumour microenvironment, cancer metabolism,

epithelial-mesenchymal transition (EMT), altered drug targets, altered DNA damage repair, inactivated drug chemistry, oxidative stress, and evading apoptosis (Figure 1). These factors could emanate alone or in combination for cancer cells to overcome cytotoxic stimuli (Zunino and Gatti, 2005; Housman et al., 2014; Cree and Charlton, 2017; Benko et al., 2021; Nussinov et al., 2021). Resistance mechanisms differs depending on the specificity of the drug, drug exposure routines, applied combinational strategies, stage of cancer and tissue/cell origin (Lippert, Ruoff and Volm, 2011).

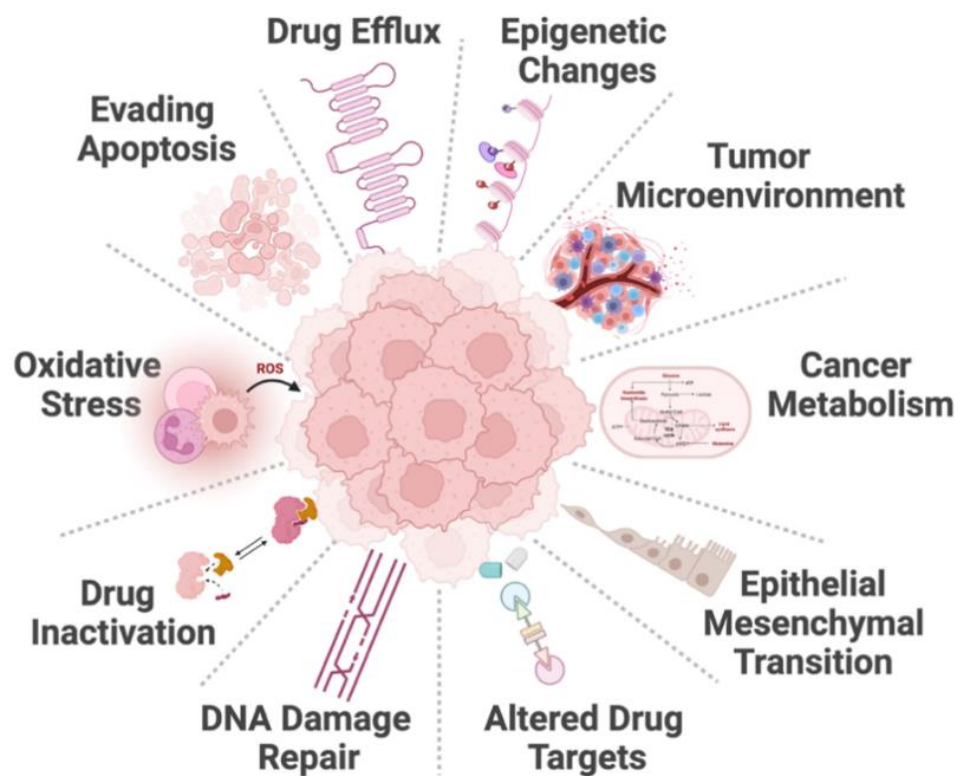


Figure 1. Schematic representation of hallmarks of intrinsic and acquired drug resistance in cancers (Source: Nussinov et al., 2021; created with BioRender.com, accessed in 2022).

1.3.1. Hallmarks of Drug Resistance

Increased drug efflux by ATP binding cassette (ABC) superfamily transmembrane transporters endures cellular homeostasis against chemical imbalance as well as cytotoxicity (Szakács, Homolya, Sarkadi & Váradi, 2008). Cancer cells

increase the number of ABC transmembrane transporters to lower/overcome intracellular toxicity prior or after the chemotherapeutic agent introduction (Wang et al., 2019). There are 48 human ABC superfamily genes classified in to 7 sub-groups ABC^{A-G} and each includes minimum of 3 members. ABCB1 (Permeability glycoprotein (P-gp)), ABCC1 (Multidrug Resistance Protein 1 (MRP1)) and ABCG2 (Breast Cancer Resistance Protein (BCRP)/Mitoxantrone Resistance Protein (MRP)) ATP dependent transporters are overexpressed in cancers. Aberrant activation of these transmembrane exporters induces Cisplatin, Doxorubicin, Mitoxantrone, Epirubicin, Etoposide, Adriamycin, Vincristine and 5-flourouracil resistance in cancers (Ughachukwu and Unekwe, 2012). Intracellular drug concentration can also be decreased by drug inactivation strategy of cancer cells inducing aberrant expression of metabolic enzymes to biochemically modify drug's structure. Cytochrome P450, carboxylesterases, foyl polyglutamate synthase, cytarabine triphosphate and glutathione-S-transferase enzyme superfamilies accommodates pivotal roles in both catabolism of fatty acids, cell proliferation, differentiation, and apoptosis (Zahreddine & Borden, 2013). Their overexpression induces resistance against high profile chemotherapeutics such as tamoxifen, 5-flourouracil, cisplatin and doxorubicin (Dong et al., 2019). Epigenetic alterations, DNA methylation, chromatin remodelling, histone and noncoding RNA modifications initiates impaired gene expression in cancer cells that results in drug resistance (Zeller and Brown, 2010). ABCB1 hypomethylation, abnormal histone methylation, decreased acetylation, altered chromatin structures, translational repression of microRNA, changes in the nucleosome density through non-coding RNA's induces multidrug resistance against platinum based drugs and recurrence in cancers (Aziz and Ahmad, 2020).

Metabolism is firing requirement of constantly growing and dividing cancer cells. It is the gateway to becoming less vulnerable in thdrug-induced microenvironment. Dependent on the cancer cell heterogeneity, cells have with different levels of energy requirements compared to homeostatic healthy cells (Gertler et al., 2019). Migrating to the nearest efficient blood supply for both nutrition, growth factors and oxygen support becomes vital for pre-metastatic cancer cells. This results in overall cancer treatment failure with resistant and relapsed cellular phenotype. Studies provide proximity difference in cancer cells to the oxygen supply induces acidic varieties in the tumor microenvironment (Feron and Corbet, 2017). This phenomenon refers as the Warburg effect and it explains cancer cell's ability to use glucose as the main energy

supply with aerobic conditioning, normal cells on the other hand, produces lactate under anaerobic conditions via glycolysis (Gillies et al., 2011). Lactate overproduction results in excessive bicarbonic acid/bicarbonate that further acidities the tumor microenvironment. Cancer cells form two acidic/acidosis conditions that either can be acute and chronic due to flow in the pH differences. Noncancerous breast cells balance extracellular pH as 7.4 and intracellular pH as 7.2 however, in ductal carcinoma in situ, acute acidosis represents as 6.8 extracellular and 7.4 intracellular pH levels whereas chronic acidosis refers to extracellular pH as 6.5 to 6.7 and intracellular pH being approximately at 7.2 (Longo et al., 2019). Under acidosis conditions, ATP production can be conducted independently from oxygen levels in anaerobic metabolism by stimulating the mitochondrial metabolic pathways. Mitochondrial respiration differences play crucial step in drug resistance phenotype formation (Khacho et al., 2014). Acidic changes can stimulate cellular insensitivity against chemotherapeutic that being used for treatment by blocking the drugs activity (Feron and Corbet, 2017). Over acidic conditions, cell membrane pumps (ABC transporter family and P-glycoproteins) found to be overly active that results in intracellular drug concentration to be lowered by using cells natural toxic material defense mechanism via drug efflux stimulation (Zhang et al., 2017).

Drugs in clinical oncology fails due to severe toxicity and side effects of drugs either not active or harmfully active to the environment caused by acidosis environment. For instance, anti-cancer agents found to be over-influxed inside the normal cells under acidosis conditions and resulted in apoptosis more than cancerous ones because normal cells are alkaline. This selective toxicity produces severe side effects and drug dose escalation for the possible future treatments due to drug resistance (Kobayashi et al., 2017; Milito et al., 2018). Chemotherapeutics can add into dynamic irregularity of the tumour microenvironment and thus result in drug resistance. Acidic environment interferes with the weak acidic drugs and increase pronation of the drugs and increase intracellular passive diffusion of the drugs known as ion trapping phenomenon. One example for this phenomenon can be given as when extracellular pH is around 7.4, Cisplatin and Docetaxel toxicity found to be increasing and forcing cells to undergo apoptosis whereas when extracellular pH is around 6.6 drug toxicity decreases significantly (Geckle et al., 2014). Acidosis also increases the cancer stem cell marker CD44 and stimulate recurrence and metastatic phenotypes (Rohani et al., 2019). Connectedly, increase in the cancer stem cell markers initiate drug resistance and cancer

relapse. Acidosis conditions stimulate invasiveness in MCF-7 and MDA-MB-231 breast cancer cells (Mo et al., 2014). Raghuand et al., suggested that modern drugs (alkylating agents, pathway inhibitors, and hormone therapies) require further structural inspection and checking deeply under physiological ionization conditions counting on acidosis as a disadvantage (2000).

Morphological changes such as EMT induce molecular events through reduction of E-cadherin, Laminin-1, Cytokeratin, ZO1 and Desmoplakin involved in epithelial morphology and increase in the expression of Vimentin, Snail 1/2, N-cadherin, B-catenin, Zeb 1/2, Twist 1/2, Slug and Fibronectin through mesenchymal state of cells (Challagundla et al., 2015) (Figure 2). Mesenchymal tumour cells present increase in the metabolic activities, generation of hypoxic conditions and eventually drug resistance (Huang et al., 2016). Degree of EMT shift changes due to cancer's heterogeneity which then stimulates morphological changes and metastatic behaviours as known to be responsible for cancers aggressiveness and drug resistance (Gupta et al., 2019).

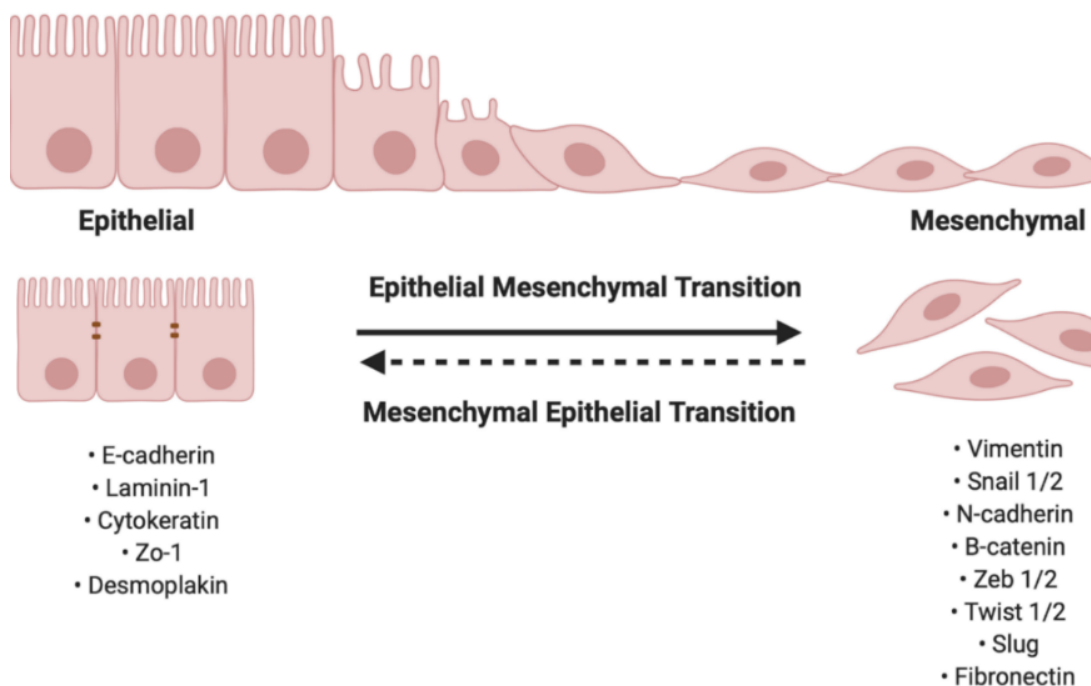


Figure 2. EMT transitions and genes involved in stimulation of epithelial and mesenchymal state of the cell shape (Source: Gupta et al., 2019; created with BioRender.com, accessed in 2022).

Prior or after chemotherapies cancer cells induce dysregulated DNA damage repair mechanisms to overcome drug toxicity. Drug based treatments (cisplatin, vincristine, doxorubicin, and 5-fluorouracil) mostly introduce DNA lesions, which result in programmed cell death of cancer cells. However, genomic instability of cancer cells results in evasion of cell death to display drug resistance and cancer recurrence (Li et al., 2021). Programmed cell death markers, Bcl-2 family, TRAIL-R3/4, TRAF, inhibitor of apoptotic proteins (IAPs), BAX, BAK, p53, caspase 3/7/8 restricts chemotherapeutic activity (Rathore et al., 2017).

Overactivated DNA damage repair mechanisms and their active regulatory proteins; base excision repair (Poly (Adenosine diphosphate-Ribose) Polymerase 1 (PARP1)), homologous recombination (Breast Cancer 1 and 2 (BRCA1 and 2), Ataxia-Telangiectasia and Mantle cell lymphoma (ATM) and RAD51), non-homologous end joining (Ku70/80), nucleotide excision repair (ERCC Excision Repair 1/4 (ERCC1/4)), mismatch repair (MutS homolog 2 (MSH2) and MutL homolog 1 (MLH1)) and direct repairs (O-6-Methylguanine-DNA Methyltransferase (MGMT)) stimulate drug-resistance in cancers (Chang and Zou, 2020; Nephytou et al., 2021).

Reactive oxygen species (ROS); hydrogen peroxide, the hydroxyl radical, superoxide and singlet oxygen maintain cellular oxi/antioxidants further for cell fate determination. Increase in the ROS production stimulates cancer prognosis and chemoresistance through overactivation of drug efflux transporters (Liu et al., 2016). Due to all these hallmarks, drug resistance paradox lingers to challenge success of treatment strategies for curing cancers (Vasan, Baselga and Hyman 2019).

1.4. Notch Signalling Pathway in Cancer

Notch is complex and conserved signalling pathway that involves cell-to-cell interactions (Figure 3). It plays an important role in regulating cell proliferation, differentiation, and apoptosis (Han et al., 2011; Zlobin and Olsauskas Kuprys, 2013). Dysregulation of Notch signaling pathway elements are associated with cancers' worse prognostic outcome, drug resistance and cancer recurrence (Han et al., 2011; Zlobin and Olsauskas Kuprys, 2013). Targeting Notch signaling activity is currently in high demand for both pre and clinical stages in treating cancers (Hossain et al., 2018).

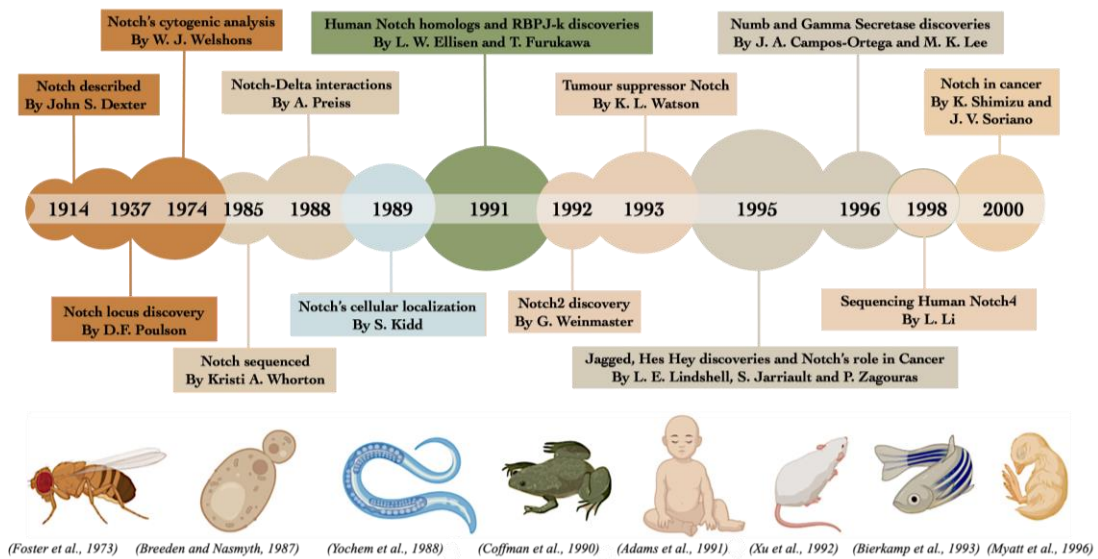


Figure 3. Key events of Notch signalling pathway discovery (Source: Dexter, 1914; Poulson et al., 1937; Foster et al., 1973; Welshons, 1974; Whorton et al., 1985; Breden and Nasmyth, 1987; Yonchem et al., 1988; Preiss et al., 1988; Kidd et al., 1989; Coffman et al., 1990; Ellisen et al., 1991; Adams et al., 1991; Frukawa et al., 1991; Xu et al., 1992; Weinmaster et al., 1992; Bierkamp et al., 1993; Watson et al., 1993; Lindshell et al., 1995; Jarriault et al., 1995; Zagouras et al., 1995; Myatt et al., 1996; Ortega et al., 1996; Lee et al., 1996; Li et al., 1998; Shimizu et al., 2000 and Soriano et al., 2000; created with BioRender.com, accessed in 2022).

1.4.1. Notch signalling pathway

Mammalian Notch signaling involves five ligands (Jagged 1, 2, Delta like 1 (DLL1), 3, and 4) on the signal sending cells and four receptors (Notch 1, 2, 3 and 4) on the signal receiving cells (Tsakonas et al., 1995). Ligand-receptor interactions are highly stable and based on each component structure units occurs in favorable combinations such as, Notch1 interacts with Jagged1, 2, Notch2 with DLL1, Notch3 with DLL3 and Notch4 interacts with DLL4 (Henrique and Schweisguth, 2019). Receptors have three main components based on their cellular location: Notch extracellular complex, Notch transmembrane domain and Notch intracellular domain (Zlobin and Olsauskas Kuprys, 2013). Notch receptors carry Epidermal Growth Factor

like repeat (EGF) sequences that can vary between 29 to 36 repeats among receptors and contain calcium binding sites required for stable and authentic receptor-ligand bindings. Diversely, Notch ligands have Cysteine rich *lin12* repeats (LNR) and heterodimerization domains (HD) responsible for sufficient binding stability and cleavage site accuracy. Negative regulatory regions (NRR) are the checkpoints of Notch activation based on ligand accuracy (Henrique and Schweisguth, 2019).

Defects on the sequence of receptors disrupt cell homeostasis as in, HD or NRR mutations induce uncontrolled Notch activation and stimulates cancerous cell phenotype. Region rich in proline (P), glutamine (E), serine (S) and threonine (T) residues (PEST) and HD contain hotspot regions reported being responsible for various diseases (Mas et al., 2017). On the other hand, each ligand also carries EGF-like repeats that vary between 8 to 16 repeats and component numbers matter for binding affinities (Gordon et al., 2009 and Mas et al., 2017). For instance, DLL1/4 requires extracellular signal initiation based on its recognition at PDLZ component whereas DLL3 can be expressed and stimulated through intracellular initiation for further signaling (Pancewicz and Nicot, 2011).

Jagged (Jag) and DLL family of ligands also contains, MNNL region, PDZL domain at C-terminus in Delta like family ligands 1, 4, cysteine rich sequences in Jagged family ligands and signal peptides. Binding of Notch receptor to the ligand stimulates Notch signaling pathway activation and further induction of Notch target genes transcription (Arruga et al., 2018).

Notch receptor production and pre-processing starts in the Endoplasmic reticulum (ER) by sequential addition of O-fucose by O-fucosyltransferases 1 (POFUT1), addition of N-acetylglucosamine by one of the N-acetylglucosaminetransferases (Lunatic Fringe (LFNG), Manic Fringe (MFNG), and Radical Fringe (RFNG)), then it is cleaved by Furin for further processing (Steinbuck et al., 2018) (Figure 4).

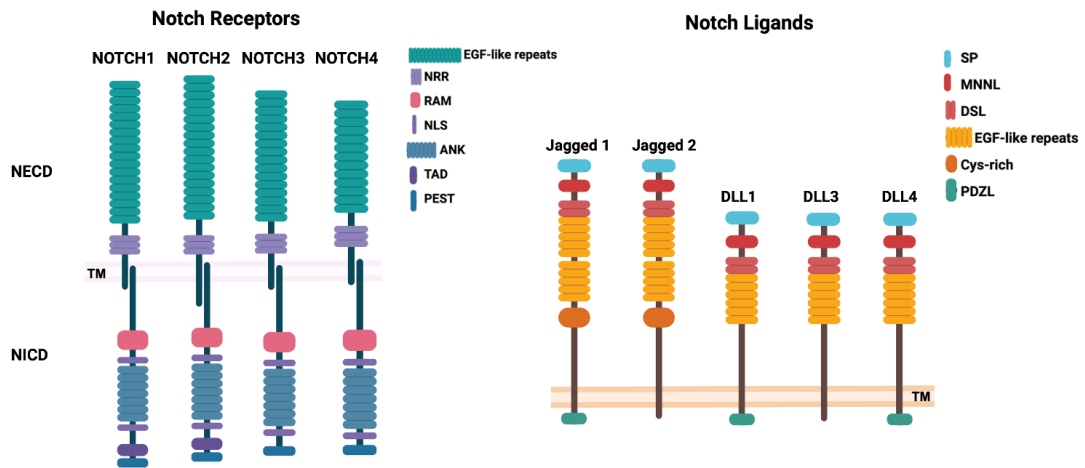


Figure 4. Schematic structures of Notch receptors and ligands. Abbreviated terms represents; Epidermal growth factor (EGF)-like repeats, negative regulatory region (NRR), recombination signal binding protein for immunoglobulin kappa J region association molecule (RAM), LIN12-Notch repeats (NLS), ankyrin repeat sequence (ANK), transactivation domain (TAD), Proline Serine and threonine to maintain protein stability (PEST), (Feng et al., 2020) and Notch ligands; Signal Peptide (SP), Module at N-terminal Domain of Notch Ligands (MNNL), Delta, Serrate and LAG-2 Domain (DSL), EGF-like repeats, cysteine rich region, PDZ ligand domain (PDZL). Notch extracellular domain (NECD), Notch intracellular domain (NICD) and Transmembrane (TM) (Source: Arruga et al., 2018; created with BioRender.com, accessed in 2022).

Tagged Notch receptors then transported to the cell surface for further ligand interaction and signaling pathway activation. Interacted complex can further be cleaved at three specific sites; S1 (Furin cleavage) required for either receptor production or recycling through cell surface transports, S2 (Metalloprotease; ADAM/TACE) at close location on the membrane and S3 (gamma secretase cleavage) at intramembrane, which releases the NICD to the cytoplasm (Ayaz and Osborne, 2014). Furin like protease is critical for Notch receptor maturation as the Notch receptor undergoes post-translational modifications through fringe glycosylation and proteolysis occurs in the Golgi apparatus before being transported to the cell membrane. S1 cleavage generates a non-covalently associated heterodimer at the cell surface which is necessary for Notch ligand

recognition (Handford et al, 2012). S2 cleavage starts with the endocytosis of the Notch-ligand complex by the ligand-expressing cells, leads to ADAM metalloprotease mediated cleavage at S2 and removes the extracellular fragment of the heterodimer formed by the Furin-like proteases (Feng et al., 2020) (Figure 5).

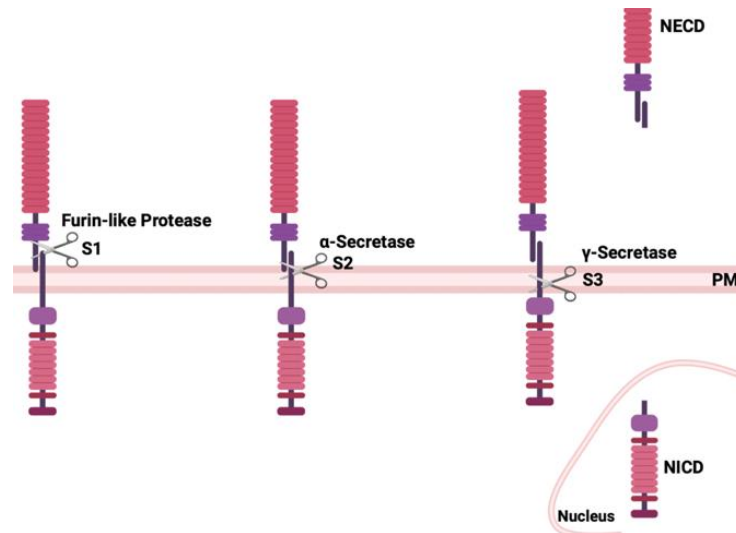


Figure 5. Cleavage locations required for activation of Notch signaling (Source: Crabtree, Singleton, and Miele, 2016; Craig & Brady-Kalnay, 2010; created with BioRender.com, accessed in 2022).

Gamma secretase complex is composed of four core subunits; PS (catalytic domain; including PS1 and PS2), nicastrin, anterior pharynx defective 1 (APH-1), and presenilin enhancer 2 (stabilizer; PEN- 2) at the membrane and each component builds up a complex in sequential manner (Takasugi et al. 2003; Zhang et al., 2014). Presenilin complex; presenilin 1 and 2: proteolytic/catalytic cores. Nicastrin, is responsible to stabilize PSEN and coordinate correct positioning for the complex searching for HD and RAM sequences (Keewan & Naser, 2020). APH1 forms seven transmembrane domains, responsible for proteolytic activity and proof checks to stabilize the assembled complex location. PEN2 is a presenilin enhancer, responsible for locating APH1 and nicastrin close to presenilin complex to form gamma secretase complex. Five components are necessary for gamma secretase cleavage. Aberrant activation of such complex results in cancers (Feng et al., 2020) (Figure 6).

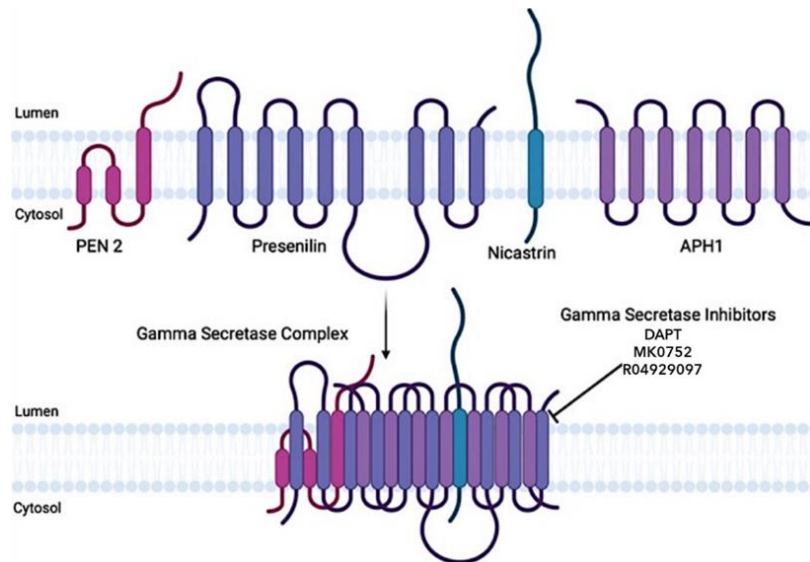


Figure 6. Illustration of Gamma secretase complex assembly and clinically available inhibitors; DAPT/MK0752 and R04929097 (Source: Zhang et al., 2014; created with BioRender.com, accessed in 2022).

Notch signaling pathway can proceed canonical or non-canonical based on the NICD being CSL-dependent or –independent activity. Canonical Notch signaling pathway, NICD translocation to nucleus initiates inhibition of suppressor proteins and stimulates histone acetyltransferases to be active. NICD then proceeds to binding to continuously repressed Co-Repressor and CBF1, Suppressor of Hairless, Lag-1 (CSL) transcription factors to activate gene transcription. Co-Activator and CSL becomes active for further transcriptional activation of Notch target genes such as Hey Hes c-myc Bcl-2 cyclin D1 IRF6 Sox2 and p21 (Han et al., 2011; Zlobin and Olsauskas-Kuprys, 2013). Such genes are crucial for neuronal development, apoptosis, and cellular homeostasis. Transcriptional corepressors (BCL-6, Bend6, CtBP1, NKAP etc.), histone deacetylases (HDCA1,2 and sirtuin 1), CSL/RBPJ and Mastermind like (MAML) bound Notch target genes, are also transcriptionally repressed when NICD is inside the nucleus. MAML and p300 stimulates HDAC activation (Talora et al., 2008). NICD then stimulates activation of CSL/RBPJ for further transcriptions (Chillakuri et al., 2012). After downstream genes are transcribed, NICD undergoes proteasomal degradation (Kopan and Ilagan, 2009). Non-canonical Notch signaling pathway regulates Wnt/ β -Catenin, p53, PI3K/AKT, mTORC2, NF κ B and HIF1- α which are necessary for cell survival and homeostasis (Dsouza et al., 2010) (Figure 7).

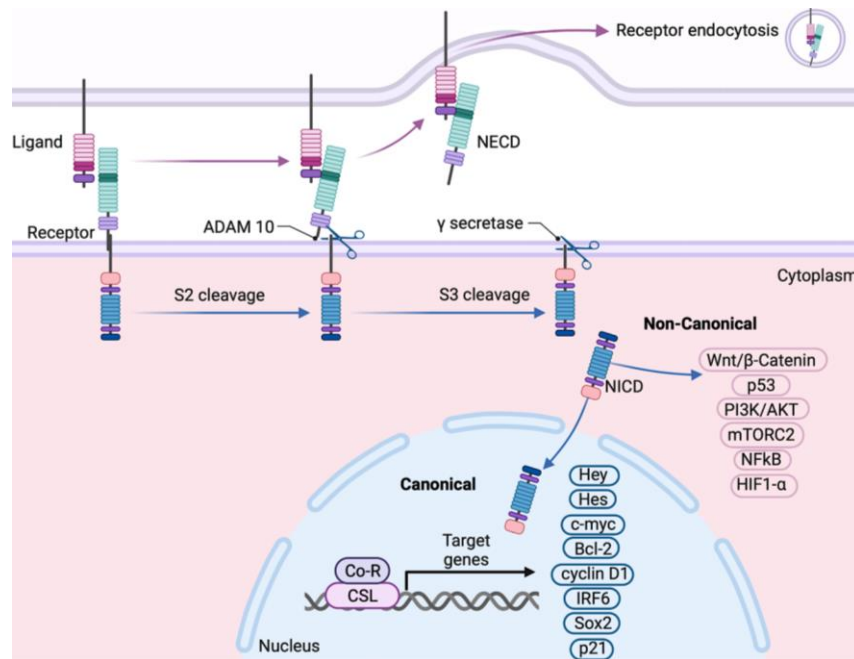


Figure 7. Overall schematic representation of Notch signaling pathway (Source: Bazzoni and Bentivegna, 2019; created with BioRender.com, accessed in 2022).

After signaling activity, Notch receptors can be recycled by endocytosis and/or degraded by alpha adaptin protein and Numb which sequentially ubiquitinylates receptors for lysosomal destruction. Recycling process of Notch ligands occurs via Mind bomb 1 (ubiquitinated by ligase) and receptors are recycled via Epsin, Clathrin, Picalm and Dynamin or lysosomal degradation. Such process initiates with the extra help from pulling action of actin cytoskeleton components (Tetering et al., 2009). Recycling and uptake of Notch ligands or receptors starts with NICD release into the cell which induces ubiquitination of Notch components and bound to the clathrin on the membrane. PKC triggers its phosphorylation and clathrin dependent endocytosis takes place in cytoplasm. Clathrin recognition and vesicle formation are dictated by Rab family proteins (Rab 4, 5 and 11). Then, Epsin binds to clathrin-Notch receptor complex to be taken back into the cell for further endocytosis and degradation. Ligand-receptor interaction stimulates all these cellular uptake mechanisms. Proteasomal degradation occurs when Nedd4 (E3 ubiquitin ligase) and numb polyubiquitinylates ligand by Deltex for both ligand and receptors. Homeostasis in the production and recycling is crucial for appropriate Notch signaling (Kopan and Ilagan 2010).

1.4.2. Role of Notch Signalling Pathway in Breast and Ovarian Cancers

Notch is a conserved ligand–receptor signaling pathway. It is essential for cellular machinery as it helps the embryonic development, organogenesis, and tissue homeostasis (Cappacione et al., 2013). Notch can both function as an oncogene or a tumor suppressor and it is dysregulated in many cancers. Disrupted differentiation ratios stimulate increased levels of transmembrane glycoprotein cluster of differentiation 44 (CD44) cancer stem cell marker and decreases CD24 which mediates Sox2 transcription factor for growth to be active and initiates tumour formation. Reversing the activity of Notch1 overcomes tumor growth and metastasis (Braune and Seshire, 2018). Such change also reverses drug resistant phenotype. Hypoxia markers HIF1/2 alpha stimulates Notch overexpression and induces Hes1/Hey1 transcription factors to be overactive in addition to its regulative role in cancer stem cell elimination (Yuan et al., 2015; Francesco and Maggiolini, 2018; Yan et al., 2018). DLL-Notch4 interaction triggers epithelial mesenchymal transition markers to be overly active and this ends up with more aggressive type of endothelial cells and stimulates drug resistance (Nami et al., 2017; Kar et al., 2019). In breast cancer, Notch activity stimulates decreased levels of E-cadherin and increased levels of N-cadherin, vimentin, Snail, Slug, Zeb1, β -catenin for migration (Shao et al., 2015). Numb defects also induce EMT and invasive behaviour in breast cancer cells. DLL4 induces overexpression of VEGFR so creates angiogenic behaviour in breast cancer cells. Notch dysregulation stimulates overactive MDM2 which destroys p53 and induces cancer (Sun et al., 2017; Tamagnone et al., 2018). Notch can bind to p53 and downregulates its phosphorylation and blocks its DNA binding function (Zhang et al., 2019). Furthermore, Delta/Notch complex was found responsible for PI3K/AKT based breast cancer metastatic behaviour and drug resistance (Wang et al., 2019). Notch1 downregulation by small interfering RNA (siRNA) treatment generates chemosensitivity in doxorubicin resistant MCF-7 breast cancer cells (Alshaer et al., 2019). Notch1 inhibits PTEN signaling stimulates Her2+ breast cancer cell survival and therapy resistance (Baker et al., 2018). For instance, Notch3 ICD (intracellular domain) found highly expressed in mice and caused development of mammary neoplasia. Notch pathway regulates and controls mammary gland development (Guo et al., 2010). Notch components when overexpressed induces

mammary cells breaking the asymmetric cell division strategy and induces cancerous tissue formation (Mollen et al., 2018; Locatelli and Curr, 2017).

Breast cancer patients with high levels of Notch1 and Jagged1/2 showed a poorer prognostic profile and lower survival rates. Notch receptor, Notch1 overexpression induces mammary tumour relapse in mouse models (Simmons et al., 2012). On the other hand, ERBB2 positive breast cancer cells are also becoming trastuzumab and lapatinib sensitive when Notch1 is silenced (Pandya et al., 2016). Mammary epithelia found overexpressing Notch4 and overexpression of Notch3 and Notch4 also leads to murine mammary tumor formation (Pan et al., 2014). Controversially, Notch2 signaling reported to function as a tumor suppressor in breast cancer (Wang et al., 2010). In ovarian cancer, Notch receptors (Notch1-4) and ligands (Jagged1/2 and Dll1/3) are dysregulated and responsible for cancers poor prognosis, drug resistance and recurrence (Rose et al., 2010; Groeneweg, et al., 2014). More than 50% of human of ovarian tumors express reduced protein levels of Numb, which has been associated with high-grade breast cancers (Brennan and Clarke, 2012). Notch signalling components balances ovarian stem cell differentiation (Rizzo et al., 2011). Notch3 overexpression induces ovarian cancer cells for distant metastasis in metastatic xenografts (Leontovich et al., 2018; Boelens et al., 2015). Ovarian cancer cisplatin and paclitaxel resistance induces overexpressions of cancer stem cell markers CD44, CD117 and increase in protein levels of Notch receptors in spheroids (Groeneweg et al., 2014). Serous ovarian cancer exhibits overactive EMT induced through Notch signalling pathway (Gupta et al., 2013). Notch 1 and Notch 3 overactivation prolongs OC development (Lu et al., 2004; Hopfer et al., 2005; Park et al., 2006). Additionally, increased expressions of PSEN2 complex in ovarian cancer found diagnostic in drug resistance and cancer recurrence patterns (Steg et al., 2012). Due to its oncogenic properties in both breast and ovarian cancer, targeting Notch signaling pathway is promising therapeutic approach (Hossain et al., 2018).

1.5. Inhibition of Notch Signalling as a therapeutic approach in cancer

Therapeutic approaches targeting Notch, are focus of the clinical perspective treating and eliminating recurrence phenomenon when treating advance stages of

cancers (Venkatesh et al., 2018). Gamma secretase inhibitors are used to overcome resistance patterns in preclinical and clinical studies to balance aberrant Notch signaling pathway (Kontomanolis et al., 2018; Lamy et al., 2017). Unlike other pathways, Notch signalling pathway does not require intense signalling, that turns hardship of complete inhibition of its components to an ease.

Notch signalling can be inhibited through either targeting notch receptor ligand cleavage (via gamma secretase inhibitors) (GSI) or ligand interaction (via monoclonal antibodies) (mAbs) (Allen and Mailard, 2021). GSI treatments were the first set of treatment passed clinical development in oncology. Although, there are more than 100 GSI's produced, only few could make successful clinical outcome such as DAPT, MK0752, RO4929097, BMS906024 and LY3039478 (NCT001001152, NCT00106145, NCT00572182, NCT00645333, NCT01098344, NCT00803894, NCT00756717, NCT01653470 and NCT01695005). Notch mAbS such as OMP-59R5, OMP21M18, REGN421 and OMP52M51 prevent ligand-receptor interaction between DLL-4 and Notch1-3 results in anti-tumour response (NCT01277146, NCT01647828, NCT00744562, NCT01189942, NCT01189968, NCT01189929, NCT00871559 and NCT01778439).

There are 52 promising single agent GSI and 19 combinational treatments reported to be resulting in chemosensitivity, decreased tumour size, invasion, tumour cell spheroids formation and cancer stem cell renewal (Tamagnone et al., 2018). However, prevention of Notch interactions results in severe side effects in the clinic which makes GSI treatments preferable. GSI's and mAb's single use or combinations with common chemotherapeutics (docetaxel, cisplatin, and gemcitabine) show anti-neoplastic outcome, decreasing cancer stem cell production and angiogenesis in thyroid, lung, colorectal, breast, ovarian and intracranial cancers, as well as sarcomas (Zhou et al., 2022).

1.5.1. Gamma secretase inhibitor; Dual Antiplatelet Therapy (DAPT)

DAPT was primarily used to prevent cleavage of a β -amyloid protein by gamma secretase complex for Alzheimer's disease. However, it is also a GSI which inhibits the proteolysis of Notch receptors. It blocks the presenilin- γ -secretase complex to prevent Notch activation (Gu, 2011). Numerous other GSI's have been developed from DAPT

that are even more effective such as, LY-411,575 and LY-450,139. DAPT was tested clinically for T-cell leukemia, sarcomas, and breast cancer (Wang et al., 2011). Angiogenesis is one of the crucial hallmarks of cancer, as it is commonly stimulated by excessive Vascular Endothelial Growth Factor (VEGF) release. Notch signaling pathway is capable of regulating angiogenic signals based on its gamma secretase complex cleavage and downstream gene transcription system. Accordingly, DAPT was used to normalize such imbalance and found effective in treating angiogenesis in colon adenocarcinomas (Khazaei et al., 2013). As a single treatment, DAPT enhanced the lethality of gastric cancer cells via inhibition of extracellular signal-regulated kinase (ERK)1/2 (Yao et al., 2013). DAPT was found as inducing G2/M cell cycle arrest and/or downregulation of antiapoptotic proteins in breast cancer cell lines (Rasul et al., 2009). DAPT blocks the MRP1 expression caused by doxorubicin therapy in T47D cell lines (Harrison et al., 2010). DAPT decreases cell proliferation as well as lateral motility in MDA-MB-231 cells (Guo et al., 2009). Combination of the DAPT with phenytoin (anti-epileptic medicine used commonly to treat seizures but also found reducing breast cancer invasion) were not beneficial as the single DAPT treatment on MDA-MB-231 breast cancer cells (Aktas, Zeybek and Piskin, 2015). DAPT causes apoptotic effects with melphalan (antineoplastic/chemotherapeutic drug) in MCF-7 breast cancer cells. It reduces CSCs population and tumor self-renewal ability both in vitro and in vivo (Kim et al., 2015). Downregulation of Hes1 were associated with DAPT inhibition of Notch cascade in ovarian cancer cells (Wang et al., 2014). DAPT directly down-regulates the expression of Notch1 in MDA-MB-231 cells and this inhibition is associated with Integrin β 1, FAK, Akt, β -catenin, that is important for migration/invasion of breast cancer cells (Harrison et al., 2010). Recent article suggested that the cisplatin and DAPT combination has effectively treated osteosarcoma (Wang et al., 2013). In another study, DAPT was used for both in combination with cisplatin, as pretreatment and as secondary treatment to sensitize cisplatin resistant ovarian cancer cells against chemotherapy (Wang et al., 2014). DAPT also inhibited cancer stem cell formation when given with cisplatin for treating gastric cancer (Kato et al., 2018). Notch signaling pathway inhibition via DAPT in combination with cisplatin treatment also leads to enhanced toxicity in resistant osteosarcoma (Dai et., al 2018).

On the other hand, downregulation of Notch1 found to be inducing chemosensitivity of cisplatin and docetaxel treatments in head and neck squamous cell carcinoma which was studied under DAPT treatment model (Zhang et al., 2019). DAPT

treatment in combination with cisplatin reduces side effects of organ toxicity (Soni, Matthews, Pallikkuth, Gangaraju & Adebisi, 2018). Preclinical studies with breast tumor graft models proved that Docetaxel and DAPT combination decreases cancer stem cell formation (Schott et al., 2013). DAPT with cisplatin or docetaxel in short term induces Notch1 inhibition which caused sensitivity in cancer cells by also reducing cancer stem cell formation (Zhao et al., 2016).

1.5.2. Gamma secretase inhibitor; R04929097

R04929097 inhibits Notch signaling pathway through the blockage of Gamma Secretase complex and induces apoptotic outcome (Albain et al., 2010). R04929097 were used to treat ER positive, HER2 negative, Triple negative breast cancer, advanced and metastatic breast cancers and found safe and effective according to mid-reports (NCT01149356, NCT01151449, NCT01217411 and NCT02299635). R04929097 was also combined with various chemotherapeutics such as vismodegib, paclitaxel and carboplatin to treat metastatic breast cancer patients (NCT01071564 and NCT01238133) (Schott et al., 2010). Its combination with Letrozole and Tamoxifen in separate studies were promising to treat early to late stage breast cancer patients (NCT00756717 and NCT01208441). However, R04929097 studies were terminated due to drug's distribution issues (Kontomanolis et al., 2018; Lamy et al., 2017).

1.5.3. Gamma secretase inhibitor; MK0752

MK0752 is a non-competitive synthetic GSI, which is used as chemotherapeutic agent. It targets overactivated Notch signaling pathway and results in cell cycle (G_0/G_1) arrest and/or cell death in tumor cells (Zlobin and Olsauskas-Kuprys, 2013). MK0752 had successful preclinical activity for many cancers as well as breast cancer (Takebe et al., 2013). It is being combined with docetaxel in locally advanced/metastatic breast cancer at clinical phase II to find whether this combination kills the breast cancer stem cells (NCT00645333). Letrozole; chemotherapeutic agent was combined with and MK-0752 (combined also with another estrogen receptor modulator; tamoxifen) in separate studies to treat early to late staged breast cancer patients (NCT00756717 and NCT01208441). Even short period of MK0752 oral usage reduced cancer stem cell

production and resulted in pro-apoptotic outcome (Albain et al., 2010; Wang et al., 2010). MK-0752 decreases tumour growth in both *vitro* and *vivo* studies of ovarian cancer (Chen et al., 2016). Clinical trial phase I's are ongoing; with hormone (endocrine) therapy and combination with tamoxifen and letrozole in early-stage breast cancer (Deangleo et al., 2006). MK0752's combination with ridaforolimus (MK-8669) is now on preclinical stage in patients with advanced solid sarcomas (Zlobin and Olsauskas-Kuprys, 2013). Chemoresistance studies were not yet conducted based on the cytotoxicity of continuous treatment because of grade 3/4 gastrointestinal side effects (Thomas et al., 2014). Clinical trial phase I patients with T-cell acute lymphoblastic leukemia tolerated this GSI well and, it was shown that MK0752 therapies were dose dependent by reducing the NICD (Krop et al., 2012). MK0752 is also found being synergistically useable with docetaxel combinational therapies for metastatic breast cancers by reducing cancer stem cell formation (Takebe et al., 2013) (Clinical trial number: NCT00645333). Both MK0752 monotherapy and combinational therapy with cisplatin found to induce cell cycle arrest and apoptosis in ovarian cancer cells both *in vitro* and *in vivo* studies which can initiate clinical studies for combinational therapies using gamma secretase inhibitors with antineoplastic drugs (Chen et al., 2016).

CHAPTER 2

AIMS AND OBJECTIVES OF THE PROJECT

Cancer cells acquire new phenotypes to overcome both intrinsic and acquired resistance through Notch signalling pathway. Leading questions to the pathway related response observations stimulated Notch pathway inhibitors, including GSIs, to become under the glass for targeted therapy research. Use of DAPT, R04929097 and MK0752 as single treatments and in combinations with Docetaxel or Cisplatin resulted in successful preclinical/clinical outcome for breast and ovarian cancers. Drug resistance is a hallmark for cancer cells to survive under toxic environments, which leads to therapy failures over the long run. Potential resistance mechanism behind DAPT, R04929097 and MK0752 remains unstudied. This project aims to uncover both morphological and molecular responses of breast (MDA-MB-231 and MCF-7) and ovarian (IGROV-1, BG-1, SKOV-3 and A2780) cells against DAPT, R04929097 and MK0752 resistance. Intrinsic and acquired resistance studies were carried out for single agent GSI treatments and combinations of GSIs with chemotherapeutic agents for both cancer types under 2D and 3D cell culture conditions. Every treatment and cell line combination aimed to be investigated for, drug toxicities, synergistic capability, viability changes, morphological alterations, and mRNA expressions levels, migration behaviours, and the proteomic variations. Overall, this study aimed to reveal intrinsic and acquired resistance responses and mechanisms against DAPT, R04929097 and MK0752 with their Docetaxel or Cisplatin combinations in both breast and ovarian cancer cell lines.

CHAPTER 3

MATERIALS AND METHODS

3.1. Cell lines and Cell Culture Conditions

Human triple negative breast adenocarcinoma cell line MDA-MB-231 (ATCC[®] HTB26[™]) and Oestrogen and Progesterone receptors positive breast adenocarcinoma cell line MCF-7 (ATCC[®] HTB22[™]) were used as breast cancer models. IGROV-1 (SCC203, Sigma) endometrioid stage III ovarian cancer cells lacking hormone receptors, SKOV-3 (ATCC[®] HTB77[™]), ascites originated ovarian adenocarcinoma, BG-1 (SCC415, Sigma) stage III solid primary ovarian adenocarcinoma, A2780 (93112519, Sigma) ovarian endometrioid adenocarcinoma cell lines were used as ovarian cancer models. Cisplatin-resistant IGROV-1 clones were provided by Linköping University, Dr. Padraig Darcy's laboratory. MDA-MB-231 and MCF-7 breast cancer cells were cultured in Dulbecco's Modified Eagle Medium (DMEM) (Sigma) with 1% Penicillin/Streptomycin (Thermo), 10% Fetal Bovine Serum (Biological Industries) at 37 C° in 5% CO₂ incubation conditions. IGROV, A2780, BG-1 and SKOV3 ovarian cancer cells were cultured in RPMI (Sigma) medium with 1% Penicillin/Streptomycin (Thermo), 10% Fetal Bovine Serum (Biological Industries). Cells, when reached confluency level of 80-90%, washed with room temperature phosphate buffer saline (PBS) and trypsinized (0.05%) for further passaging and cryofreezing.

3.2. Measuring Half-Maximal Inhibitory Concentrations (IC₅₀)

R04929097 (ADOOQ), DAPT (Cayman), MK0752 (Cayman), Docetaxel (TOCRIS) were prepared in Dimethyl sulfoxide (DMSO), Cisplatin (Sigma) were dissolved in 0.9% Sodium Chloride (NaCl). Each solvent was included as a control throughout experiments. IC₅₀ dose determinations were conducted by using MTT (3-

(4,5-Dimethylthiazol-2-yl)-2,5 Diphenyltetrazolium Bromide) assay. Cells were plated into 96 well plates and treated with increasing doses of R04929097, DAPT, MK0752, Docetaxel and Cisplatin (from 1nM to 100 μ M) or respective solvent control (DMSO or 0.9% NaCl) for 24, 48 or 72 hours. The cells were treated with 5mg/mL of 3-(4,5-Dimethylthiazol-2-yl)-2,5 Diphenyltetrazolium Bromide (Amnesco) for 4 hours, followed by dissolving of tetrazolium salts in 10% Sodium Dodecyl Sulfate (SDS) and 0.01M Hydrochloric acid (HCl). Then, the absorbance values at 570 nm and 650 nm were measured in a microtiter plate reader (Thermo Scientific Multiskan Spectrum). Intrinsic resistances were scaled as; $IC_{50}<1$ ratio, highly sensitive, $IC_{50}=1-50$ ratio, Sensitive, $IC_{50}=50-100$ ratio, Resistant, and IC_{50} values higher than 100 ratio called as Highly Resistant.

3.2.1. Measuring Drug Synergies

Drug doses in combinations were selected according to each cell line's IC_{50} values. $IC_{12.5}$, IC_{25} , IC_{50} and IC_{100} dose combinations were tested for DAPT, MK0752 with Docetaxel and Cisplatin. MTT absorbance values of three independent combination conditions were analysed for synergistic activity by using Synergy Finder tool. Bliss test was used to confirm effectiveness of two independent drugs combinations. Values between -10-0 refers for additive effects obtained by two drug combinations whereas 0-10 refers to synergistic activity. Each independent experimental setup was replicated at least three times and normalized to control group.

3.3. Proliferation Assay and Multidrug treatment strategies

Breast and ovarian cancer cell lines were seeded 10,000 cell per well into 96 well plates. Treatment was applied as a single agent, combinational and sequential treatments of DAPT, MK0752, Docetaxel and Cisplatin (Figure 8). DAPT and MK0752 treatments were applied for 24 hours, Docetaxel and Cisplatin for 48 and 72 hours, respectively, based on each drugs' half-life. After treatments MTT cell proliferation assay was applied for the proliferation rate determinations. Each set up was repeated at

least three times and results were graphed by GRAPH PAD Prism 9. Two-way ANOVA, multiple comparisons and paired t tests were applied to analysis (Figure 8).

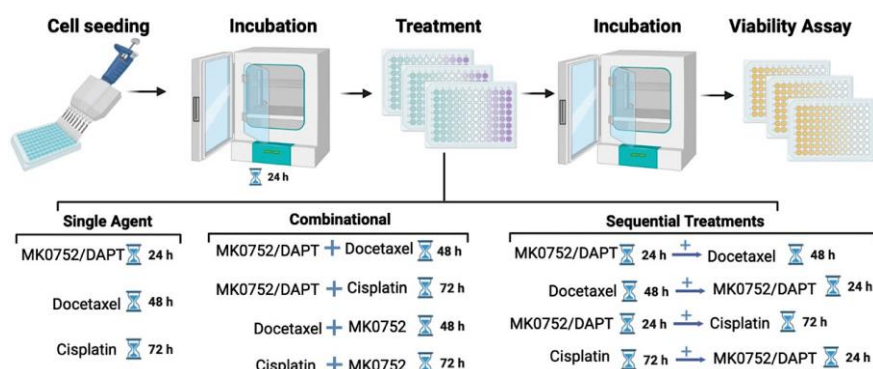


Figure 8. Treatment strategies. Multidrug treatments were divided into three categories; single agent treatment, combinational treatments where two drugs were applied at the same time and sequential treatments where the first treatment with one drug is followed by the second treatment with another drug. Treatments times were scheduled based on drugs half-life time points.

3.4. Generating Intrinsic and Acquired resistance

Intrinsic and Acquired resistance definitions were specified by McDermott et al.'s published protocol (2014). Cells' initial response to IC_{100} of R04929097, DAPT, MK0752, Docetaxel and Cisplatin were measured via MTT assay to determine intrinsic resistance. To generate acquired resistance, cells were treated with gradually increasing doses of R04929097, DAPT or MK0752 from half of the IC_{50} value (IC_{25}) to a four-fold IC_{50} value (IC_{200}). Drug treatments started twenty-four hours after cells were seeded into six-well plates. After reaching 80-90% of confluency in the presence of drug, approximately in ten days, media was removed, and cells were maintained in a drug-free medium for twenty-four hours. During the confluency period of ten days, media was refreshed when needed without the drug treatments. Then, the unconfirmed resistant cells were visualized under the light microscope for morphological analysis, flash frozen for mRNA expression analysis, and cryofreezed for further experiments. Each dose exposure was repeated twice. The treatment procedure including treatment free cycles took six months. DAPT's solvent; Dimethyl sulfoxide (DMSO) was included

as the control. Cell numbers were set to 15,000 per condition and treatments also included DMSO controls of each treatment (Figure 9). IC₅₀ values of MK0752 treated IGROV-1, BG-1, SKOV-3 and A2780 was measured again for resistance cell line confirmations and results were specified as Resistance index ratio.

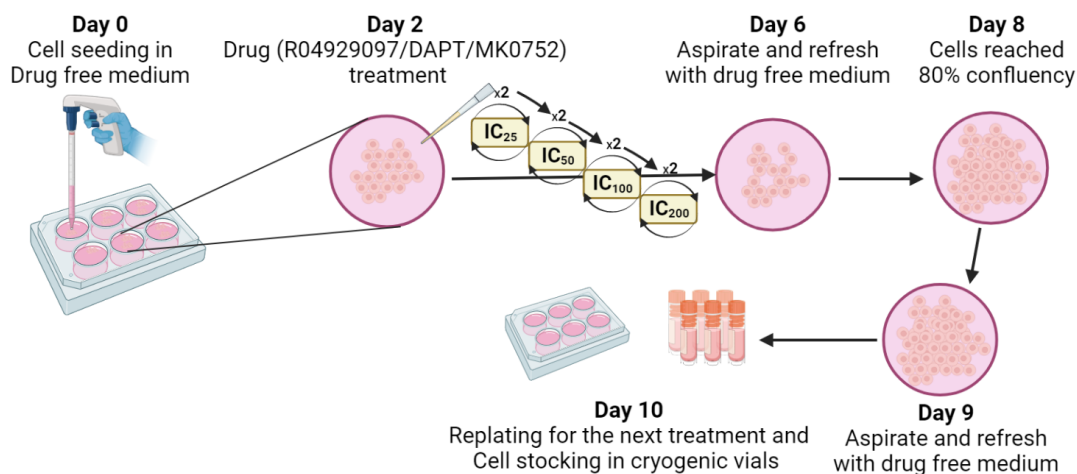


Figure 9. The schematic explanation of the protocol used to generate R04929097, DAPT and MK0752 resistant cells is shown. Each treatment with a specific dose was twice, along with DMSO controls. Cells then were preserved for further analysis. Viability changes of DAPT-resistant cells were confirmed with MTT assay.

3.5. Quantitative Real Time-PCR

Total RNA was isolated using PureLink RNA Mini isolation kit (Invitrogen). 1 µg of total RNA was used to synthesize cDNA using the RevertAid First Strand cDNA Synthesis Kit (Fermentas). PCR amplification and detection were done on LightCycler 96 Real Time PCR detection system (Roche) using Maxima SYBR Green qPCR Master Mix (Fermentas). The primer sequences are listed on Table 1. The comparative delta-delta Ct method was applied and TATA box- binding protein (TBP) expression was used for normalization. PCR reactions for each individual gene were repeated three times. One-way ANOVA combined with paired t-test were used to determine statistical significance.

Table 1. List of primers used for quantitative real-time PCR (Q-RT-PCR).

Primers	Primer sequences (5'-3')	Product size (bp)
Notch 1	F: CACTGCGAGGTCAACACAGA	143
	R: GCACACTCGTCCACATCGTA	
Notch 2	F: TGTGCCTCAAATCCATGCCT	221
	R: ATGGTACACCGCTGACCTTG	
Notch 3	F: GCAGCGATGGAATGGGTTTC	243
	R: CTGCCAGGTTGGTGCAGATA	
Notch 4	F: TTCCACTGTCCTCCTGCCAGAA	142
	R: TGGCACAGGCTGCCTTGAATC	
Snail-2	F: CTCCTCATCTTTGGGGCGAG	136
	R: TTCAATGGCATGGGGGTCTG	
Zo-1	F: ATGGAGGAAACAGCTATATGGGA	68
	R: CCAAATCCAAATCCAGGAGCC	
E-cadherin	F: CAGCACGTACACAGCCCTAA	111
	R: GGTATGGGGGCGTTGTCATT	
N-cadherin	F: GGCTTCTGGTGAAATCGCAT	159
	R: GCAGGCTCACTGCTCTCATA	
Hey-1	F: AGTGCGGACGAGAATGGAAA	161
	R: CTGGGTACCAGCCTTCTCAG	
TBP	F: TAGAAGGCCTTGTGCTCACC	109
	R: TCTGCTCTGACTTTAGCACCTG	
Hes-1	F: AACACGACACCGGATAAACC	109
	R: TCAGCTGGCTCAGACTTCA	
Slug	F: CTAGGCCCTGGCTGCTACAA	189
	R: TGTGGAGCAGGGACATTCTG	
Hes-5	F: ACATCCTGGAGATGGCTGTC	85
	R: TAGTCCTGGTGCAGGCTCTT	

3.6. Wound Healing Assay

MDA-MB-231 (5×10^5 cells per well) and MCF-7 cells (7.5×10^5 cells per well) were seeded in 24-well plates to grow in a monolayer. 24 hours later, cells were incubated with 5 μ g/ml Mitomycin C (SantaCruz) at 37 °C for 3 hours. Then the medium is removed, and a sterile 10 μ L pipette tip was held vertically to scratch across in each well. The detached cells were removed by washing with PBS and cells were monitored in 500 μ L of fresh serum-free medium per well. The wound closure was monitored at 3 different positions per well and imaged in 1-hour intervals for 24 hours using a Leica SP8 microscope at 4x magnification. Images were analysed via Image J. Data are

represented as the means and \pm standard deviation (SD) of three independent experiments, graphed by using Graph Pad PRISM 9. One-way ANOVA and t test analysis was used for statistical analysis.

3.7. Circularity analysis

MDA-MB-231 and MCF-7 cells including DAPT and R04929097 resistant lines (1×10^4 cells per well) were seeded in 6-well plates to grow in a monolayer for 24 hours for morphological analysis. Phase contrast, light microscopy images at 20x magnification were taken using Leica DMI8 confocal microscope. 100 cells were imaged for each condition and analysed with Image J's circularity testing with the circularity baseline set to 4π ($\text{area}/\text{perimeter}^2$).

3.8. Spheroid formation and Area Measurement

MDA-MB-231, MCF-7, IGROV-1, IGROV-1^{CisR}, BG-1, SKOV-3 and A2780 cells were seeded as 5.000 cell per well of U bottom 96 well plate for 3-4 days in growth media of each cell line. Treatments were done after spheroid formation and images were taken by Incucyte Cell Analysis Systems up to 72 hours. Treatment dose determined as IC₁₀₀ of DAPT, MK0752, Docetaxel and Cisplatin. Each cell line and treatment conditions were repeated at least three times and images were analysed with Image J's Spheroid J plugin (Figure 10).

3.8.1 Acid Phosphatase Assay

Treated and control spheroids were treated with p-NPP solution with sodium acetate buffer and Triton-X-100 (0.1%) was added and incubated at 37 C° for 90 minutes. 0.2% 1N NaOH was used to terminate phosphatase reaction and measured at 405 nm absorbance in a microtiter plate reader (Thermo Scientific Multiskan Spectrum). Conditions were normalized to each cell lines' untreated conditions. Results then graphed and analysed via Two-way ANOVA, multiple comparisons, and paired t test by using Graph Pad Prism software.

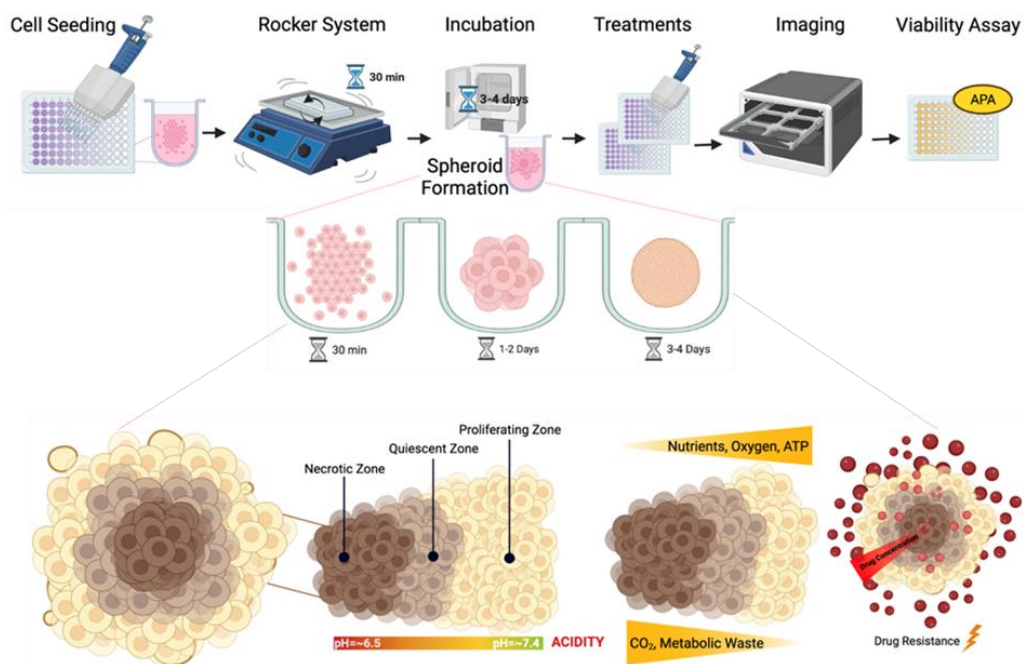


Figure 10. Spheroid assays and Spheroid formations. Spheroids are formed fully after 3-4 days, and treatment was applied for further imaging and viability assays.

3.9. Protein extraction and Western Blotting

Monolayer and spheroids of MK0752 resistant and parental IGROV-1, BG-1, SKOV-3 and A2780 cells were incubated with IC_{100} of MK0752 for 6 hours in six-well plates. Cells then washed with cold PBS and RIPA lysis buffer (Millipore) with protease inhibitor was used for the lysis. Protein concentrations were measured by using DC protein assay kit (Bio-Rad). Total of 25 μ g of protein with sample reducing agent and loading dye (NuPAGE) was incubated for 5 minutes at 95°C before loading to 4–12% Bis-tris gels (NuPAGE) with the protein molecular weight standard, precision all blue (Bio-Rad). Proteins were transferred to nitrocellulose membrane by using Thermo Scientific Pierce G2 Fast Blot and membranes were incubated with blocking solution of PBST and 5% skimmed milk for one hour on the shaker. Primary antibodies: C-Myc (Cell Signalling, 1:1000 dilution ratio), OXPHOS antibody cocktail (Abcam, 1x dilution ratio) and B-actin (Thermo Fisher, 1:5000 dilution ratio) were diluted in PBST with 2% BSA overnight at 4°C. Membranes then washed and further incubated with the secondary antibody diluted in PBST with 5% skimmed milk for an hour at room

temperature. Blots were developed using Clarity Western ECL substrate (Bio-Rad) and imaged using ChemiDoc MP Imager (Bio-Rad). Images were analysed by ImageJ and graphed after Two-way ANOVA, multiple comparison tests and paired t tests via Graph Pad Prism 9.

3.10. LC-MS/MS and Label-Free Quantification

IGROV-1, IGROV-1^{CisR} and IGROV-1^{MK0752R} peptide digests were desalted by using Pierce C18 desalting columns (Thermo). The desalted peptide solution is then dried in a vacuum concentrator, reconstituted with 0.5% Formic acid, and analyzed using LTQ Orbitrap Velos Pro mass spectrometer (Thermo) coupled to an EASY-nLC II (Thermo Scientific) chromatography system. Peptides were separated by reverse-phase chromatography using a 20 mm x 100 μ m C18 precolumn followed by a 100 mm x 75 μ m C18 column with a 5 μ m particle size (NanoSeparations) using the following solvent system: Buffer A, 0.1% Formic Acid v/v in water; Buffer B, 0.1% Formic Acid v/v in Acetonitrile. The mass spectrometer was operated using XCalibur software v2.6 (Thermo Scientific) and analysis was done in positive ionization mode. Full scans were performed at a resolution of 30,000. The top 20 most intense ions were fragmented with Collision-induced dissociation (CID) using a normalized collision energy of 35%, isolation width of 2.0, and activation time of 10 ms. Protein identification and quantification were done with Proteome Discoverer 2.5.0.400 (Thermo) using the Sequest HT search engine. All searches were performed on human reference proteome obtained from UniProt (<http://www.uniprot.org> Accessed: 19 September 2022). Cysteine carbamidomethylation was set as a fixed modification and methionine oxidation as a variable modification. Label-free quantification of proteins was done, and protein abundances were quantified based on precursor intensity. The abundances were then normalized based on the total peptide amount.

CHAPTER 4

RESULTS

4.1. DAPT resistance in MDA-MB-231 triple-negative breast cancer cells

Half maximal doses (IC_{50}) of DAPT, Cisplatin and Docetaxel were measured for intrinsic resistance scaling and determining tolerable dose range for further acquired resistance studies. IC_{50} values of DAPT, Cisplatin and Docetaxel were determined by MTT cell viability assay for the MDA-MB-231 triple-negative breast cancer cell line. Dose-dependent normalized inhibition response was recorded as $8.2 \mu\text{M}$ for DAPT, $1.01 \mu\text{M}$ for Cisplatin and $0.5 \mu\text{M}$ for Docetaxel. The intrinsic resistance scale represented MDA-MB-231's high sensitivity pattern against Docetaxel and Cisplatin and moderate sensitivity to DAPT (Figure 11).

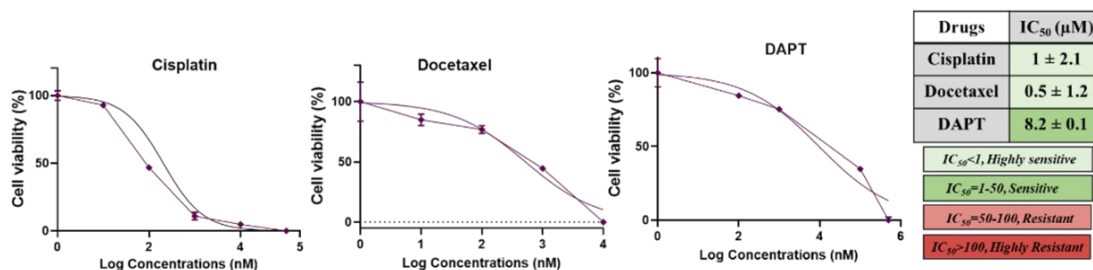


Figure 11. IC₅₀ curves of DAPT, Docetaxel, and Cisplatin treatments for MDA-MB-231 breast cancer cell line. MTT absorbance values were normalized and graphed by using GraphPad Prism 8.

To further model acquired resistance, MDA-MB-231 cells were treated with gradually increasing doses of DAPT, starting from half (IC₂₅) to four times (IC₂₀₀) the IC₅₀ value. Eventually, MDA-MB-231 cells were obtained that can grow to 90% confluency in the presence of IC₂₀₀ of DAPT, which is referred to as MDA-MB-231-R throughout this section (Figure 2A). The control (MDA-MB-231-C) MDA-MB-231 cells were treated with the respective volumes of DMSO while MDA-MB-231-R cells received DAPT treatments. Altered morphologies were stated as one of the hallmarks of drug resistance. To test this, MDA-MB-231-C MDA-MB-231-R cells were monitored for 120 hours. Cellular shapes were not altered for both MDA-MB-231-C and MDA-MB-231-R cells after 24 and 120 hours after the DAPT treatments (Figure 12). The difference in the viability ratios was measured with an MTT cell viability assay to record probable differences between MDA-MB-231-C and MDA-MB-231-R cells. Moreover, MDA-MB-231-R cells expanded significantly by 40% more than the MDA-MB-231-C cells. (Figure 13). Mesenchymal phenotype lingers to be the passageway for cancer cells' increased migration and development of drug resistance. To compare potential resistance-dependent changes in mesenchymal phenotype, cells were plated at a lower density and visualized with higher magnification (Figure 14A). The mean circularity (a.u) of the MDA-MB-231-C cells was 0.38 and reduced to 0.36 in MDA-MB-231-R cells. However, the change was not statistically significant and presumed as MDA-MB-231-R cells showed no comparable difference in mesenchymal morphology (Figure 14B).

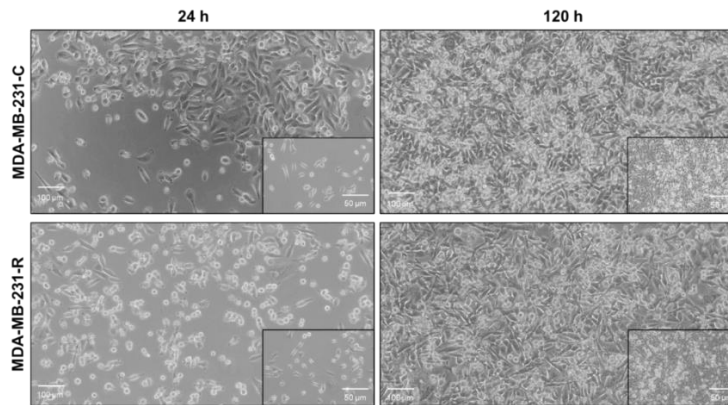


Figure 12. MDA-MB-231-R breast cancer cells reach confluency in the presence of DAPT. Light microscopy images of MDA-MB-231 cells resistant to IC₂₀₀ DAPT treatment (MDA-MB-231-R) and DMSO-treated control cells (MDA-MB-231-C) were taken at 24 h and 120 h respectively after the IC₂₀₀ of DAPT and respective DMSO treatments (Scale bar: 50 and 100 µm).

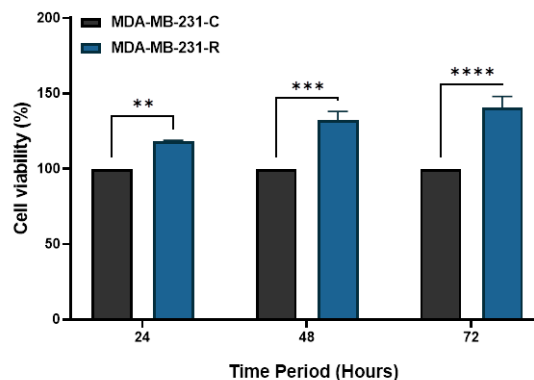


Figure 13. DAPT-resistant MDA-MB-231 cells exhibit increased viability than the MDA-MB-231-C cells. MDA-MB-231-R and MDA-MB-231-C cells were cultured in drug-free media and the viability analyses were performed at three different time points (24, 48 and 72 hours). One-way ANOVA analysis and student t-test confirmed the significance of the conditions. Data represent means and \pm SD of three independent experiments (** $p < 0.01$, *** $p < 0.001$, **** $p \leq 0.0001$).

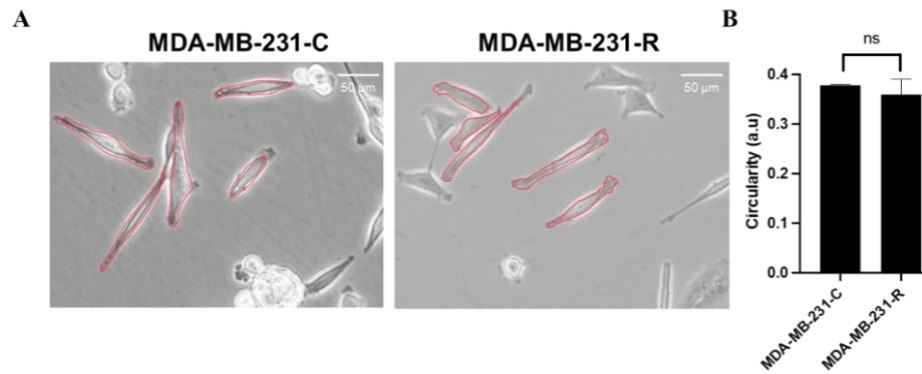


Figure 14. Circularity analysis of DAPT resistant and control MDA-MB-231 cells.(A) Representative phase-contrast images of MDA-MB-231-C and MDA-MB-231-R cells plated in a drug-free medium. Red outlines representing the cell borders were used to assess circularity. (Scale bar, 50 μm) (B) The circularity values (a.u) of control and resistant cells are shown. Student t-tests confirmed the significance of the conditions. Data represents the means and \pm SD of randomly selected 100 cells (ns: not significant).

4.1.1. DAPT-resistant MDA-MB-231 cells alter Notch receptors, Notch target genes and Epithelial-Mesenchymal Transition markers' mRNA expression levels

The Notch signalling pathway regulates multiple downstream targets. To gain a wider insight into understanding the mechanism behind the DAPT resistance in MDA-MB-231, mRNA expression levels of Notch receptors (Notch1,2,3 and 4), Notch's main downstream targets (Hes5, Hes1, Hey1) and EMT regulators (E-Cadherin, ZO1, Snail2, Snail1 and N-Cadherin) were measured. mRNA expression profiles were analysed by quantitative real-time Q-RT-PCR. In MDA-MB-231-R cells, mRNA expression of Notch receptors Notch1 and Notch2 was downregulated by 12% and 1%, respectively. Notch3 and Notch4 were downregulated by 6%, and (Figure 15A). Notch target genes Hes5 and Hey1 were downregulated by 5% and 2% as well as Hes1 by 12% (Figure 15B). E-Cadherin was increased by 10-fold while ZO1 decreased by 7% (Figure 15C). On the contrary, mRNA expressions of epithelial-mesenchymal transition (EMT) regulator Snail2 were increased by 4-fold. Mesenchymal marker N-Cadherin was decreased by 36% as well as Snail1 by 14% (Figure 15D).

Collectively, MDA-MB-231-R suppresses the expression of Notch receptors, and this is supposed to decrease the expression of its targets; Hes5, Hes1, Hey1 as observed in the data. An increase in the EMT/MET shift is known to be associated with the characteristics of drug resistance. However, no clear pattern of a shift towards any of the phenotypes was detected in the mRNA analysis as where one epithelial marker increases other decreases. Mesenchymal stimulators, Snail2 expression increases yet Snail1 expression decreases. Morphological changes were also not observed; thus, we could not conclude whether EMT is a potential route in DAPT for MDA-MB-231 breast cancer cells.

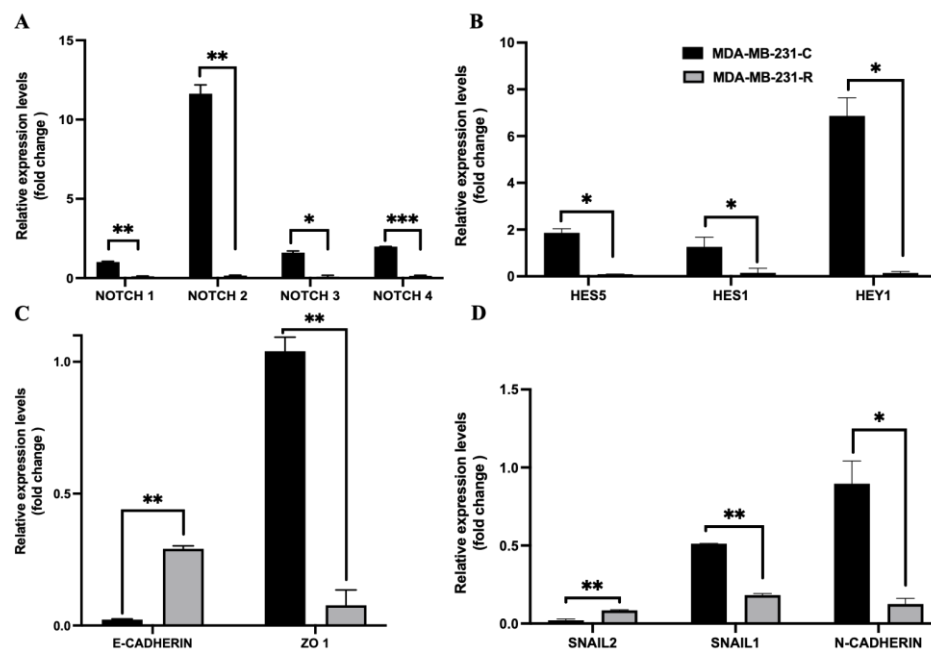


Figure 15. mRNA expression analysis of Notch receptors, downstream targets, and EMT markers for DAPT resistant-MDA-MB-231 cells. mRNA expression levels of (A) Notch receptors (Notch 1,2,3 and 4), (B) Notch pathway downstream target genes (Hes5, Hes1, Hey1), (C) EMT regulators, epithelial markers (E-Cadherin, ZO1), and (D) mesenchymal markers (Snail2, N-Cadherin, and Snail1) of MDA-MB-231-C and MDA-MB-231-R cells were shown. Data represent the means and \pm SD of 3 independent experiments One-way ANOVA analysis and student t-test confirmed the significance for conditions (* $p < 0.05$, ** $p < 0.01$, *** $p < 0.001$).

4.1.2. DAPT resistant MDA-MB-231 cells exhibit increased migration

Increased EMT shift established to be associated with increased migration potential to overcome drug toxicity and induce resistance behaviour in cancers. To test this, MDA-MB-231-R cells were evaluated for potential changes in the migration phenotype by wound healing assay. The wound area for MDA-MB-231-C cells was closed by 30% whereas MDA-MB-231-R cells reduced the gap by 52% in 10 hours. Overall closure of the wound for MDA-MB-231 control cells was 67% and MDA-MB-231-R cells reduced the gap by 89% in 20 hours indicating an increased migration potential of DAPT-resistant cells (Figure 16).

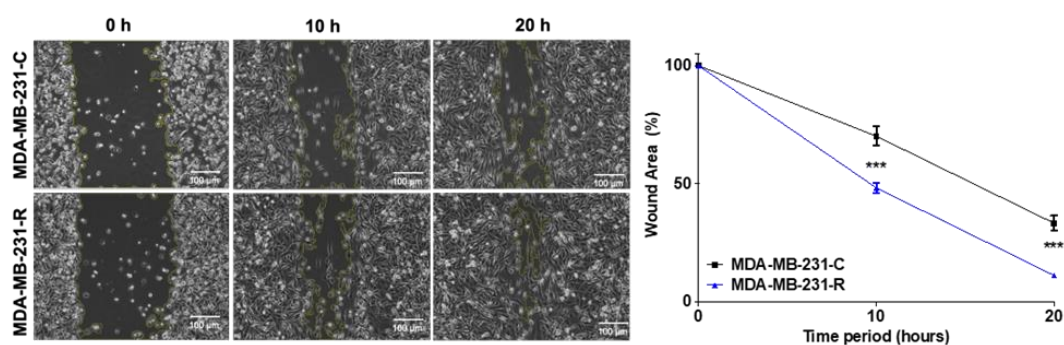


Figure 16. DAPT resistance increases migration in MDA-MB-231 breast cancer cells. Migration phenotype was evaluated by wound healing assay. Time-lapse microscopy images of wound closure of MDA-MB-231-C and MDA-MB-231-R cells at $t=0$, 10, and 20 h after the wound formation. Cells were treated with IC_{200} of DAPT, and images were analyzed via Image J. Yellow lining defines the area lacking cells. Scale bars, 100 μ m. (B) Quantification of the wound area after the DAPT treatment in MDA-MB-231-C and MDA-MB-231-R cells. Results represent three independent experiments (***) ($p < 0.001$).

4.1.3. Docetaxel and Cisplatin's synergistic activities with DAPT in MDA-MB-231 cells

Commonly used chemotherapeutics Docetaxel and Cisplatin's combinations with various GSIs including DAPT exhibits successful preclinical/clinical outcomes for

breast cancer. Yet, the synergistic effect of such a combination remains unstudied. To investigate DAPT's potential synergistic outcomes with Cisplatin and Docetaxel, cell viability data were plotted, and Bliss synergy scores were quantified. A Bliss score less than -10 represents two drugs are likely to be antagonistic, from -10 to 10 two drugs are likely to be additive and larger than 10 two drugs are likely to be synergistic. Bliss scores of DAPT combinations with Cisplatin were 17.7 (Figure 17) and 15.3 with Docetaxel for the MDA-MB-231 cell line (Figure 18). DAPT's combination with Cisplatin and Docetaxel showed a highly synergistic pattern. These results suggest that MK0752 can be used in further combinational treatments with Cisplatin and Docetaxel to explore potential responses against GSI's intrinsic resistance.

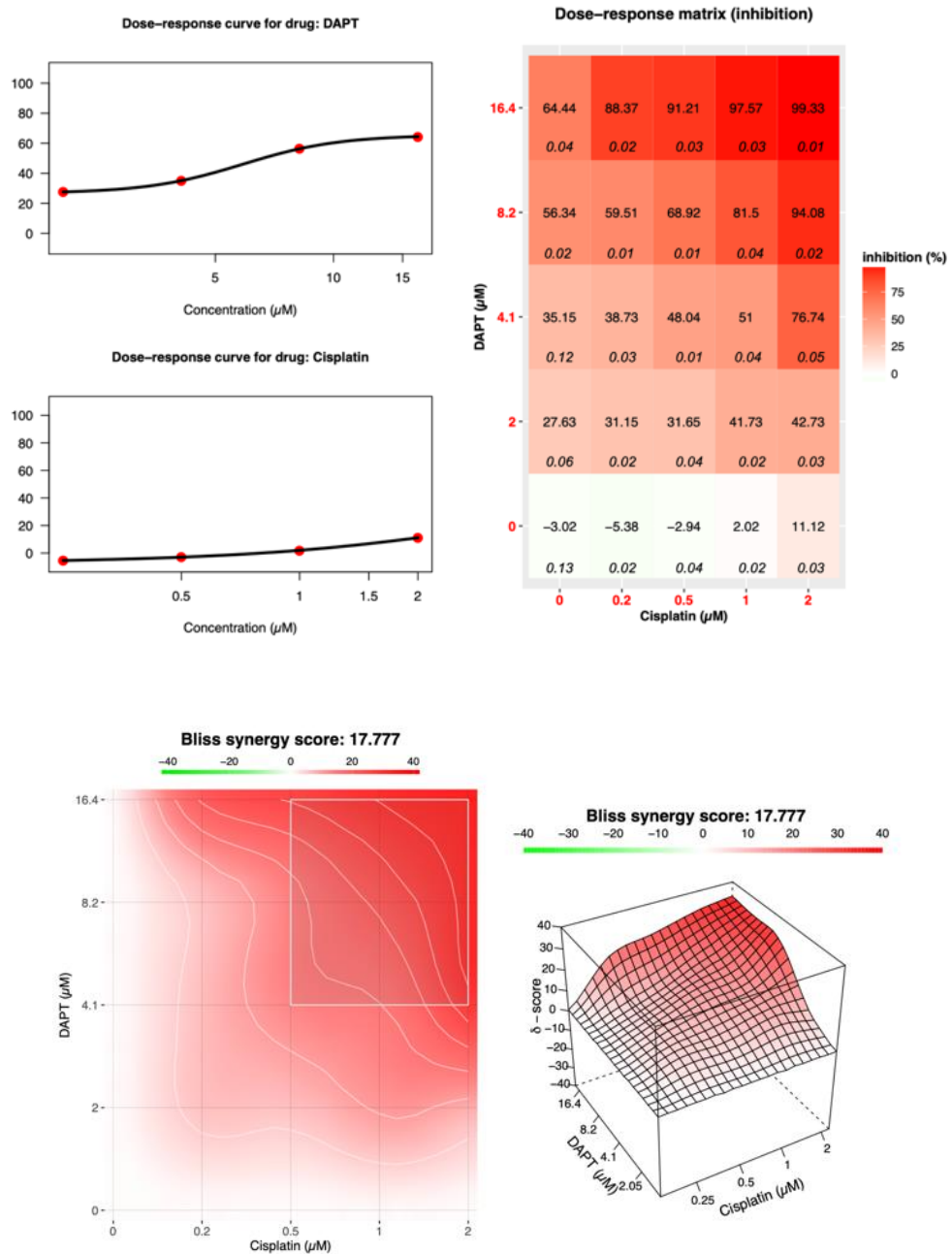


Figure 17. DAPT and Cisplatin have synergistic effects for MDA-MB-231 cells. Drug synergy analysis of DAPT with Cisplatin was conducted by Synergy Finder tool. Bliss synergy scores of three independent experiments were analyzed for combinations. The drug response curve with the inhibition matrix and heatmap shows IC_{100} for DAPT and Cisplatin was the optimum dose combination for MDA-MB-231 cell lines.

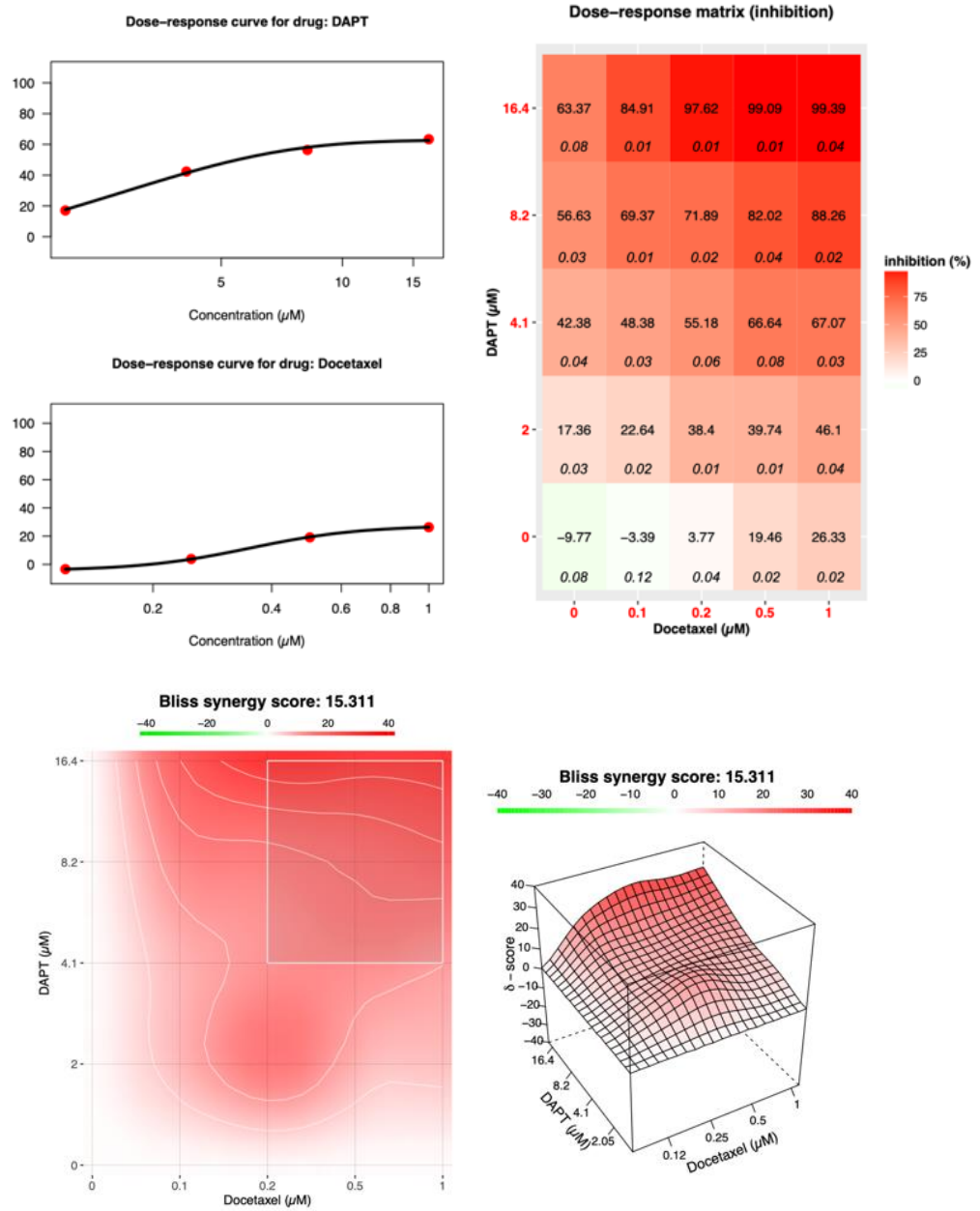


Figure 18. DAPT and Docetaxel have synergistic effects for MDA-MB-231 cells. Drug synergy analysis of DAPT with Docetaxel was conducted by Synergy Finder tool. Bliss synergy scores of three independent experiments were analyzed for combinations. The drug response curve with the inhibition matrix and heatmap shows IC_{100} for DAPT and Docetaxel was the optimum dose combination for MDA-MB-231 cell lines.

Effects of the DAPT, Docetaxel and Cisplatin's single agent and combinational treatments on MDA-MB-231 cells viability were measured by the MTT assay based on the optimum synergistic doses (IC_{100} of each drug) calculated via the Bliss charts. Viability was decreased to 51% for DAPT, to 35% for Docetaxel and Cisplatin single agent treatments. DAPT single treatments compared to its combination with Docetaxel showed a decrease in cell viability to 25% where Cisplatin combinations decreased to 21%. Docetaxel single agent treatments when compared to its DAPT combinations showed a 10% difference. Cisplatin single agent treatments compared to its combinations with DAPT showed 14% additional decrease in cell viability (Figure 19).

Clinical studies referred to the success of sequential treatments of GSIs with common chemotherapeutics to increase their anti-cancer effects. To test this, DAPT, Docetaxel and Cisplatin pre-treatment studies were conducted sequentially one after initial treatments of the selected drug. In the first group, the cells were initially treated with DAPT (IC_{100}) for 24 hours, which was followed by Docetaxel (IC_{100}) (DAPT_Docetaxel) for 48 hours, or Cisplatin (IC_{100}) (DAPT_Cisplatin) treatment for 72 hours. In the second group, DAPT (IC_{100}) treatment for 24 hours was applied after the cells were initially treated with Docetaxel (IC_{100}) (Docetaxel_DAPT) for 48 hours or Cisplatin (IC_{100}) (Cisplatin_DAPT) for 72 hours.

DAPT pre-treatments followed by Docetaxel treatments resulted in a decreased viability to 40% and Cisplatin treatments showed a 23% reduction compared to the non-treated cells. Both Docetaxel and Cisplatin pre-treatments decreased the cell viability to 23%. DAPT_Docetaxel treatments compared to Docetaxel_DAPT showed an additional decrease by 17%. DAPT_Cisplatin treatments compared to Cisplatin_DAPT induced a decrease by 11% (Figure 20).

DAPT single-agent treatments were compatible with Docetaxel and Cisplatin, which confirms its potential success in single-agent treatments. Either combinational or sequential treatments of DAPT with Docetaxel and Cisplatin resulted in lessened cell viability in MDA-MB-231 cells which strengthens their synergistic activities and supposes a promising treatment plan.

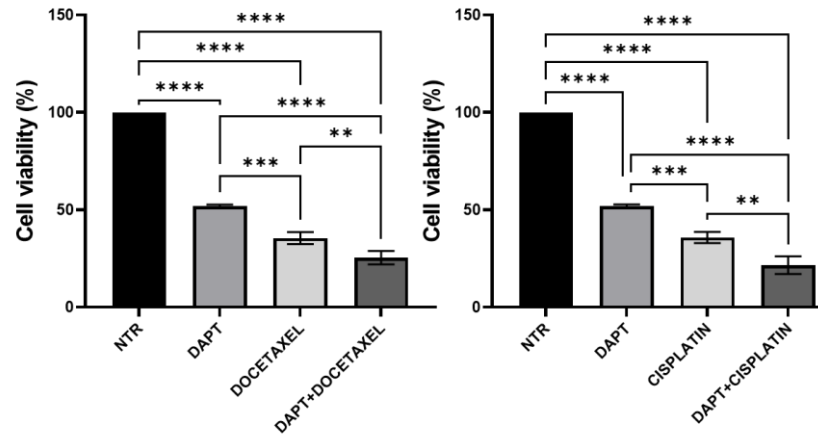


Figure 19. Decreased viability percentages of MDA-MB-231 cells in response to DAPT, Docetaxel and Cisplatin treatments. MTT assay was carried out after the cells were treated with IC₁₀₀ of DAPT (for 24 hours), Docetaxel (for 48 hours), and Cisplatin (for 72 hours) alone or in combinations applied simultaneously. Combinational treatments were performed with Docetaxel for 48 hours and with Cisplatin for 72 hours. (**p<0.01, ***p<0.001, ****p ≤ 0.0001).

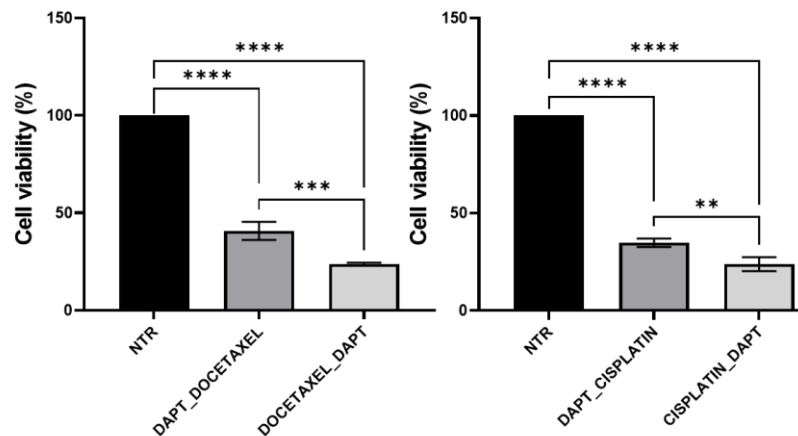


Figure 20. Decreased viability percentages of MDA-MB-231 cells in response to sequential DAPT, Docetaxel and Cisplatin treatments. MTT absorbance values were normalized to untreated groups and graphed by Graph Pad PRISM 8. NTR: non-treated. (**p<0.01, ***p<0.001, ****p ≤ 0.0001).

4.1.4. DAPT Combinations with Cisplatin and Docetaxel in MDA-MB-231 spheroids

Tumors evade apoptosis and induce drug resistance through the regulation of pH and acidity through various events. 3D cell cultures mimic such pH alterations and acidosis that are commonly used for monolayer culture comparisons. Comparing both monolayers (2D) and spheroid (3D) setups were conducted to understand the potential effects of acidosis on DAPT and its combinations with Docetaxel and Cisplatin's tolerance in breast cancer. MDA-MB-231 spheroids were treated with IC_{100} of DAPT and its combinations with IC_{100} of Docetaxel or Cisplatin the optimum synergistic dose measured by the Bliss chart. Spheroid areas were measured by Spheroid J plugin and days (0, 1, 2 and 3) were compared within the experiment group. Results were normalized to the untreated condition and each treatment's day 0 condition (Figure 21). DAPT-treated MDA-MB-231 spheroids decreased to 61% at day 3. Docetaxel-treated spheroids decreased the sphere size to 21% whereas its DAPT combinations showed 19% sphere size difference when compared to single agent Docetaxel treatments. Cisplatin single-agent treatments for spheroids decreased to 41% whereas its DAPT combination showed 35% shrunken sphere size (Figure 22).

Spheroid volume analysis was followed by the APA cell viability experiments with the same conditions and doses. DAPT single agent treatments showed 35%, Docetaxel treatments 32% and Cisplatin treatments 27% decrease when compared to treatment-free MDA-MB-231 cells (Figure 23A and B). DAPT combinations with Docetaxel resulted in 43% decrease, and Cisplatin combinations resulted in a 49% decrease when compared to the non-treated group. DAPT combined with Docetaxel and Cisplatin represents a significant decrease when compared to their single treatments (Figure 23 C). Images of spheroids were analyzed for area comparisons to understand the approximate shrinking in the spheroid size followed by the APA cell viability assessments upon a single agent or combinational treatments. Total toxicity of DAPT, Docetaxel and Cisplatin including their combinational treatments showed a synergistic effect of DAPT in both 2D and 3D MDA-MB-231 cell cultures.

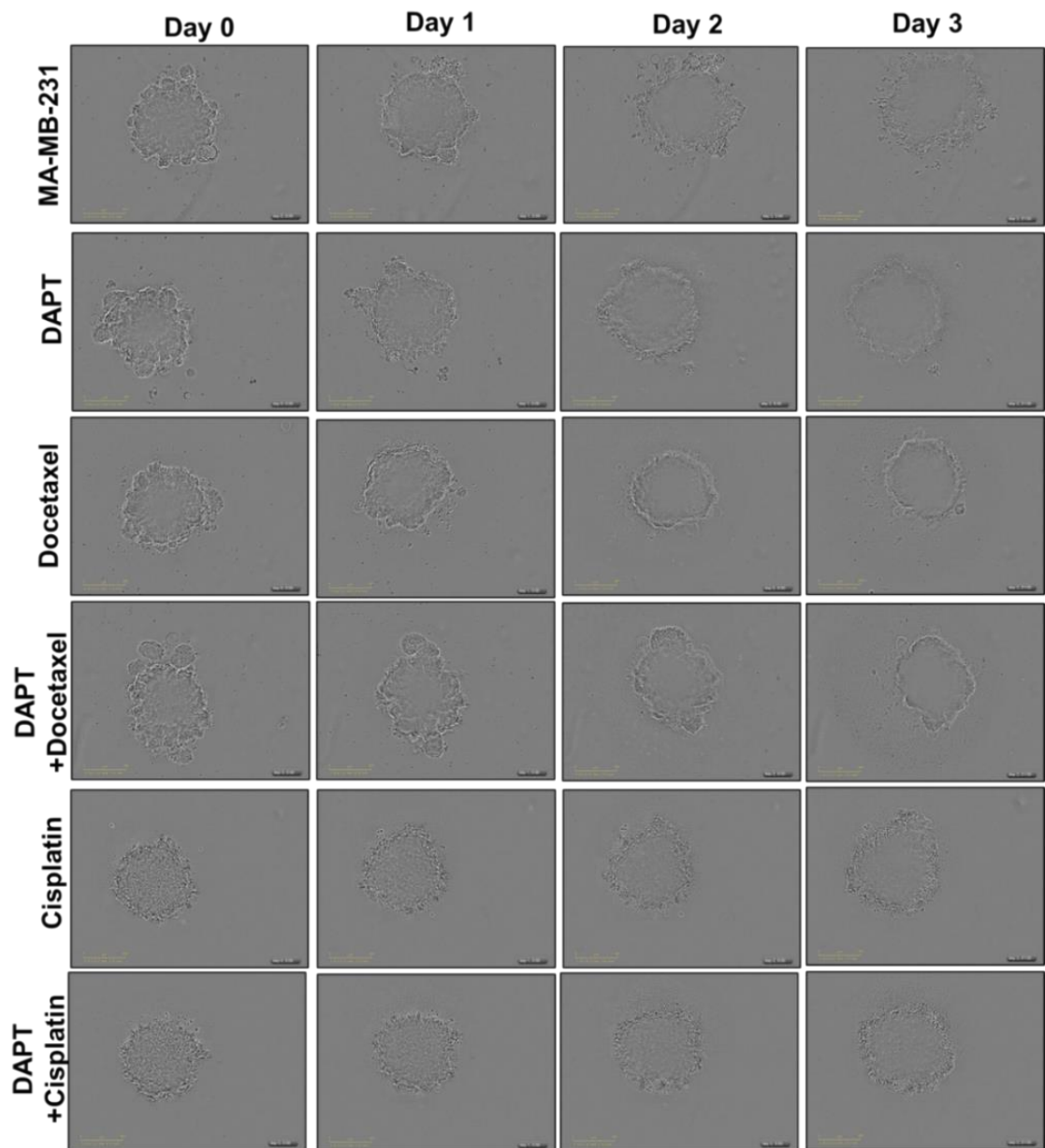


Figure 21. DAPT, Docetaxel and Cisplatin's both single agent and combinational treatments decrease MDA-MB-231 sphere size. DAPT (for 24 hours), Docetaxel (for 48 hours) and Cisplatin (for 72 hours) treatments were applied after the spheroids were formed. Doses were set to IC_{100} of DAPT, Docetaxel and Cisplatin. Images taken by Incucyte Cell Analysis Systems.

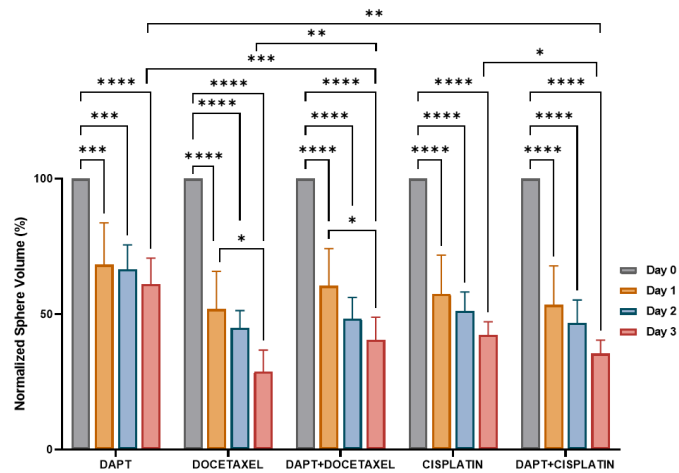


Figure 22. DAPT, Docetaxel and Cisplatin reduces MDA-MB-231 sphere size. Normalized Area of measured from spheroid images were graphed. DAPT (for 24 hours), Docetaxel (for 48 hours) and Cisplatin (for 72 hours) treatments were applied after the spheroids were formed. Doses were set to IC₁₀₀ of DAPT, Docetaxel and Cisplatin. (*p<0.05, **p<0.01, ***p<0.001 and ****p<0.0001).

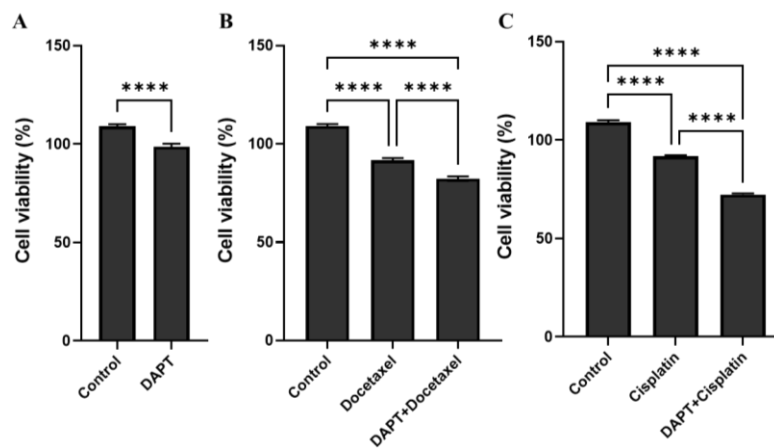


Figure 23. Decreased viability of MDA-MB-231 spheroids in response to DAPT, Docetaxel and Cisplatin treatments and their combinations. (A) IC₁₀₀ of DAPT (for 24 hours), (B) Docetaxel (for 48 hours) and (C) Cisplatin (for 72 hours) and their respective combinational treatments were applied after the spheroids were formed. (****p ≤ 0.0001).

4.2. DAPT resistance in ER/PR+ MCF-7 breast cancer cells

Half maximal doses (IC_{50}) of DAPT, Cisplatin and Docetaxel were measured for intrinsic resistance scaling and determining tolerable dose range for further acquired resistance studies. IC_{50} values of DAPT, Cisplatin and Docetaxel was determined by MTT cell viability assay for the MCF-7 breast cancer cell line. Dose-dependent normalized inhibition response was recorded as 102 μ M for DAPT, 0.2 μ M for Cisplatin and 0.6 μ M for Docetaxel. The intrinsic resistance scale represents MCF-7's high sensitivity profile to Docetaxel and Cisplatin and its highly resistant pattern against DAPT (Figure 24).

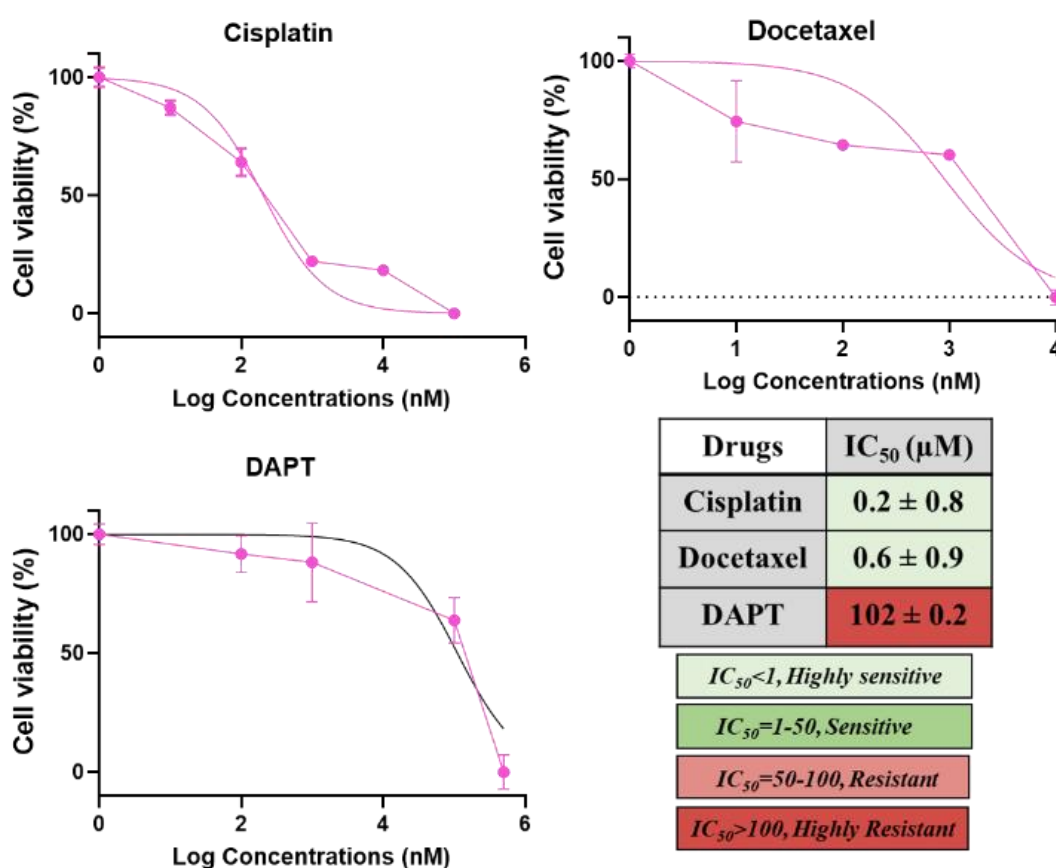


Figure 24. IC_{50} curves of MCF-7 breast cancer cell line to DAPT, Docetaxel, and Cisplatin treatments. MTT absorbance values were normalized and graphed by using GraphPad Prism 8.

To further model DAPT's acquired resistance, MCF-7 cells were treated with gradually increasing doses of DAPT, from half (IC_{25}) to four times (IC_{200}) of IC_{50} value. Eventually, MCF-7 cells were obtained that can grow to 90% confluency in the presence of IC_{200} of DAPT, which is referred to as MCF-7-R (Figure 25). The control MCF-7 (MCF-7-C) cells were treated with the respective volumes of DMSO as MCF-7-R cells received the DAPT treatments. Morphological data showed mesenchymal-like structures for MCF-7-R cells. In contrast to the control MCF-7-C cells, which have an epithelial-like phenotype, MCF-7-R cells were a more elongated phenotype (Figure 25). The growth rate assessment by MTT analysis showed that MCF-7-R cells expand significantly more by 39% than the control MCF-7-C cells (Figure 26). Increased proliferation could be correlated with DAPT-resistant MCF-7 cell's mesenchymal-like shapes. To further assess MCF-7-R cells mesenchymal morphology, cells were plated at a lower density and visualized with higher magnification (Figure 27A). The mean circularity of the control cells was 0.88, while it was reduced to 0.61 in MCF-7-R cells, representing a more elongated shape (Figure 27B). Increased mesenchymal phenotype and growth rate represents MCF-7 cell's potential escape routes to tolerate DAPT toxicity.

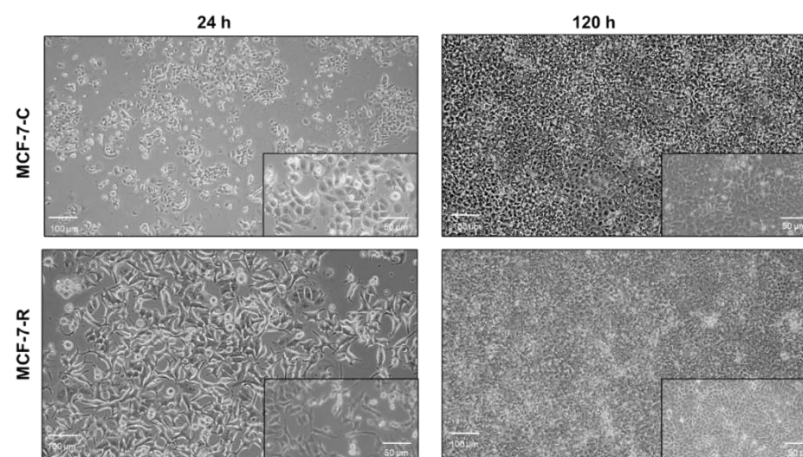


Figure 25. MCF-7-R breast cancer cells reach confluency in the presence of DAPT. Light microscopy images of MCF-7 cells resistant to IC_{200} DAPT treatment (MCF-7-R) and DMSO treated control cells (MCF-7-C) were taken at 24 h and 120 h after IC_{200} of DAPT and respective DMSO treatments. (Scale bar: 50 and 100 μ m).

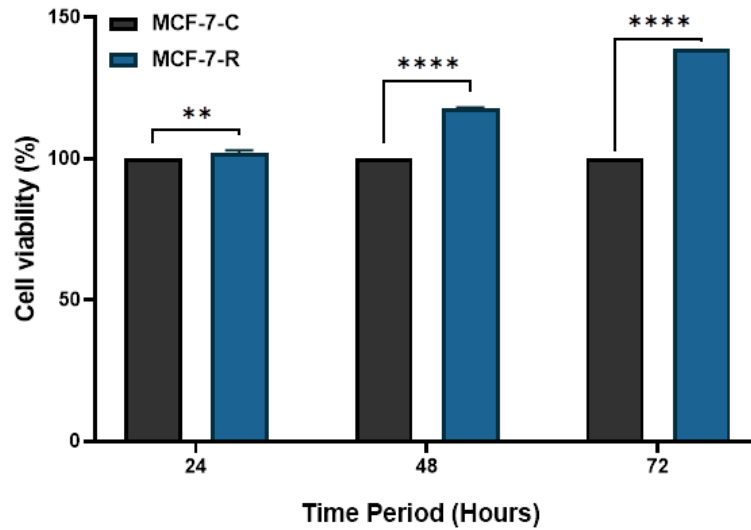


Figure 26. DAPT resistant MCF-7 cells exhibits increased viability than the MCF-7-C cells. MCF-7-R and MCF-7-C cells cultured in drug-free media at three different time points. (** $p < 0.01$, **** $p \leq 0.0001$).

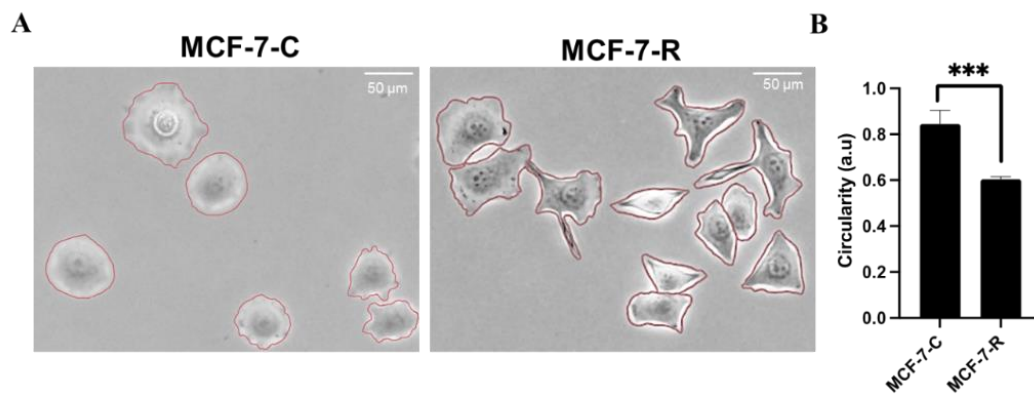


Figure 27. Circularity analysis of DAPT resistant- and control MCF-7 cells. (A) Representative phase-contrast images of MCF-7-C and MCF-7-R cells plated in a drug-free medium. Red outlines representing the cell borders were *Cont.* used to calculate circularity. (Scale bar, 50 μm) (B) The circularity values (a.u) of control and resistant cells are shown. Data represents the means and \pm SD of randomly selected 100 cells. The student t-test confirmed the significance for conditions (***) $p < 0.001$).

4.2.1. DAPT resistant MCF-7 cells alter Notch receptors, Notch target genes and Epithelial-Mesenchymal Transition markers' expression levels

The Notch signalling pathway regulates multiple downstream targets. To gain wider insight into understanding possible pattern behind the DAPT resistance in MCF-7 cells, mRNA expression levels of Notch receptors (Notch1,2,3 and 4), Notch's main downstream targets (Hes5, Hes1, Hey1) and EMT regulators (E-Cadherin, ZO1, Snail2, Snail1 and N-Cadherin) were measured. mRNA expression profiles were analysed by quantitative real-time Q-RT-PCR.

In MCF-7-R cells, mRNA expression of Notch receptors Notch1 and Notch2 were downregulated by 50% and 60%, respectively, while Notch3 was upregulated by 2-fold, and Notch 4 did not change (Figure 28A). Notch target genes Hes5 and Hey1 were upregulated by 1.8-fold, while Hes1 was decreased by 50% (Figure 28B). Two epithelial markers showed an opposite trend that E-Cadherin was increased by 1.3-fold, while ZO1 decreased by 50% (Figure 28C).

On the contrary, mRNA expressions of epithelial-mesenchymal transition (EMT) regulator Snail2 and mesenchymal marker N-Cadherin were increased by 2- and 3-fold, respectively, while another EMT regulator Snail1 was not changed in MCF-7-R cells (Figure 28D).

Overall, MCF-7-R cells showed decreased Notch1 and increased Notch3 expressions which direct to Hes5, E-Cadherin, Snail2, Snail1 and N-Cadherin expressions escalation. Furthermore, with ZO1 expression suppression, mRNA expression profiles for MCF-7-R reflects elevated mesenchymal transition which is additionally represented in morphological changes.

Thus, explains previously observed morphological changes and its association with the increased EMT shift that possibly roots for drug tolerance, and this could explain the potential DAPT resistance route for MCF-7 breast cancer cells.

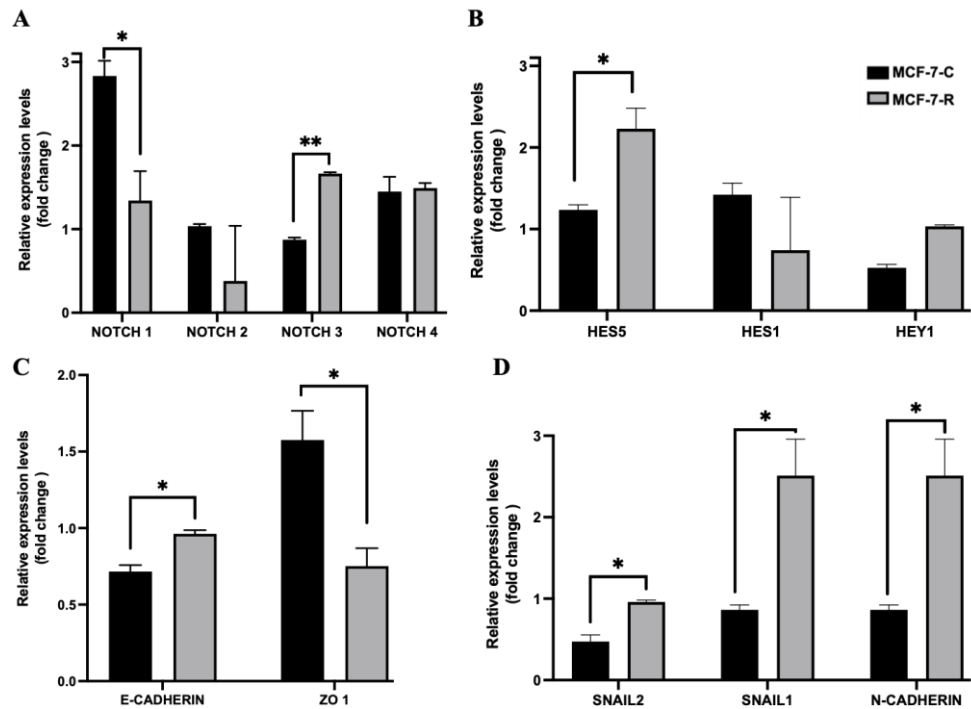


Figure 28. Expression analysis of Notch pathway components and EMT markers for DAPT resistant-MCF-7 cells. mRNA expression levels of (A) Notch receptors (Notch 1,2,3 and 4), (B) Notch pathway target genes (Hes5, Hes1, Hey1), (C) epithelial markers (E-Cadherin, ZO1), and EMT regulators (D) mesenchymal markers (Snail2, Snail1 and N-Cadherin) of MCF-7-C and MCF-7-R cells are shown. Data represents the means and \pm SD of 3 independent experiments. (ns: not significant, * $p < 0.05$, ** $p < 0.01$, *** $p < 0.001$).

4.2.2. DAPT resistant-MCF-7 cells exhibit increased migration

Mesenchymal morphology is often associated with the increased migration capacity, which is a common trait of invasive and metastatic tumours. Drug resistance is also known to be correlated with the expression of mesenchymal traits. Thus, we analysed whether mesenchymal-like MCF-7-R cells had an increased migration capacity using wound healing assay. While only 13.2 % of the open wound was closed by the control cells, MCF-7-R cells reduced the gap by 51.1% in 20 hours (Figure 29) indicating elevated migratory phenotype in correlation with its mesenchymal morphology.

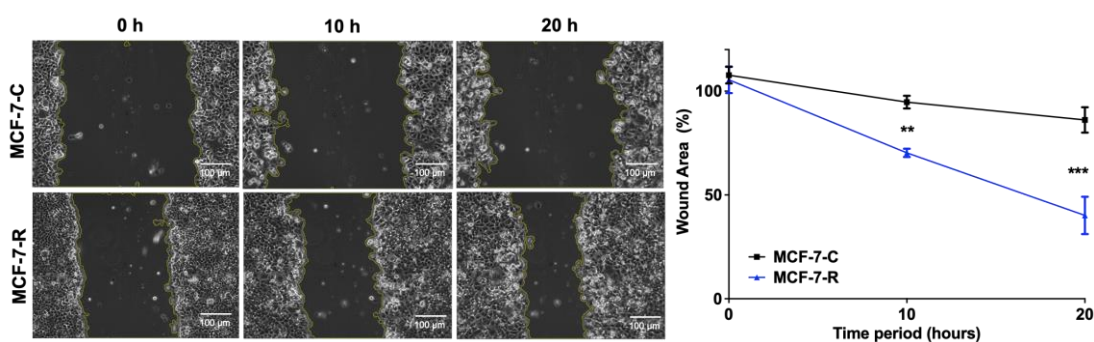


Figure 29. DAPT resistance increases migration in MCF-7 breast cancer cells. Migration phenotype was evaluated by wound healing assay. Time-lapse microscopy images of wound closure of MCF-7-C and MCF-7-R cells at $t=0$, 10, and 20 h after the wound formation. Cells were treated with IC₂₀₀ of DAPT, and images were analyzed via Image J. Yellow lining defines the area lacking cells. Scale bars, 100 μm . (B) Quantification of the wound area after the DAPT treatment in MCF-7-C and MCF-7-R cells. Results represent three independent experiments and One-way ANOVA analysis, and the student t-test confirmed the significance for conditions (***) $p < 0.001$).

4.2.3. Docetaxel and Cisplatin's synergistic activities with DAPT in MCF-7 cells

Docetaxel and Cisplatin's successful preclinical/clinical outcome when combined with GSIs further investigated in this study as the synergistic effects of such combination remain unstudied. To investigate potential synergistic outcomes with Cisplatin and Docetaxel, cell viability data was plotted and measured by Bliss synergy score. Bliss scores for DAPT combinations of MCF-7 cell line with Cisplatin resulted as 25.2 (Figure 30) and with Docetaxel 17.9 (Figure 31). DAPT's combination either with Cisplatin or Docetaxel showed a highly synergistic pattern. Synergistic pattern suggests that DAPT can be used in combinational treatments with Cisplatin and Docetaxel for further MCF-7 treatments.

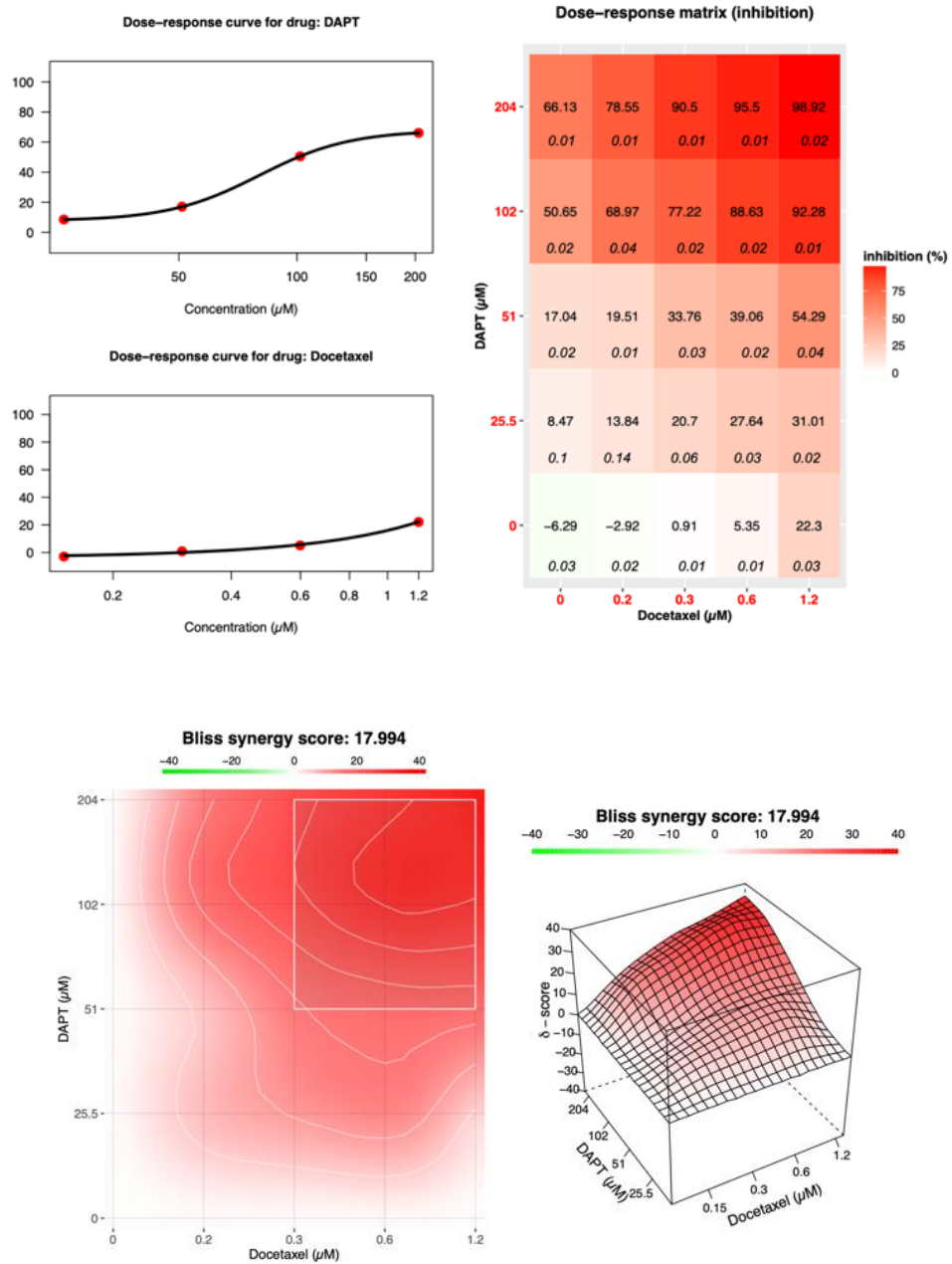


Figure 30. DAPT’s combination with Docetaxel results in synergistic effect for MCF-7 cells. Drug synergy analysis of DAPT with Docetaxel was conducted by Synergy Finder tool. Bliss synergy score of three independent experiments were analyzed for combinations. The drug response curve with the inhibition matrix and heatmap shows IC_{100} for DAPT and Docetaxel was the optimum dose combination for MCF-7 cell lines.

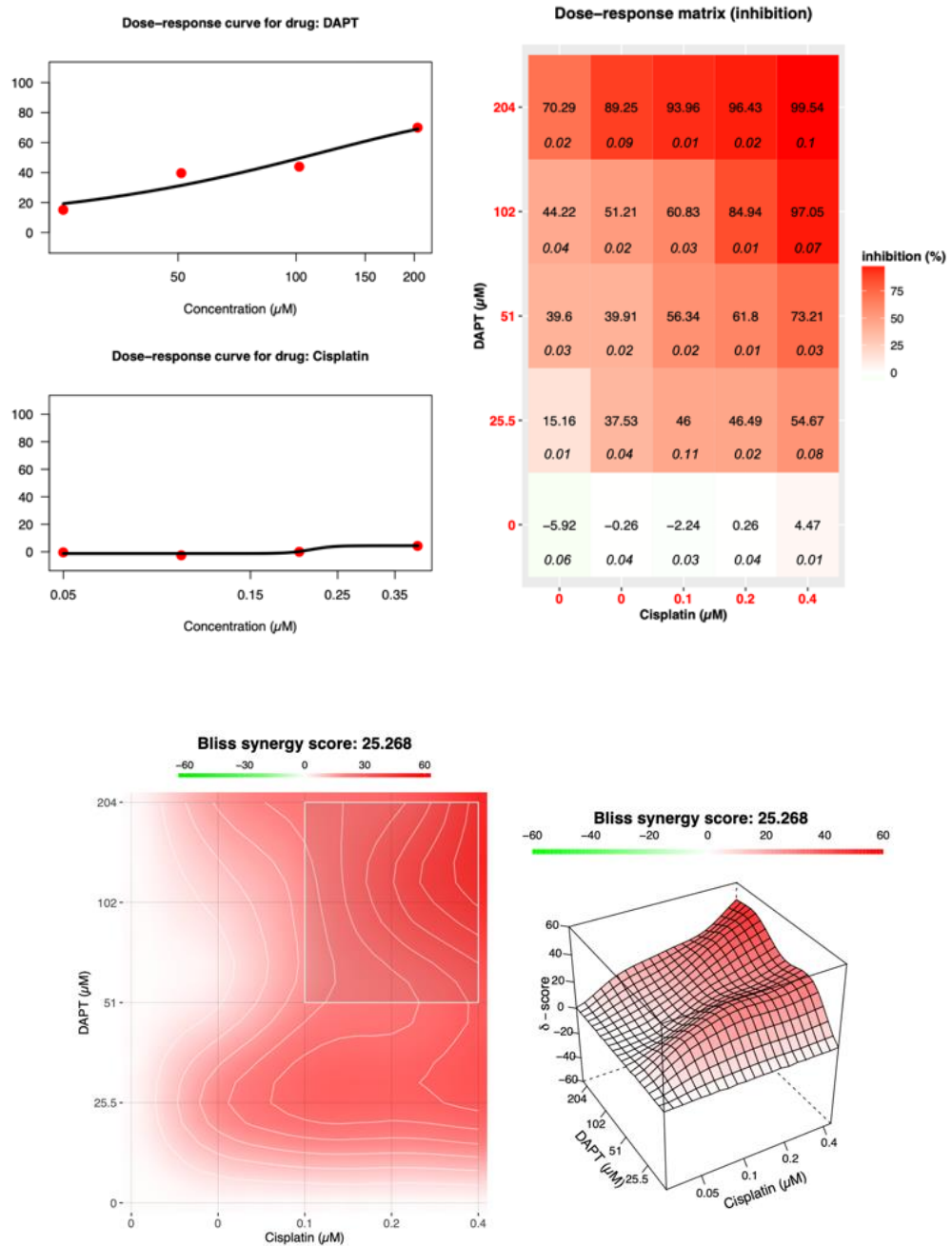


Figure 31. DAPT’s combination with Cisplatin results in synergistic effect for MCF-7 cells. Drug synergy analysis of DAPT with Cisplatin was conducted by Synergy Finder tool. Bliss synergy score of three independent experiments were analyzed for combinations. The drug response curve with the inhibition matrix and heatmap shows IC_{100} for DAPT and Cisplatin was the optimum dose combination for MCF-7 cell lines.

According to the suggested optimum synergistic dose (IC₁₀₀ of each drug) determined by the Bliss chart, DAPT combinational treatments were performed by MTT cell viability assay. Viability was decreased to 41% for DAPT, to 45% for Docetaxel and to 41% for Cisplatin single agent treatments. DAPT single treatments showed a decrease in cell viability by 17% when compared to its combination with Docetaxel. Cisplatin combinations decreased by 16% than the DAPT or Cisplatin single agent treatments (Figure 32).

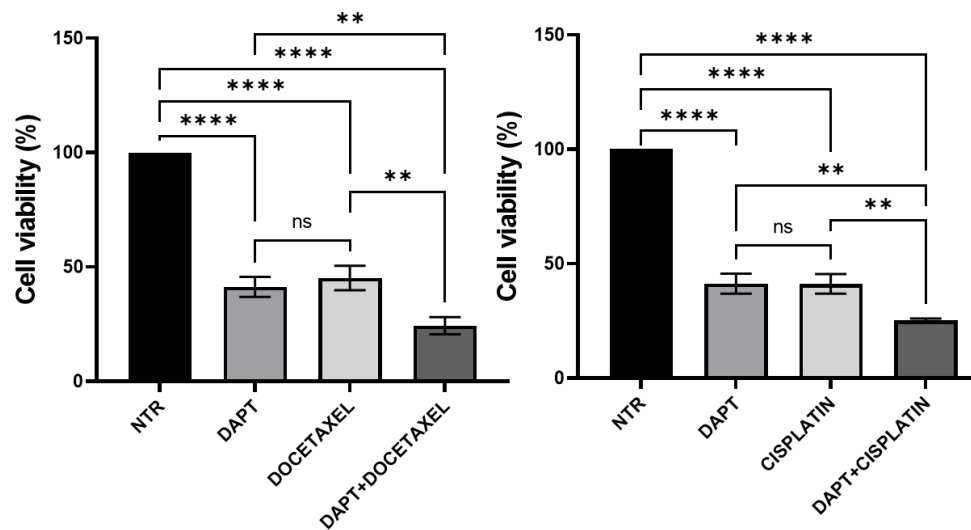


Figure 32. Decreased viability ratios of MCF-7 cells in response to DAPT, Docetaxel and Cisplatin treatments. MTT assay was carried out after the cells were treated with IC₁₀₀ of DAPT (for 24 hours), Docetaxel (for 48 hours), Cisplatin (for 72 hours) alone or in combinations which applied simultaneously. Combinational treatments performed with Docetaxel for 48 hours and with Cisplatin for 72 hours. (ns: not significant, *p<0.05, **p<0.01, ***p<0.001).

Clinical studies referred to the success of sequential treatments of GSIs with common chemotherapeutics to increase their anti-cancer effects. To test this, DAPT, Docetaxel and Cisplatin pre-treatment studies were conducted sequentially one after initial treatments of the selected drug. In the first group, the cells were initially treated with DAPT (IC₁₀₀) for 24 hours, which was followed by Docetaxel (IC₁₀₀) (DAPT_Docetaxel) for 48 hours, or Cisplatin (IC₁₀₀) (DAPT_Cisplatin) treatment for

72 hours. In the second group, DAPT (IC₁₀₀) treatment for 24 hours was applied after the cells were initially treated with Docetaxel (IC₁₀₀) (Docetaxel_DAPT) for 48 hours or Cisplatin (IC₁₀₀) (Cisplatin_DAPT) for 72 hours. DAPT pre-treatments followed by Docetaxel treatments resulted in a decreased viability to 27% and Cisplatin treatments showed a 74% reduction compared to the non-treated cells. Docetaxel_DAPT treatments compared to DAPT_Docetaxel showed an additional decrease by 1%. Cisplatin_DAPT treatments compared to DAPT_Cisplatin induced a decrease by 8%. DAPT single-agent treatments were compatible with Docetaxel and Cisplatin treatments which confirms its potential success over single-agent treatments. Either combinational or sequential treatments of DAPT with Docetaxel and Cisplatin resulted in decreased cell viability in MCF-7 cells which strengthens their synergistic activities and supposes a promising treatment plan (Figure 33).

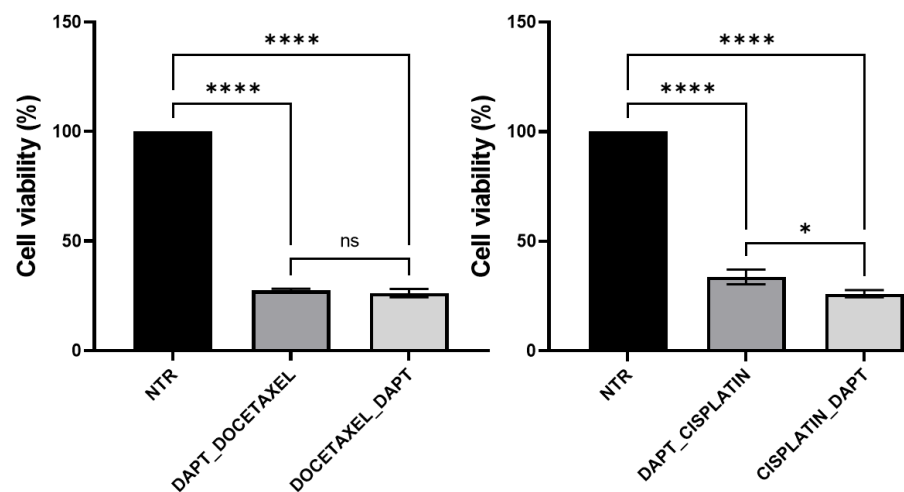


Figure 33. Decreased viability ratios of MCF-7 cells in response to sequential DAPT, Docetaxel and Cisplatin treatments. In the first group, the cells were initially treated with DAPT (IC₁₀₀) for 24 hours, which was followed by Docetaxel (IC₁₀₀) (DAPT_Docetaxel) for 48 hours, or Cisplatin (IC₁₀₀) (DAPT_Cisplatin) treatment for 72 hours. In the second group, DAPT (IC₁₀₀) treatment for 24 hours was applied after the cells were initially treated with Docetaxel (IC₁₀₀) (Docetaxel_DAPT) for 48 hours or Cisplatin (IC₁₀₀) (Cisplatin_DAPT) for 72 hours. (ns: not significant, *p<0.05, **p<0.01, ***p<0.001).

4.2.4. DAPT Combinations with Cisplatin and Docetaxel in MCF-7 spheroids

Tumours evade apoptosis and induce drug resistance through the regulation of pH and acidity through various events. 3D cell cultures mimic such pH alterations and acidosis that are commonly used for monolayer culture comparisons. Comparing both monolayers (2D) and spheroid (3D) setups were conducted to understand the potential effects of acidosis on DAPT and its combinations with Docetaxel and Cisplatin's tolerance in breast cancer. MCF-7 spheroids were treated with the optimum synergistic dose measured by the Bliss chart, IC_{100} of DAPT and its combinations with IC_{100} of Docetaxel or Cisplatin. Spheroid areas were measured by Spheroid J plugin and days (0,1,2 and 3) were compared within the experiment group to the addition of comparisons to treatments day 3 data (Figure 34). All data were normalized to the untreated condition and each treatment's day 0 condition. DAPT single-agent treatments were decreased to 85% on day 2 yet recovered back to 98% on day 3. Docetaxel single agent treatments showed an increase in the area to 151% at day 3 whereas DAPT combined with Docetaxel showed 108% in the spheroid volume. Each day of Docetaxel treatments showed a significant increase in the spheroid volume. MCF-7 spheroids treated with Cisplatin showed no significant change yet when compared with DAPT differed by 9%. (Figure 35).

MCF-7 spheroid treatment's APA cell viability results showed DAPT single treatments showed 32%, Docetaxel treatments at 38% and Cisplatin treatments decreased by 48% when compared to the control group (Figure 36A). DAPT combinations with Docetaxel resulted in no change when compared to Docetaxel single-agent treatments (Figure 36B). Cisplatin combinations showed a 39% change when compared to the non-treated group. Moreover, Cisplatin combinations compared to Cisplatin single agent treatments induced a decrease by an additional 9% (Figure 36C). Images of spheroids were analysed for area comparisons to understand the approximate shrinking in the spheroid size followed by the APA cell viability assessments upon a single agent or combinational treatments. Total toxicity of DAPT, Docetaxel and Cisplatin including their combinational treatments showed their increased synergistic effects of DAPT in both 2D and 3D MCF-7 cell cultures.

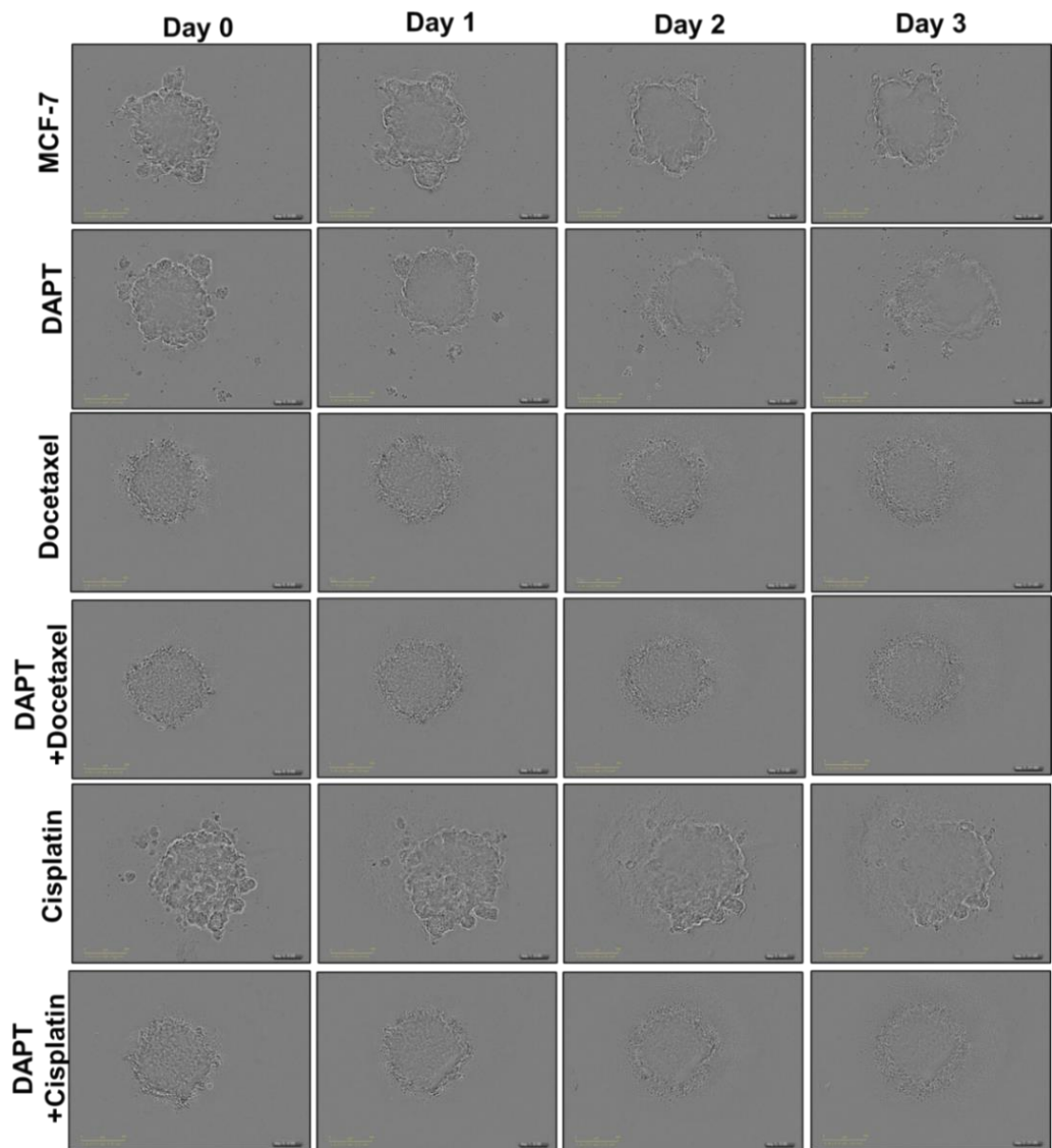


Figure 34. DAPT, Docetaxel and Cisplatin's both single agent and combinational treatments decreases MCF-7 sphere size. DAPT (for 24 hours), Docetaxel (for 48 hours) and Cisplatin (for 72 hours) treatments were applied after the spheroids were formed. Doses were set to IC_{100} of DAPT, Docetaxel and Cisplatin. Images taken by Incucyte Cell Analysis Systems.

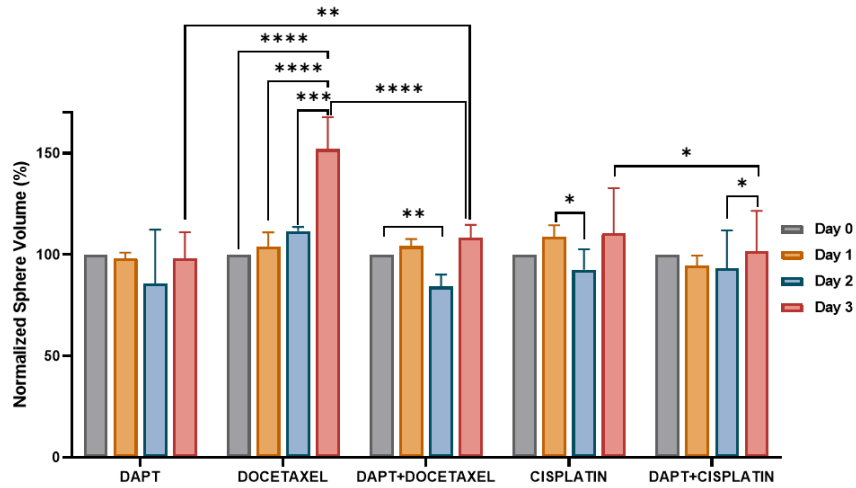


Figure 35. DAPT, Docetaxel and Cisplatin their combinations reduce MCF-7 sphere size. Normalized Area of measured from spheroid images were graphed. DAPT (for 24 hours), Docetaxel (for 48 hours) and Cisplatin (for 72 hours) treatments were applied after the spheroids were formed. Doses were set to IC₁₀₀ of DAPT, Docetaxel and Cisplatin. (*p<0.05, **p<0.01, ***p<0.001 and ****p<0.0001).

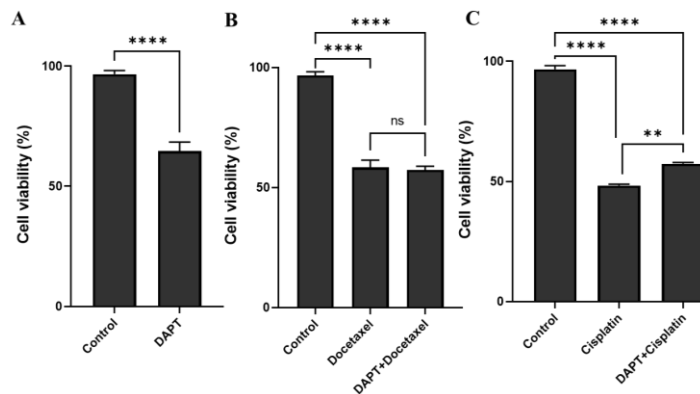


Figure 36. Decreased viability of MCF-7 spheroids in response to DAPT, Docetaxel and Cisplatin treatments and their combinations. (A) IC₁₀₀ of DAPT (for 24 hours), (B) Docetaxel (for 48 hours) and (C) Cisplatin (for 72 hours) treatments and their respective combinations were applied after the Control: non-treated. (ns: not significant, **p<0.01, ***p<0.001, ****p<0.0001).

4.3. R04929097 resistance in MDA-MB-231 triple negative breast cancer cells

Half maximal doses (IC_{50}) of R04929097 were measured for intrinsic resistance scaling and determining tolerable dose range for further acquired resistance studies. IC_{50} of R04929097 for MDA-MB-231 triple negative breast cancer cells were determined by the MTT assay and inhibition response was normalized as $0.01\mu\text{M}$ (Figure 37). Sensitivity scale represents MDA-MB-231's natural hypersensitivity against R04929097.

To model acquired resistance, MDA-MB-231 cells were treated with gradually increasing doses of R04929097, from half the value (IC_{25}) up to four times the value (IC_{200}) of IC_{50} . In the end, MDA-MB-231 cells were obtained which can grow to 90% confluency in the presence of IC_{200} of R04929097, which is referred as MDA-MB-231-R in this section. MDA-MB-231-C cells were treated with the respective volumes of DMSO whereas MDA-MB-231-R cells received respective R04929097 treatments.

Morphological changes were not observed 24 and 120 hours after the R04929097 compared to MDA-MB-231-C versus MDA-MB-231-R cells (Figure 38). MDA-MB-231-R cells were not significantly more proliferative than the MDA-MB-231-C cells. (Figure 39).

To further compare potential resistance-dependent morphological changes, cells were plated at a lower density and visualized with higher magnification. The mean circularity of the control cells was 0.37, while it was reduced to 0.35 in MDA-MB-231-R cells. MDA-MB-231-R cells showed no difference in growth rate, mesenchymal phenotype (Figure 40). R04929097 resistance might not depend on increased growth rate, or EMT phenotype including increased migration. Thus, these data suggest alternative paths for R04929097 resistance in MDA-MB-231 cells.

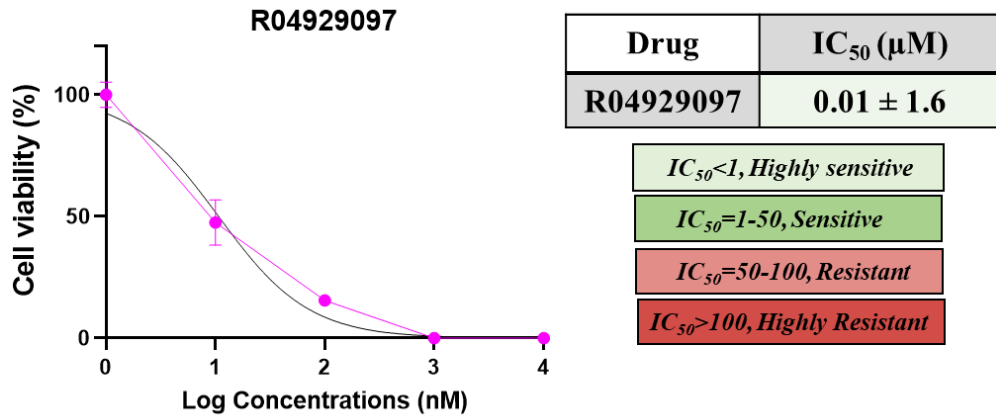


Figure 37. IC₅₀ curves of MDA-MB-231 breast cancer cell line to R04929097 treatments. MTT absorbance values were normalized and graphed by using GraphPad Prism 8.

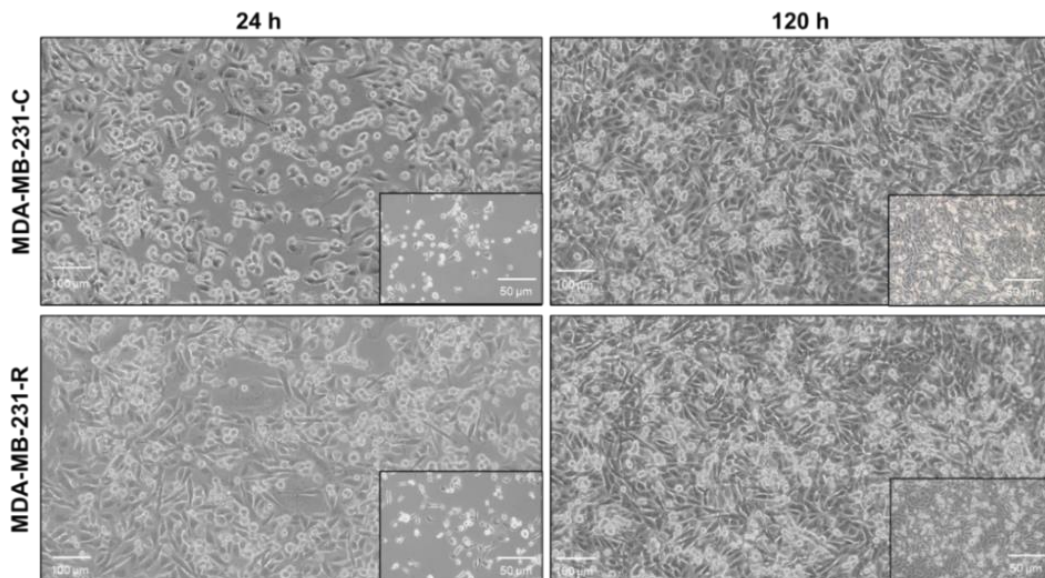


Figure 38. MDA-MB-231-R breast cancer cells reach confluency in the presence of R04929097. Light microscopy images of MDA-MB-231 cells resistant to IC₂₀₀ R04929097 treatment (MDA-MB-231-R) and DMSO treated control cells (MDA-MB-231-C) were taken at 24 h and 120 h after IC₂₀₀ of R04929097 and respective DMSO treatments (Scale bar: 50 and 100 μm).

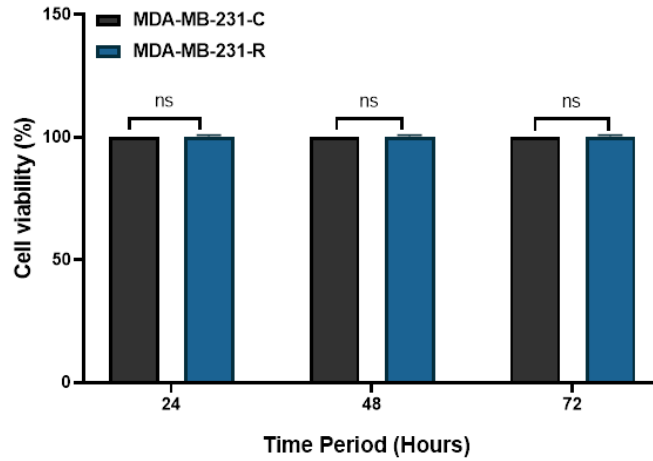


Figure 39. R04929097 resistant MDA-MB-231 cells exhibit no changes in viability. MDA-MB-231-R and MDA-MB-231-C cells cultured in drug-free media at three different time points. Data represents the means and \pm SD of three independent experiments. (ns: not significant).

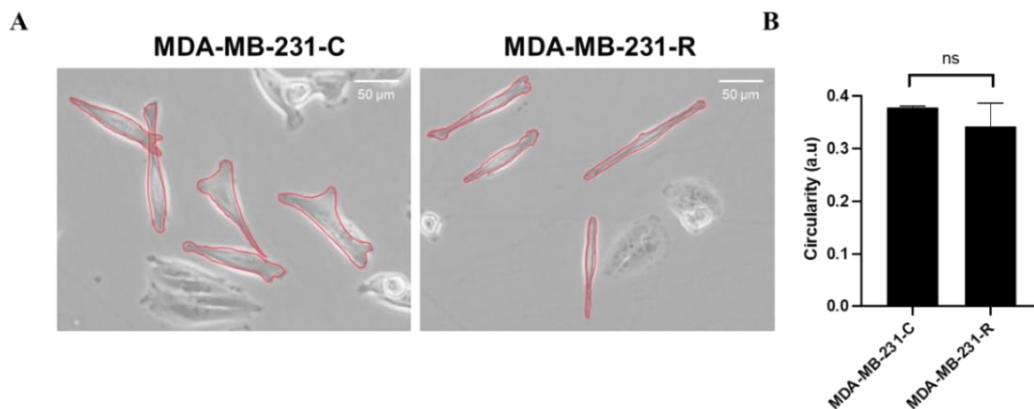


Figure 40. Circularity analysis of R04929097 resistant- and control MDA-MB-231 cells. (A) Representative phase-contrast images of MDA-MB-231-C and MDA-MB-231-R cells plated in a drug-free medium. Red outlines representing the cell borders were used to calculate circularity. (Scale bar, 50 μ m) (B) The circularity values (a.u) of control and resistant cells are shown. Data represents the means and \pm SD of randomly selected 100 cells. (ns: not significant).

4.3.1. R04929097 resistant MDA-MB-231 cells alter Notch receptors, Notch target genes and Epithelial-Mesenchymal Transition markers' expression levels

The Notch signalling pathway regulates multiple downstream targets. To gain wider insight into understanding the pattern behind the R04929097 resistance in MDA-MB-231, mRNA expression levels of Notch receptors (Notch1,2,3 and 4) and Notch's main downstream targets (Hes5, Hes1, Hey1) and EMT regulators (E-Cadherin, ZO1, Snail2, Snail1 and N-Cadherin) were measured. mRNA expression profiles were analysed by quantitative real-time Q-RT-PCR. MDA-MB-231-R cells downregulated expressions of Notch receptors, Notch1 by 2% as well as Notch2 Notch3 and Notch4 by 0.1% (Figure 41A).

Resistant cells expressed decreased levels of Hes5 by 2% and Hey1 by 0.1%, while Hes1 expression was decreased by 7% (Figure 41B). Reduced trend of ZO1 expressions by 1% were also observed (Figure 41C).

N-Cadherin was repressed by 6% as well as Snail2 by 3.2-fold in MDA-MB-231-R cells compared to MDA-MB-231-C. R04929097 resistance showed downregulation in the expression of Snail1 by 1% (Figure 41D).

Decreased mRNA expressions of Notch1,2,3 and 4 resulted in overall suppression of Notch's main downstream targets (Hes5, Hes1 and Hey1) and EMT regulators (E-Cadherin, ZO1, Snail2, Snail1 and N-Cadherin).

Thus, the data suggests R04929097's continuous treatments result in successful inhibition of all four Notch receptors and thus interrupts EMT homeostasis in MDA-MB-231-R cells yet this is not enough to confirm potential R04929097 routes for MDA-MB-231 cells.

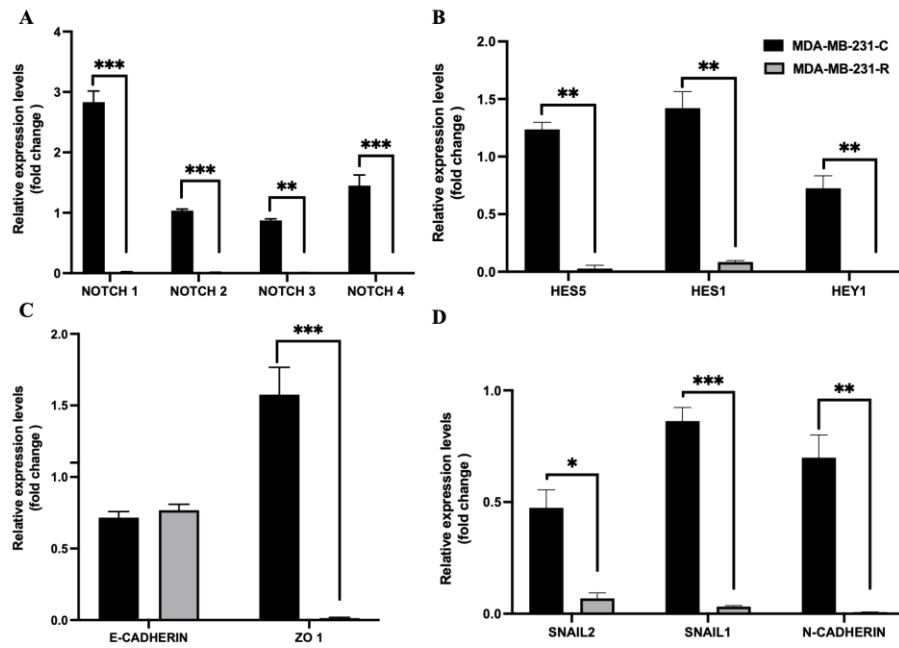


Figure 41. Expression analysis of Notch pathway components and EMT markers for R04929097 resistant-MDA-MB-231 cells. mRNA expression levels of (A) Notch receptors (Notch 1,2,3 and 4), (B) Notch pathway target genes (Hes5, Hes1, Hey1), (C) epithelial markers (E-Cadherin, ZO1), and EMT regulators (D) mesenchymal markers (Snail2, N-Cadherin, and Snail1) of MDA-MB-231-C and MDA-MB-231-R cells are shown. (ns: not significant, * $p < 0.05$, ** $p < 0.01$, *** $p < 0.001$).

4.3.2. R04929097 resistant MDA-MB-231 cells display accelerated migration

Dysregulations in the homeostatic stage of EMT known to be associated with increased migrative behaviours in breast cancer to overcome drug toxicity and induce resistance pattern. To assess this, MDA-MB-231-R cells were analysed for potential changes in the migration phenotype by wound healing assay. MDA-MB-231-R cells were then analysed for migrative changes by wound healing assay. The wound for MDA-MB-231-C cells were closed by 12% whereas MDA-MB-231-R cells reduced the gap by 43% in 10 hours. Overall closure of the wound for MDA-MB-231-C cells was fully closed whereas 10% of the area was left for closure (Figure 42). Although mRNA expressions of EMT regulators were aberrantly expressed, MDA-MB-231-R cells

showed no difference in proliferation or mesenchymal morphology. R04929097 resistance might potentiate through another drug resistance patterns in MDA-MB-231 cells.

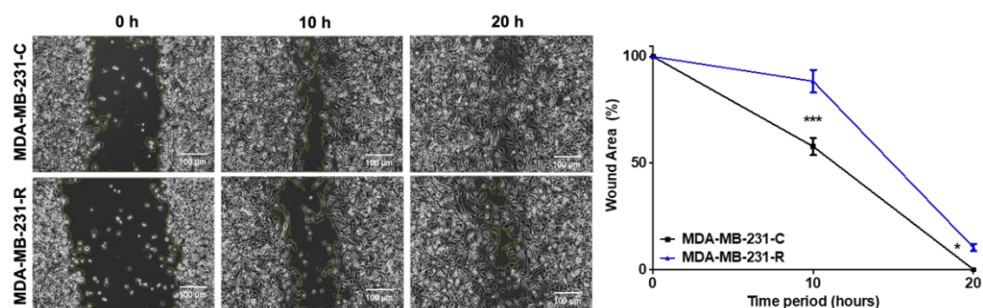


Figure 42. R04929097 resistance delays migration rate in MDA-MB-231 breast cancer cells. Migration phenotype was evaluated by wound healing assay. Time-lapse microscopy images of wound closure of untreated and treated with R04929097 (IC_{200}) MDA-MB-231 cells at $t=0$, 10, and 20 h after the wound formation were analyzed via Image J. Yellow lining defines the area lacking cells. Scale bars, 100 μ m. (B) Quantification of the wounded area invaded control and R04929097 treated MDA-MB-231 cells. (* $p<0.05$, *** $p<0.001$).

4.4. R04929097 resistance in ER/PR+ MCF-7 breast cancer cells

Half maximal doses (IC_{50}) of R04929097 were measured for intrinsic resistance scaling and determining tolerable dose range for further acquired resistance studies. IC_{50} of R04929097 for ER/PR+ MCF-7 breast cancer cell line was initially determined by MTT assay and inhibition response was normalized as 0.01 μ M (Figure 43). Sensitivity scale represents MCF-7's intrinsic high sensitivity profile against R04929097. To model acquired resistance, MCF-7 cells were treated with gradually increasing doses of R04929097, from half the value (IC_{25}) up to four times the value (IC_{200}) of IC_{50} . In the end, MCF-7 cells were obtained which can grow to 90% confluency in the presence of IC_{200} of R04929097, which is referred as MCF-7-R (Figure 44). As the control (MCF-7-C), MCF-7 cells were treated with the respective volumes of DMSO as MCF-7-R cells received R04929097 treatments. Morphological changes were not observed 24 and

120 hours after the R04929097 compared to MCF-7-C versus MCF-7-R cells. Cell viability ratios showed that MCF-7-R cells were not significantly different than the MCF-7-C cells (Figure 45). Cells were plated at a lower density to compare potential resistance-dependent morphological changes and visualized with higher magnification (Figure 46A). The mean circularity of the control cells was 0.72, while it was reduced to 0.70 in MCF-7-R cells, (Figure 46B). MCF-7-R cells showed no difference in proliferation or mesenchymal morphology.

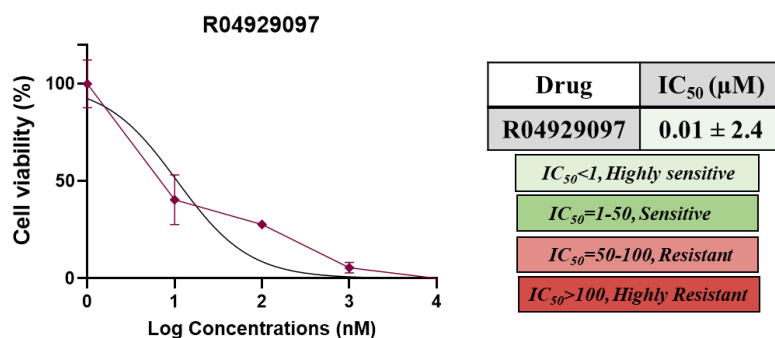


Figure 43. IC₅₀ curves of MCF-7 breast cancer cell line to R04929097 treatments.

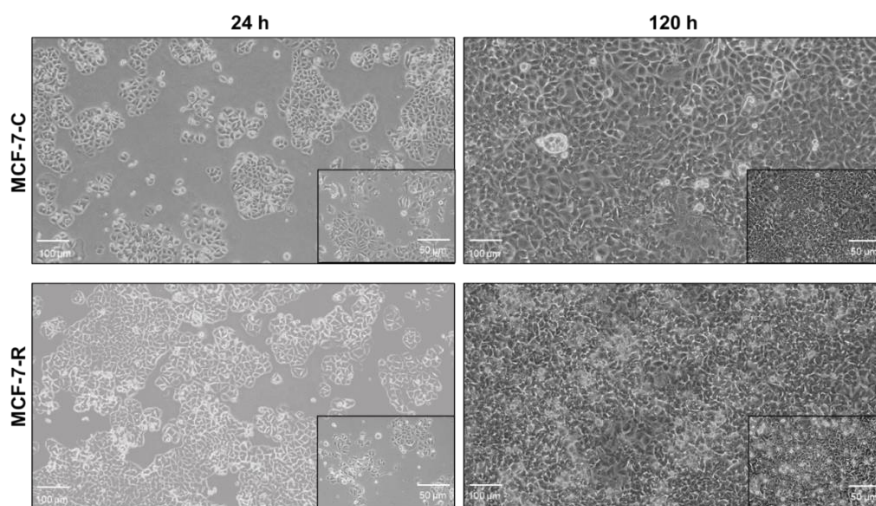


Figure 44. MCF-7-R breast cancer cells reach confluency in the presence of R04929097. Light microscopy images of MCF-7 cells resistant to IC₂₀₀ R04929097 treatment (MCF-7-R) and DMSO treated control cells (MCF-7-C). (Scale bar: 50 and 100 μm).

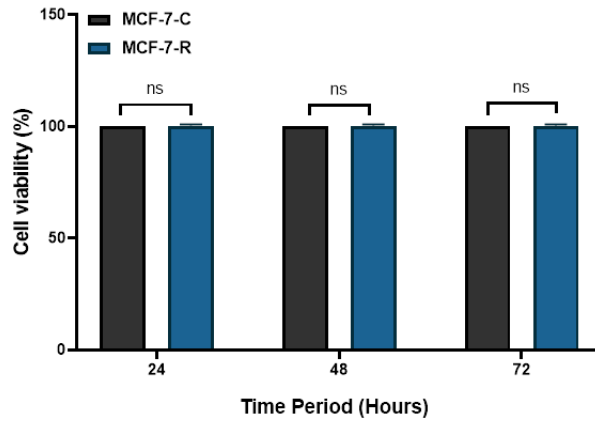


Figure 45. R04929097 resistant MCF-7 cells exhibits no changes in viability. MCF-7-R and MCF-7-C cells cultured in drug-free media at three different time points. Data represents the means and \pm SD of three independent experiments. (ns: not significant).

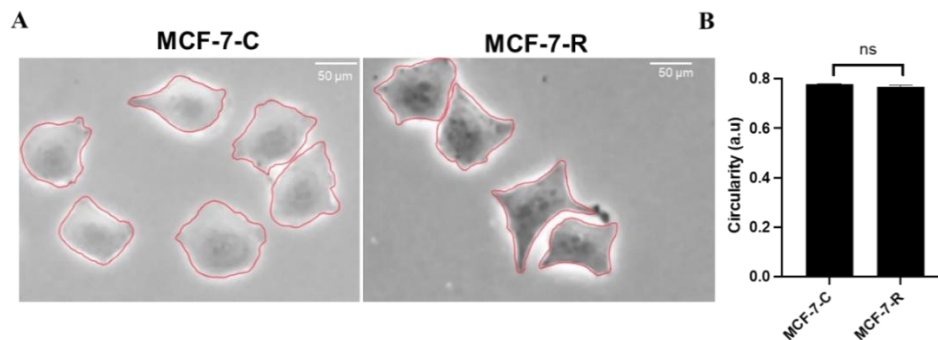


Figure 46. Circularity analysis of R04929097 resistant MCF-7 and control cells. (A) Representative phase-contrast images of MCF-7-C and MCF-7-R cells plated in a drug-free medium. Red outlines representing the cell borders were used to calculate circularity. (Scale bar, 50 μ m) (B) The circularity values (a.u.) of control and resistant cells are shown. Data represents the means and \pm SD of randomly selected 100 cells. Student t-test confirmed the significance for conditions (ns: not significant).

4.4.1. R04929097 resistant MCF-7 cells alter Notch receptors, Notch target genes and Epithelial-Mesenchymal Transition marker's expression levels

The Notch signalling pathway regulates multiple downstream targets. To gain wider insight into understanding the mechanism behind the R04929097 resistance in MCF-7, mRNA expression levels of Notch receptors (Notch1,2,3 and 4) and Notch's main downstream targets (Hes5, Hes1, Hey1) and EMT regulators (E-Cadherin, ZO1, Snail2, Snail1 and N-Cadherin) were measured. mRNA expression profiles were analysed by quantitative real-time Q-RT-PCR.

MCF-7-R cells downregulated expressions of Notch receptors, Notch1 by 23% and Notch2 by 69%, Notch3 expression by 71%, and upregulated Notch 4 by 1.11-fold change (Figure 47A). Resistant cells expressed decreased levels of Hes1 by 72% and increased levels of Hey1 by 1.48-fold as well as Hes5 by 1.07-fold change (Figure 47B). Elevated expressions of E-Cadherin by 1.59-fold and an increased trend of ZO1 expressions by 11-fold were also observed (Figure 47C).

R04929097 resistance showed decrease in the expression of Snail1 by 1.09-fold (Figure 47D). Decreased Notch1 expression led to Hes1 and Snail1 suppression. On the other hand, Hes5, Hey1 and ZO1 expressions were increased significantly. Thus, accounts for partial inhibition of the Notch receptors induces dysregulations in EMT markers which might indicate a potential resistance route for R04929097 in MCF-7 cells, yet this is not enough to confirm such route.

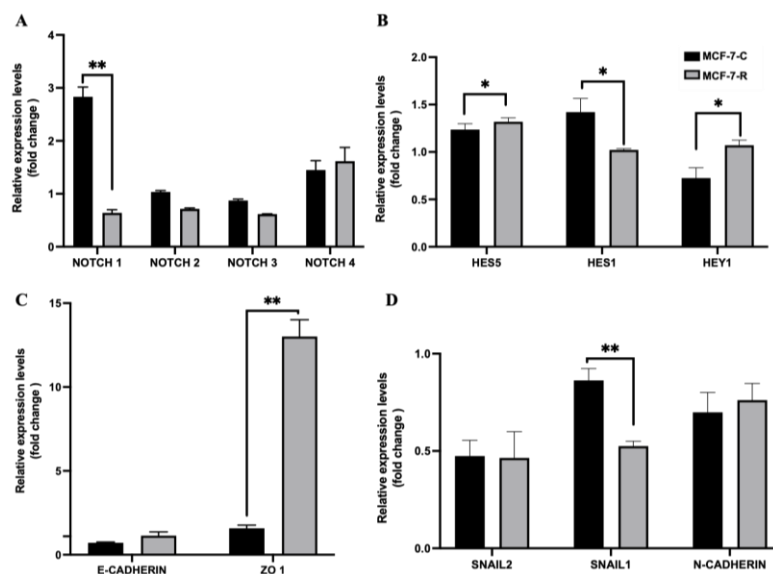


Figure 47. Expression analysis of Notch pathway components and EMT markers for R04929097 resistant-MCF-7 cells. mRNA expression levels of (A) Notch receptors (Notch 1,2,3 and 4), (B) Notch pathway target genes (Hes5, Hes1, Hey1), (C) epithelial markers (E-Cadherin, ZO1), and EMT regulators (D) mesenchymal markers (Snail2, N-Cadherin, and Snail1) of MCF-7-C and MCF-7-R cells are shown. (* $p < 0.05$, ** $p < 0.01$).

4.4.2. R04929097 resistant MCF-7 cells exhibits no change in the migration potential

Dysregulations in the homeostatic stage of EMT known to be associated with increased migrative behaviours in breast cancer to tolerate drug toxicity. To assess this MCF-7-R cells were then analysed for migrative changes by wound healing assay. The wound for MCF-7-C cells were closed by 13% same as MCF-7-R cells in 10 hours. Overall closure of the wound for MCF-7-C cells were 27% and MCF-7-R cells reduced the wound by 25% in 20 hours (Figure 48) indicating no changes in the migratory phenotype of resistant cells. Although mRNA expressions of EMT regulators were aberrantly expressed, MCF-7-R cells showed no difference in growth rate and mesenchymal morphology. R04929097 resistance might potentiate through another drug resistance patterns in MCF-7 cells.

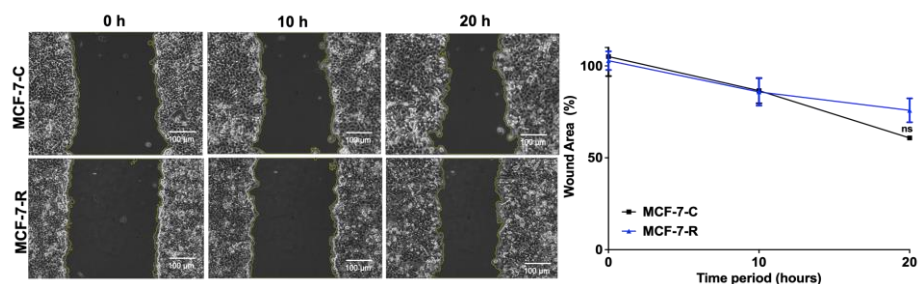


Figure 48. R04929097 resistance shows no change in the migration rate for MCF-7 breast cancer cells. Migration phenotype was evaluated by wound healing assay. Time-lapse microscopy images of wound closure of untreated and treated with R04929097 (IC_{200}) MCF-7 cells at $t=0$, 10, and 20 h after the wound formation were analyzed via Image J. Yellow lining defines the area lacking cells. Scale bars, 100 μm . (B) Quantification of the wounded area invaded control and R04929097 treated MCF-7 cells. (ns: not significant).

4.5. Intrinsic MK0752 resistance and Docetaxel and Cisplatin's synergistic activities with MK0752 in MDA-MB-231 cells

Half maximal doses (IC_{50}) of MK0752 were measured for intrinsic resistance scaling. IC_{50} of MK0752, for the MDA-MB-231 triple-negative breast cancer cell line, was initially determined by MTT assay and inhibition response was normalized as 66 μM for MK0752 (Figure 49).

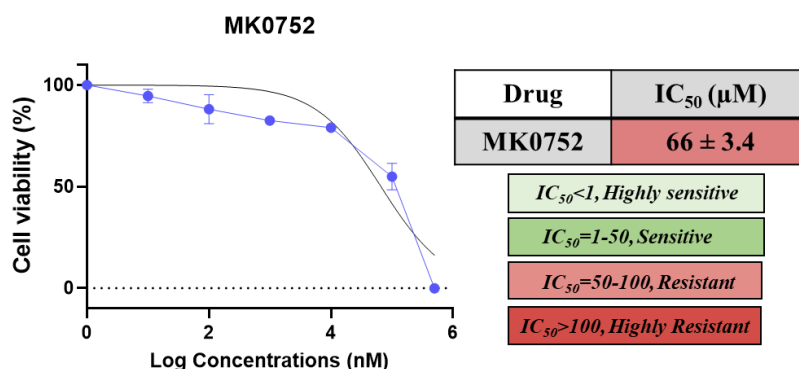


Figure 49. IC_{50} curves of MDA-MB-231 breast cancer cell line to MK0752 treatments.

The sensitivity scale represents MDA-MB-231's innate resistance against MK0752. Docetaxel and Cisplatin is combined with various GSIs exhibits successful preclinical/clinical outcome for breast cancer. Yet the synergistic effect of such combination remains unstudied for MK0752. To investigate potential synergistic outcomes with Cisplatin and Docetaxel, cell viability data was plotted and measured by Bliss synergy score. Bliss score of MK0752 combinations of MDA-MB-231 with Docetaxel 3.6 (Figure 50) and Cisplatin represented as 8.2 (Figure 51) and MK0752's combination either with Cisplatin or Docetaxel showed a highly additive pattern. These results suggest that MK0752 can be used in combinational treatments with Cisplatin and Docetaxel for MDA-MB-231 treatments.

According to the suggested optimum synergistic dose (IC_{100} of each drug) determined by the Bliss chart, MK0752 combinational treatments were performed by MTT cell viability assay. Cell viability of non-treated MDA-MB-231 decreased by 56% for MK0752 and Docetaxel treatments and Cisplatin by 47%. MK0752 single treatments compared to MK0752's combination with Docetaxel showed additional decrease by 6%. Docetaxel treatments compared to its MK0752 combinations were decreased further by 12%, Cisplatin combinations with MK0752 decreased the viability to 52% (Figure 52). MK0752_Docetaxel sequential treatments resulted in 87%, MK0752_Cisplatin treatments by 88%, Cisplatin_MK0752 treatments showed 86% decrease when compared to control groups. Sequential treatments indicated no difference between the order of treatments (Figure 53).

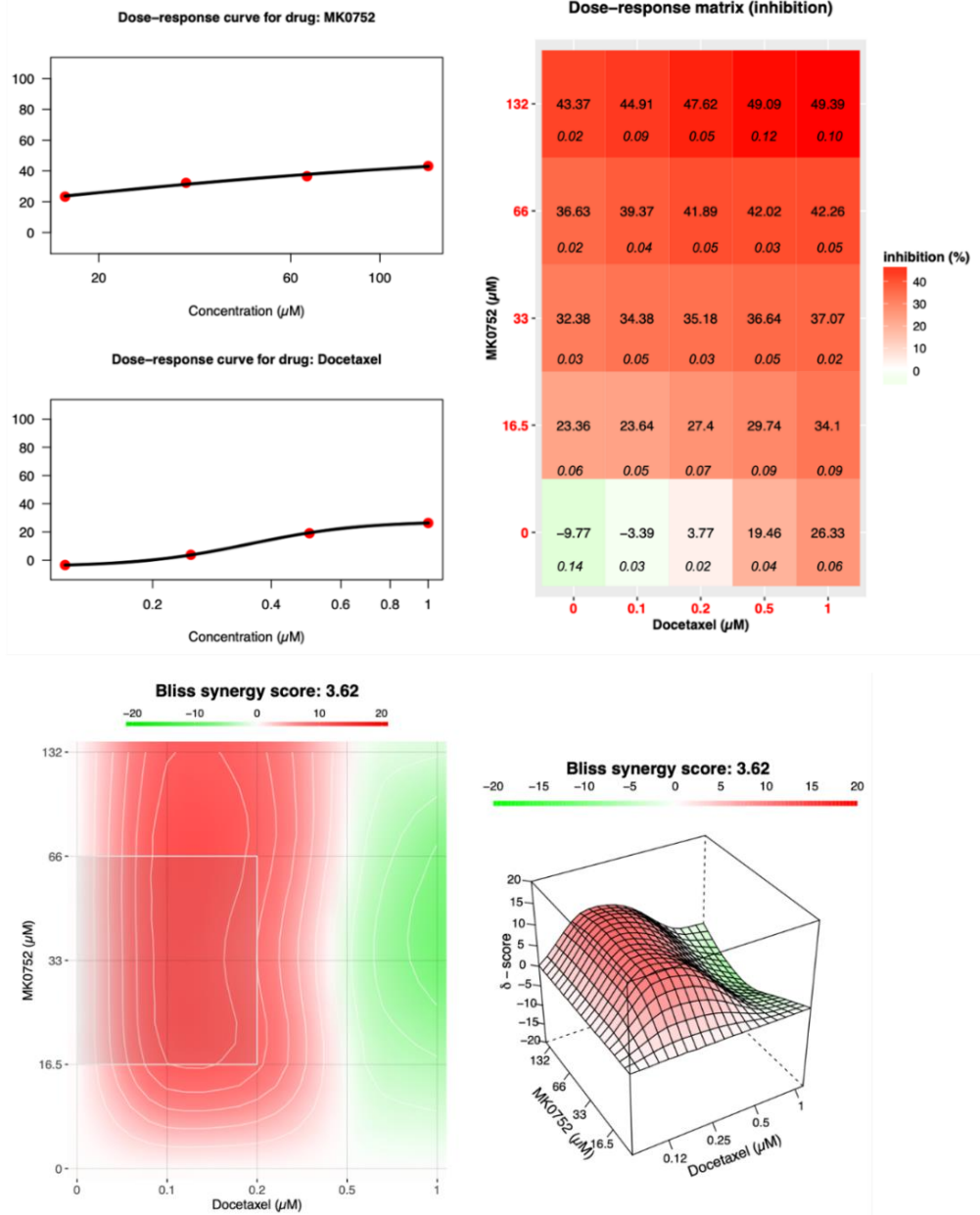


Figure 50. MK0752’s combination with Docetaxel results in additive effect for MDA-MB-231 cells. Drug synergy analysis of MK0752 with Docetaxel was conducted by Synergy Finder tool. Bliss synergy score of three independent experiments were analyzed for combinations. The drug response curve with the inhibition matrix and heatmap shows IC100 for MK0752 and Docetaxel was the optimum dose combination for MDA-MB-231 cell lines.

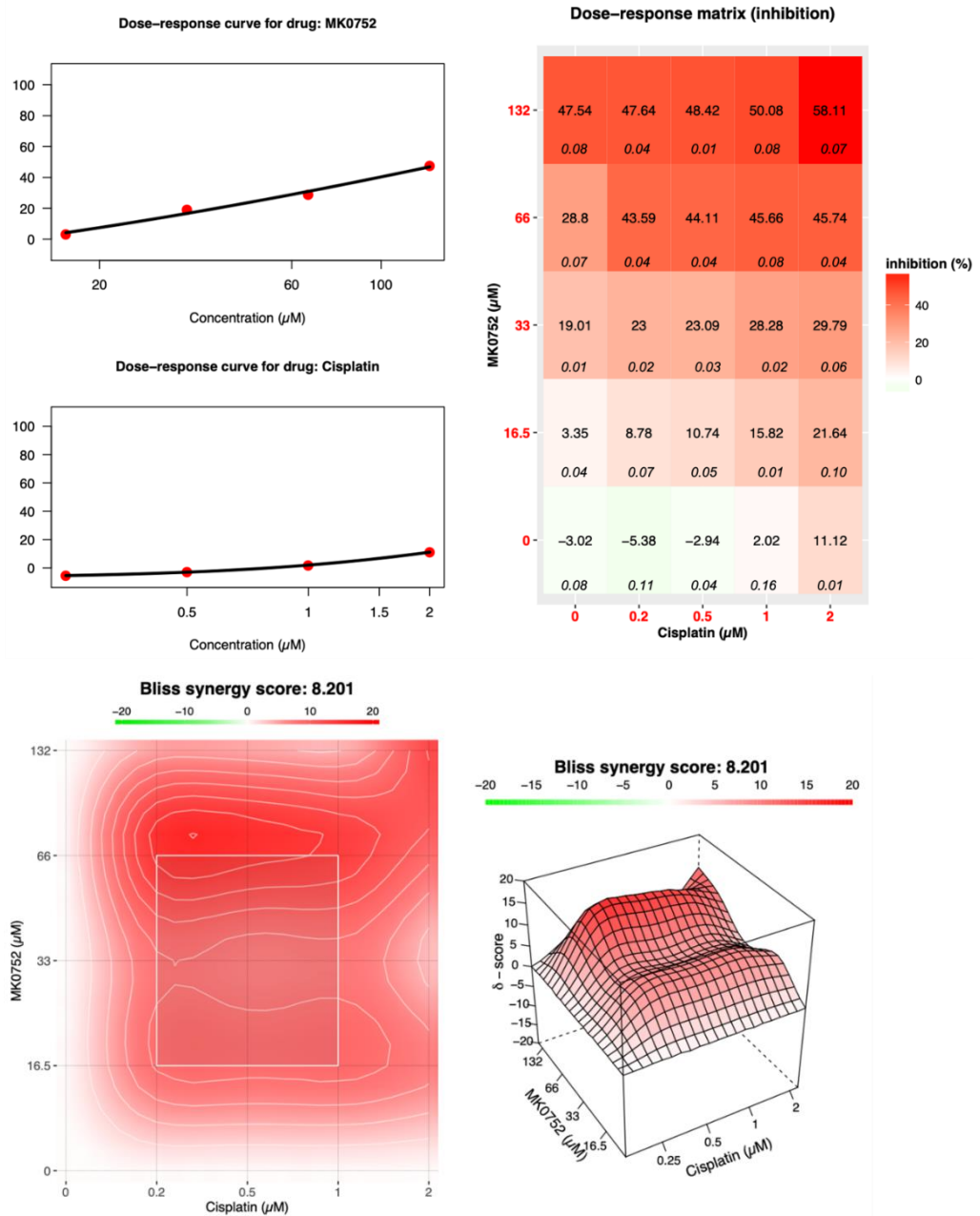


Figure 51. MK752’s combination with Cisplatin results in additive effect for MDA-MB-231 cells. Drug synergy analysis of MK752 with Cisplatin was conducted by Synergy Finder tool. Bliss synergy score of three independent experiments were analyzed for combinations. The drug response curve with the inhibition matrix and heatmap shows IC₁₀₀ for MK752 and Cisplatin was the optimum dose combination for MDA-MB-231 cell lines.

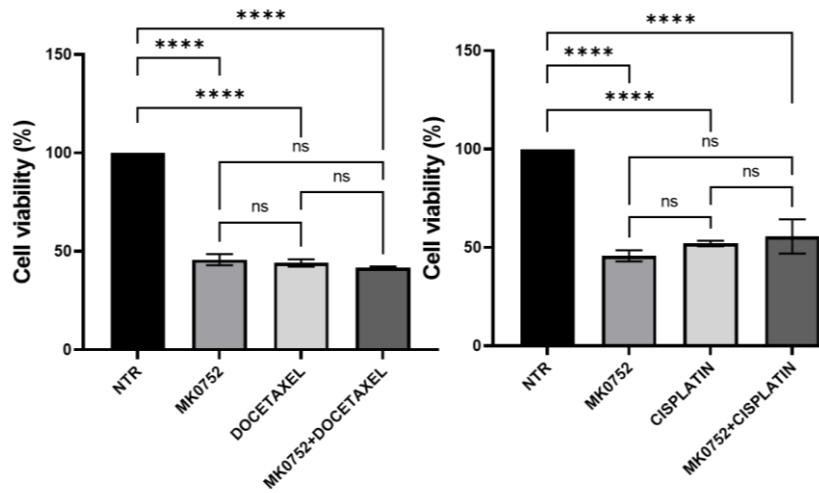


Figure 52. Decreased viability ratios of MDA-MB-231 cells in response to MK0752, Docetaxel and Cisplatin treatments. MTT assay was carried out after the cells were treated with IC₁₀₀ of MK0752 (for 24 hours), Docetaxel (for 48 hours), Cisplatin (for 72 hours) alone or in combinations which applied simultaneously. Combinational treatments performed with Docetaxel for 48 hours and with Cisplatin for 72 hours. (ns: not significant, *p<0.05, **p<0.01, ***p<0.001).

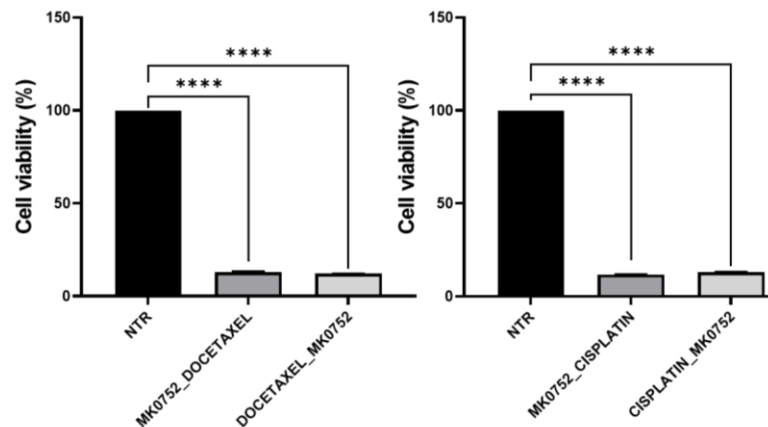


Figure 53. Decreased viability ratios of MDA-MB-231 cells in response to sequential MK0752, Docetaxel and Cisplatin treatments. (ns: not significant, *p<0.05, **p<0.01, ***p<0.001).

4.5.1. MK0752 Combinations with Cisplatin and Docetaxel in MDA-MB-231 spheroids

Tumors evade apoptosis and induce drug resistance through the regulation of pH and acidity through various events. 3D cell cultures mimic such pH alterations and acidosis that are commonly used for monolayer culture comparisons. Comparing both monolayers (2D) and spheroid (3D) setups were conducted to understand the potential effects of acidosis on MK0752 and its combinations with Docetaxel and Cisplatin's tolerance in breast cancer. MDA-MB-231 spheroids were treated with IC₁₀₀ of MK0752 and its combinations with IC₁₀₀ of Docetaxel or Cisplatin the optimum synergistic dose measured by the Bliss chart. Spheroid areas were measured by Spheroid J plugin and days (0,1,2 and 3) were compared within the experiment group. Results were normalized to the untreated condition and each treatment's day 0 condition (Figure 54). MK0752 treated MDA-MB-231 spheroids represented 65% decrease in the sphere size. Docetaxel single agent treatments showed no change when compared to MK0752 combined Docetaxel treatments as well as Cisplatin treatments. Yet, MK0752 combined with Cisplatin resulted in 45% decreased sphere size. Each day of Docetaxel and its MK0752 combinations showed a significant decrease in the spheroid volume (Figure 55). MDA-MB-231 spheroid treatment's APA cell viability results showed MK0752 single treatments showed 47%, Docetaxel treatments 59% and Cisplatin treatments decreased by 53% when compared to the control group (Figure 56A). MK0752 combinations with Docetaxel resulted in 66% decrease, and Cisplatin resulted in 62% decrease when compared to the control group (Figure 56B). MK0752 combined with Docetaxel and MK0752 combined with Cisplatin represents significant change when compared to their single treatments. Cisplatin combinations showed 15% change when compared to MK0752 single-agent treatments. Docetaxel or Cisplatin's single agent treatments compared to their combination with MK0752 treatments resulted in 18% difference, although the change did not reach to a statistically significant level (Figure 56C). MK0752 single-agent treatments were compatible with Docetaxel and Cisplatin treatments which confirms its potential success in further single-agent treatments. Either combinational or sequential treatments of MK0752 with Docetaxel and Cisplatin resulted in lessened cell viability in MDA-MB-231 cells for both 2D and 3D cultures which strengthens their synergistic activities and supposes a promising treatment plan.

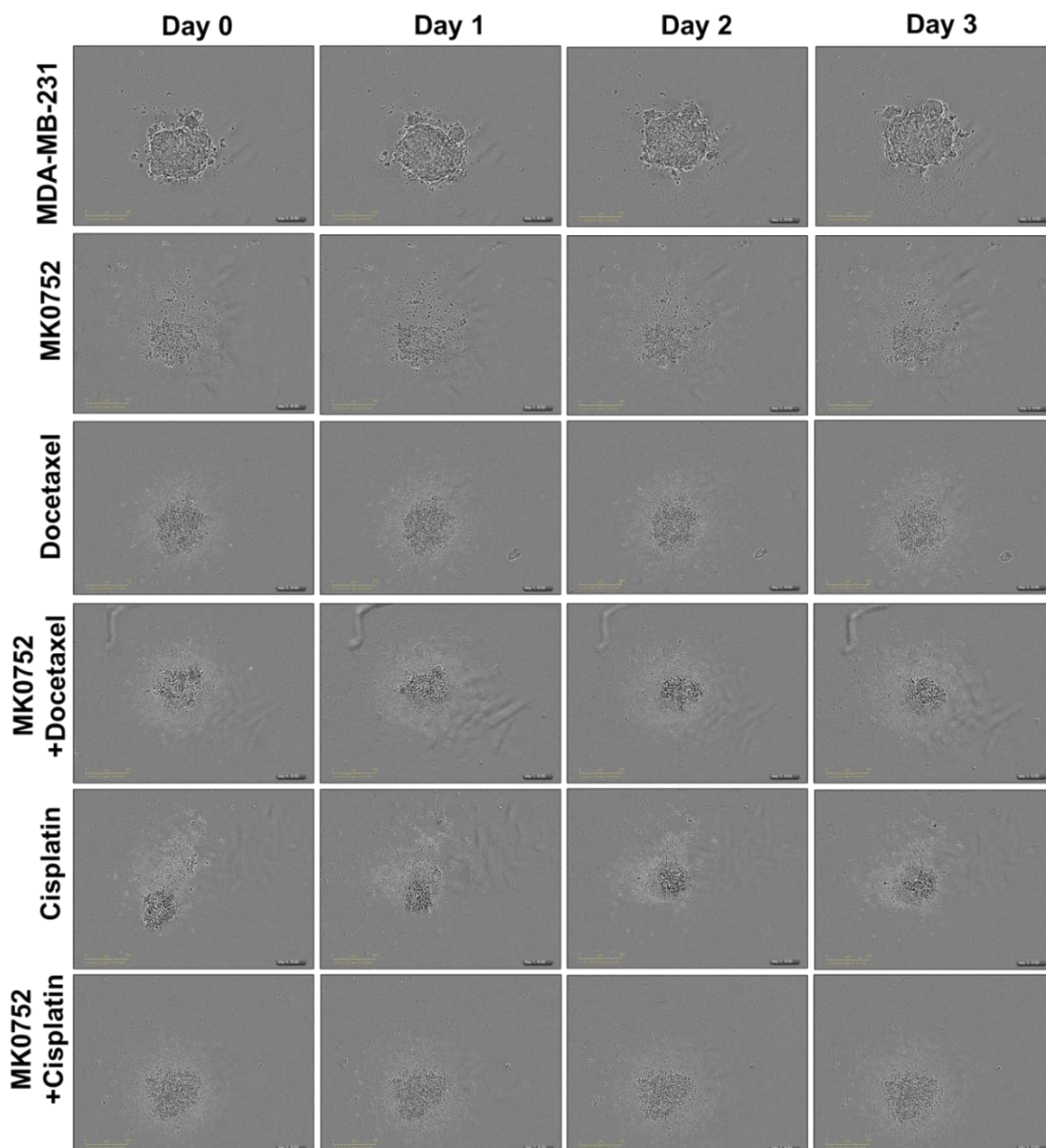


Figure 54. MK0752, Docetaxel and Cisplatin's both single agent and combinational treatments decreases MDA-MB-231 sphere size. MK0752 (for 24 hours), Docetaxel (for 48 hours) and Cisplatin (for 72 hours) treatments were applied after the spheroids were formed. The doses were set to IC₁₀₀ of MK0752, Docetaxel and Cisplatin. Images taken by Incucyte Cell Analysis Systems.

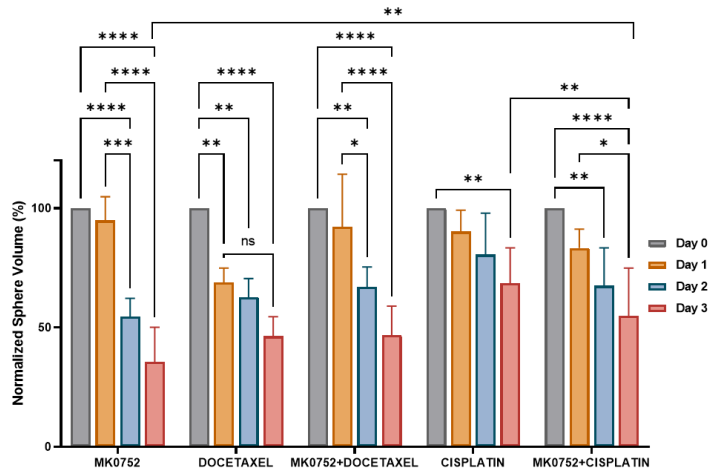


Figure 55. MK0752, Docetaxel, Cisplatin and their combinations reduces MDA-MB-231 sphere size. Normalized Area of measured from spheroid images were graphed. MK0752 (for 24 hours), Docetaxel (for 48 hours) and Cisplatin (for 72 hours) treatments were applied after the spheroids were formed. The doses were set to IC_{100} of MK0752, Docetaxel and Cisplatin. (* $p < 0.05$, ** $p < 0.01$, *** $p < 0.001$ and **** $p < 0.0001$).

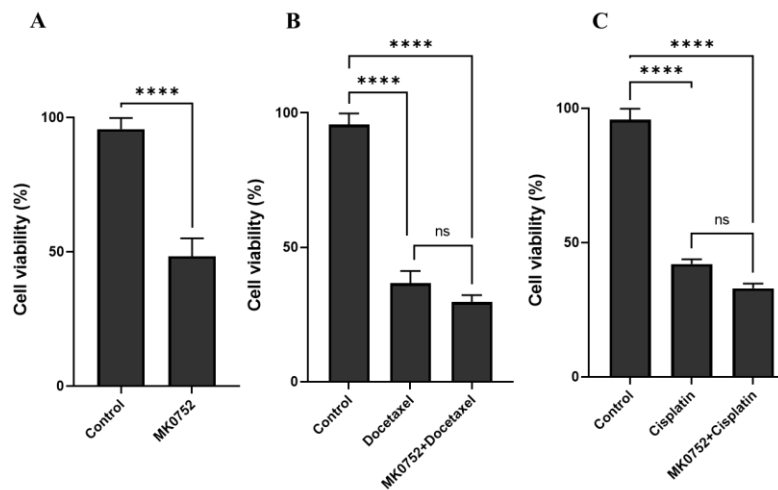


Figure 56. Decreased viability of MDA-MB-231 spheroids in response to MK0752, Docetaxel and Cisplatin treatments and their combinations. (A) MK0752 (for 24 hours), (B) Docetaxel (for 48 hours) and (C) Cisplatin (for 72 hours) (ns: not significant, * $p < 0.05$, ** $p < 0.01$, *** $p < 0.001$, **** $p < 0.0001$).

4.6. Intrinsic MK0752 resistance and Docetaxel and Cisplatin's synergistic activities with MK0752 in MCF-7 cells

Half maximal doses (IC_{50}) of MK0752 were measured for intrinsic resistance scaling. IC_{50} of MK072, for MCF-7 breast cancer cell line was initially determined by MTT assay and inhibition response was normalized as 75 μ M for MK0752 treatments. Sensitivity scale represents MCF-7's natural resistance against MK0752 (Figure 57). To investigate MK0752's potential synergistic outcomes with Cisplatin and Docetaxel, cell viability data was plotted and measured by Bliss synergy score. Bliss score of MK0752 combinations of wereF-7 with Docetaxel was 11.8 (Figure 58) indicating a synergistic and with Cisplatin it was 6.1 (Figure 59) indicating an additive effect. These results suggests that DAPT can be used in combinational treatments with Cisplatin and Docetaxel for MCF-7 treatments. According to the suggested optimum synergistic dose determined by the Bliss chart, MK0752 combinational treatments were performed via MTT cell viability assay. Cell viability of non-treated MCF-7 decreased to 54% for MK0752, Docetaxel to 34% and Cisplatin treatments to 46%. MK0752's combination with Docetaxel decreased to 18% and its Cisplatin combination decreased to 23%. Docetaxel treatments compared to MK0752 combinations were decreased by 16%, Cisplatin single agent treatments compared to MK0752, and Cisplatin combinations showed 23% decrease. (Figure 60).

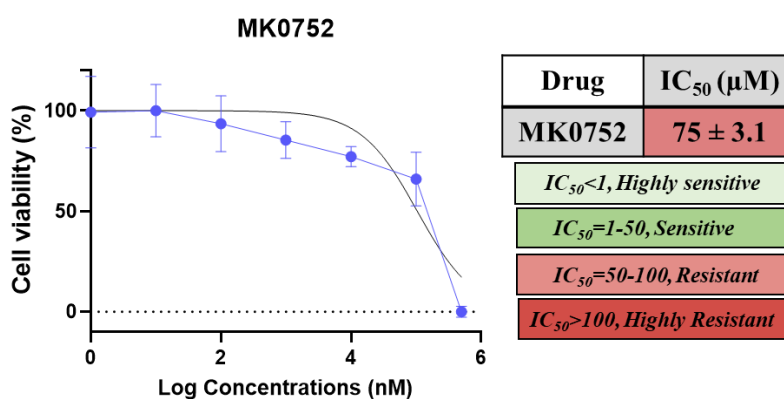


Figure 57. IC_{50} curves of MCF-7 cell lines to MK0752 treatments. MTT absorbance values were normalized and graphed by using Graph Pad PRISM 8.

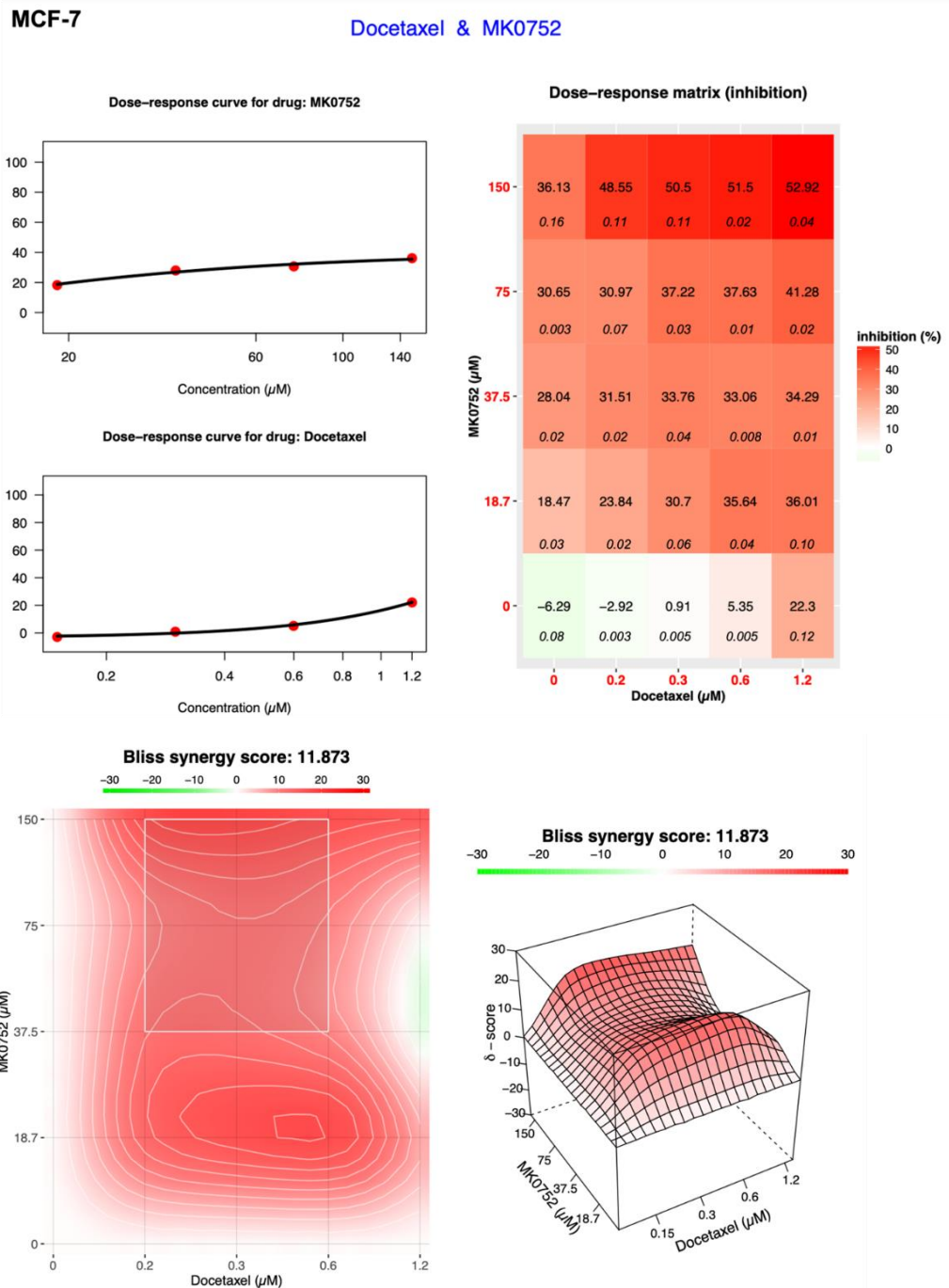


Figure 58. MK0752's combination with Docetaxel results in synergistic effect for MCF-7 cells. Drug synergy analysis of MK0752 with Docetaxel was conducted by Synergy Finder tool. Bliss synergy score of three independent experiments were analyzed for combinations. The drug response curve with the inhibition matrix and heatmap shows IC₁₀₀ for MK0752 and Docetaxel was the optimum dose combination for MCF-7 cell lines.

MCF-7

Cisplatin & MK0752

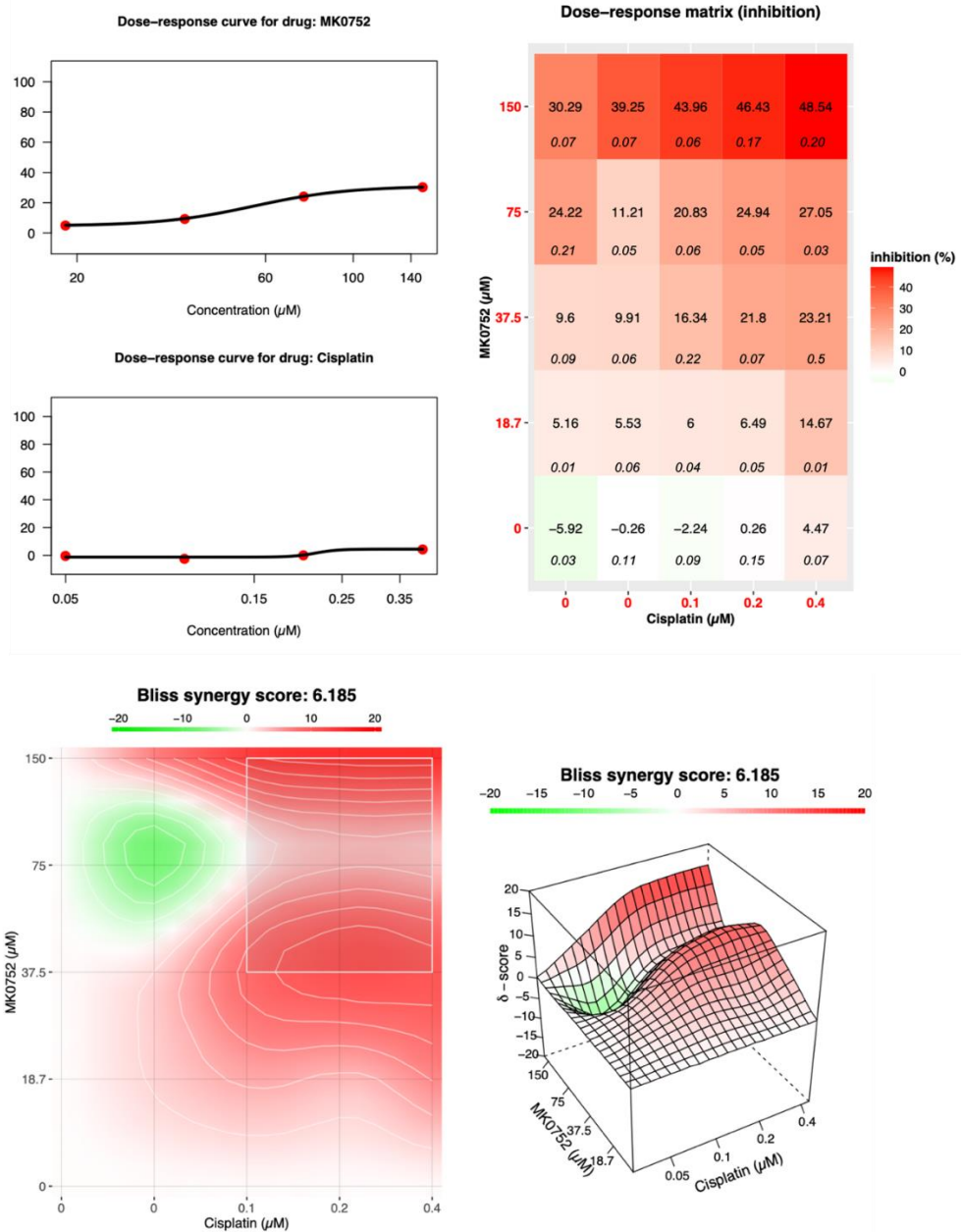


Figure 59. MK0752's combination with Cisplatin results in additive effect for MCF-7 cells. Drug synergy analysis of MK0752 with Cisplatin was conducted by Synergy Finder tool. Bliss synergy score of three independent experiments were analyzed for combinations. The drug response curve with the inhibition matrix and heatmap shows IC_{100} for MK0752 and Cisplatin was the optimum dose combination for MCF-7 cell lines.

MK0752_Docetaxel sequential treatments resulted in 31% decrease as well as MK0752_Cisplatin treatments to 23%. Cisplatin_MK0752 treatments showed 10% viability when compared to control groups. MK0752_Cisplatin compared to Cisplatin_MK0752 treatments showed 13% difference and MK0752_Docetaxel compared to Docetaxel_MK0752 treatments showed 8% difference (Figure 61).

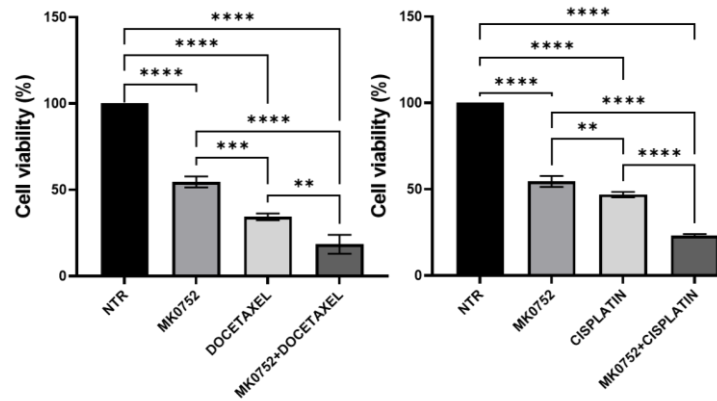


Figure 60. Decreased viability ratios of MCF-7 cells in response to MK0752, Docetaxel and Cisplatin treatments. MTT assay was carried out after the cells were treated with IC₁₀₀ of MK0752 (for 24 hours), Docetaxel (for 48 hours), Cisplatin (for 72 hours) alone or in combinations which applied simultaneously. (**p<0.01, ***p<0.001, ****p<0.0001).

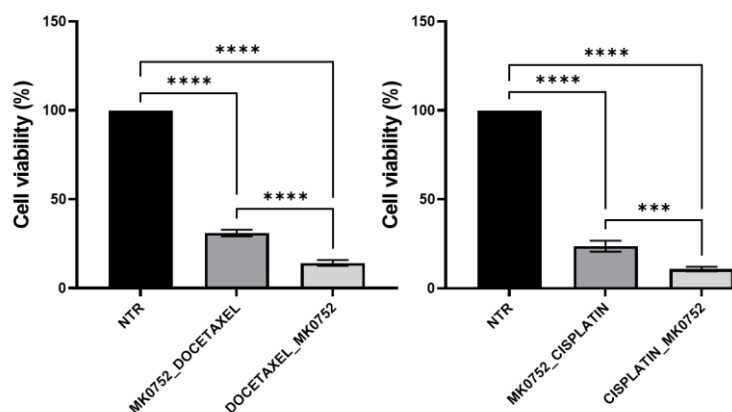


Figure 61. Decreased viability ratios of MCF-7 cells in response to sequential MK0752, Docetaxel and Cisplatin treatments. (**p<0.001, ****p<0.0001).

4.6.1. MK0752 Combinations with Cisplatin and Docetaxel in MCF-7 spheroids

Tumours evade apoptosis and induce drug resistance through the regulation of pH and acidity through various events. 3D cell cultures mimic such pH alterations and acidosis that are commonly used for monolayer culture comparisons. Comparing both monolayers (2D) and spheroid (3D) setups were conducted to understand the potential effects of acidosis on MK0752 and its combinations with Docetaxel and Cisplatin's tolerance in breast cancer. MCF-7 spheroids were treated with IC_{100} of MK0752 and its combinations with IC_{100} of Docetaxel or Cisplatin the optimum synergistic dose measured by the Bliss chart. Spheroid areas were measured by Spheroid J plugin and days (0,1,2 and 3) were compared within the experiment group. Results were normalized to the untreated condition and each treatment's day 0 condition. MCF-7 spheroids were treated with the optimum synergistic dose measured by the Bliss chart, IC_{100} of MK0752 and its combinations with IC_{100} of Docetaxel or Cisplatin. Spheroid areas were measured by Spheroid J plugin and days were compared within the experiment group to the addition of comparisons to treatments day 3 data (Figure 62). All data was normalized to the untreated condition and each treatment's day 0 condition. MK0752 treated MCF-7 spheroids represented shrinking to 72% at day 3. Docetaxel single agent treatments showed 50% decrease and its MK0752 combinations represented 57% decrease in sphere volume. Each day of Docetaxel and MK0752 combinations with Cisplatin showed significant decrease in the spheroid volume. Cisplatin single agent treatments showed 61% sphere size whereas its MK0752 combination decrease the sphere volume to 41% (Figure 63). MCF-7 spheroid treatment's APA cell viability results showed MK0752 single treatments showed 35%, Docetaxel treatments 32% and Cisplatin treatments decreased by 27% when compared to the control group (Figure 64 A). MK0752 combinations with Docetaxel resulted in 40% decrease, and Cisplatin resulted in 41% decrease when compared to MK0752 single agent treatments. MK0752 combined with Docetaxel and MK0752 combined with Cisplatin represents significant change when compared to their single treatments. Docetaxel single treatments showed 37% decrease when compared to the control group. Cisplatin combinations showed 57% change when compared to the nontreated group. Docetaxel or Cisplatin's single agent treatments compared to their combination with

MK0752 treatments resulted in 22% difference (Figure 64 B and C). MK0752 single-agent treatments were compatible with Docetaxel and Cisplatin treatments which confirms its potential success in further single-agent treatments. Either combinational or sequential treatments of MK0752 with Docetaxel and Cisplatin resulted in decreased cell viability in MCF-7 cells for both 2D and 3D cultures which strengthens their synergistic activities and suggest a promising treatment plan.

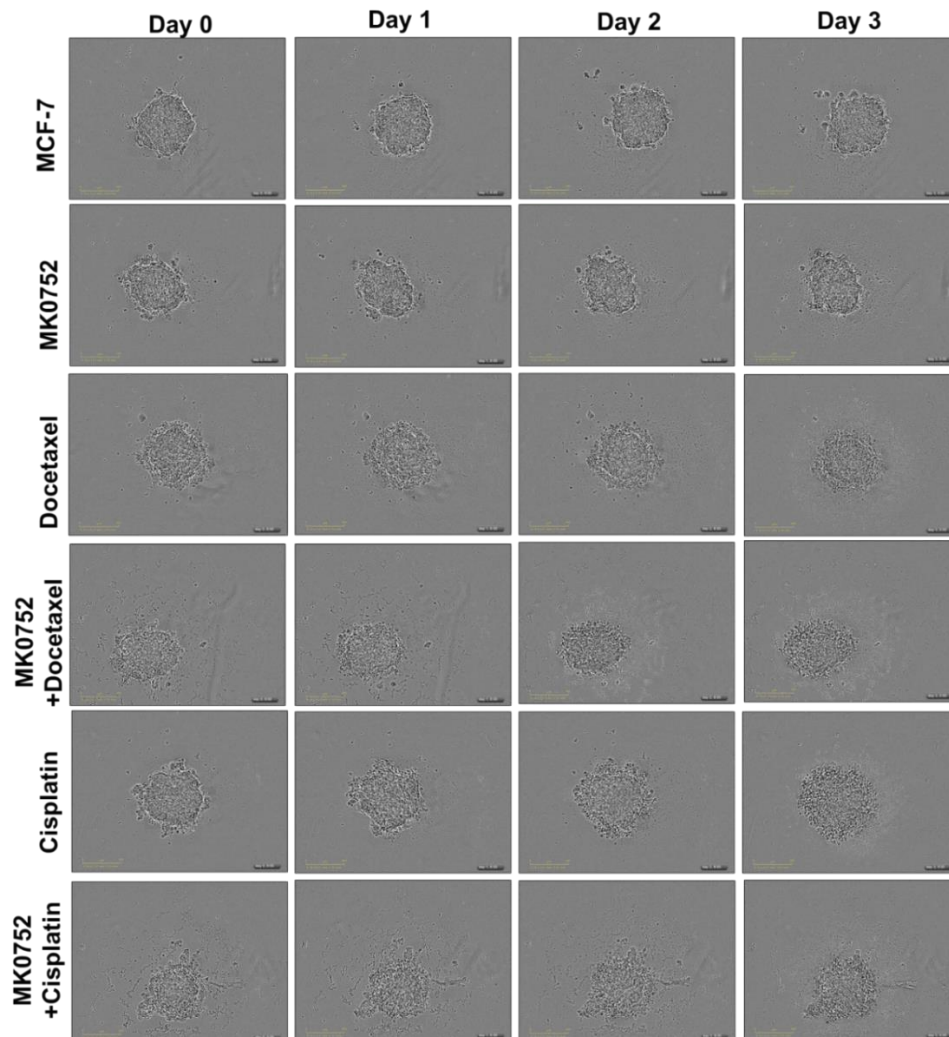


Figure 62. MK0752, Docetaxel and Cisplatin's both single agent and combinational treatments decreases MCF-7 sphere size. MK0752 (for 24 hours), Docetaxel (for 48 hours) and Cisplatin (for 72 hours) treatments were applied after the spheroids were formed. The doses were set to IC_{100} of MK0752, Docetaxel and Cisplatin. Images taken by Incucyte Cell Analysis Systems.

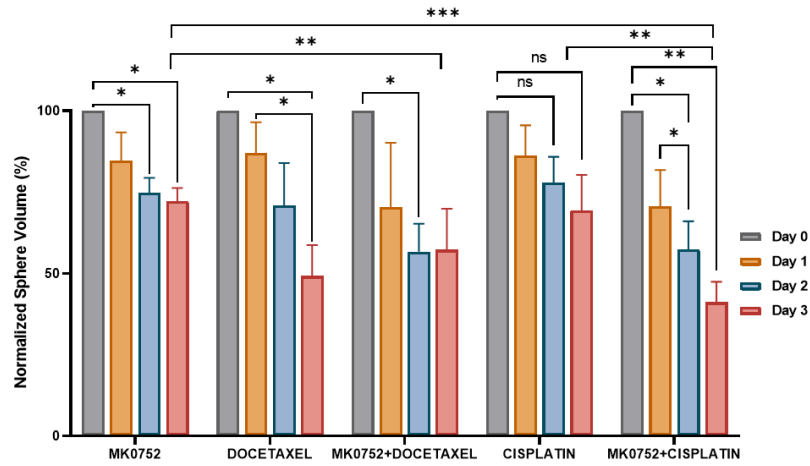


Figure 63. MK0752, Docetaxel, Cisplatin and their combinations reduces MCF-7 spheroid size. Normalized Area of measured from spheroid images were graphed. MK0752 (for 24 hours), Docetaxel (for 48 hours) and Cisplatin (for 72 hours) treatments were applied after the spheroids were formed. (* $p < 0.05$, ** $p < 0.01$, *** $p < 0.001$ and **** $p < 0.0001$).

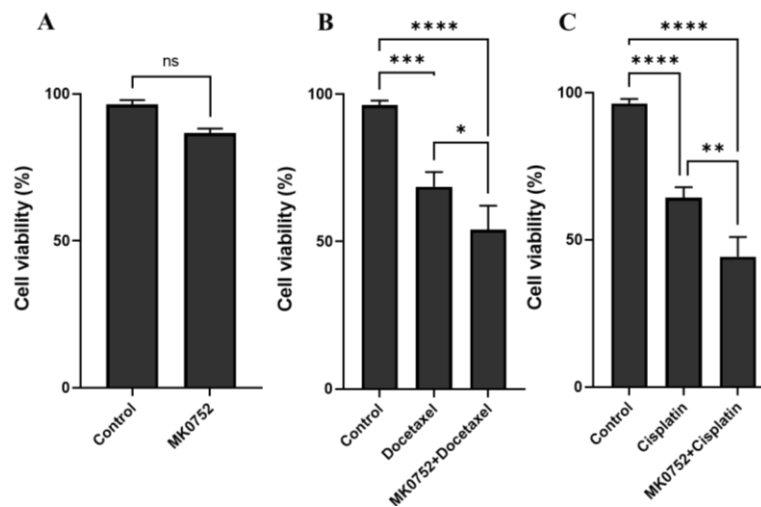


Figure 64. Decreased viability of MCF-7 spheroids in response to MK0752, Docetaxel and Cisplatin treatments and their combinations. (A) MK0752 (for 24 hours), (B) Docetaxel (for 48 hours) and (C) Cisplatin (for 72 hours) treatments were applied after the spheroids were formed. (ns: not significant, * $p < 0.05$, ** $p < 0.01$, *** $p < 0.001$, **** $p < 0.0001$).

4.7. MK0752 Resistance in Ovarian Cancer Cells

4.7.1. Intrinsic MK0752 resistance and Docetaxel, Cisplatin synergistic effects in Ovarian Cancer Cells

Half maximal doses (IC_{50}) of MK0752, Cisplatin and Docetaxel were measured for intrinsic resistance scaling and determining tolerable dose range for further acquired resistance studies. SKOV-3, IGROV-1, A2780, BG-1 ovarian cancer cell lines were treated with logarithmically increasing doses of MK0752 for 24 hours and MTT absorbances were normalized and set into toxicity response curve of Graph Pad PRISM 8. IGROV-1's IC_{50} for Cisplatin 2.2 μ M, Docetaxel 7.7 μ M and MK0752 was 68 μ M. A2780's IC_{50} for Cisplatin 0.2 μ M, Docetaxel 0.06 μ M and MK0752 was 66 μ M. BG-1's IC_{50} for Cisplatin 0.5 μ M, Docetaxel 0.05 μ M and MK0752 was 0.2 μ M. SKOV-3's IC_{50} for Cisplatin 2.9 μ M, Docetaxel 2.2 μ M and MK0752 was 0.9 μ M. A2780, BG-1, SKOV-3 cells were highly sensitive and IGROV-1 cells were moderate sensitive to Cisplatin and Docetaxel (Figure 65). Continuously, IGROV-1 and A2780 responses were moderate resistant, and BG-1 and SKOV-3 were highly sensitive to MK0752 treatments. Docetaxel and Cisplatin is combined with various GSIs exhibits successful preclinical/clinical outcome for breast cancer. Yet the synergistic effect of such combination remains unstudied for MK0752. To investigate potential synergistic outcomes with Cisplatin and Docetaxel, cell viability data was plotted and measured by Bliss synergy score. Synergistic effects of MK0752 with Docetaxel and Cisplatin were assessed by Bliss synergy scoring. IGROV-1 cells synergistic score with Docetaxel 1.8 (Figure 66) and with Cisplatin were measured as -5.3 (Figure 67). IGROV-1^{CisR} cells Bliss synergistic score with Docetaxel were measured as 7.8 (Figure 68) and with Cisplatin 1.45 (Figure 69). All drug interactions for ovarian cancer cell lines showed additive effect of MK0752 on Cisplatin and Docetaxel combinations.

IGROV-1 and IGROV-1's Cisplatin resistant cell line IGROV-1^{CisR} were treated with MK0752, Docetaxel and Cisplatin single agent, combinational and sequential treatments. Treated IGROV-1's showed no difference when compared with IGROV-1^{CisR} except the Cisplatin treatments. Docetaxel treatments were not significantly different from Cisplatin treatments for IGROV-1 cells. IGROV-1 is sensitive to IC_{100} of Cisplatin treatments and MK0752 combinations decrease viability to 45% (Figure 70).

IGROV-1 and IGROV-1^{CisR} sequential treatments of initial MK0752 with Docetaxel resulted in 59% and 69% viability respectively. Docetaxel initial treatments decreased the cell viability to 6.9% for IGROV-1 and 12% for IGROV-1^{CisR} cells. MK0752 initial treatments followed by Cisplatin resulted in 61% cell viability for IGROV-1^{CisR} cells. Cisplatin initial treatments followed by MK0752, decreased the viability the most to 7% for IGROV-1 and 11% IGROV-1^{CisR} cells (Figure 71).

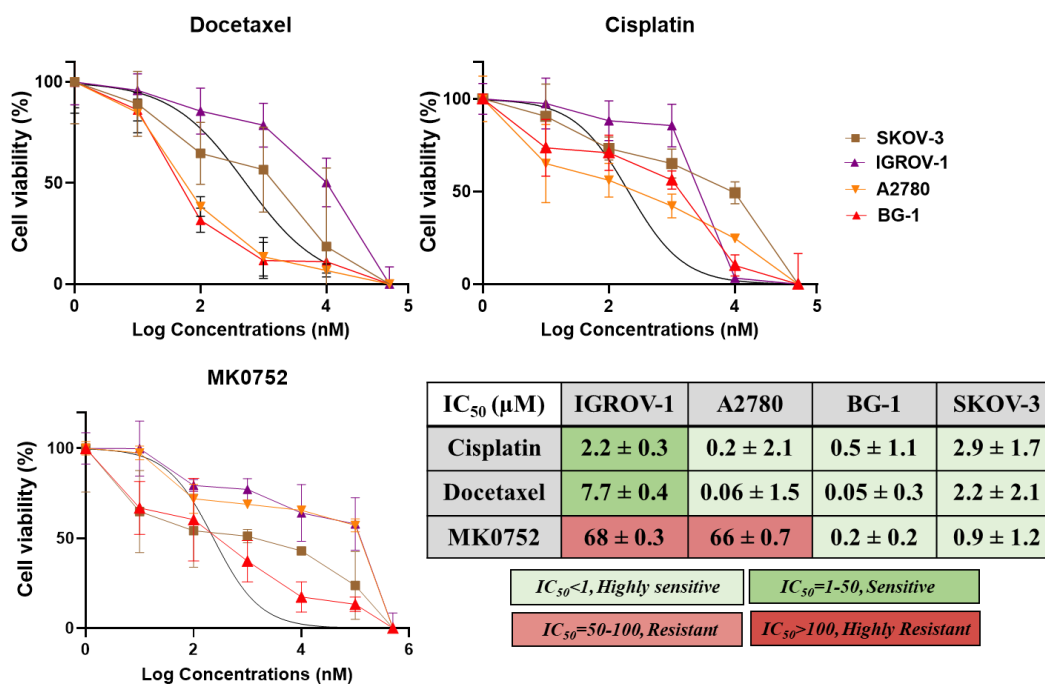


Figure 65. IC₅₀ curves of IGROV-1, SKOV3, A2780 and BG-1 cell lines to MK0752, Docetaxel, and Cisplatin treatments. MTT absorbance values were normalized and graphed by using Graph Pad PRISM 8.

IGROV-1

Docetaxel & MK0752

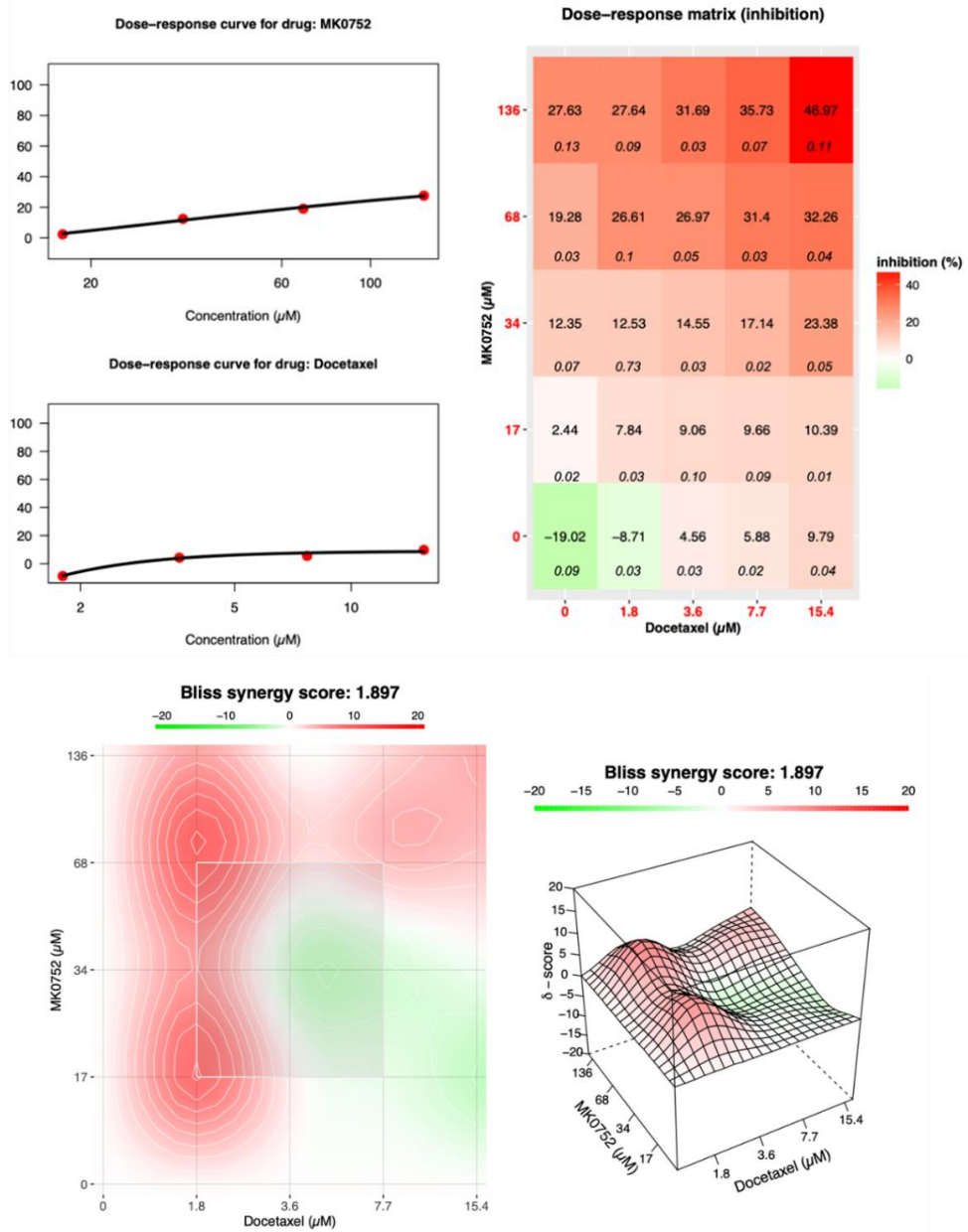


Figure 66. MK0752’s combination with Docetaxel results in additive effect for IGR-OV-1 cells. Drug synergy analysis of MK0752 with Docetaxel was conducted by Synergy Finder tool. Bliss synergy score of three independent experiments were analyzed for combinations. Drug response curve with the inhibition matrix and heatmap shows IC_{100} for MK0752 and Docetaxel was the optimum dose combination for IGROV-1 cell lines.

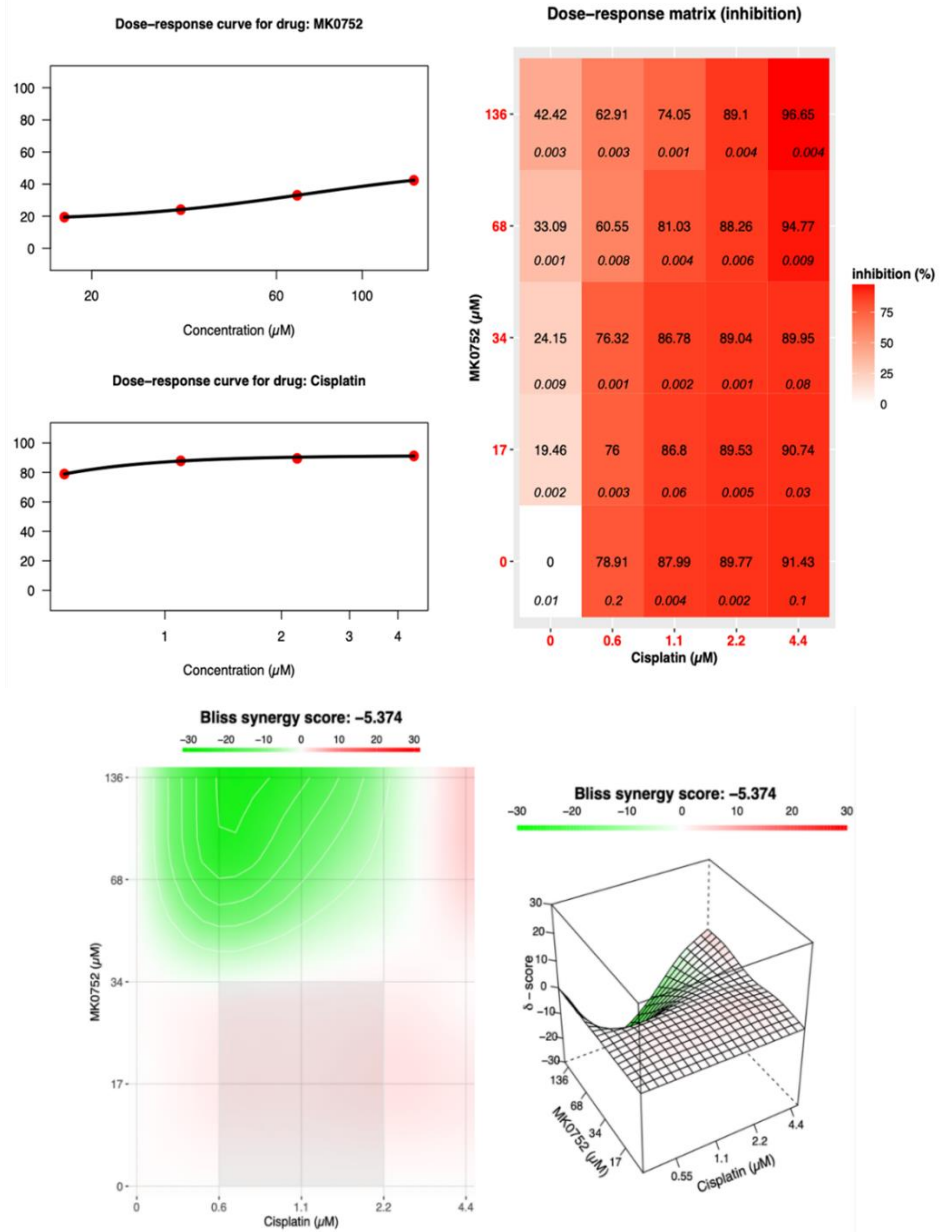


Figure 67. MK0752's combination with Cisplatin results in additive effect for IGROV-1 cells. Drug synergy analysis of MK0752 with Cisplatin was conducted by Synergy Finder tool. Bliss synergy score of three independent experiments were analyzed for combinations. Drug response curve with the inhibition matrix and heatmap shows IC_{100} for MK0752 and Cisplatin was the optimum dose combination for IGROV-1 cell lines.

IGROV-1CisR

Docetaxel & MK0752

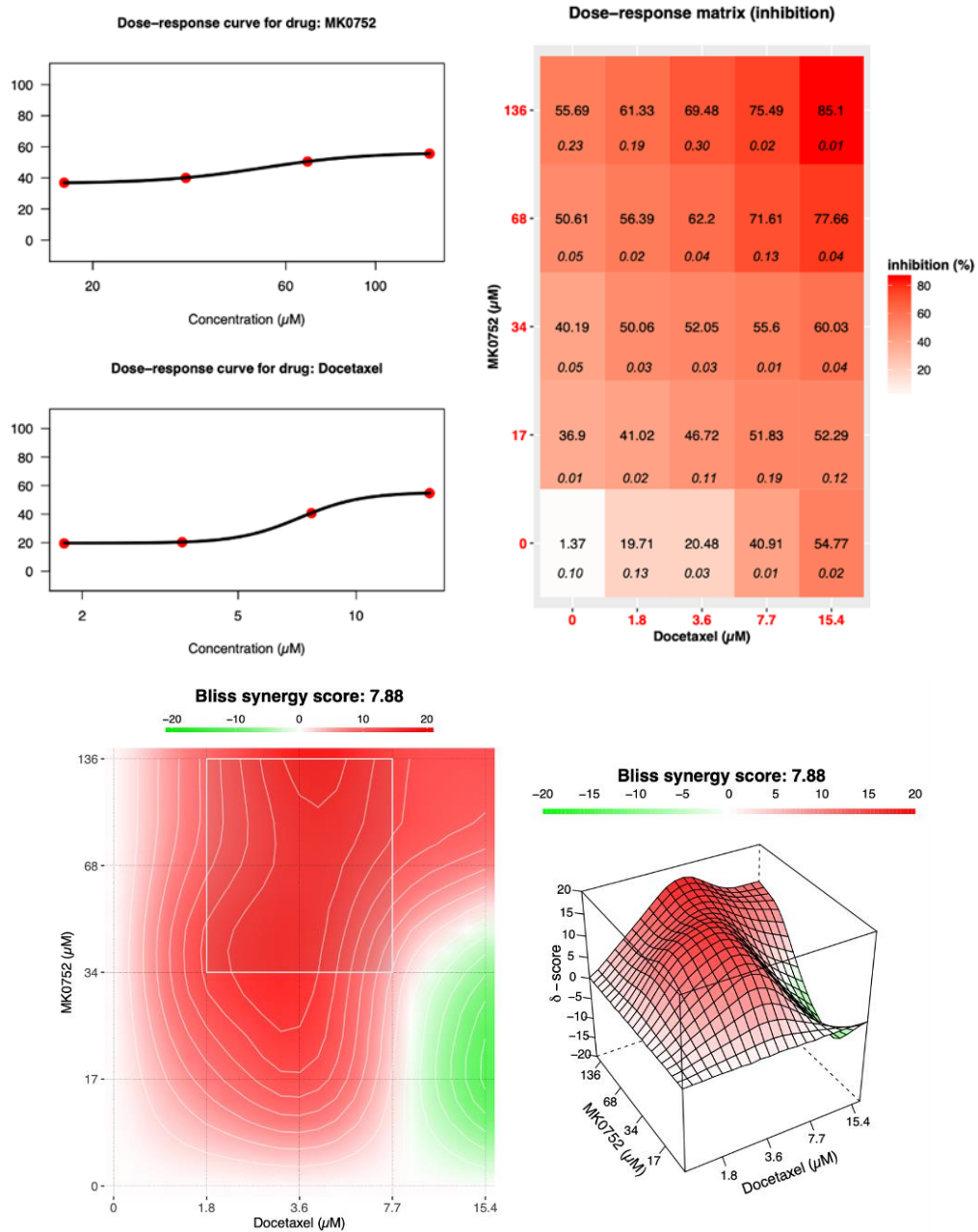


Figure 68. MK0752's combination with Docetaxel results in additive effect for IGR-OV-1^{CisR} cells. Drug synergy analysis of MK0752 with Docetaxel was conducted by Synergy Finder tool. Bliss synergy score of three independent experiments were analyzed for combinations. The drug response curve with the inhibition matrix and heatmap shows IC₁₀₀ for MK0752 and Docetaxel was the optimum dose combination for IGROV-1^{CisR} cell lines.

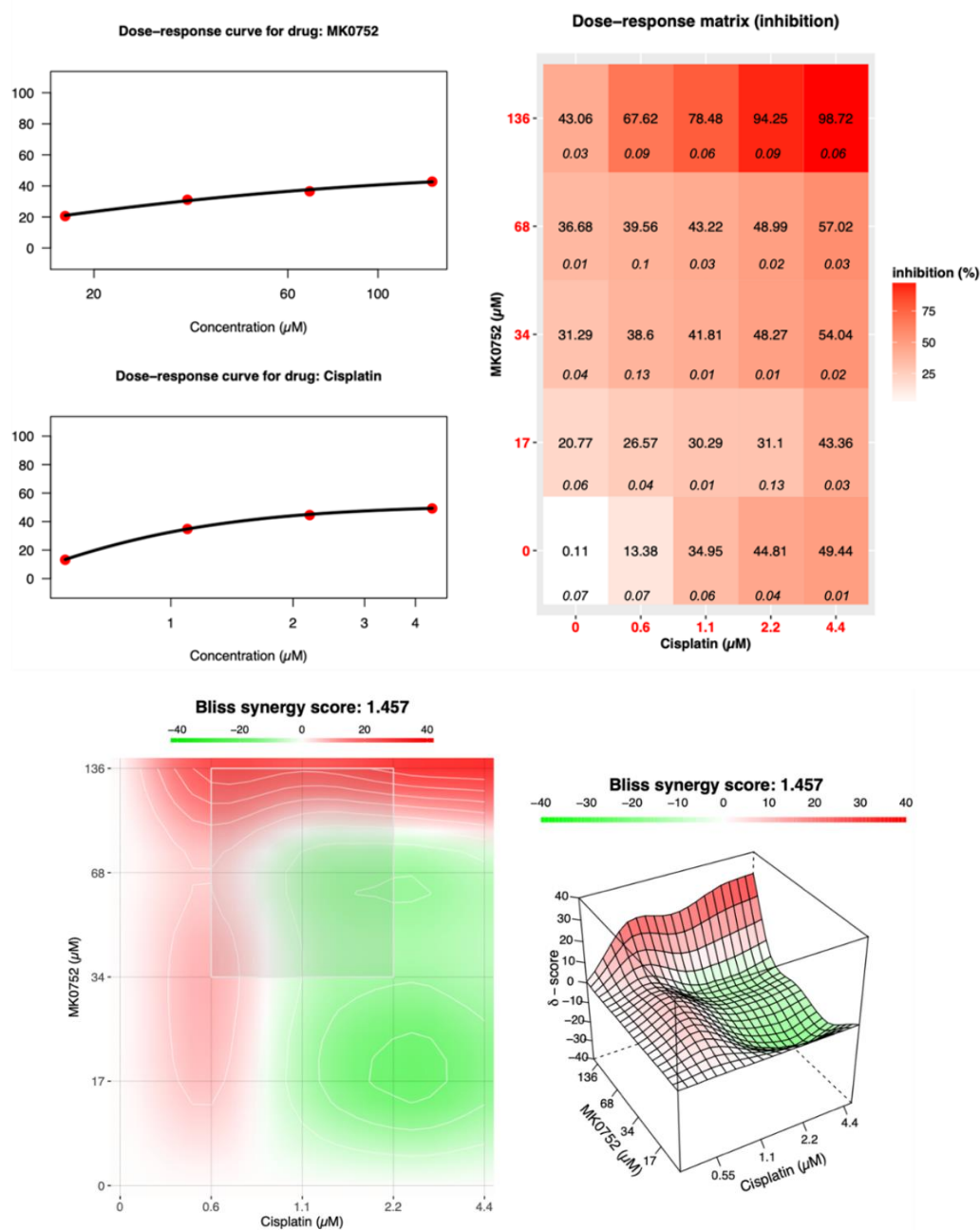


Figure 69. MK0752's combination with Cisplatin results in additive effect for IGROV-1^{CisR} cells. Drug synergy analysis of MK0752 with Cisplatin was conducted by Synergy Finder tool. Bliss synergy score of three independent experiments were analyzed for combinations. The drug response curve with the inhibition matrix and heatmap shows IC₁₀₀ for MK0752 and Cisplatin was the optimum dose combination for IGROV-1^{CisR} cell lines.

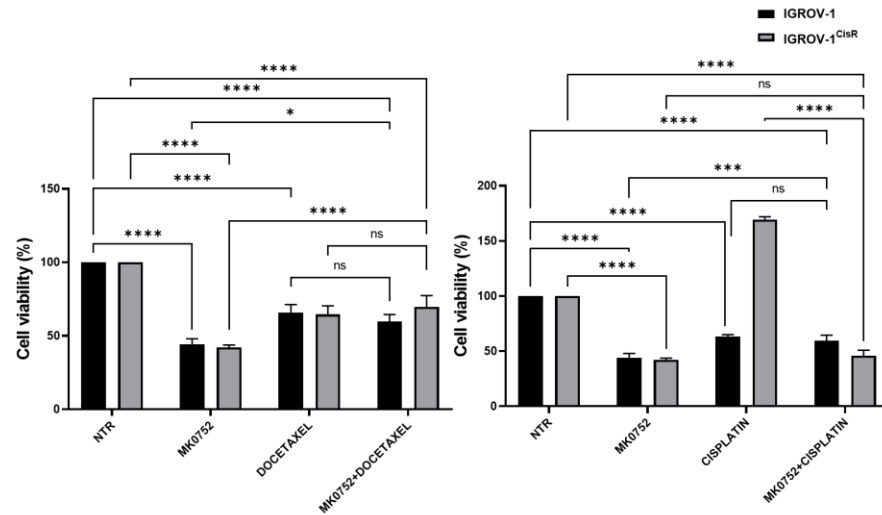


Figure 70. Decreased viability ratios of IGROV-1 and IGROV-1^{CisR} cells in response to MK0752, Docetaxel and Cisplatin treatments. MTT assay was carried out after the cells were treated with IC₁₀₀ of MK0752 (for 24 hours), Docetaxel (for 48 hours), Cisplatin (for 72 hours) alone or in combinations which applied simultaneously. (ns: not significant, *p<0.05, **p<0.01, ***p<0.001, ****p<0.0001).

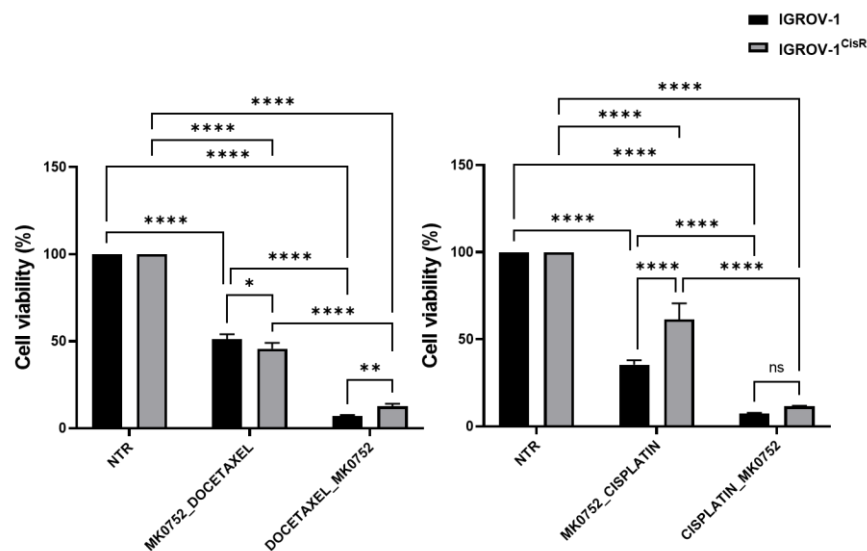


Figure 71. Decreased viability ratios of IGROV-1 and IGROV-1^{CisR} cells in response to sequential MK0752, Docetaxel and Cisplatin treatments. (ns: not significant, *p<0.05, **p<0.01, ***p<0.001).

A2780 cells synergistic score with Docetaxel were measured as 3.2 (Figure 72) and with Cisplatin 8.5 (Figure 73). A2780's single treatments indicated decrease when treated with MK0752 by 32%, with Docetaxel 48%, and with Cisplatin treatments by 37%. Docetaxel combinations with MK0752 decreased the viability to 58% and Cisplatin combinations with MK0752 decreased cell viability to 43% when compared to the nontreated control group. Docetaxel single agent treatments compared to its combinations with MK0752 resulted in decrease by 6%. Cisplatin combinations resulted in 20% difference when compared with Cisplatin single-agent treatments (Figure 74). MK0752 pre-treatments with Docetaxel decreased the viability to 28% and MK0752's pre-treatments with Cisplatin decreased the cell viability to 43%. Docetaxel initial treatment followed by MK0752 decreased to 18% and Cisplatin initial treatments decreased to 31% when compared to their nontreated conditions. Sequential treatments initially with Docetaxel differed by 10% and Cisplatin initial treatments changed the viability by 12% when compared with their MK0752 initial treatment combinations (Figure 75). Bliss score of MK0752 combinations of BG-1 cells with Docetaxel was 7.5 (Figure 76) whereas with Cisplatin was 4.1 (Figure 77). BG-1's single agent treatments showed decreased cell viability with MK0752 to 67%, Docetaxel to 86% and Cisplatin to 83%. Docetaxel combinations with MK0752 resulted in 53% and MK0752's Cisplatin combinations resulted in 61% viability. Docetaxel combinational treatments compared to single agents induced 43% difference whereas cisplatin combinational treatments with MK0752 compared to single agent treatments resulted in 21% difference. (Figure 78). MK0752 initial treatments with Docetaxel were decreased the viability to 26% and MK0752 sequential Cisplatin treatments to 24%. Docetaxel initial treatments followed by MK0752 resulted in 13% and Cisplatin initial treatments resulted in 27% cell viability. MK0752 sequential treatments with Docetaxel showed 13% difference when compared with Docetaxel initial treatments whereas Cisplatin sequential treatments showed 3% difference in cell viability (Figure 79). Bliss score of MK0752 combinations of SKOV-3 cells with Docetaxel was 7.5 (Figure 80) whereas with Cisplatin was 6.1 (Figure 81).

A2780

Docetaxel & MK0752

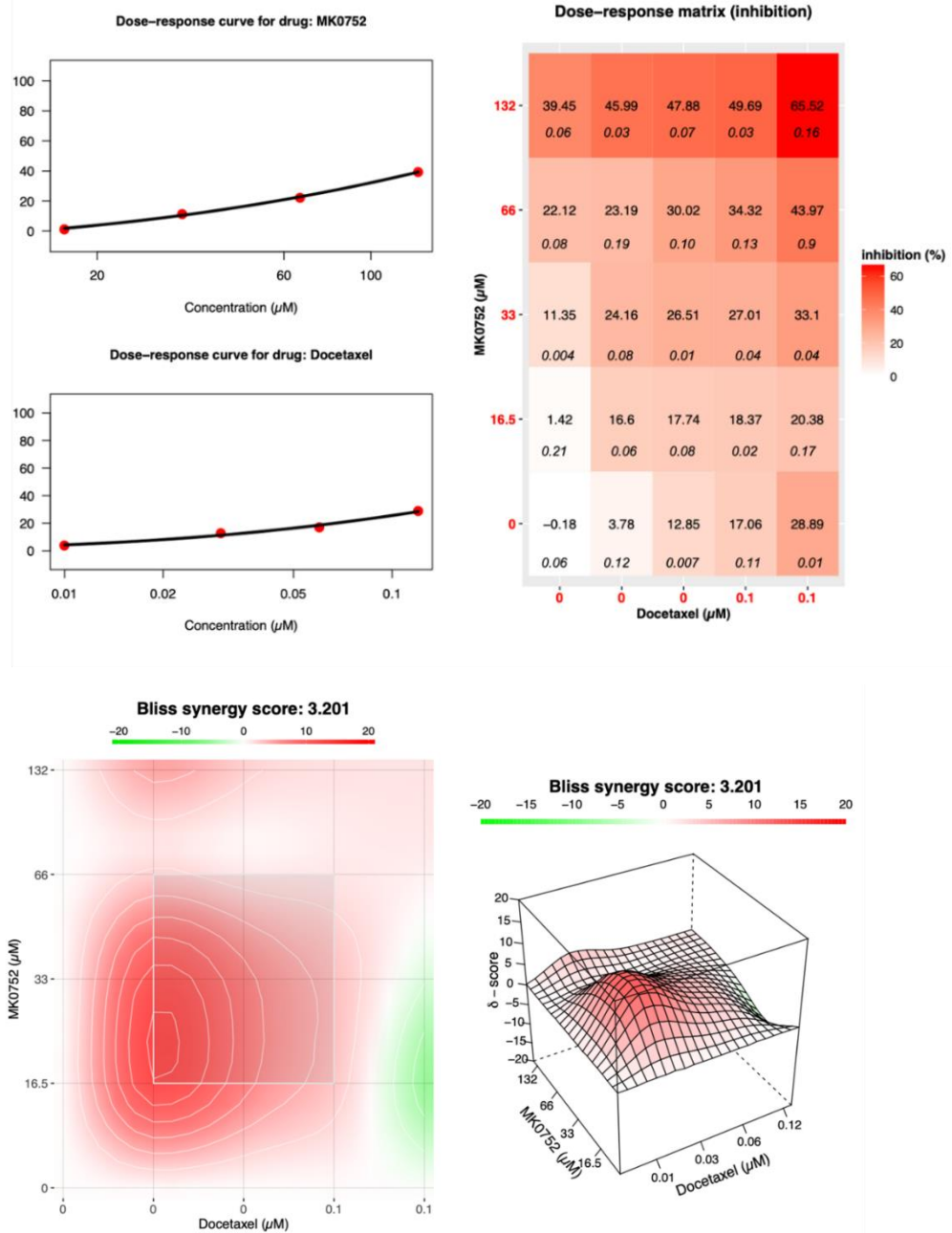


Figure 72. MK0752's combination with Docetaxel results in additive effect for A2780 cells. Drug synergy analysis of MK0752 with Docetaxel was conducted by Synergy Finder tool. Bliss synergy score of three independent experiments were analyzed for combinations. The drug response curve with the inhibition matrix and heatmap shows IC_{100} for MK0752 and Docetaxel was the optimum dose combination for A2780 cell lines.

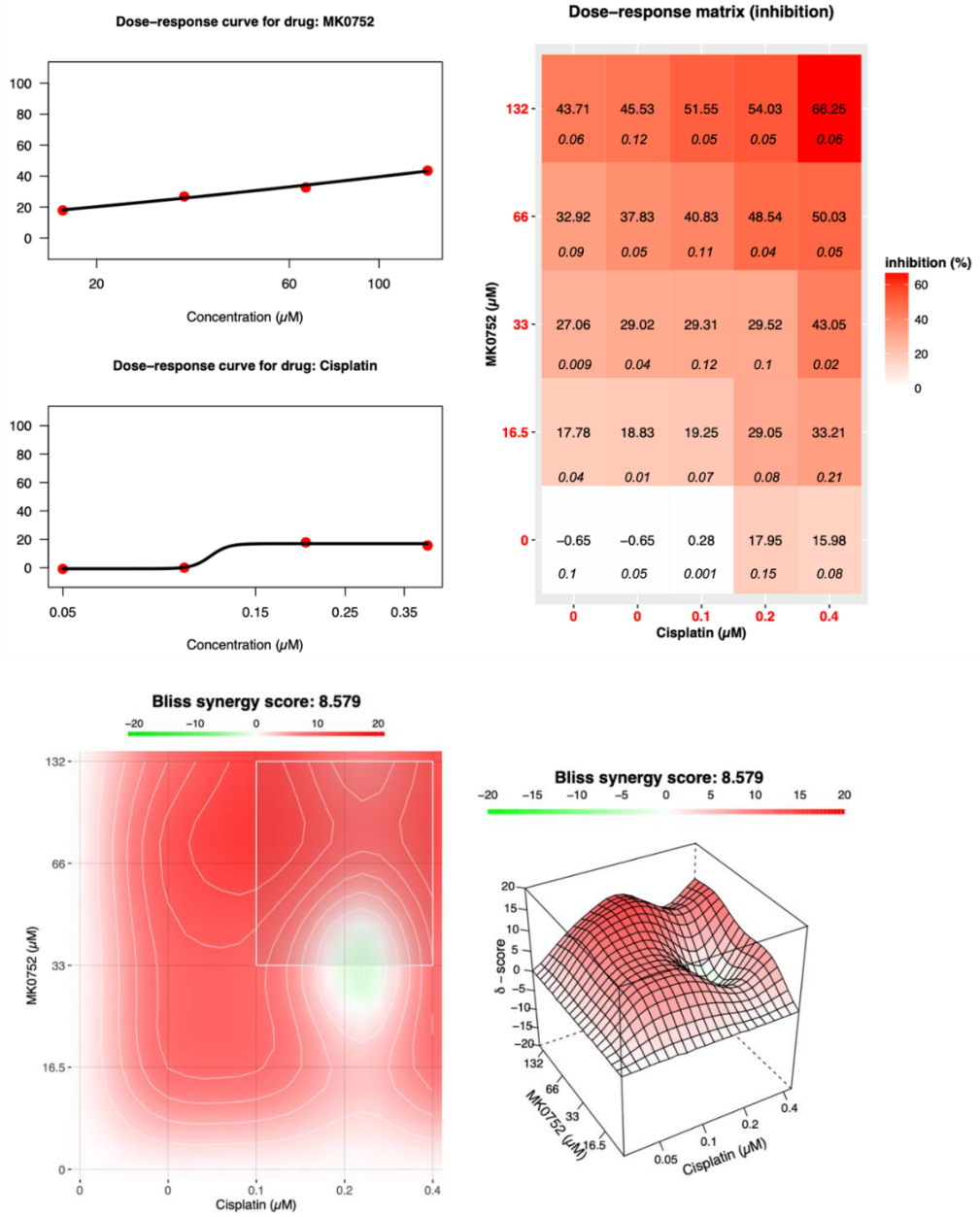


Figure 73. MK0752’s combination with Cisplatin results in additive effect for A2780 cells. Drug synergy analysis of MK0752 with Cisplatin was conducted by Synergy Finder tool. Bliss synergy score of three independent experiments were analyzed for combinations. The drug response curve with the inhibition matrix and heatmap shows IC_{100} for MK0752 and Cisplatin was the optimum dose combination for A2780 cell lines.

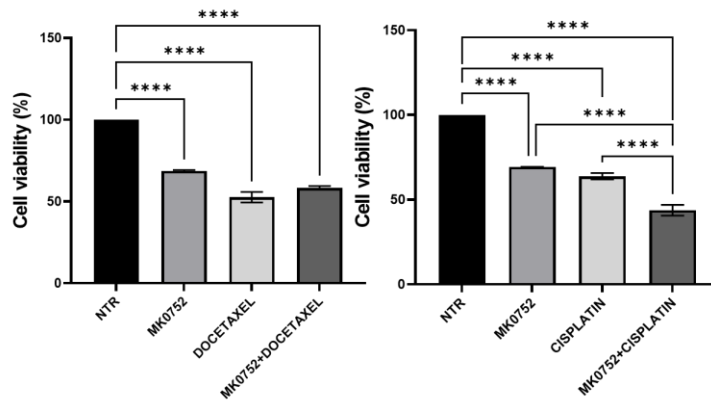


Figure 74. Decreased viability ratios of A2780 cells in response to MK0752, Docetaxel and Cisplatin treatments. MTT assay was carried out after the cells were treated with IC₁₀₀ of MK0752 (for 24 hours), Docetaxel (for 48 hours), Cisplatin (for 72 hours) alone or in combinations which applied simultaneously. (*p<0.05, **p<0.01, ***p<0.001, ****p<0.0001).

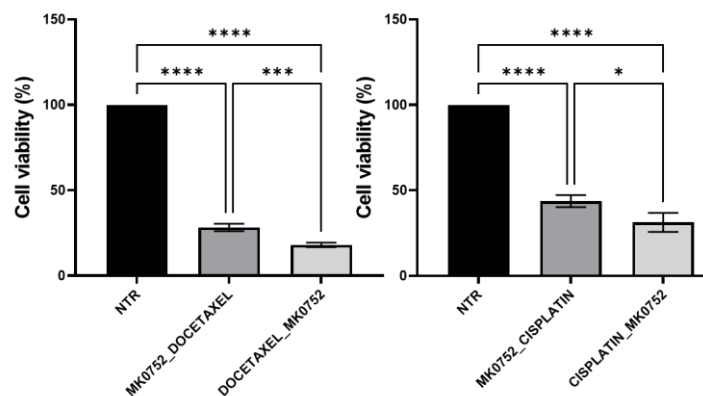


Figure 75. Decreased viability ratios of A2780 cells in response to sequential MK0752, Docetaxel and Cisplatin treatments. (*p<0.05, ***p<0.001, ****p<0.0001).

BG-1's single agent treatments showed decreased cell viability with MK0752 to 63%, Docetaxel to 62% and Cisplatin to 61%. Docetaxel combinations with MK0752 resulted in 52% and MK0752's Cisplatin combinations resulted in 54% viability. Docetaxel combinational treatments compared to single agents induced 10% and Cisplatin combinational treatments with MK0752 resulted in 7% difference. Docetaxel single agent and combinational treatments were not significantly different (Figure 82).

BG-1

Docetaxel & MK0752

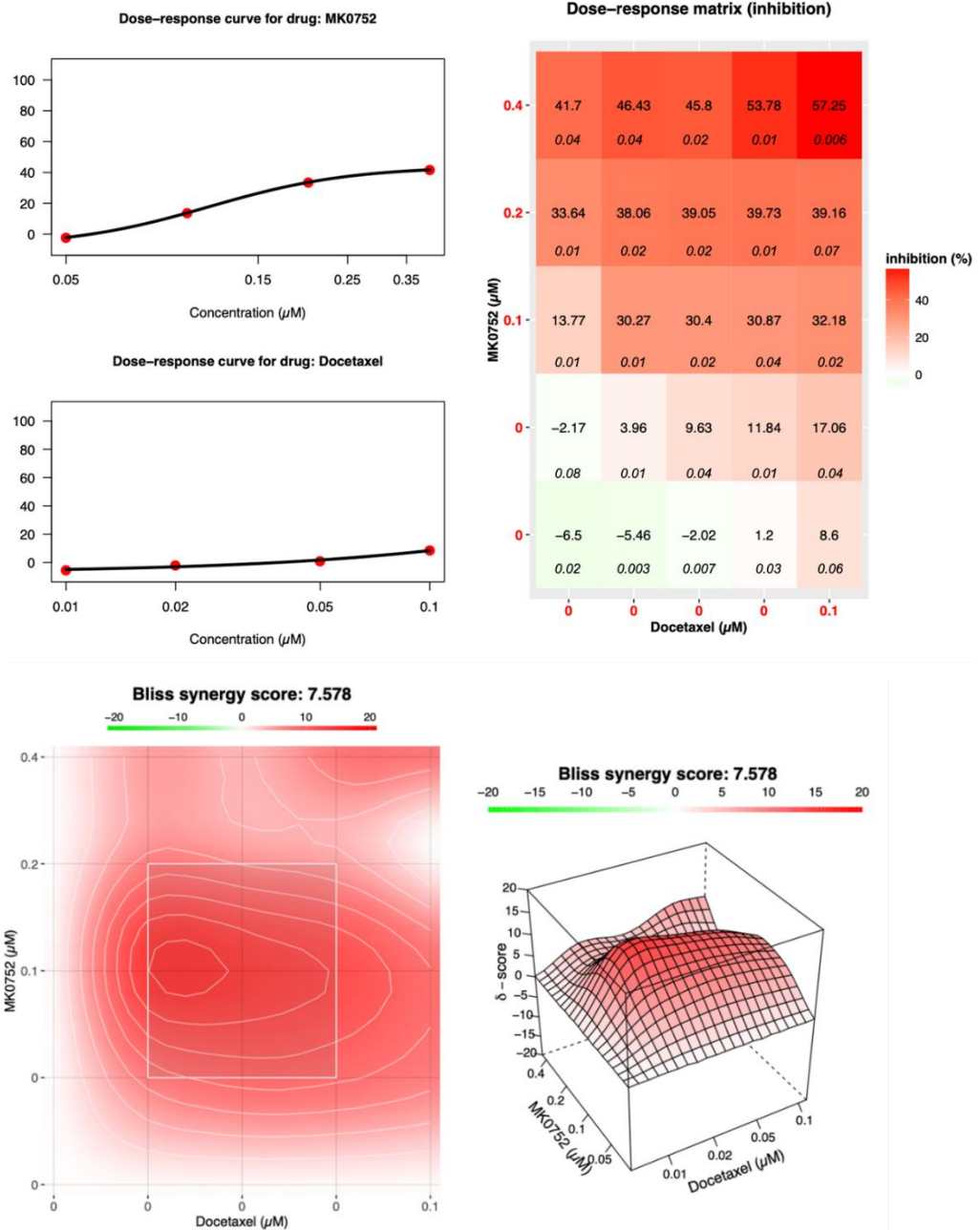


Figure 76. MK0752's combination with Docetaxel results in additive effect for BG-1 cells. Drug synergy analysis of MK0752 with Docetaxel was conducted by Synergy Finder tool. Bliss synergy score of three independent experiments were analyzed for combinations. The drug response curve with the inhibition matrix and heatmap shows IC_{100} for MK0752 and Docetaxel was the optimum dose combination for BG-1 cell lines.

BG-1

Cisplatin & MK0752

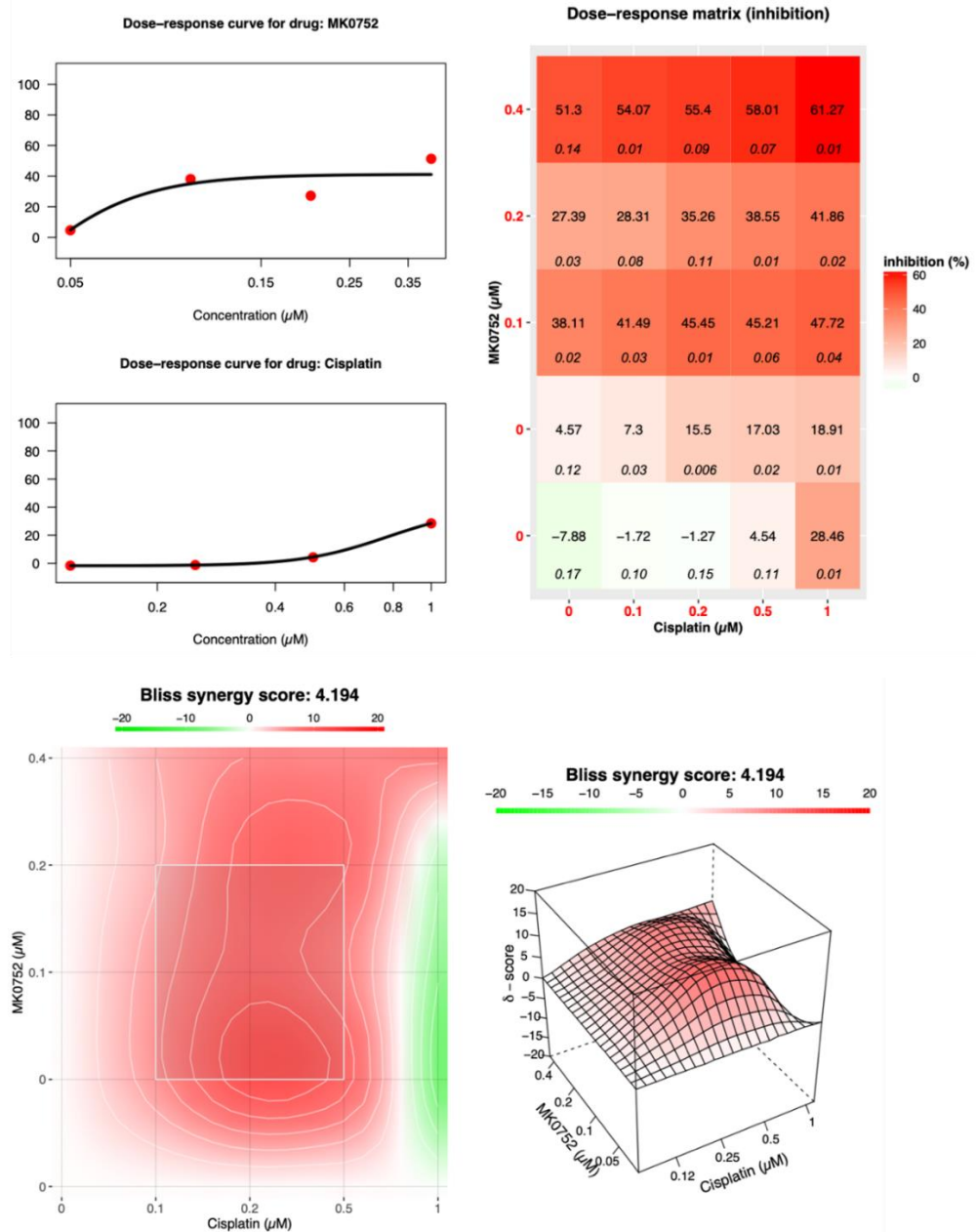


Figure 77. MK0752's combination with Cisplatin results in additive effect for BG-1 cells. Drug synergy analysis of MK0752 with Cisplatin was conducted by Synergy Finder tool. Bliss synergy score of three independent experiments were analyzed for combinations. The drug response curve with the inhibition matrix and heatmap shows IC_{100} for MK0752 and Cisplatin was the optimum dose combination for BG-1 cell lines.

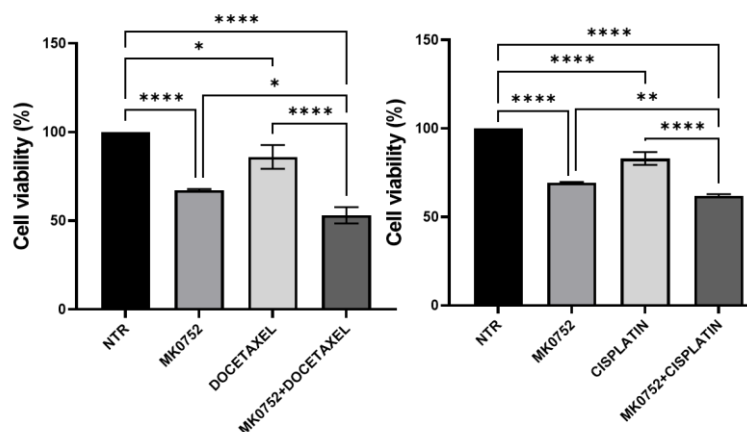


Figure 78. Decreased viability ratios of BG-1 cells in response to MK0752, Docetaxel and Cisplatin treatments. MTT assay was carried out after the cells were treated with IC₁₀₀ of MK0752 (for 24 hours), Docetaxel (for 48 hours), Cisplatin (for 72 hours) alone or in combinations which applied simultaneously. (*p<0.05, ***p<0.001, ****p<0.0001).

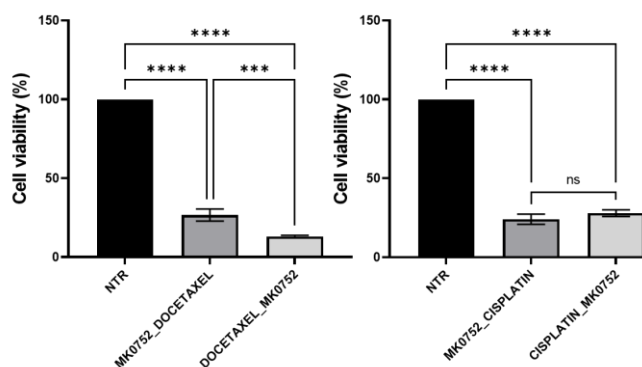


Figure 79. Decreased viability ratios of BG-1 cells in response to sequential MK0752, Docetaxel and Cisplatin treatments. (ns: not significant, *p<0.05, ***p<0.001, ****p<0.0001).

MK0752 initial treatments with Docetaxel and Cisplatin were decreased to 52% and Docetaxel initial treatments followed by MK0752 resulted in 42% cell viability. Cisplatin initial treatments resulted in 10% viability. MK0752 sequential treatments with Docetaxel showed 10% difference when compared with Docetaxel initial treatments whereas Cisplatin sequential treatments differed by 42% (Figure 83).

SKOV-3

Docetaxel & MK0752

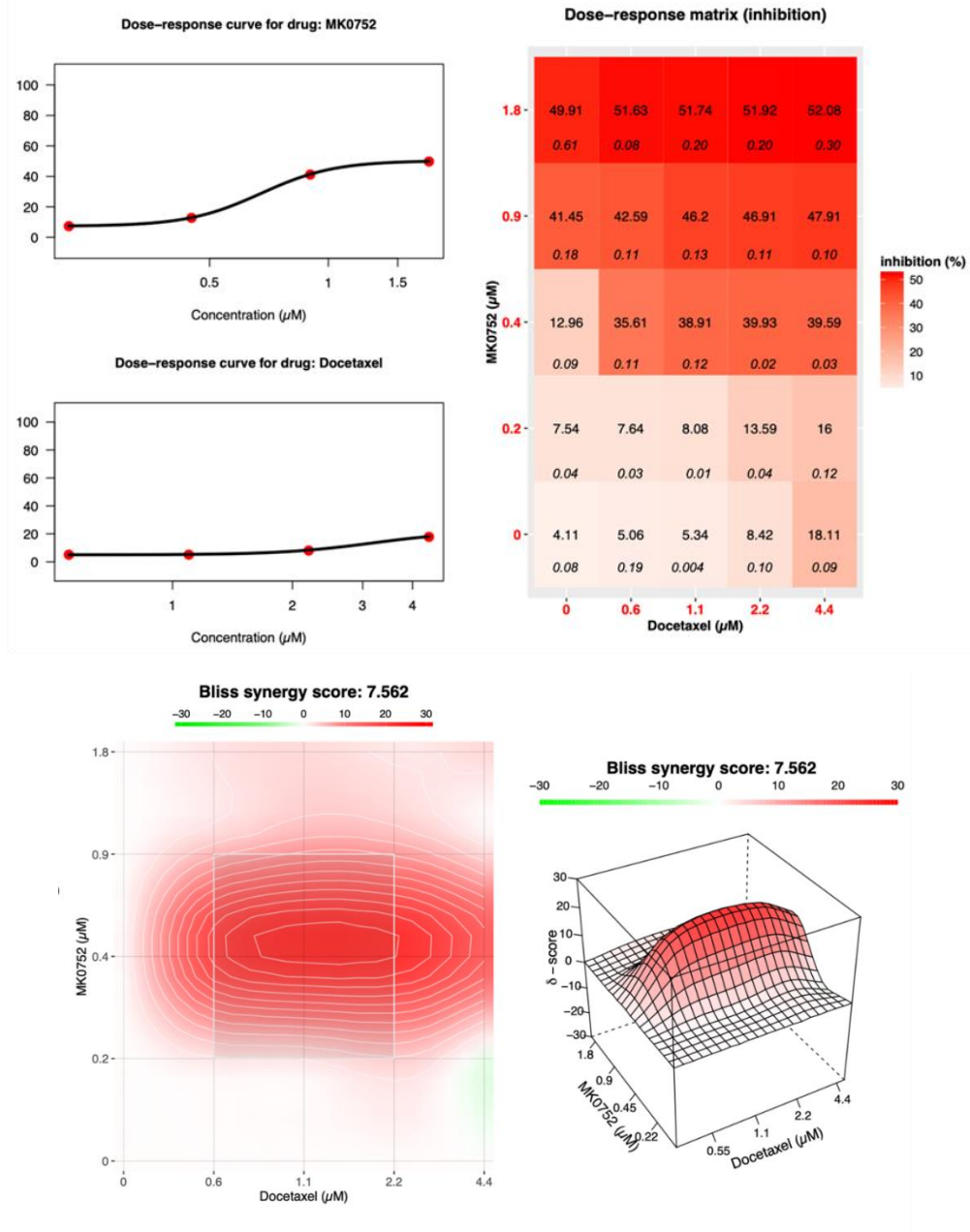


Figure 80. MK0752's combination with Docetaxel results in additive effect for SKOV-3 cells. Drug synergy analysis of MK0752 with Docetaxel was conducted by Synergy Finder tool. Bliss synergy score of three independent experiments were analyzed for combinations. The drug response curve with the inhibition matrix and heatmap shows IC_{100} for MK0752 and Docetaxel was the optimum dose combination for SKOV-3 cell lines.

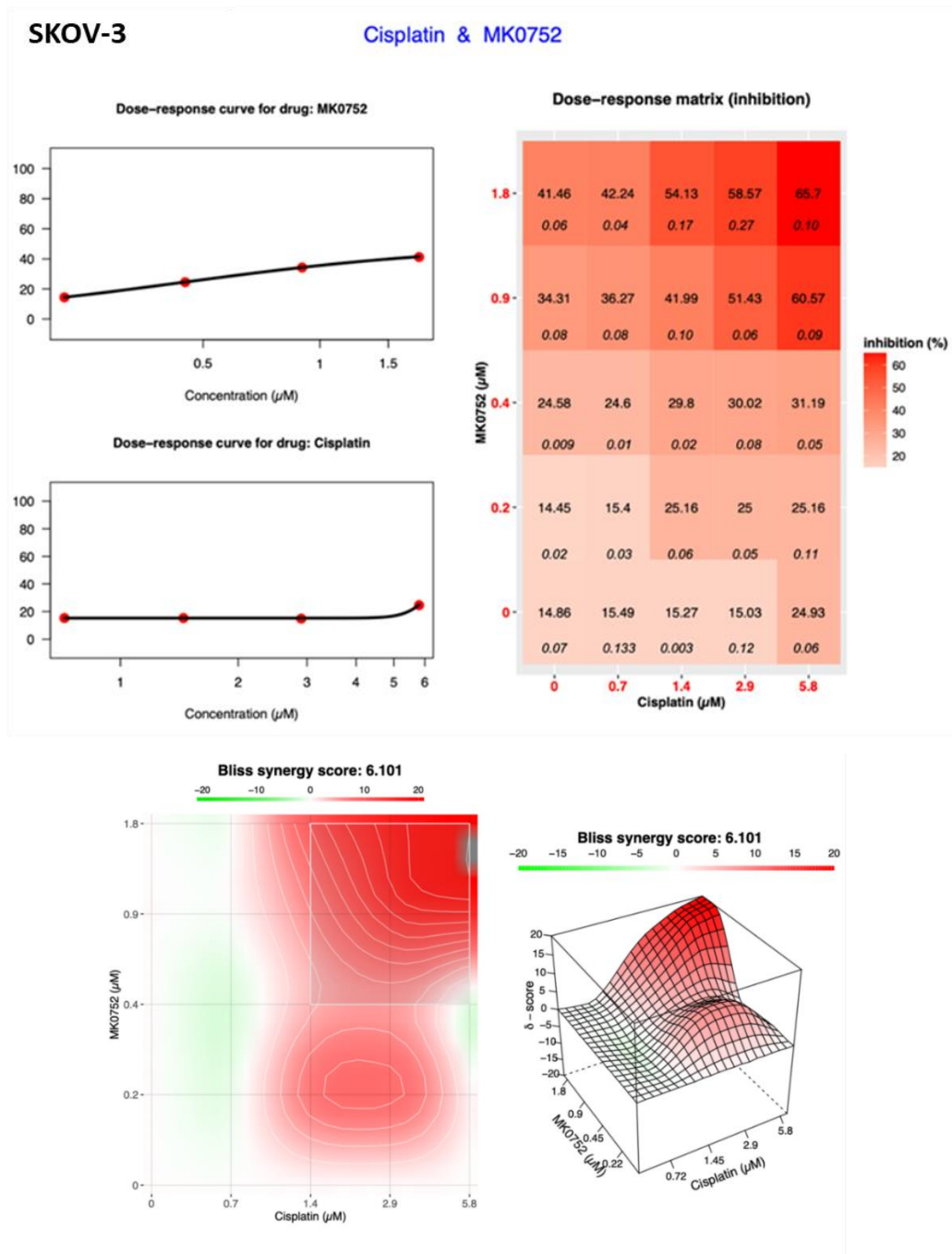


Figure 81. MK0752's combination with Cisplatin results in additive effect for SKOV-3 cells. Drug synergy analysis of MK0752 with Cisplatin was conducted by Synergy Finder tool. Bliss synergy score of three independent experiments were analyzed for combinations. The drug response curve with the inhibition matrix and heatmap shows IC_{100} for MK0752 and Cisplatin was the optimum dose combination for SKOV-3 cell lines.

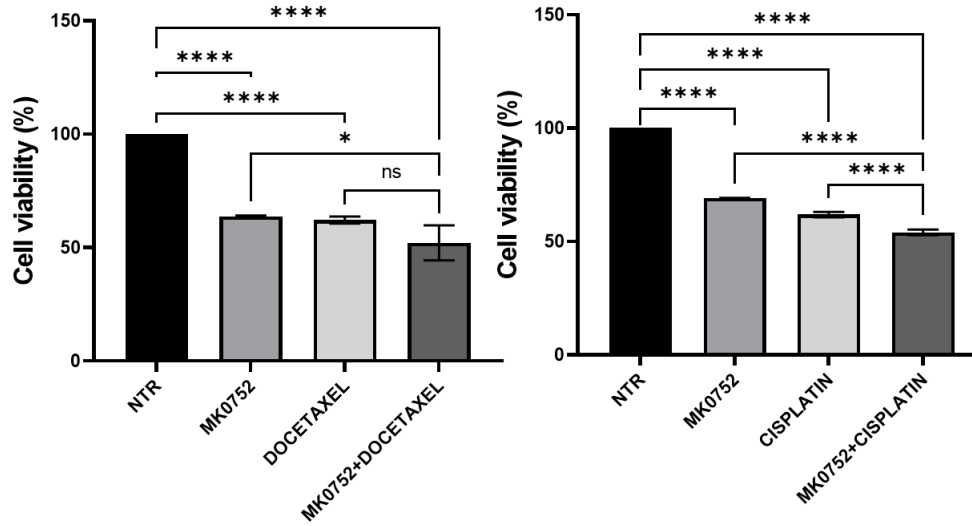


Figure 82. Decreased viability ratios of SKOV-3 cells in response to MK0752, Docetaxel and Cisplatin treatments. MTT assay was carried out after the cells were treated with IC₁₀₀ of MK0752 (for 24 hours), Docetaxel (for 48 hours), Cisplatin (for 72 hours) alone or in combinations which applied simultaneously. (ns: not significant, *p<0.05, ***p<0.001, ****p<0.0001).

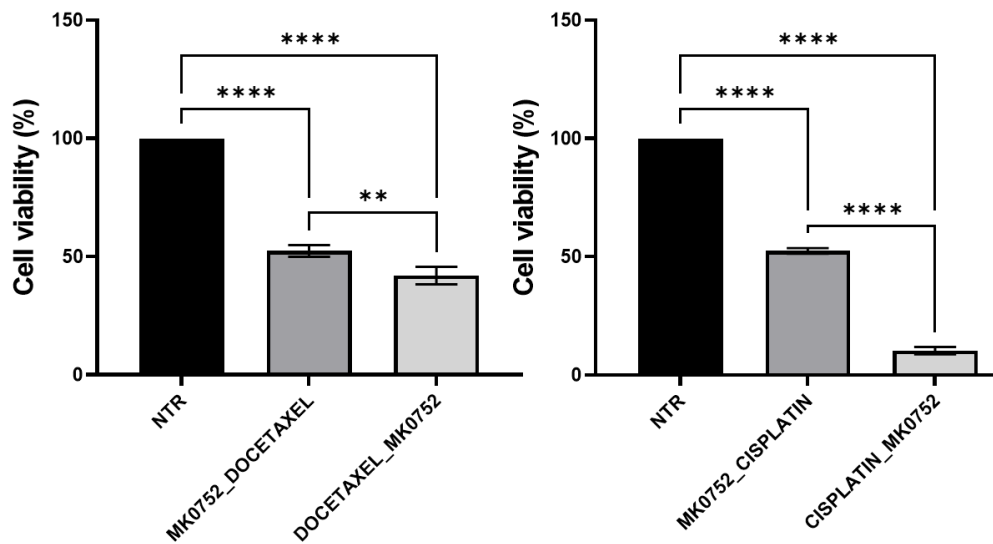


Figure 83. Decreased viability ratios of SKOV-3 cells in response to sequential MK-0752, Docetaxel and Cisplatin treatments. (**p<0.01, ****p<0.0001).

4.7.2. Acquired MK0752 resistance in Ovarian Cancer Cells

To model MK0752 acquired resistance, IGROV-1, A2780, BG-1 and SKOV-3 cells were treated with gradually increasing doses of MK0752, from their IC_{25} up to IC_{200} values. Resistant cells were obtained by their ability to grow up to 90% confluency in the presence of IC_{200} of MK0752. Resistance confirmations after treatments were conducted by recalculating IC_{50} values of MK0752 for resistant cell lines (Figure 84). Resistance index ratio were applied and, accordingly, A2780 and IGROV-1 cells resulted in 2.5-fold, SKOV-3 was 40-fold and BG-1 cells resulted in 160-fold increase of IC_{50} values which confirms resistant cell line generations (Table 2).

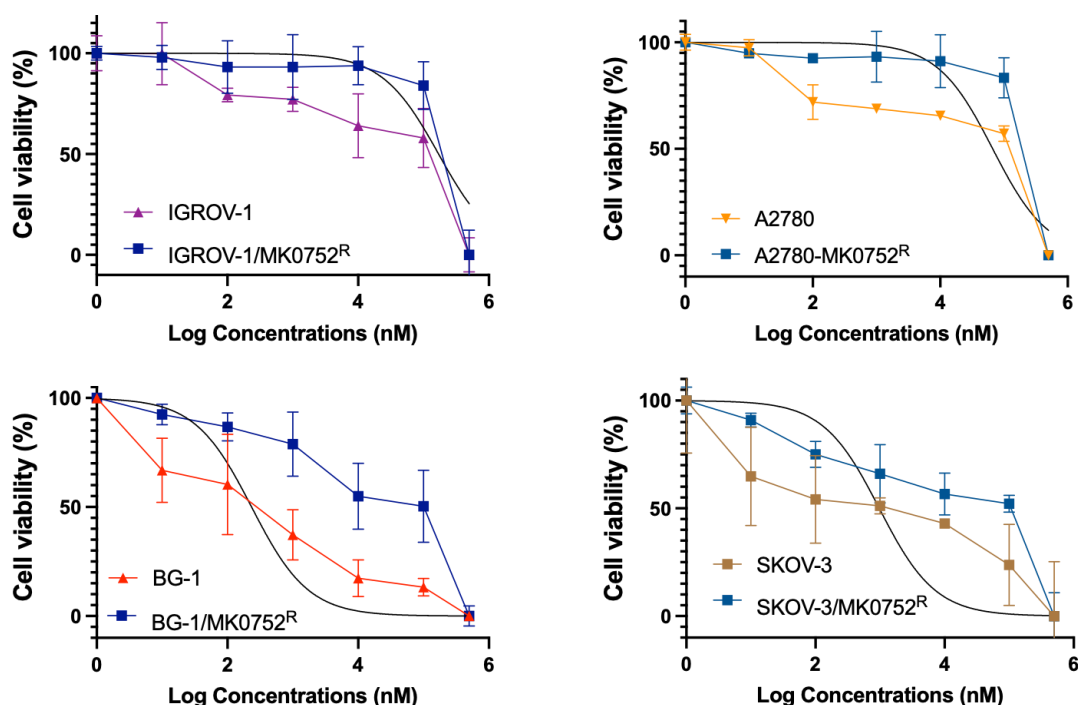


Figure 84. IC_{50} curves of parental and MK0752 resistant IGROV-1, A2780, BG-1 and SKOV-3 cell lines. MTT absorbance values were normalized and graphed by using GraphPad PRISM 8. Each dose represents at least three independent experiments.

Table 2. IC₅₀ values of MK0752 resistant ovarian cancer cell lines, IGROV-1, A27-80, BG-1 and SKOV-3. RI: Resistance Index signifies resistance scaling (Standard deviations represented as ±).

IC ₅₀ (μM)	IGROV-1	A2780	BG-1	SKOV-3
Parental	68 ± 0.3	66 ± 0.7	0.2 ± 0.2	0.9 ± 1.2
MK0752^R	170 ± 2.1	166 ± 1.4	32 ± 0.9	36 ± 0.2
RI	2.5	2.5	160	40
	<i>RI=2-10, Moderate Sensitivity</i>		<i>RI>10, Highly Resistant</i>	

Morphologies were recorded for potential resistance behaviour and changes were not observed for BG-1, SKOV-3, IGROV-1 whereas A2780 cells exhibited mesenchymal like shapes (Figure 85). Viability rates of A2780 cells compared to A2780^{MK0752R} cells showed no significant changes until 72 hours of comparisons by 17% (Figure 86). BG-1^{MK0752R} cells increased by 81% in the growth rate when compared to 72 hours (Figure 87). IGROV-1^{CisR} showed higher viability by 73% whereas IGROV-1^{MK0752R} cells exhibited growth increase by 7% compared to IGROV-1 cell lines (Figure 88). SKOV-3^{MK0752R} resistant cell lines increased by 34% difference in viability when compared to SKOV-3 cells at 72 hours (Figure 89). MK0752 resistant A2780, BG-1 and SKOV-3 cells showed increased growth rate which is related to common drug resistance pattern.

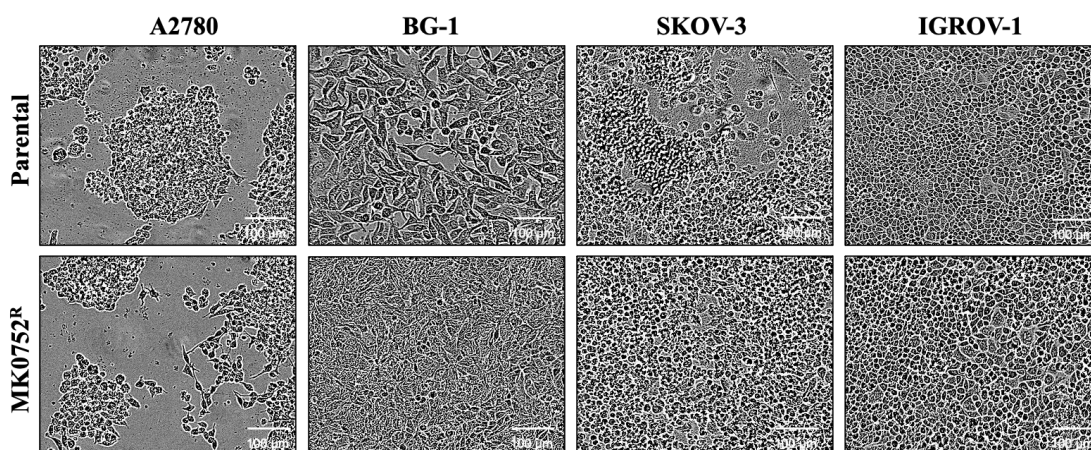


Figure 85. Morphological changes of parental and MK0752 resistant A2780, BG-1, SKOV-3, and IGROV-1 ovarian cancer cell lines. Scale bars is 100 μm.

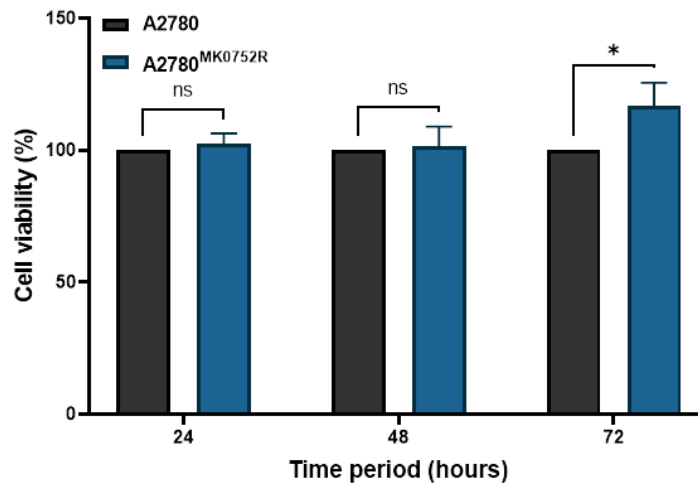


Figure 86. A2780^{MK0752R} cells exhibits increased viability when compared to A2780. A2780 and A2780^{MK0752R} cells cultured in drug-free media at three different time points. Data represents the means and \pm SD of three independent experiments. One-way ANOVA analysis confirmed significance for conditions (ns: not significant, * $p < 0.05$).

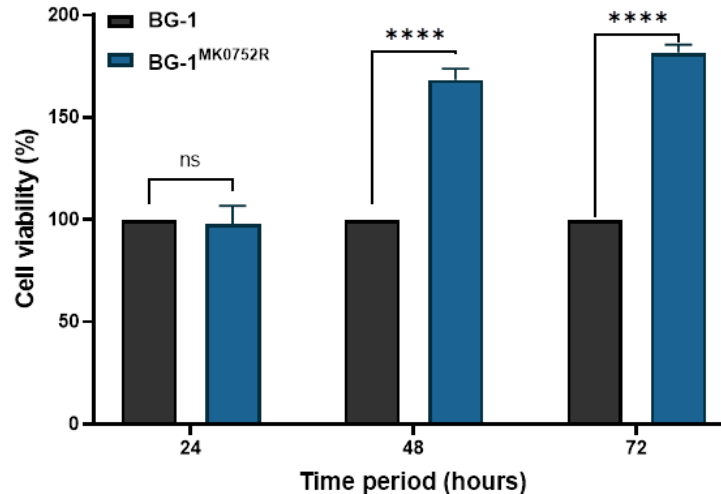


Figure 87. BG-1^{MK0752R} cells exhibits increased viability when compared to BG-1. BG-1 and BG-1^{MK0752R} cells cultured in drug-free media at three different time points. Data represents the means and \pm SD of three independent experiments. One-way ANOVA analysis confirmed significance for conditions (ns: not significant, **** $p < 0.0001$).

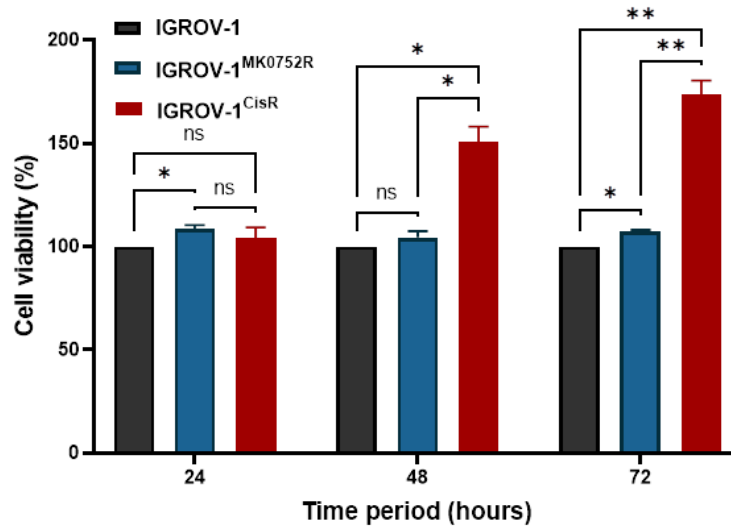


Figure 88. IGROV-1^{CisR} cells exhibits increased viability when compared to IGROV-1^{MK0752R}, IGROV-1, IGROV-1^{CisR} and IGROV-1^{MK0752R} cells cultured in drug-free media at three different time points. (ns: not significant, * $p < 0.05$, **** $p \leq 0.0001$).

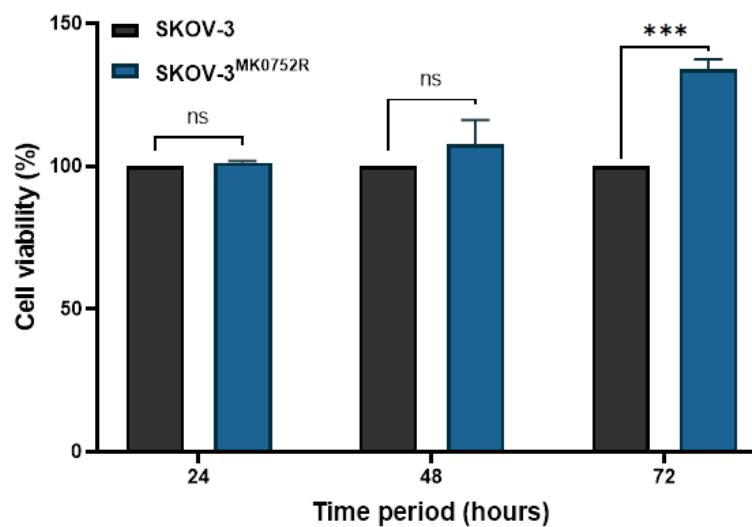


Figure 89. SKOV-3^{MK0752R} cells exhibits increased viability when compared to SKOV-3. SKOV-3 and SKOV-3^{MK0752R} cells cultured in drug-free media at three different time points. One-way ANOVA analysis confirmed significance for conditions (ns: not significant, **** $p < 0.0001$).

4.7.2.1. MK0752, Cisplatin and Docetaxel treatments in 2D and 3D cultures in parental and MK0752 resistant ovarian cancer cells

Acidosis is a drug tolerating pathway of tumors to evade cell death through regulation the pH. Comparing both monolayer (2D) and spheroid (3D) setups were conducted to understand potential effects on cancer's acidity on drug tolerance and resistance.

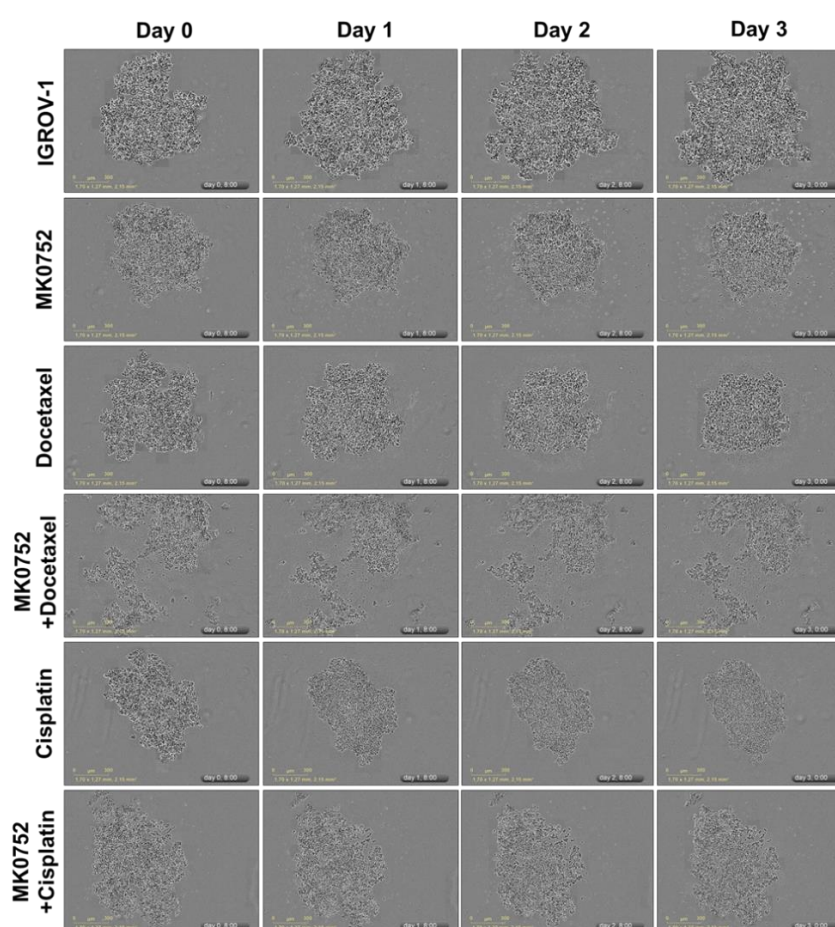


Figure 90. MK0752, Docetaxel and Cisplatin's both single agent and combinational treatments decreases IGROV-1 sphere size. MK0752 (for 24 hours), Docetaxel (for 48 hours) and Cisplatin (for 72 hours) treatments were applied after the spheroids were formed.

IGROV-1, BG-1, SKOV-3 and A2780 spheroids were treated with the optimum synergistic dose measured by the Bliss chart, IC₁₀₀ of MK0752 and its combinations with IC₁₀₀ of Docetaxel or Cisplatin. Spheroid areas were measured by Spheroid J plugin and days were compared within the experiment group to the addition of comparisons to treatments day 3 data. All data was normalized to the untreated condition and each treatment's day 0 condition. IGROV-1 and IGROV-1^{CisR} spheroids showed no significant change on daily trend (Figure 90 and 91). Day 2 of IGROV-1^{MK0752R} cells showed decreased spheroid volume however cells recovered back to day 0 ratio at day 3 (Figure 92). IGROV-1, IGROV-1^{MK0752R} and IGROV-1^{CisR} spheroids showed no significant difference when treated with IC₁₀₀ of MK0752. IGROV-1 spheroids were decreased to 25% for MK0752, 55% for Docetaxel and 52% for Cisplatin single agent treatments at day 3 which represents moderate sensitivity yet effective treatments. There were 21% difference between Docetaxel and its MK0752 combination. 24% difference in sphere area between Cisplatin's MK0752 combinations compared to Cisplatin single agent treatments (Figure 90 and 91).

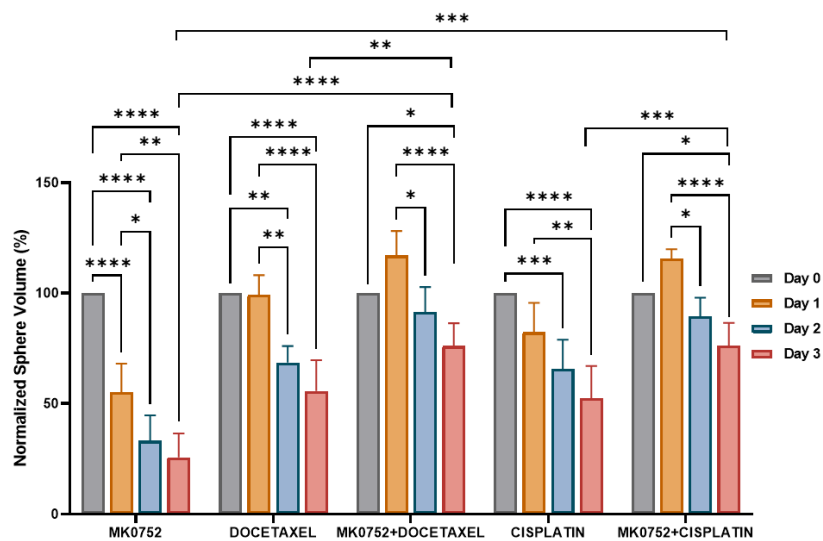


Figure 91. MK0752, Docetaxel, Cisplatin and their combinations reduce IGROV-1 sphere size. Normalized Area of measured from spheroid images were graphed. MK0752 (for 24 hours), Docetaxel (for 48 hours) and Cisplatin (for 72 hours) treatments were applied after the spheroids were formed. (*p<0.05, **p<0.01, ***p<0.001 and ****p<0.0001).

IGROV-1^{CisR} spheroids were decreased to 43% for MK0752 and increased to 108% for Docetaxel and 206% for Cisplatin single agent treatments at day 3 that shows its resistance behavior to Cisplatin and non-responsiveness to Docetaxel treatments. Almost 50% decrease for MK0752 IC₁₀₀ shows IGROV-1^{CisR}'s sensitiveness against MK0752 retreatments. There were 48% difference between Docetaxel and its MK0752 combination. 80% difference in the sphere area was observed when Cisplatin's MK0752 combinations were compared to Cisplatin single agent treatments. IGROV-1^{CisR} MK0752 combinations with retreatment of Cisplatin induced significant sensitivity which can be promising for further studies (Figure 92 and 93).

IGROV-1^{MK0752R} spheroids were decreased to 53% for MK0752 and increased to 97% for Docetaxel and 148% for Cisplatin single agent treatments at day 3. Thus shows IGROV-1^{MK0752R} spheres remains sensitivity against re-treatments of MK0752 and reflects resistance against Docetaxel and Cisplatin. that shows moderate sensitivity yet effective treatments. There were 37% difference between Docetaxel and its MK0752 combination. 7% difference in the sphere area was observed when Cisplatin's MK0752 combinations were compared to Cisplatin single agent treatments (Figure 94 and 95). Collectively, MK0752 resistant spheroids of IGROV-1, induces Docetaxel and/or Cisplatin resistance yet their combinational treatments remain effective.

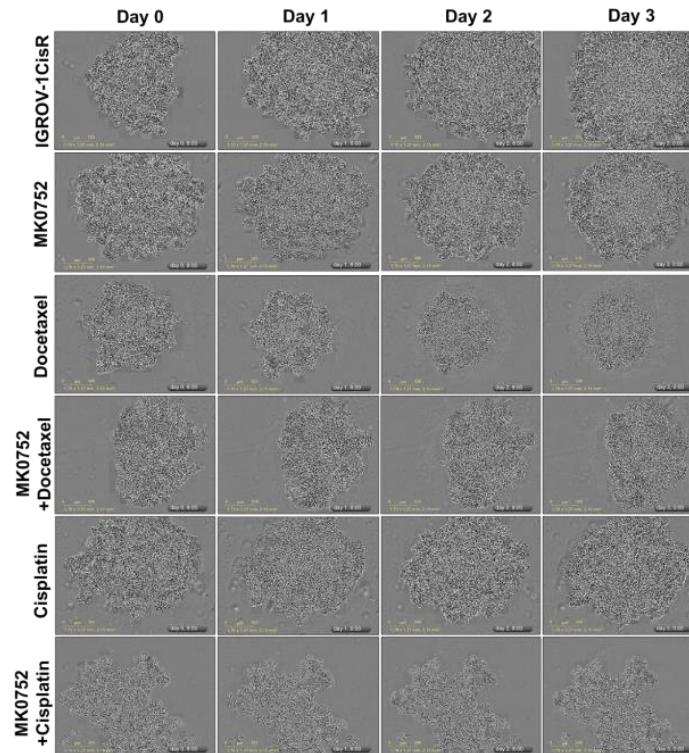


Figure 92. MK0752, Docetaxel and Cisplatin's both single agent and combinational treatments decreases IGROV-1^{CisR} sphere size. MK0752 (for 24 hours), Docetaxel (for 48 hours) and Cisplatin (for 72 hours) treatments were applied after the spheroids were formed.

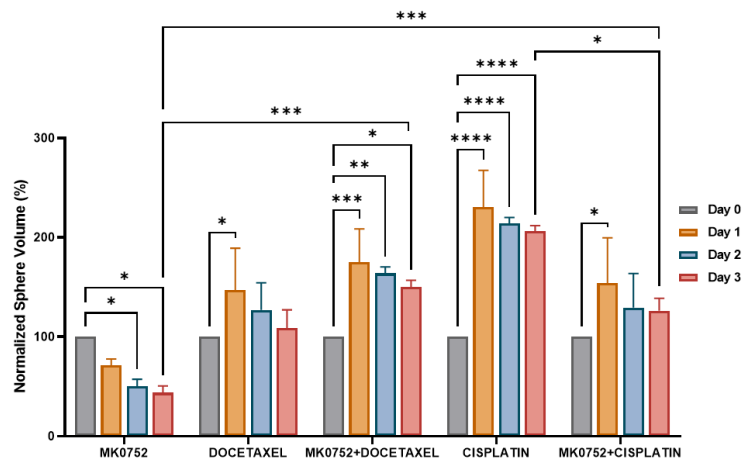


Figure 93. MK0752, Docetaxel, Cisplatin and their combinations reduce IGROV-1^{CisR} sphere size. (* $p < 0.05$, ** $p < 0.01$, *** $p < 0.001$ and **** $p < 0.0001$).

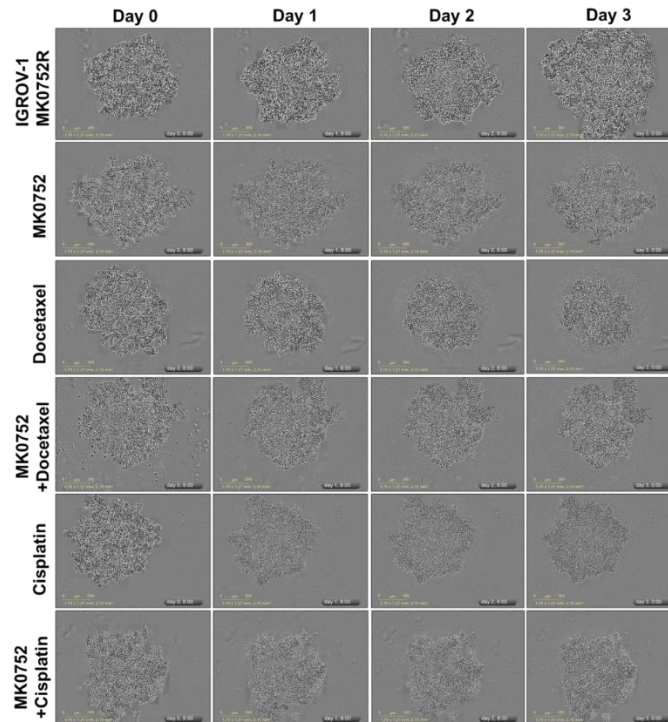


Figure 94. MK0752, Docetaxel and Cisplatin's both single agent and combinational treatments decreases IGROV-1^{MK0752R} sphere size. MK0752 (for 24 hours), Docetaxel (for 48 hours) and Cisplatin (for 72 hours) treatments were applied after the spheroids were formed.

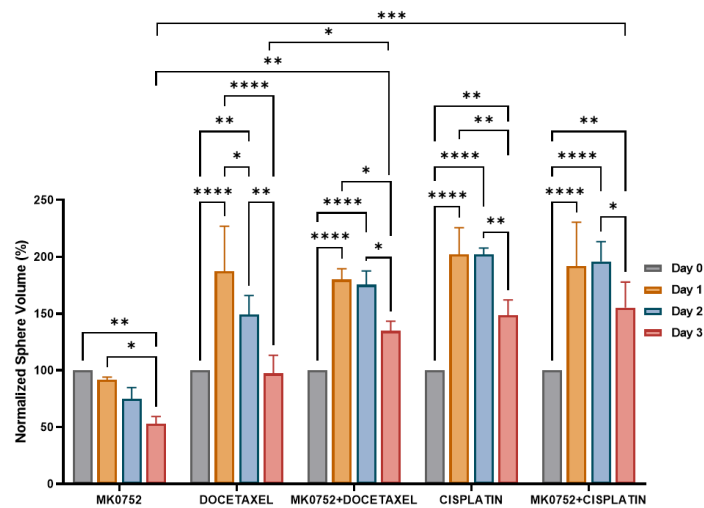


Figure 95. MK0752, Docetaxel, Cisplatin and their combinations reduces IGROV-1^{MK0752R} sphere size. (*p<0.05, **p<0.01, ***p<0.001 and ****p<0.0001).

BG-1 spheroids were decreased to 42% for MK0752, 31% for Docetaxel and 30% for Cisplatin single agent treatments at day 3. There were 20% difference between Docetaxel and its MK0752 combination. 11% additional shrinking in the sphere area was observed when Cisplatin's MK0752 combinations were compared to Cisplatin single agent treatments (Figure 96 and 97).

BG-1^{MK0752R} spheroids were decreased to 90% for MK0752, 69% for Docetaxel and 50% for Cisplatin single agent treatments at day 3. Only 10% decrease for MK0752 IC₁₀₀ retreatments shows BG-1^{MK0752R}'s resistant outcome. There were 36% difference between Docetaxel and its MK0752 combination. 11% additional shrinking in the sphere area was observed when Cisplatin's MK0752 combinations were compared to Cisplatin single agent treatments (Figure 98 and 99).

BG-1 represents success of MK0752 both as a single agent and combinational treatments with Docetaxel and Cisplatin. On the other hand, BG-1^{MK0752R} spheres remain sensitive to single agent chemotherapeutics and Cisplatin's MK0752 combinations which reflects its promising responsiveness.

SKOV-3 and SKOV-3^{MK0752R} spheroids represented changes for MK0752 single agent treatments when compared with in day comparisons. SKOV-3 spheroids were decreased to 42% for MK0752, 48% for Docetaxel and 43% for Cisplatin single agent treatments at day 3. There were 14% difference between Docetaxel and its MK0752 combination. 6% additional shrinking in the sphere area was observed when Cisplatin's MK0752 combinations were compared to Cisplatin single agent treatments (Figure 100 and 101).

SKOV-3^{MK0752R} spheroids were decreased to 51% for MK0752, 40% for Docetaxel and 31% for Cisplatin single agent treatments at day 3. Almost 50% decrease for MK0752 IC₁₀₀ retreatments shows SKOV-3^{MK0752R}'s sensitiveness against MK0752 retreatments. There were 4% difference between Docetaxel and its MK0752 combination. 1% additional shrinking in the sphere area was observed when Cisplatin's MK0752 combinations were compared to Cisplatin single agent treatments (Figure 102 and 103).

SKOV-3 and its MK0752 resistant clone's spheres represented similar sensitivity patterns against MK0752, Docetaxel and Cisplatin in addition to further sphere size decrease when in combinations might be promising for further studies.

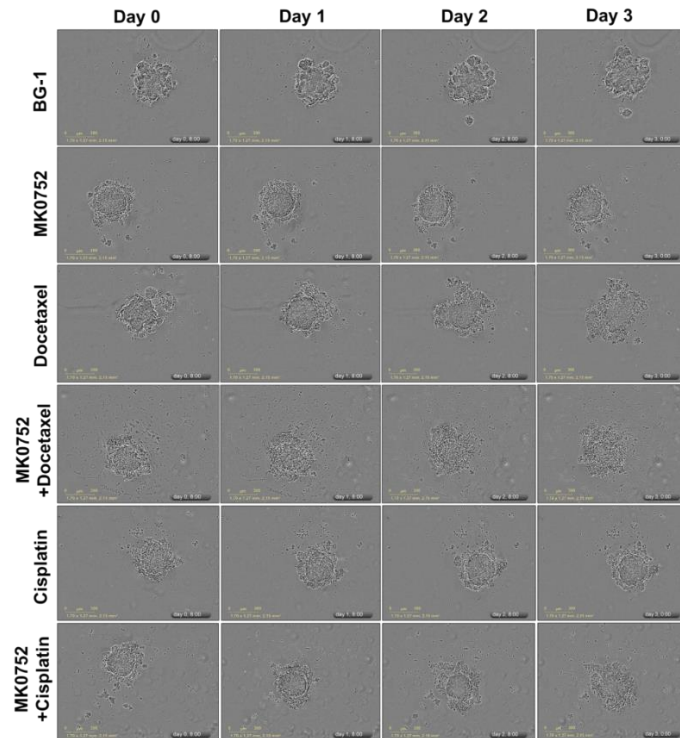


Figure 96. MK0752, Docetaxel and Cisplatin's both single agent and combinational treatments decreases BG-1 sphere size. MK0752 (for 24 hours), Docetaxel (for 48 hours) and Cisplatin (for 72 hours) treatments were applied after the spheroids were formed.

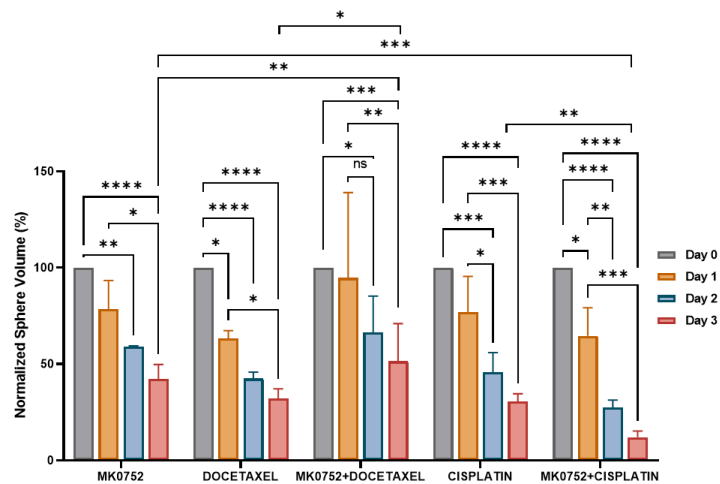


Figure 97. MK0752, Docetaxel, Cisplatin and their combinations reduce BG-1 sphere size. (* $p < 0.05$, ** $p < 0.01$, *** $p < 0.001$ and **** $p < 0.0001$).

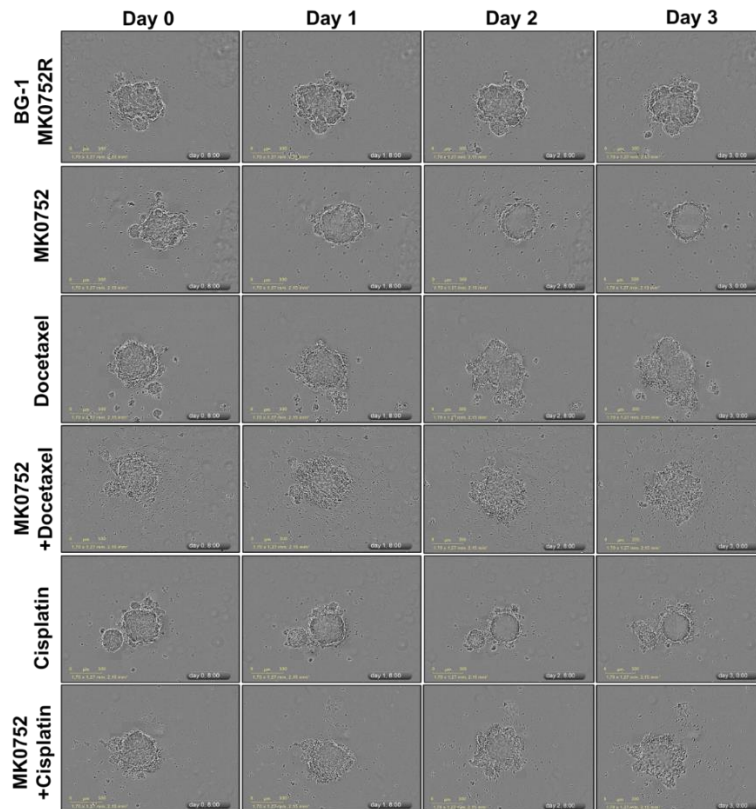


Figure 98. MK0752, Docetaxel and Cisplatin's both single agent and combinational treatments decreases BG-1^{MK0752R} sphere size. MK0752 (for 24 hours), Docetaxel (for 48 hours) and Cisplatin (for 72 hours) treatments were applied after the spheroids were formed.

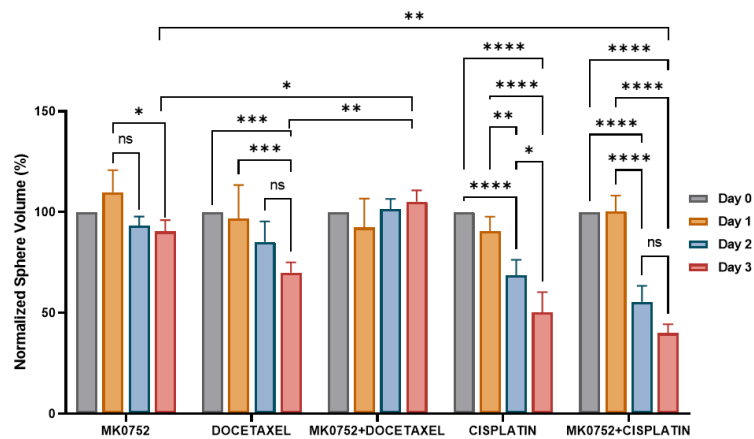


Figure 99. MK0752, Docetaxel, Cisplatin and their combinations reduces BG-1^{MK0752R} sphere size. (* $p < 0.05$, ** $p < 0.01$, *** $p < 0.001$ and **** $p < 0.0001$).

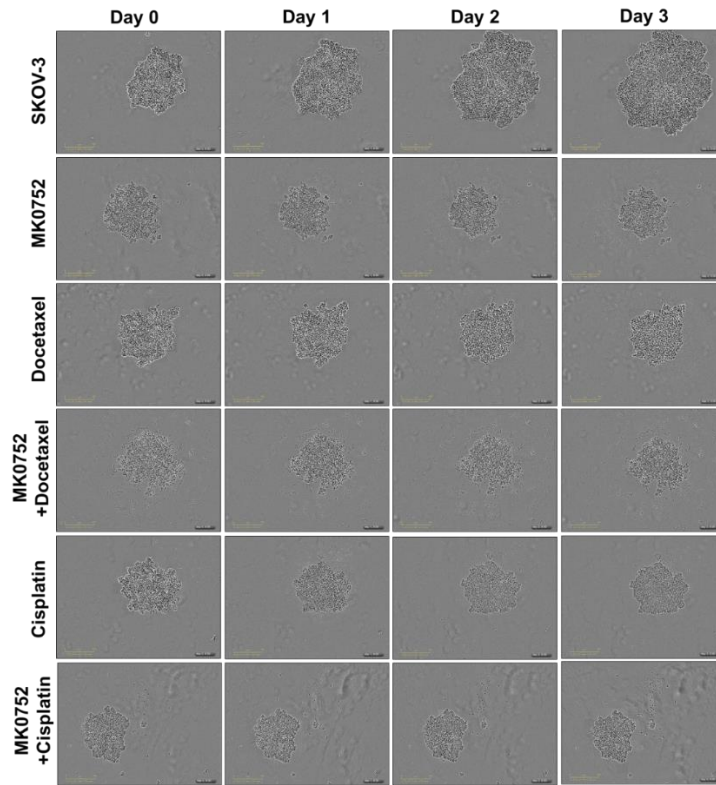


Figure 100. MK0752, Docetaxel and Cisplatin's both single agent and combinational treatments decreases SKOV-3 sphere size. MK0752 (for 24 hours) Docetaxel (for 48 hours) and Cisplatin (for 72 hours) treatments were applied after the spheroids were formed.

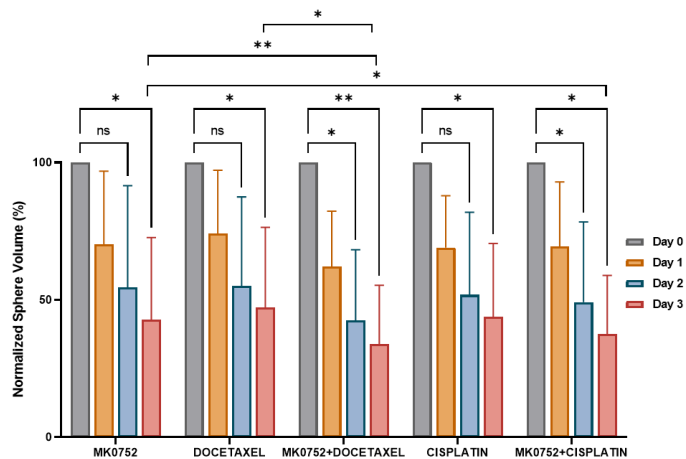


Figure 101. MK0752, Docetaxel, Cisplatin and their combinations reduces SKOV-3 sphere size. (* $p < 0.05$, ** $p < 0.01$, *** $p < 0.001$ and **** $p < 0.0001$).

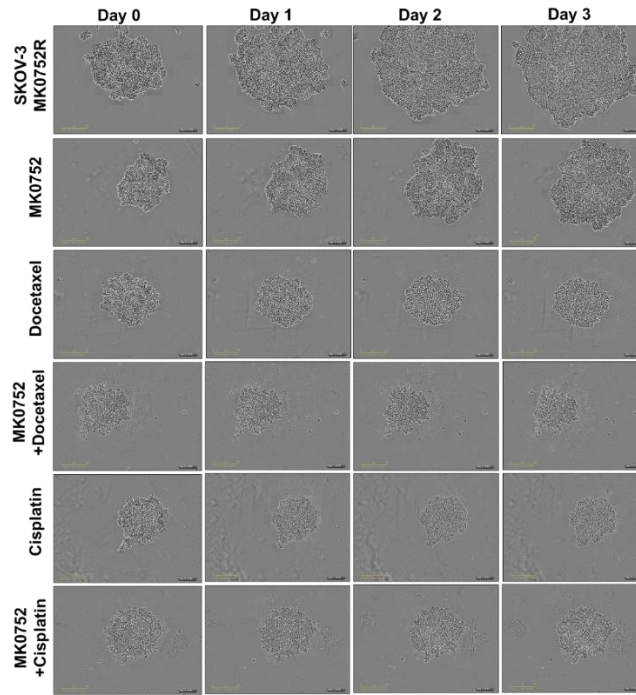


Figure 102. MK0752, Docetaxel and Cisplatin's both single agent and combinational treatments decreases SKOV-3^{MK0752R} sphere size. MK0752 (for 24 hours), Docetaxel (for 48 hours) and Cisplatin (for 72 hours) treatments were applied after the spheroids were formed.

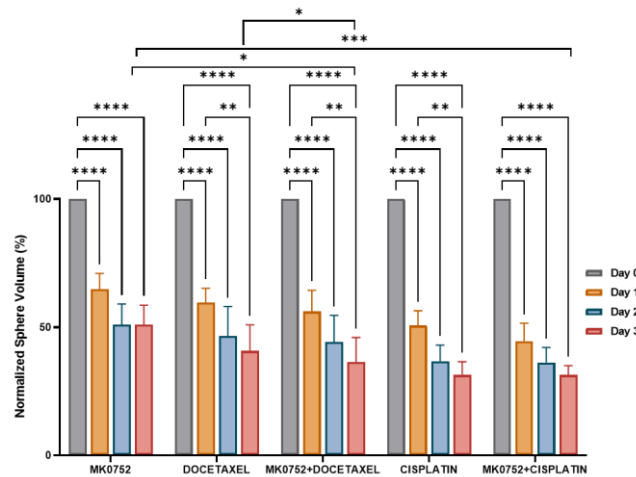


Figure 103. MK0752, Docetaxel, Cisplatin and their combinations reduces SKOV-3^{MK-0752R} sphere size. (*p<0.05, **p<0.01, ***p<0.001 and ****p<0.0001).

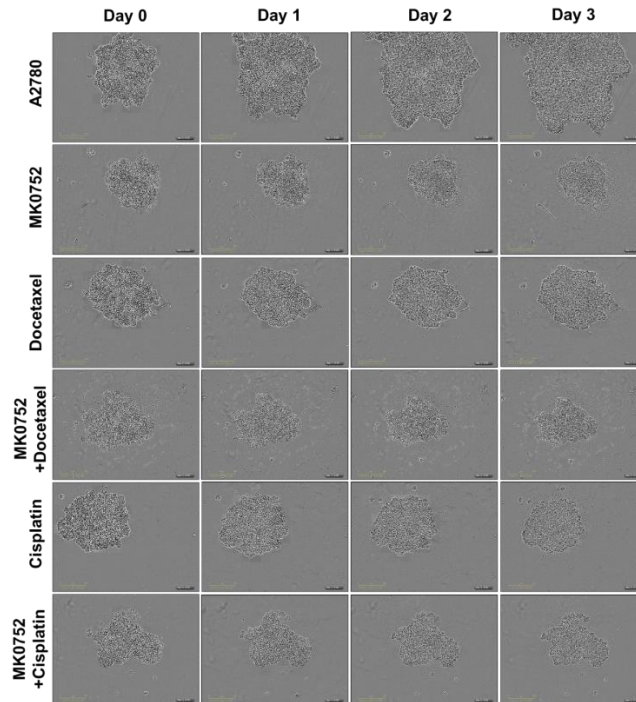


Figure 104. MK0752, Docetaxel and Cisplatin's both single agent and combinational treatments decreases A2780 sphere size. MK0752 (for 24 hours), Docetaxel (for 48 hours) and Cisplatin (for 72 hours) treatments were applied after the spheroids were formed.

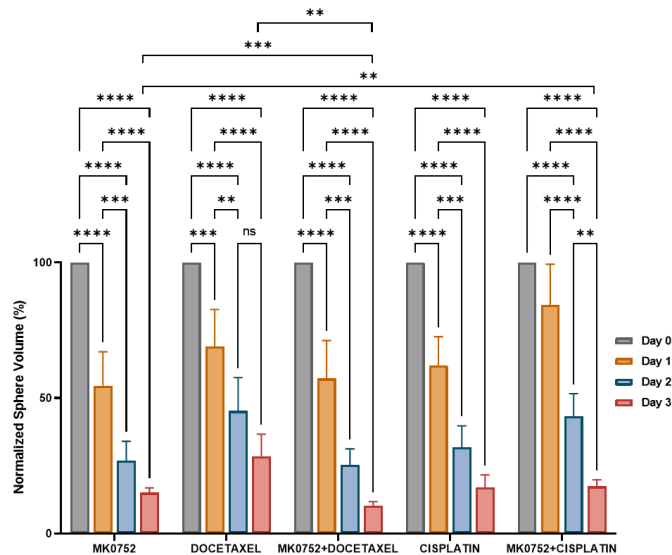


Figure 105. MK0752, Docetaxel, Cisplatin and their combinations reduces A2780 sphere size. (* $p < 0.05$, ** $p < 0.01$, *** $p < 0.001$ and **** $p < 0.0001$).

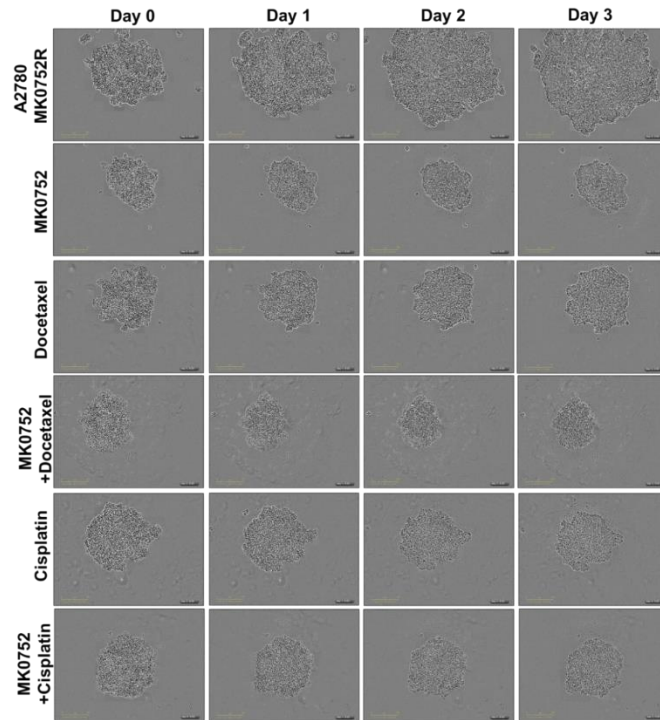


Figure 106. MK0752, Docetaxel and Cisplatin's both single agent and combinational treatments decreases A2780^{MK0752R} sphere size. MK0752 (for 24 hours), Docetaxel (for 48 hours) and Cisplatin (for 72 hours) treatments were applied after the spheroids were formed.

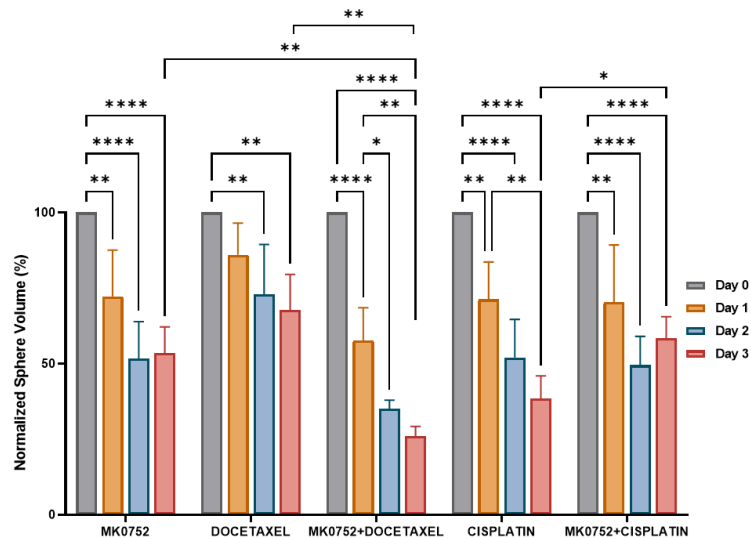


Figure 107. MK0752, Docetaxel, Cisplatin and their combinations reduces A2780^{MK0752R} sphere size. (*p<0.05, **p<0.01, ***p<0.001 and ****p<0.0001).

A2780 spheroids were decreased to 15% for MK0752, 28% for Docetaxel and 17% for Cisplatin single agent treatments at day 3 which represents oversensitivity to single agent treatments. There were 18% difference between Docetaxel and its MK0752 combination. There was no change in sphere area between Cisplatin's MK0752 combinations compared to Cisplatin single agent treatments (Figure 104 and 105). A2780^{MK0752R} spheroids were decreased to 53% for MK0752, 67% for Docetaxel and 38% for Cisplatin single agent treatments at day 3 that shows moderate sensitivity yet effective treatments. Almost 50% decrease for MK0752 IC₁₀₀ retreatments shows A2780^{MK0752R}'s sensitiveness against MK0752 retreatments. There were 41% difference between Docetaxel and its MK0752 combination. 20% difference in the sphere area was observed when Cisplatin's MK0752 combinations were compared to Cisplatin single agent treatments (Figure 106 and 107). A2780 spheres showed higher sensitivity to MK0752, Docetaxel and Cisplatin single agent and combinational treatments as well as A2780^{MK0752R} spheres. Thus, represents despite A2780^{MK0752R} resistance behaviour, it remains responsive to single agent and combinational treatments.

Acid phosphatase activity of MK0752 treatments for A2780 and A2780^{MK0752R} cells resulted in no different than non-treated controls. MK0752 combinations with Docetaxel resulted in 93% difference when compared to Docetaxel single agent treatments for A2780^{MK0752R} (Figure 108 A). MK0752 combinations with Docetaxel showed 102% decreased pattern when compared to non-treated conditions. MK0752 combinations with Docetaxel resulted in 106% decrease in A2780^{MK0752R} cells when compared to non-treated conditions. A2780^{MK0752R} cells induced 98% decrease and MK0752 combinations indicated 80% decrease when compared to the non-treated group. Cisplatin single treatments for A2780 cells showed 91% decrease in cell viability compared to nontreated controls (Figure 108 B and C). BG-1, Acid phosphatase activity of MK0752 treatments resulted in no different than the non-treated controls (Figure 109 A). BG-1 cells showed 11% decrease in single agent Docetaxel treatments and MK0752 combinations with Docetaxel by 22% decrease compared to nontreated conditions. BG-1^{MK0752R} cells when combined with MK0752 with Docetaxel resulted 10% decrease in viability when compared to nontreated BG-1^{MK0752R} conditions. Cisplatin treated BG-1^{MK0752R} cells resulted in 11% decrease and BG-1 cells showed 13% decrease. MK0752 combined with Cisplatin resulted in 17% decrease when compared to the non-treated control (Figure 109 B and C).

MK0752 treatments showed SKOV-3 cells decreased by 11% and when treated with MK0752 and SKOV-3^{MK0752R} showed 50% decrease (Figure 110 A). Docetaxel single treatments for SKOV-3 induced 13% decrease and its MK0752 combinations showed 23% decrease in cell viability when compared to nontreated controls. SKOV-3^{MK0752R} cells single treatment with Docetaxel and MK0752 combinations indicated 23% decrease. Cisplatin single agent treatments for SKOV-3 cells showed 21% and 28% decrease when combined with MK0752. Cisplatin single agent treatments for SKOV-3^{MK0752R} cells showed 60% decrease and 50% when combined with MK0752 (Figure 110 B and C).

IGROV-1^{CisR} cell line showed 20% decrease when compared to the non-treated group. IGROV-1 cell's Docetaxel single agent treatments resulted in 12%, its combinations with MK0752 decrease in 16% compared to non-treated condition (Figure 111 A). IGROV-1^{CisR} cells Docetaxel single agent treatments were decreased by 25% and its combinations with MK0752 were decreased by 29%. IGROV-1^{MK0752R} cells Docetaxel single agent treatments were decreased by 6% and its combinations with MK0752 decreased by 11% compared to non-treated condition. IGROV-1 cells Cisplatin single agent treatments were decreased by 19% and its combinations with MK0752 were decreased by 21% compared to non-treated condition. IGROV-1^{CisR} cells Cisplatin single agent treatments were decreased by 18% and its combinations with MK0752 were 20% compared to non-treated condition. IGROV-1^{MK0752R} cells Cisplatin single agent treatments were decreased by 6% decreased and its combinations with MK0752 decreased by 11% compared to non-treated condition (Figure 111 B and C). MK0752 treatments sensitized cells as Docetaxel and Cisplatin treatments yet their combinations increased the toxicity for IGROV-1, A2780, BG-1 and SKOV-3. IGROV-1^{CisR} cells were also sensitive to Cisplatin treatments when combined with MK0752. Overall findings represent MK0752's successful cell viability inhibition capacity. MK0752 resistant cells showed less shrinking in spheroid size that represents its fitting in common hallmarks in drug resistance catalogues. MK0752 resistant IGROV-1, A270, BG-1 and SKOV-3 was still responsive to Docetaxel and Cisplatin treatments which suggests its probable success in long term anti-cancer treatments and availability of combinational treatments.

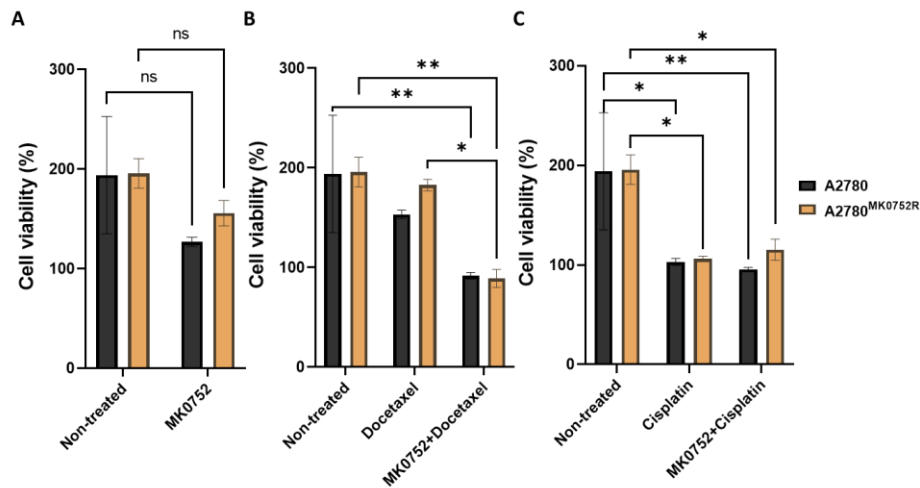


Figure 108. Decreased viability of A2780 and A2780^{MK0752R} spheroids in response to MK0752, Docetaxel and Cisplatin treatments and their combinations. (A) MK0752 (for 24 hours), (B) Docetaxel (for 48 hours) and (C) Cisplatin (for 72 hours) and their respective combinational treatments were applied after the spheroids were formed. (ns: not significant, *p<0.05, **p<0.01).

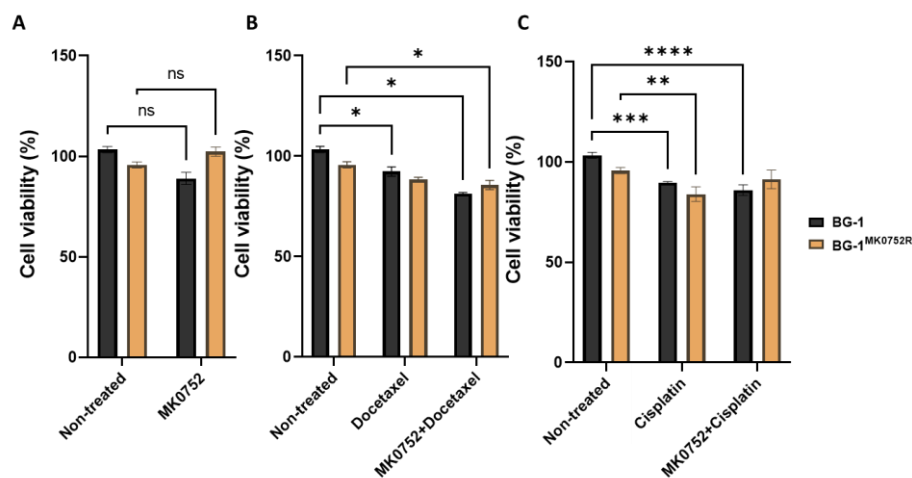


Figure 109. Decreased viability ratios of BG-1 and BG-1^{MK0752R} spheroids in response to MK0752, Docetaxel and Cisplatin treatments and their combinations. (A) MK0752 (for 24 hours), (B) Docetaxel (for 48 hours) and (C) Cisplatin (for 72 hours) and their respective combinational treatments were applied after the spheroids were formed. (ns: not significant, *p<0.05, **p<0.01, ***p<0.001, ****p<0.0001).

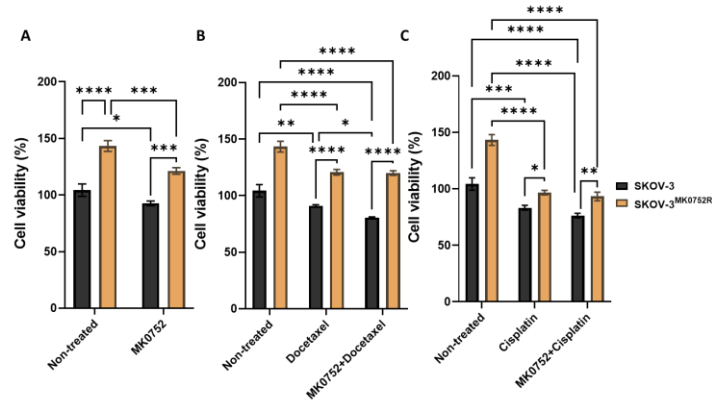


Figure 110. Decreased viability ratios of SKOV-3 and SKOV-3^{MK0752R} spheroids in response to MK0752, Docetaxel and Cisplatin treatments and their combinations. (A) MK0752 (for 24 hours), (B) Docetaxel (for 48 hours) and (C) Cisplatin (for 72 hours) and their respective combinational treatments were applied after the spheroids were formed. (*p<0.05, **p<0.01, ***p<0.001, ****p<0.0001).

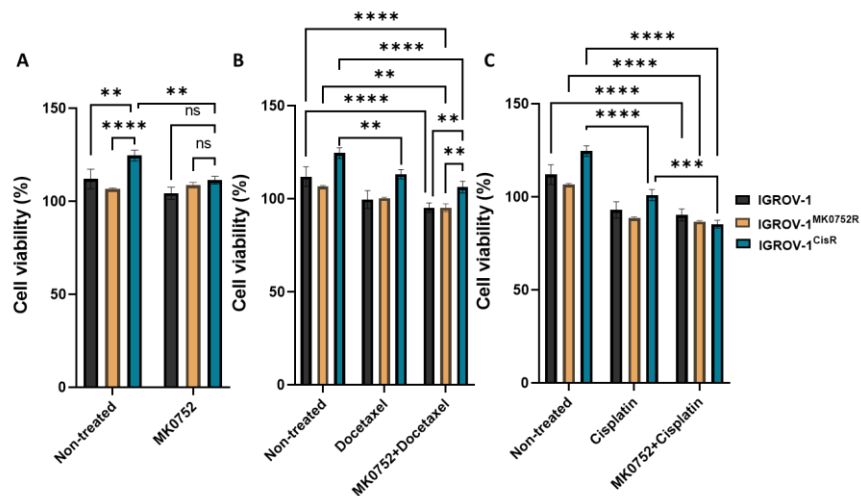


Figure 111. Decreased viability ratios of IGROV-1 and IGROV-1^{MK0752R}, and IGROV-1^{CisR} spheroids in response to MK0752, Docetaxel and Cisplatin treatments and their combinations. (A) MK0752 (for 24 hours), (B) Docetaxel (for 48 hours) and (C) Cisplatin (for 72 hours) and their respective combinational treatments were applied after the spheroids were formed. (ns: not significant, *p<0.05, **p<0.01, ***p<0.001, ****p<0.0001).

4.7.2.2. MK0752 resistant ovarian cancer cells regulates C-Myc protein expression levels

To assess potential MK0752 resistance route, protein expression levels of c-myc were profiled. C-myc is the one of the main downstream targets of Notch signalling pathway responsible for cancer recurrence and drug resistance. Its protein expression levels were compared for every single agent and combinational treatments of MK0752, Cisplatin and Docetaxel for IGROV-1, BG-1, SKOV-3 and A2780 and their MK0752 resistant clones. IGROV-1^{CisR} cells were also included in experiments. BG-1-C and BG-1^{MK0752R} cells MK0752 retreatments and Docetaxel treatments induced no significant difference of c-myc levels. BG-1^{MK0752R} cells MK0752 combinations with Docetaxel resulted in 0.73-fold decrease when compared to non-treated BG-1^{MK0752R} cells. BG-1 and BG-1^{MK0752R} cells differed by 0.84-fold c-myc expression levels when treated with MK0752 and Docetaxel. Cisplatin single agent treatments induced 0.63-fold decrease for BG-1 cells. BG-1^{MK0752R} cells MK0752 combination with Cisplatin treatments decreased by 1.2-fold when compared to its Cisplatin single agent treatments as well as when it's compared to BG-1 cells. MK0752 and Cisplatin combinations for BG-1^{MK0752R} resulted in 1-fold decrease when compared to non-treated BG-1^{MK0752R} cells (Figure 112).

A2780 cells expressed c-myc by 1.4-fold when compared to A2780^{MK0752R} cells. MK0752 treatments resulted in 1.2-fold difference between A2780 and A2780^{MK0752R} cells. Single agent Docetaxel and Cisplatin treatments showed no significance in c-myc mRNA expressions. however, MK0752 and Docetaxel combination resulted in 0.4-fold decrease and Cisplatin combinations resulted in 0.61-fold decrease when compared to A2780 cells non-treated condition. SKOV-3 and SKOV-3^{MK0752R} cells showed no protein expression of c-myc naturally (Figure 113). Though, MK0752 retreated SKOV-3^{MK0752R} cells resulted in 0.79-fold increase when compared to nontreated SKOV-3^{MK0752R} cells and to MK0752 treated SKOV-3 cells. Docetaxel treated SKOV-3^{MK0752R} cells increased the c-myc protein expression by 0.41 when compared to its MK0752 combinations and nontreated conditions. Cisplatin treated SKOV-3^{MK0752R} cells increased the c-myc protein expression by 1.2 when compared to nontreated conditions. MK0752 and Cisplatin combinations showed decreased expression by 1.02-fold when compared to Cisplatin single-agent treatments (Figure 114).

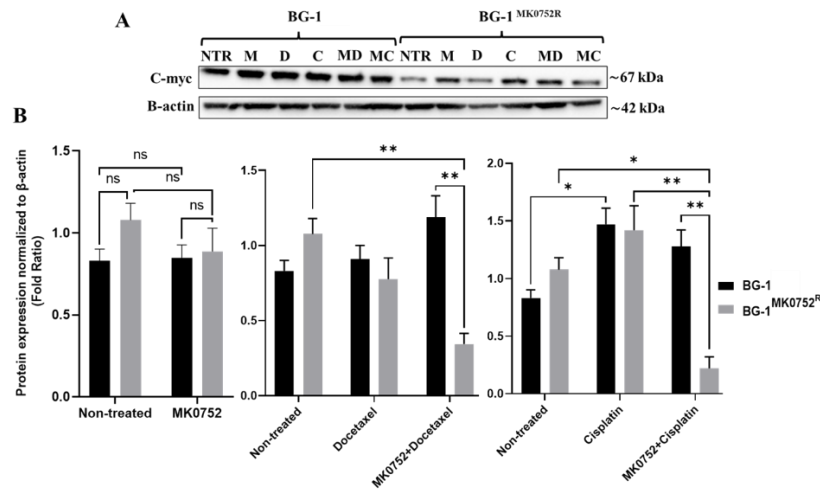


Figure 112. BG-1 and BG-1^{MK0752R} cells c-myc protein expressions with MK0752, Docetaxel and Cisplatin single agent and combinational treatments. (A) Western blot analysis of c-myc protein for treatments, (B) Normalized c-myc expression to β -actin ratios graphed for both BG-1 and BG-1^{MK0752R} cells (ns: not significant, * $p < 0.05$, ** $p < 0.01$).

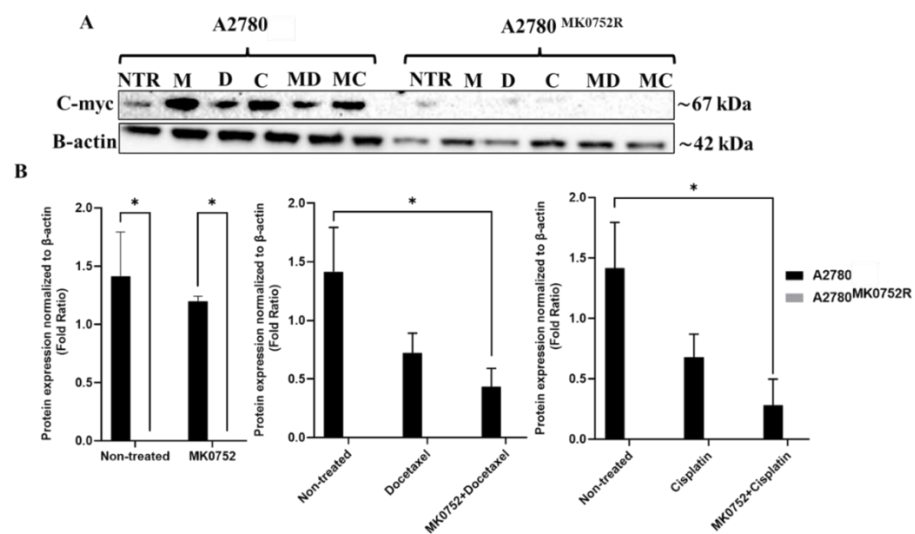


Figure 113. A2780 and A2780^{MK0752R} cells c-myc protein expressions with MK0752, Docetaxel and Cisplatin single agent and combinational treatments. (A) Western blot analysis of c-myc protein for treatments, (B) Normalized c-myc expression to β -actin ratios graphed for both A2780 and A2780^{MK0752R} cells (* $p < 0.05$).

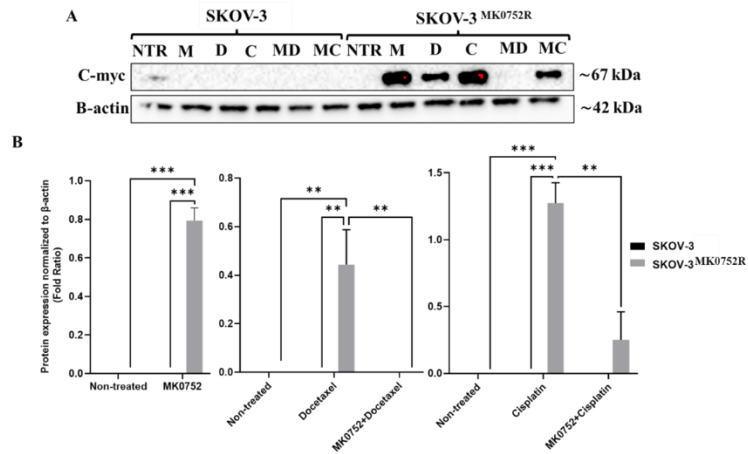


Figure 114. SKOV-3 and SKOV-3^{MK0752R} cells c-myc protein expressions with MK075-2, Docetaxel and Cisplatin single agent and combinational treatments. (A) Western blot analysis of c-myc protein for treatments, (B) Normalized c-myc expression to β -actin ratios graphed for both SKOV-3 and SKOV-3^{MK0752R} cells. (**p<0.01, ***p<0.001).

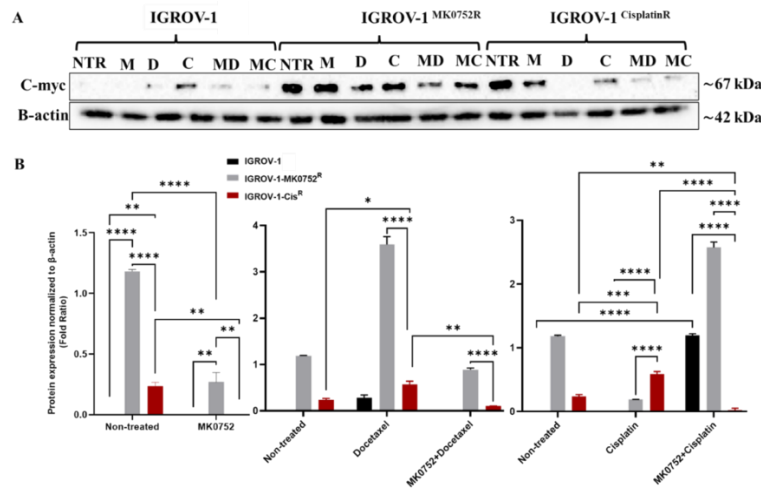


Figure 115. IGROV-1, IGROV-1^{MK0752R} and IGROV-1^{CisR} cells c-myc protein expressions with MK0752, Docetaxel and Cisplatin single agent and combinational treatments. (A) Western blot analysis of c-myc protein for treatments, (B) Normalized c-myc expression to β -actin ratios graphed for both IGROV-1, IGROV-1^{MK0752R} and IGROV-1^{CisR} cells (ns: not significant, *p<0.05, **p<0.01, ***p<0.001, ****p<0.0001).

IGROV-1 cells showed no c-myc protein expression. IGROV-1MK0752R cells showed 1.1-fold increase and IGROV-1CisR cells showed 0.81-fold increase when compared to their non-treated conditions with IGROV-1 cells. MK0752 treatments decreased the expression by 0.58-fold for IGROV-1MK0752R when compared to non-treated IGROV-1MK0752R cells whereas IGROV-1CisR's expression was totally inhibited. Docetaxel single agent treatments for IGROV-1MK0752R cells increased the expression by 2.4-fold and its combination with MK0752 decreased the expression by 1.3-fold. Protein expression levels of c-myc of IGROV-1MK0752R cells compared to IGROV-1CisR cells decreased by 0.29-fold change. Docetaxel single agent treatments compared to MK0752 combinations resulted in additional 0.13-fold decrease for IGROV-1CisR cells. IGROV-1 cells only expressed c-myc when treated with Docetaxel as a single agent by 0.28-fold. IGROV-1 cells were not expressing c-myc when treated with Cisplatin as a single agent yet its combination with MK0752 induced increase in the expression by 1.2-fold. MK0752 and Cisplatin combinational treatments for IGROV-1MK0752R showed 1.3-fold increase in the expression whereas Cisplatin's single agent treatment inhibited the expression by 0.9-fold. MK0752 and Cisplatin combinational treatments for IGROV-1CisR showed 0.38-fold decrease in the expression whereas Cisplatin's single agent treatment increased the expression by 0.42-fold (Figure 115). A2780MK0752R, BG-1MK0752R showed overall decrease in the c-myc protein expression in opposite to IGROV-1MK0752R and SKOV-3MK0752R. Thus, might explain uniqueness of the routes and regulative capacities for each ovarian cancer cell line tested in response to the MK0752 resistance. Spheroids differ in expression of various proteins to maintain 3D microenvironments homeostatic state in cancers. Comparing both monolayer (2D) and spheroid (3D) setups were conducted to understand potential effects on acidity on drug tolerance and resistance. 2D and 3D cell's C-myc's protein expression levels were compared for IGROV-1, BG-1, SKOV-3 and A2780 and their MK0752 resistant clones. SKOV-3 cells were not expressing C-myc for both 2D and 3D comparisons (Figure 116). BG-1 and BG-1^{MK0752R} cells expressed C-myc yet, there were no significant difference measured (Figure 117). A2780 cells nontreated 2D condition expressed 0.6-fold increased expression difference compared to its 3D condition as well as to A2780^{MK0752R} cells (Figure 118). IGROV-1 cells 2D and 3D results were not significantly different but, IGROV-1^{MK0752R} cells increased c-myc protein expression by 0.84-fold for 2D and for 0.75-fold for 3D experiments (Figure 119). C-myc protein expression was not the determinant factor for

the monolayer or spheroids comparisons for A2780^{MK0752R}, SKOV-3^{MK0752R}, BG-1^{MK0752R} and IGROV-1^{MK0752R}. This could be due to its potential acidosis independency as well as not being the main target in controlling environment toxicity for A2780, SKOV-3, BG-1, and IGROV-1 cells to resist MK0752.

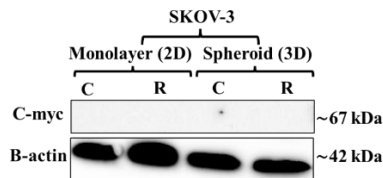


Figure 116. SKOV-3 and SKOV-3^{MK0752R} cells c-myc protein expressionS with 2D and 3D conditions. Western blot analysis of c-myc protein for treatments were represented (C represents SKOV-3 and R represents SKOV-3^{MK0752R}).

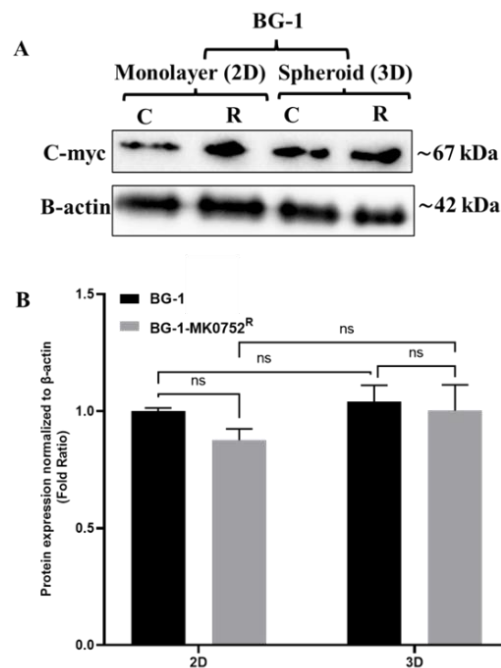


Figure 117. BG-1 and BG-1^{MK0752R} cells c-myc protein expressions with 2D and 3D conditions. (A) Western blot analysis of c-myc protein for treatments, (B) Normalized c-myc expression to β -actin ratios graphed for both BG-1 and BG-1^{MK0752R} cells by Graph Pad PRISM 8. C represents BG-1 and R represents BG-1^{MK0752R}. (ns: not significant).

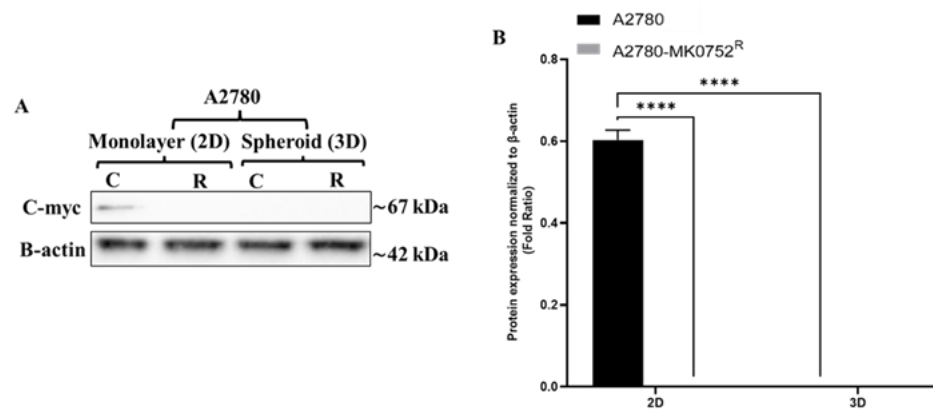


Figure 118. A2780 and A2780^{MK0752R} cells c-myc protein expressions with 2D and 3D conditions. (A) Western blot analysis of c-myc protein for treatments, (B) Normalized c-myc expression to β-actin ratios graphed for both A2780 and A2780^{MK0752R} cells by Graph Pad PRISM 8. Each experiment was performed twice. C represents A2780 and R represents A2780^{MK0752R}. (****p<0.0001).

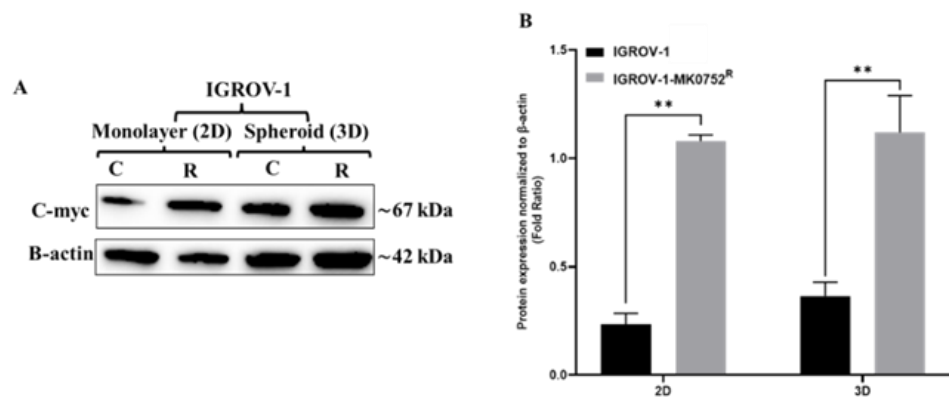


Figure 119. IGROV-1 and IGROV-1^{MK0752R} cells c-myc protein expressions with 2D and 3D conditions. (A) Western blot analysis of c-myc protein for treatments, (B) Normalized c-myc expression to β-actin ratios graphed for both IGROV-1 and IGROV-1^{MK0752R} cells by Graph Pad PRISM 8. Each experiment was performed twice. C represents IGROV-1 and R represents IGROV-1^{MK0752R}. (**p<0.01).

4.7.2.3. MK0752 resistant Ovarian cancer cells regulates Oxidative stress markers protein expression levels

Oxidative stress induces acidosis which helps cancer cells to tolerate the lack of energy source and toxic environments that is associated with drug resistance. To assess MK0752's resistance route, Oxidative stress marker's (Catalase, Smooth muscle actin (SMA), Superoxide Dismutase 1 (SOD1) and Thioredoxin) protein expression levels were compared for every single agent and combinational treatments of MK0752, Cisplatin and Docetaxel for IGROV-1, BG-1, SKOV-3 and A2780 and their MK0752 resistant clones. IGROV-1^{CisR} cells were also included in experiments. BG-1 and BG-1^{MK0752R} cells represented no significant expression difference profile for Catalase protein expressions except the Docetaxel treatments. Docetaxel's combination with MK0752 increased Catalase expression by 0.37-fold when compared to Docetaxel single agent treatments of BG-1 cells (Figure 120 A and B). SMA expressions were not observed for BG-1^{MK0752R} cells. Docetaxel's combination with MK0752 increased SMA expression by 0.11-fold when compared to Docetaxel single agent treatments of BG-1 cells (Figure 120 C).

Cisplatin single agent or combinations were not significantly different when compared to each other however, Cisplatin single agent treatments decreased the expression by 0.14-fold when compared to non-treated BG-1 cells. SOD1 expressions for BG-1^{MK0752R} cells showed 0.49-fold increase when treated with MK0752 and Docetaxel single agent treatments increased the expression by 0.34-fold when compared to non-treated conditions. Cisplatin single agent treatments, MK0752 combinational treatments showed no expression of SOD1 for BG-1^{MK0752R} cells. SOD1 protein expressions were observed stable for BG-1 cells (Figure 120 D). Thioredoxin protein expressions for MK0752 and Docetaxel single agent treatments showed not significant difference for BG-1 and BG-1^{MK0752R} cells. Cisplatin treated BG-1^{MK0752R} cells showed increased expression by 1.1-fold when compared to BG-1 cell's Cisplatin treatments. MK0752's Docetaxel combinations 0.22-fold and Cisplatin combinations, increased by 0.12-fold when compared to non-treated conditions. Cisplatin combinational treatments decreased Thioredoxin expression by 1-fold (Figure 120 E).

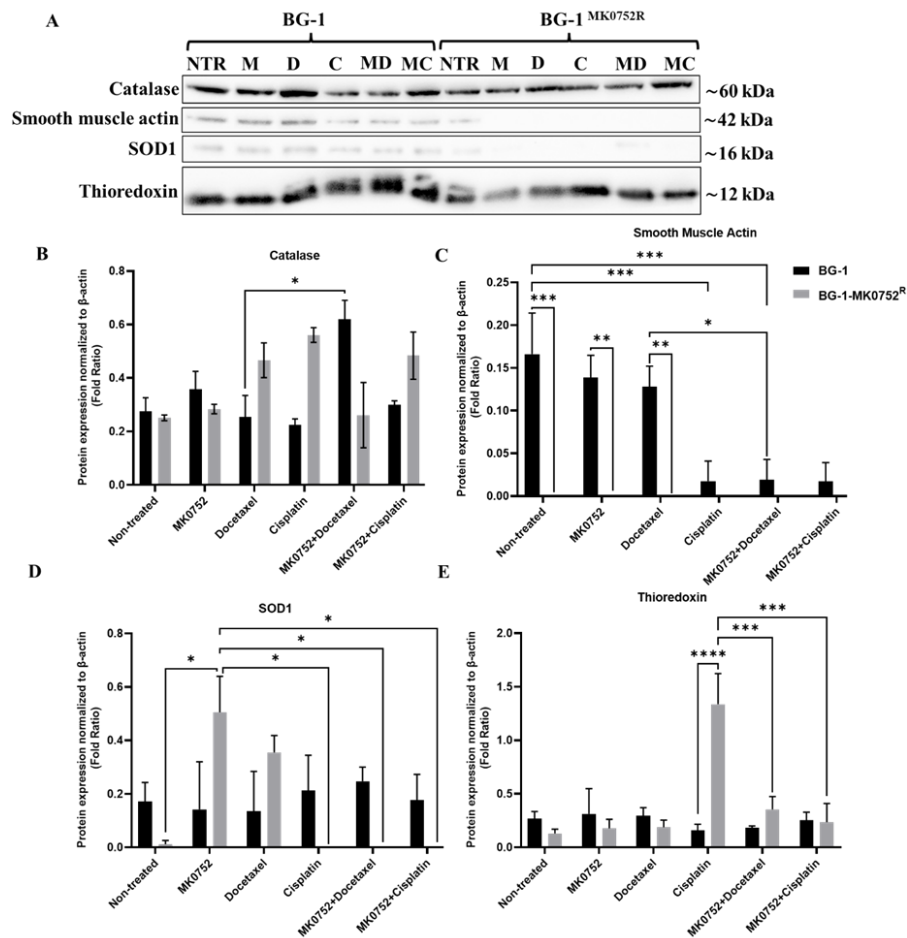


Figure 120. BG-1 and BG-1^{MK0752R} cells Catalase, Smooth muscle actin, SOD1 and Thioredoxin protein expressions with MK0752, Docetaxel and Cisplatin single agent and combinational treatments. (A) Western blot analysis of Oxidative stress marker proteins for treatments, (B) Normalized Catalase expression (C) Smooth muscle actin expression (D) SOD1 expression (E) Thioredoxin expression to β -actin ratios graphed for both BG-1 and BG-1^{MK0752R} cells (* p <0.05, ** p <0.01, *** p <0.001, **** p <0.0001).

Catalase expressions were not observed for A2780 cells whereas A2780^{MK0752R} cells showed 1.2-fold expression. Catalase expressions of A2780^{MK0752R} cells observed as decreased by 1.5-fold for MK0752, 1.59-fold for Docetaxel and 1.61-fold for Cisplatin single agent treatments when compared to non-treated controls. MK0752 combinations with Docetaxel by 0.1-fold and Cisplatin by 0.05-fold increase in the expression were observed for A2780 cells compared to their single agent treatments. MK0752 combinations with Docetaxel by 1.6-fold and Cisplatin by 1.7-fold decrease

in the expression were observed for A2780^{MK0752R} cells compared to their single agent treatments (Figure 121 A and B). SMA expressions were not observed for A2780 cells except when they were treated with MK0752's Docetaxel and Cisplatin combinations by 0.1-fold. SMA expressions of A2780^{MK0752R} cells observed as decreased by 1.2-fold for MK0752, Docetaxel and Cisplatin single agent treatments when compared to non-treated controls. MK0752 combinations with Docetaxel by 1.0-fold and Cisplatin by 1.1-fold decrease in the expression were observed for A2780^{MK0752R} cells compared to non-treated controls (Figure 121 C).

SOD1 expressions were not observed in Docetaxel and Cisplatin single agent treatments and their combinations with MK0752 except the non-treated condition by 1.3-fold for A2780^{MK0752R} cells. Cisplatin single agent treatments and MK0752 combinations showed 0.23-fold decrease when compared to non-treated controls for A2780 cells. Docetaxel combinations with MK0752 resulted in increase of SOD1 expression by 0.41-fold when compared to its single agent treatments for A2780 cells (Figure 121 D). A2780 and A2780^{MK0752R} treatments showed no significant difference of Thioredoxin protein expressions (Figure 121 E). Catalase expressions of SKOV-3^{MK0752R} cells were not observed whereas SKOV-3 cells showed increase by 1.2-fold for MK0752, 0.9-fold for Docetaxel and 0.03-fold for Cisplatin single agent treatments when compared to non-treated control (Figure 122 A and B).

SKOV-3 and SKOV-3^{MK0752R} cells showed no SMA and SOD1 protein expressions for all treatments. MK0752 combinations with Docetaxel decreased the expression by 0.8-fold when compared to Docetaxel single agent treatments for SKOV-3 cells. SKOV-3 cells showed decrease by 0.1-fold for MK0752, 0.7-fold for Docetaxel and 0.9-fold for Cisplatin single agent treatments when compared to nontreated control for Thioredoxin protein expressions. SKOV-3^{MK0752R} cells showed increase by 0.08-fold for MK0752, 0.56-fold for Docetaxel and Cisplatin single agent treatments when compared to nontreated control. MK0752 combinations with Docetaxel decreased the expression by 0.5-fold when compared to non-treated control for SKOV-3 cells and 0.6-fold for SKOV-3^{MK0752R} cells. Docetaxel and Cisplatin combinations with MK0752 showed no significant difference in Thioredoxin protein expression in their single agent treatment comparisons (Figure 122 C).

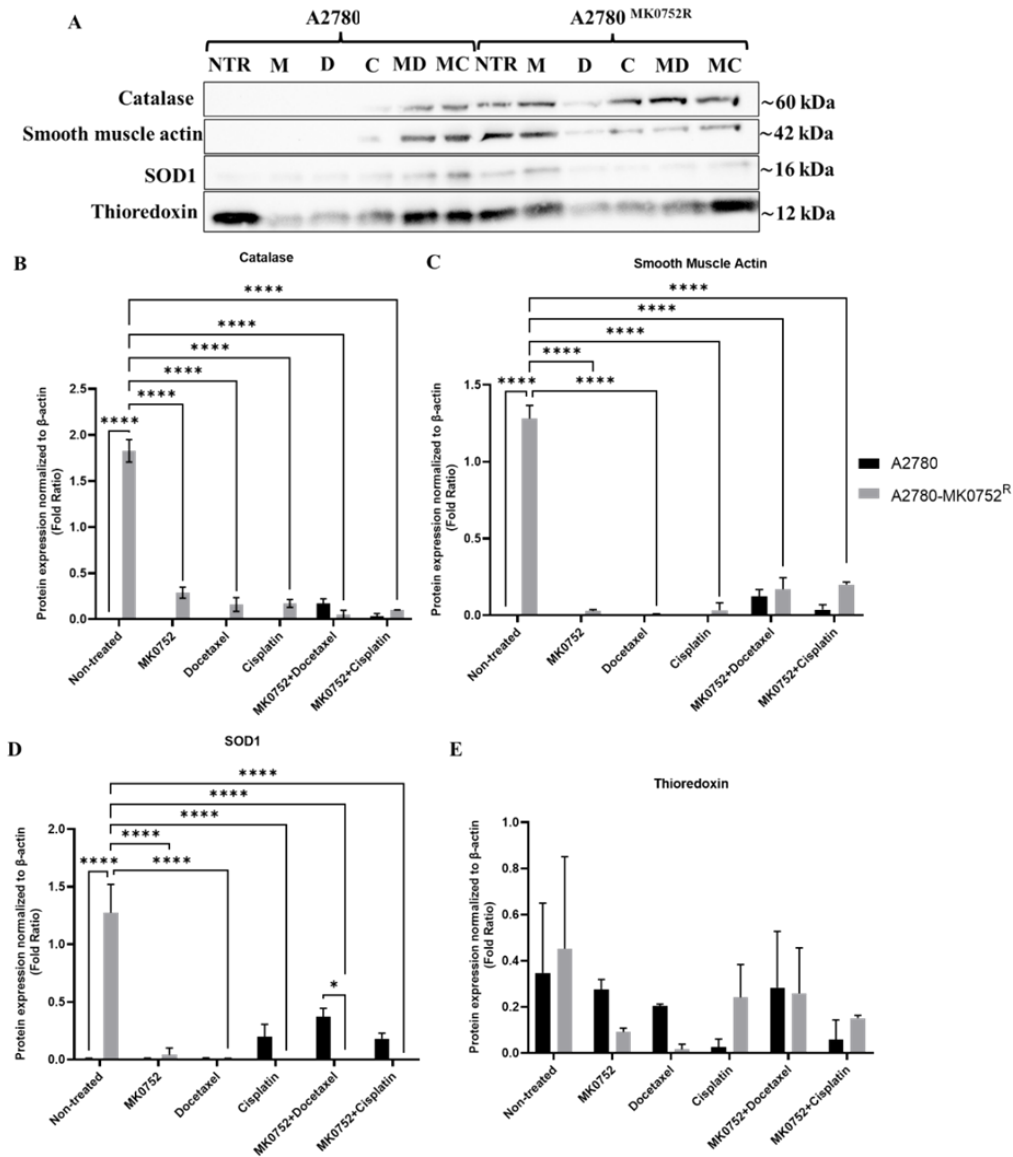


Figure 121. A2780 and A2780^{MK0752R} cells Catalase, Smooth muscle actin, SOD1 and Thioredoxin protein expressions with MK0752, Docetaxel and Cisplatin single agent and combinational treatments. (A) Western blot analysis of Oxidative stress marker proteins for treatments, (B) Normalized Catalase expression (C) Smooth muscle actin expression (D) SOD1 expression (E) Thioredoxin expression to β -actin ratios graphed for both A2780 and A2780^{MK0752R} cells by Graph Pad PRISM 8. Each experiment was performed twice. Two-way ANOVA analysis and student t-test confirmed the significance for conditions (**p<0.001, ****p<0.0001).

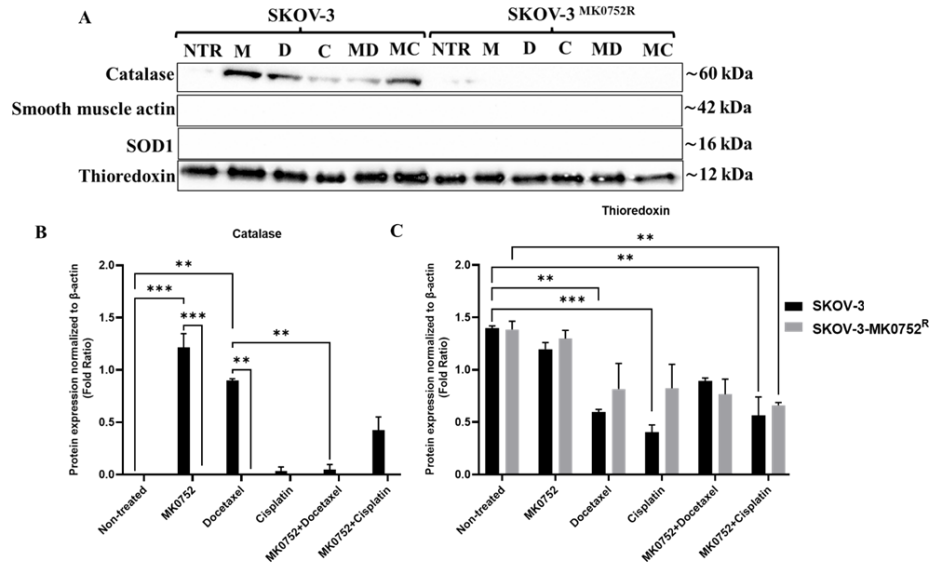


Figure 122. SKOV-3 and SKOV-3^{MK0752R} cells Catalase, Smooth muscle actin, SOD1 and Thioredoxin protein expressions with MK0752, Docetaxel and Cisplatin single agent and combinational treatments. (A) Western blot analysis of Oxidative stress marker proteins for treatments, (B) Normalized Catalase expression (C) Thioredoxin expression to β -actin ratios graphed for both SKOV-3 and SKOV-3^{MK0752R} cells by Graph Pad PRISM 8. Each experiment was performed twice. Two-way ANOVA analysis and student t-test confirmed the significance for conditions (** $p < 0.01$, *** $p < 0.001$, **** $p < 0.0001$).

Catalase protein expressions for IGROV-1, IGROV-1^{MK0752R} and IGROV-1^{CisR} cells were not significantly different from each other for MK0752, Docetaxel and Cisplatin single agent treatments (Figure 123 A and B). IGROV-1^{MK0752R} cells showed expression increase by 0.2-fold for MK0752, 1.3-fold for Docetaxel and decrease 0.49-fold for Cisplatin single agent treatments when compared to non-treated control. IGROV-1^{CisR} cells showed expression increase by 0.3-fold for MK0752, 1.2-fold for Cisplatin and decrease 0.6-fold for Docetaxel single agent treatments when compared to non-treated control. IGROV-1 cells showed expression decrease by 0.4-fold for MK0752, 0.42-fold Docetaxel for and increase 1.1-fold for Cisplatin single agent treatments when compared to non-treated control. MK0752 combinations with Docetaxel resulted in increased by 3.1-fold for IGROV-1 and by 2.3-fold for IGROV-

1^{CisR} cells when compared to their single agent treatments. IGROV-1^{MK0752R} cells combinations with Docetaxel resulted in 0.4-fold decrease compared to Docetaxel single agent treatments. MK0752 combinations with Cisplatin resulted in decreased by 2.6-fold for IGROV-1 and by 1.1-fold for IGROV-1^{CisR} cells when compared to their single agent treatments. IGROV-1^{MK0752R} cells combinations with Cisplatin resulted in 0.2-fold decrease compared to Cisplatin single agent treatments. IGROV-1, IGROV-1^{MK0752R} and IGROV-1^{CisR} cells showed no protein expression of SMA for all treatment conditions. SOD1 expressions were not significantly different between treatment and cell line groups (Figure 123 C). IGROV-1 cells showed expression decrease by 1.1-fold for MK0752, 0.6-fold for Cisplatin and increase 0.4-fold for Docetaxel single agent treatments when compared to non-treated control for Thioredoxin protein expressions. IGROV-1^{MK0752R} cells showed expression increase by 0.1-fold for MK0752, 0.05-fold for Docetaxel and decrease 0.1-fold for Cisplatin single agent treatments when compared to non-treated control. IGROV-1^{CisR} cells showed expression increase by 0.1-fold for MK0752, 0.14-fold for Cisplatin and decrease 0.05-fold for Docetaxel single agent treatments when compared to non-treated control. MK0752 combinations with Docetaxel decreased the Thioredoxin expression by 0.2-fold when compared to Docetaxel single agent treatments for IGROV-1 cells. MK0752 combinations with Cisplatin increased the expression by 1.2-fold when compared to Cisplatin single agent treatments for IGROV-1, IGROV-1^{MK0752R} and IGROV-1^{CisR} cells. MK0752 combinations with Docetaxel increased the expression by 0.3-fold when compared to Cisplatin single agent treatments for IGROV-1^{MK0752R} and IGROV-1^{CisR} cells (Figure 123 D). Aberrant expression patterns of Catalase, Smooth muscle actin, Superoxide Dismutase 1, and Thioredoxin were observed for A2780^{MK0752R}, BG-1^{MK0752R}, SKOV-3^{MK0752R} and IGROV-1^{MK0752R} cells. Dysregulations in the Oxidative stress markers might be the potential route for MK0752 resistance in A2780, BG-1, SKOV-3, and IGROV-1 ovarian cancer cells. Oxidative stress induces acidic tumor environments and pH changes which forms a hallmark of drug resistance. To test this phenomenon, both monolayer (2D) and spheroid (3D) cell's Oxidative stress marker's (Catalase, Smooth muscle actin (SMA), Superoxide Dismutase 1 (SOD1) and Thioredoxin protein expression levels were compared for IGROV-1, BG-1, SKOV-3 and A2780 and their MK0752 resistant clones. IGROV-1 cells were not expressing SMA and showed no significant difference for Catalase, SOD1 and Thioredoxin expressions when compared for both 2D and 3D experiments (Figure 124 A, B, C and D).

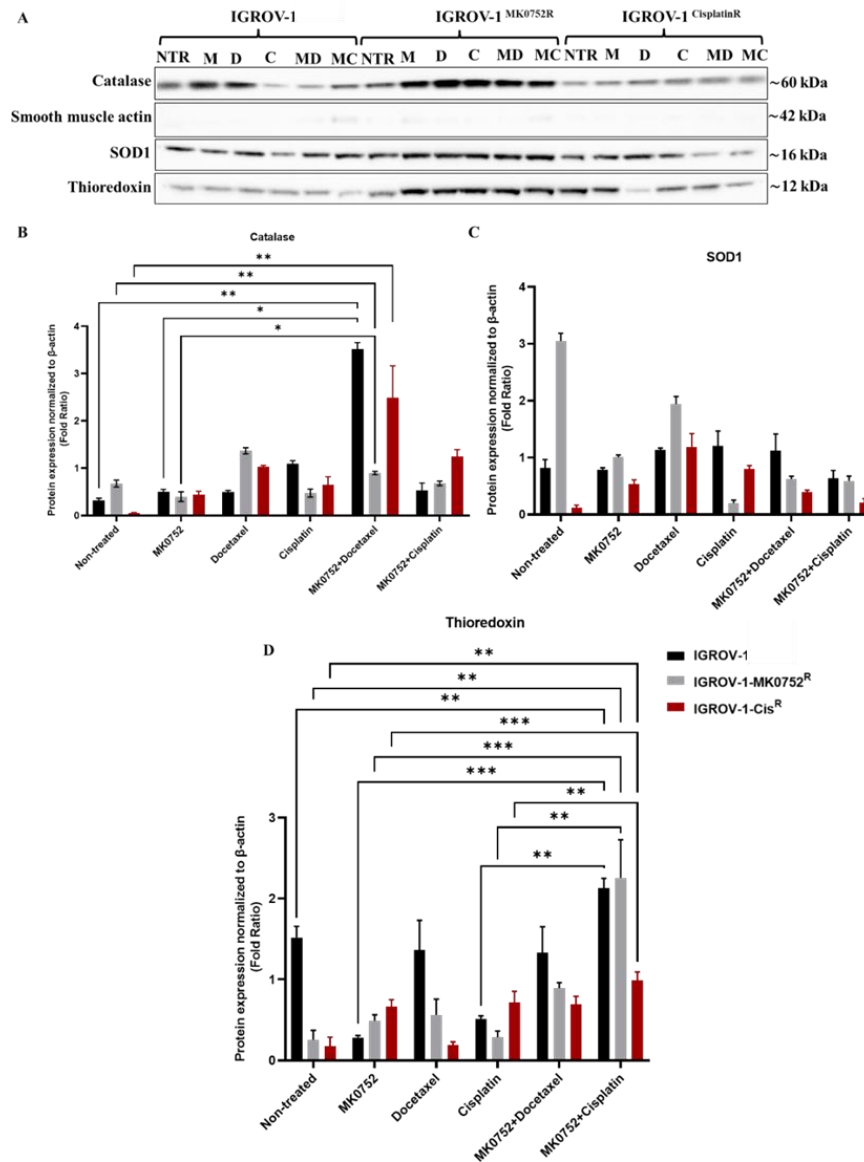


Figure 123. IGROV-1, IGROV-1^{MK0752R} and IGROV-1^{CisR} cells Catalase, Smooth muscle actin, SOD1 and Thioredoxin protein expressions with MK0752, Docetaxel and Cisplatin single agent and combinational treatments. (A) Western blot analysis of Oxidative stress marker proteins for treatments, (B) Normalized Catalase expression (C) SOD1 expression (D) Thioredoxin expression to β -actin ratios graphed for both IGROV-1, IGROV-1^{MK0752R} and IGROV-1^{CisR} cells by Graph Pad PRISM 8. Each experiment was performed twice. Two-way ANOVA analysis and student t-test confirmed the significance for conditions (* $p < 0.05$, ** $p < 0.01$, *** $p < 0.001$, **** $p < 0.0001$).

SKOV-3 cells showed no expression of Catalase, SMA and SOD1 however, Thioredoxin protein expressions were increased by 0.42-fold for 3D SKOV-3 cells and decreased 0.31-fold for 3D SKOV-3^{MK0752R} when compared to cells 2D condition. 3D SKOV-3 cells showed 0.6-fold difference when compared to 3D SKOV-3^{MK0752R} cells (Figure 125 A and B). BG-1 and BG-1^{MK0752R} cells showed no significant differences in protein expressions for Catalase, SMA and SOD1 when compared to their 2D and 3D conditions. Thioredoxin protein expressions showed 0.75-fold difference when compared to BG-1 and BG-1^{MK0752R} cell's 2D conditions and 0.53-fold for their 3D comparisons. BG-1 cells 2D condition resulted in 0.28-fold decrease when compared to BG-1 cells 3D condition. BG-1^{MK0752R} cells 2D condition resulted in 0.06-fold decrease when compared to BG-1^{MK0752R} cells 3D condition (Figure 126 A, B and C).

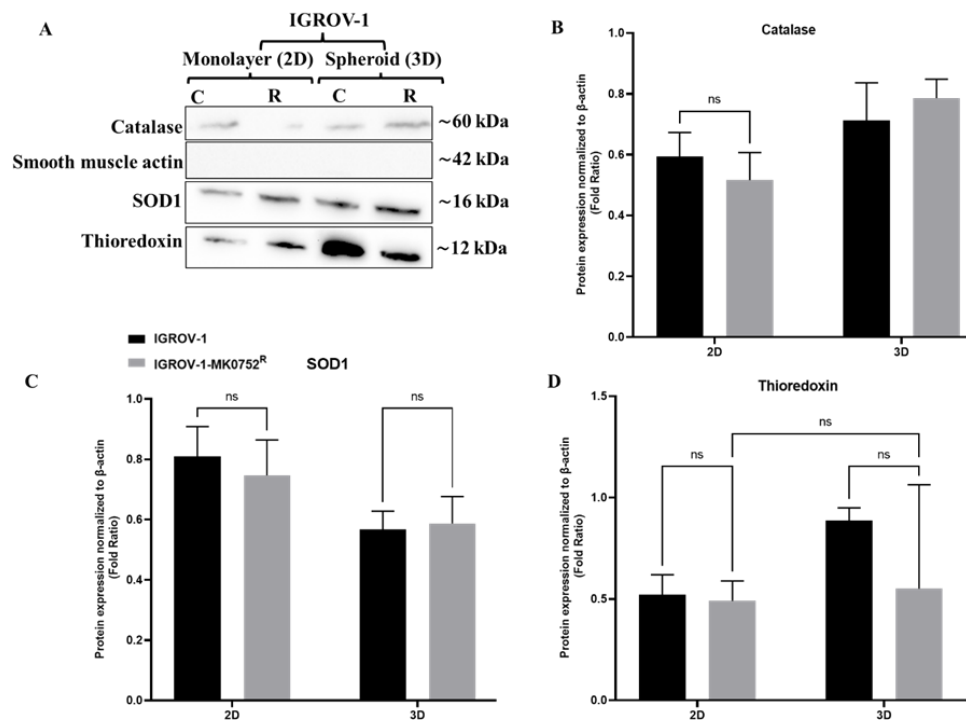


Figure 124. IGROV-1 and IGROV-1^{MK0752R} cells Catalase, Smooth muscle actin, SOD1 and Thioredoxin protein expressions with 2D and 3D conditions. (A) Western blot analysis of oxidative stress marker proteins for treatments, (B) Normalized Catalase expression (C) SOD1 expression (D) Thioredoxin expression to β -actin ratios graphed for both IGROV-1 and IGROV-1^{MK0752R} cells by Graph Pad PRISM 8. (ns: not significant).

A2780 and A2780^{MK0752R} cells showed no protein expression of Catalase and SOD1 for both 2D and 3D conditions. SMA was expressed 0.62-fold by only A2780^{MK0752R} cells for 2D conditions and Thioredoxin protein expressions resulted in no significant difference between conditions for both A2780 and A2780^{MK0752R} cells (Figure 127 A, B, C and D). Spheroids were found to be aberrantly expressing Catalase, SMA, SOD1 and Thioredoxin when compared to monolayer IGROV-1, A2780, BG-1 and SKOV-3 due to their acidic nature yet this could be a route to tolerate MK0752 treatments.

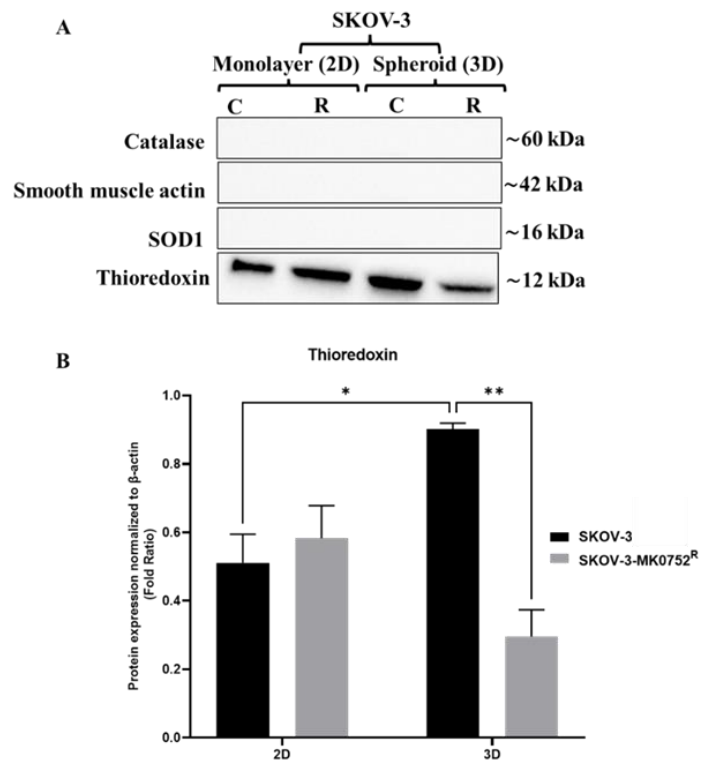


Figure 125. SKOV-3 and SKOV-3^{MK0752R} cells Catalase, Smooth muscle actin, SOD1 and Thioredoxin protein expressions with 2D and 3D conditions. (A) Western blot analysis of oxidative stress marker proteins for treatments, (B) Thioredoxin expression to β-actin ratios graphed for both SKOV-3 and SKOV-3^{MK0752R} cells by Graph Pad PRISM 8. Each experiment was performed twice. Two-way ANOVA analysis and student t-test confirmed the significance for conditions (*p<0.05, **p<0.01).

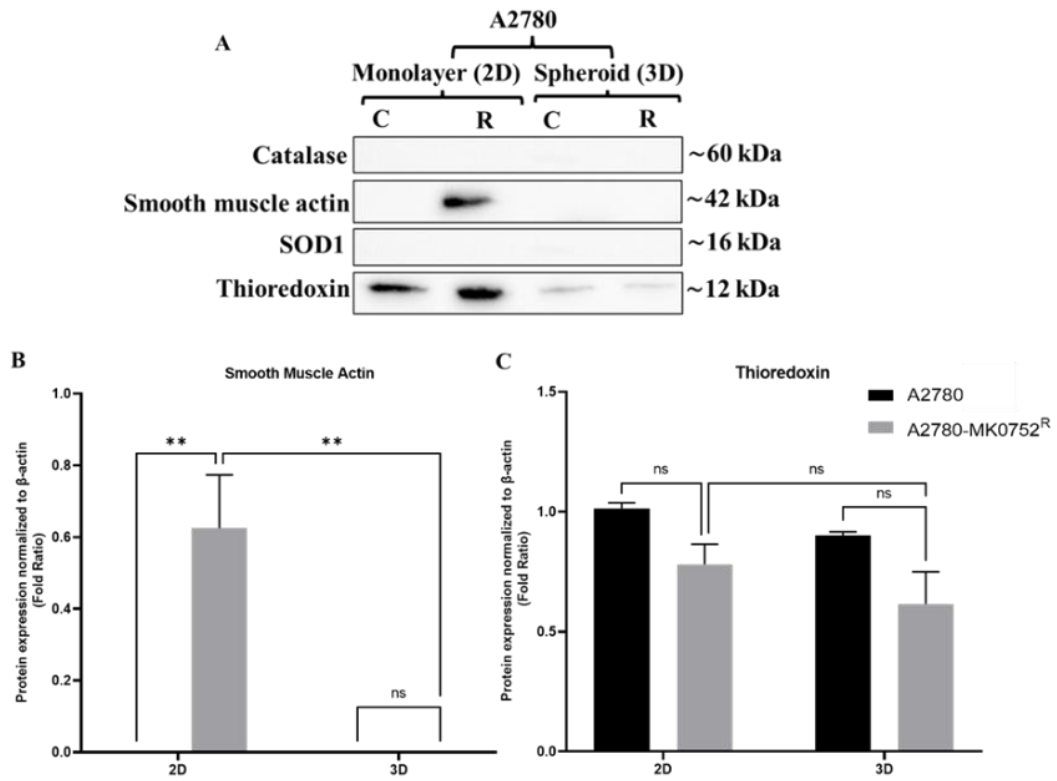


Figure 126. A2780 and A2780^{MK0752R} cells Catalase, Smooth muscle actin, SOD1 and Thioredoxin protein expressions with 2D and 3D conditions. (A) Western blot analysis of oxidative stress marker proteins for treatments, (B) Smooth muscle actin expression (C) Thioredoxin expression to β -actin ratios graphed for both A2780 and A2780^{MK0752R} cells (ns: not significant, ** $p < 0.01$).

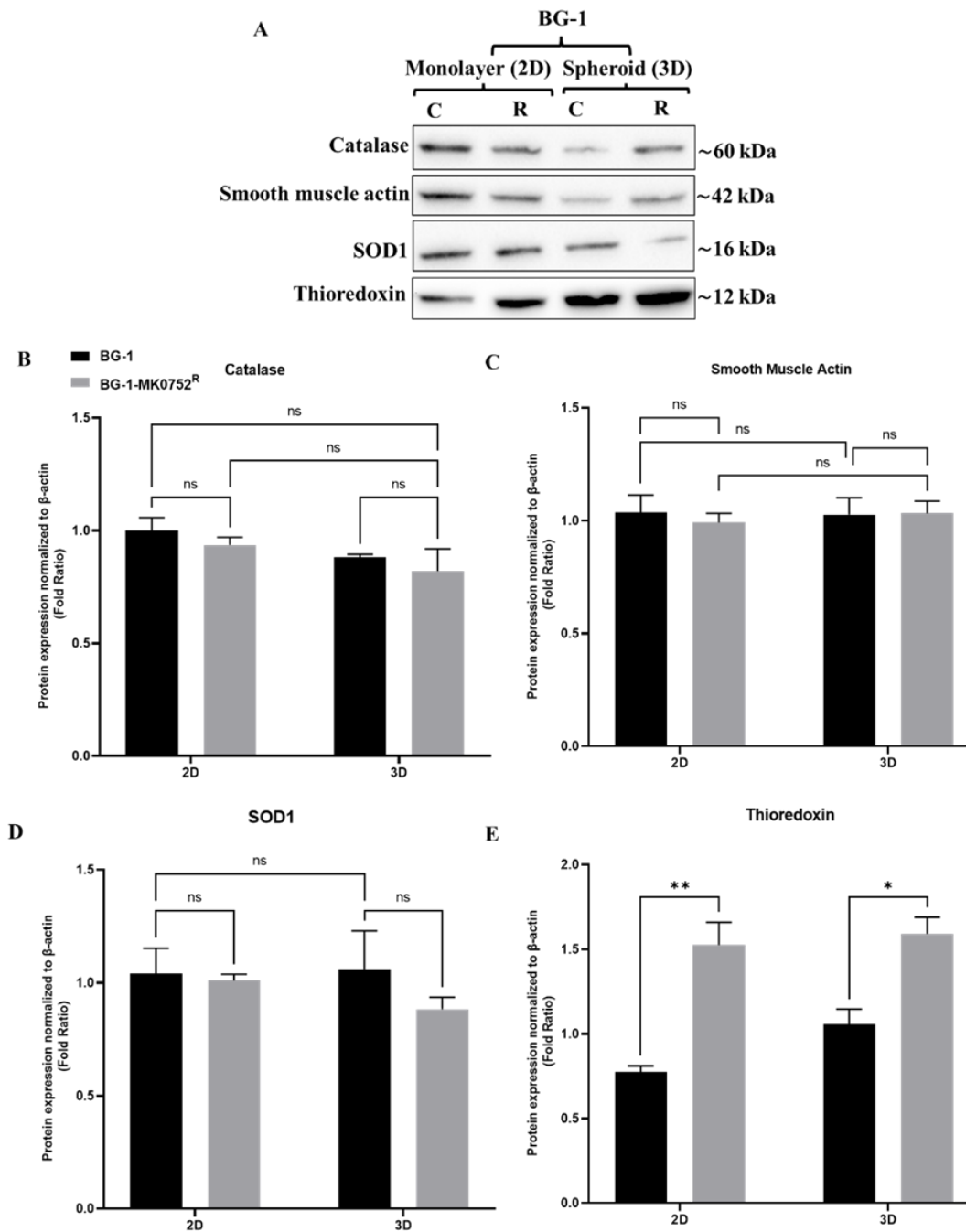


Figure 127. BG-1 and BG-1^{MK0752R} cells Catalase, Smooth muscle actin, SOD1 and Thioredoxin protein expressions with 2D and 3D conditions. (A) Western blot analysis of oxidative stress marker proteins for treatments, (B) Normalized Catalase expression (C) Smooth muscle actin expression, (D) SOD1 expression (E) Thioredoxin expression to β -actin ratios graphed for both BG-1 and BG-1^{MK0752R} cells (ns: not significant, * $p < 0.05$, ** $p < 0.01$).

4.7.2.4. Proteomic profiling and comparison of IGROV-1^{CisR} and IGROV-1^{MK0752R} cells

Drugs resistance mechanisms can differ through specific treatment induced dysregulated pathways. Proteomic profiling was conducted to uncover and compare potential altered targets for IGROV-1^{CisR} and IGROV-1^{MK0752R} cells to clarify resistance pattern. IGROV-1^{CisR} and IGROV-1^{MK0752R} cells were collected after resistance confirmations and analysed by Label-free quantification of LC-MS/MS in independent triplicates. Results were normalized to IGROV-1 parental cells and abundance ratio's including p-values were analysed. Proteomics analysis allowed an overall identification of 1477 proteins and fold changes of abundance higher than 2 were highlighted as upregulated whereas lower than -1.5 represented as downregulated. Between 2 and -1.5 abundance fold changes were also plotted due to dysregulated patterns and significance. Proteins downregulated in IGROV-1^{MK0752R} cells and upregulated in both IGROV-1^{CisR} and IGROV-1^{MK0752R} cells were listed (Table 3 and 4). Dysregulated proteins were listed for both conditions (Table 5).

Table 3. Proteins downregulated in IGROV-1^{MK0752R} cells identified by label-free proteomics approach. Fold changes in bold represent the lowest ratio compared.

Uniprot Accession	Gene Symbol	Protein Name	Fold Change MK0752R	Fold Change CISR	P-Value (-log10) MK0752R	P-Value (-log10) CISR
Q5JPU3	<i>PDHA1</i>	Pyruvate dehydrogenase E1 component subunit alpha, somatic form, mitochondrial	-2,11	-0,72	2,39	2,01
Q9Y5S9	<i>RBMSA</i>	RNA-binding protein 8A	-1,63	0,752	2,16	2,39

Table 4. Proteins upregulated in IGROV-1^{CisR} and IGROV-1^{MK0752R} cells identified by label-free proteomics approach. Fold changes in bold represent the highest ratio compared.

Uniprot Accession	Gene Symbol	Protein Name	Fold Change MK0752R	Fold Change CISR	P-Value (-log10) MK0752R	P-Value (-log10) CISR
Q5SWL8	<i>PRAMEF19</i>	PRAME family member 19	2,33	2,94	2,59	3,12
A0A075B6F9	<i>NOSIP</i>	Nitric oxide synthase interacting protein	-0,71	2,069	2,78	2,17

Table 5. Proteins dysregulated in IGROV-1^{CisR} and IGROV-1^{MK0752R} cells cells identified by label-free proteomics approach. Fold changes in bold represents the highest ratio compared.

Uniprot Accession	Gene Symbol	Protein Name	Fold Change MK0752R	Fold Change CISR	P-Value (-log10) MK0752R	P-Value (-log10) CISR
Q8TEQ6	<i>GEMIN5</i>	Gem-associated protein 5	-0.85	-0.88	2	4.3
Q14204	<i>DYNC1H1</i>	Cytoplasmic dynein 1 heavy chain 1	-0.43	-0.84	4.09	2.12
Q7Z2W4	<i>ZC3HAV1</i>	Zinc finger CCH-type antiviral protein 1	0.3	-0.73	2.07	2.01
Q7RTV0	<i>PHF5A</i>	PHD finger-like domain-containing protein 5A	-0.4	-0.7	2.43	3.6
Q7Z6Z7	<i>HUWE1</i>	E3 ubiquitin-protein ligase	-0.69	-0.63	2.03	2.11
O95865	<i>DD4H2</i>	N(G),N(G)-dimethylarginine dimethylaminohydrolase 2	-0.5	-0.61	2.33	2.7
P08240	<i>SRPR4</i>	Signal recognition particle receptor subunit alpha	0.29	-0.57	2.02	3.1
BIAPN9	<i>PP1L4</i>	Lipin-alpha-4	-1.18	-0.54	3.34	2.4
E5RFR7	<i>TPD52</i>	Tumor protein D52	-1.05	-0.53	3.79	3.5
P18583	<i>SON</i>	Protein SON	0.4	-0.52	2.18	2.9
O43765	<i>SGTA</i>	Small glutamine-rich tetrapeptide repeat-containing protein alpha	-0.64	-0.44	3.41	3.4
P53367	<i>ARFIP1</i>	Arfapin-1	-0.27	-0.44	3.26	4.1
Q9NUP9	<i>LIN7C</i>	Protein lin-7 homolog C	0.05	-0.41	2.08	2.4
P05141	<i>SIC25A5</i>	ADP/ATP translocase 2	-0.29	-0.36	2.47	3
P25398	<i>RPS12</i>	40S ribosomal protein S12	0.25	-0.36	2.36	2.4
Q32M24	<i>LRRFIP1</i>	Leucine-rich repeat flightless-interacting protein 1	-1.03	-0.31	2.21	2.71
H0Y8G5	<i>HNRNPD</i>	Heterogeneous nuclear ribonucleoprotein D0	-0.42	-0.29	2.1	2.42
P62072	<i>TIMM10</i>	Mitochondrial import inner membrane translocase subunit Tim10	-0.85	-0.28	2.19	2.5
A0A669KB05	<i>CTNND1</i>	Catenin delta-1	-0.03	-0.27	3.14	3.03
Q14315	<i>FLNC</i>	Filamin-C	-0.2	-0.17	2.9	2.5
Q9BQ70	<i>TCF25</i>	Transcription factor 25	0.5	-0.07	2.8	2.1
P22061	<i>PCMT1</i>	Protein-L-isoaspartate(D-aspartate) O-methyltransferase	-0.1	0.427	2.16	2.31
A0A2R8Y5S7	<i>RDY</i>	Radixin	0.54	0.46	2.05	2.97
Q9NZM1	<i>MYOF</i>	Myoferlin	-0.52	0.503	2.33	4.1
Q9HBR0	<i>SLC38A10</i>	Putative sodium-coupled neutral amino acid transporter 10	-0.31	0.574	2.18	2.11
P60174	<i>TPH1</i>	Tryptophan hydroxylase 1	-0.02	0.58	3.81	2.3
Q07812	<i>BAX</i>	Bcl-2-associated X protein	-0.95	0.602	2.07	3
Q86XP3	<i>DDX42</i>	ATP-dependent RNA helicase DDX42	-0.3	0.647	2	2.8
Q9UNH7	<i>SNX6</i>	Sorting nexin-6	0.55	0.653	2.86	2.4
H0Y4V9	<i>LARP4B</i>	La-related protein 4B (Fragment)	-0.3	0.698	4.07	2.2
Q96919	<i>WWP2</i>	WW domain-binding protein 2	-0.9	0.711	2.12	2.3
J3KPS8	<i>CLIP1</i>	CAP-Gly domain-containing linker protein 1	-0.35	0.746	2.22	3.6
Q95336	<i>PGLS</i>	6-phosphogluconolactonase	-0.43	0.756	2.01	2.7
FSW114	<i>ITPR3</i>	Intraflagellar transport protein 81 homolog	0.31	0.763	2.44	2.4
Q14573	<i>ITPR3</i>	Inositol 1,4,5-trisphosphate receptor type 3	-0.53	0.85	2.13	2.1
P54886	<i>ALDH18A1</i>	Delta-1-pyrroline-5-carboxylate synthase	-0.73	0.868	2.05	2.02
Q14651	<i>PLS1</i>	Plastin-1	-1.34	0.886	2.36	2
Q00515	<i>LADI</i>	Lactinin-1	-0.92	1.018	2.27	3.1
P58107	<i>EPPLK1</i>	Epplakin	-1.04	1.021	2.23	3.4
Q9BS18	<i>ESYT1</i>	Extended synaptotagmin-1	-0.58	1.235	2.42	2.5
A0A669KAX3	<i>WFS1</i>	Wolframin	1.28	1.323	2.83	3.4
Q7L710	<i>H2AF</i>	Histone H2A type 3	0.03	1.92	2.13	3

Identifying dysregulated proteins from IGROV-1^{CisR} and IGROV-1^{MK0752R} cells, MaxQuant label-free algorithm (LFQ) was applied to analyse the relative protein abundance created via spectral intensity. Significance was set by using t-test and False Discovery Rate (FDR) were set <0.05 as significance base and fold-change ratio's as >2 or <-1.5 for differential abundance limit. In such profiling, there were no proteins found as significant and less than a -1.5-abundance fold ratio. p-values and fold ratios of the data represented as volcano plots showing both significant and nonsignificant differences between IGROV-1^{CisR} and IGROV-1^{MK0752R} (Figure 128A). Significantly dysregulated 46 hits were represented as a heatmap showing up or downregulation of genes for both IGROV-1^{CisR} and IGROV-1^{MK0752R} conditions (Figure 128B).

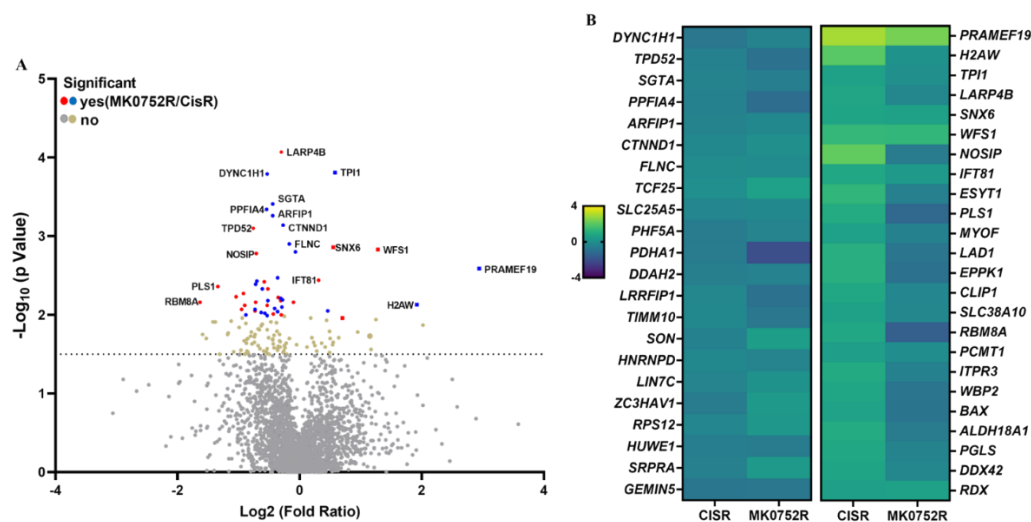


Figure 128. Proteomics data interpretation and visualization of IGROV-1^{MK0752R} and IGROV-1^{CisR} cells. (A) Volcano plot comparing differential protein expression in IGROV-1^{CisR} and IGROV-1^{MK0752R} samples. The proteins significantly upregulated are red or blue dots and those upregulated are in a square shape, while the grey dots represent the proteins with insignificant expression. Only a few protein names were written due to lack of space. The p-value <0.05 was used for this significance cut-off. (B) Heatmap analysis of 46 significantly dysregulated proteins for IGROV-1^{CisR} and IGROV-1^{MK0752R} with FDR, p-value<0.05 as significance threshold and fold-change >2 or <-1.5 as the differential abundance threshold.

The functional proteome distribution of 46 dysregulated proteins for both IGROV-1^{CisR} and IGROV-1^{MK0752R} were represented as pie charts. Analysis was performed by Panther Tool and represented in enriched categories as molecular function, cellular component, biological processes, protein class categories and pathways. Utmost enriched terms in molecular function were transporter activity (10.5%) and catalytic activity (15.8%) (Figure 129 A). Cellular component was divided into a cellular anatomical entity (79.7%) and protein-containing complex (20.3%) (Figure 129 B).

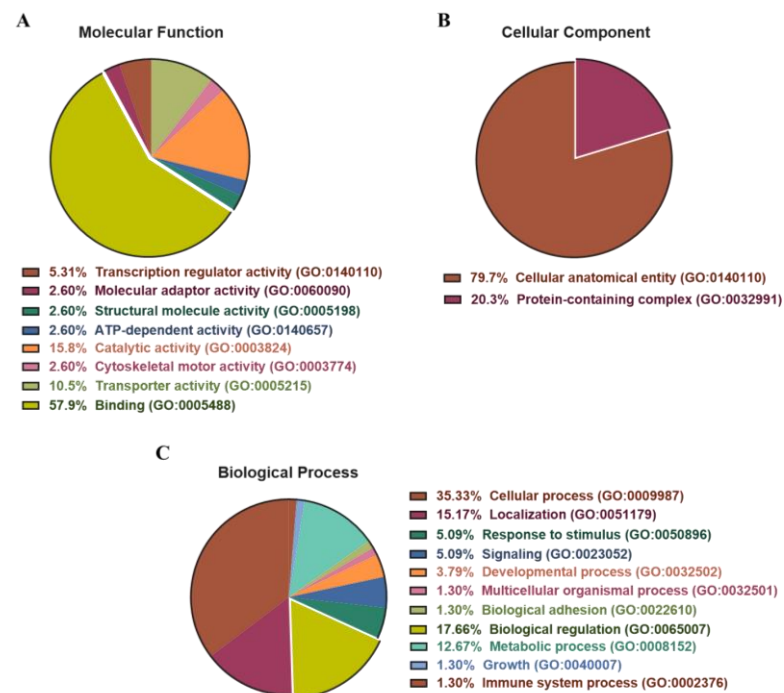


Figure 129. Pie charts showing the proteome distribution on molecular function, cellular component, and biological processes. All dysregulated proteins identified in IGROV-1^{CisR} and IGROV-1^{MK0752R} samples were annotated with the PANTHER Classification system (<http://www.pantherdb.org/>, accessed on 19 October 2022) according to their (A) molecular function, (B) cellular component and (C) biological process.

Biological processes represented cellular process (35.33%), localization (15.17%) and biological regulation (17.66%) as most enriched (Figure 129 C). The dysregulated proteins were predominantly in cytoskeletal (14%), transporter (9.21%),

RNA metabolism (11.21%), translational (10.21%), metabolite interconversion enzyme (20.22%) in class categories (Figure 130A). Pathway interactions were distributed equally among signaling and activation routes (Figure 130B). Collectively, Notch's vital role in cell fate reflects in IGROV-1's MK0752 resistance through dysregulations of its downstream pathways.

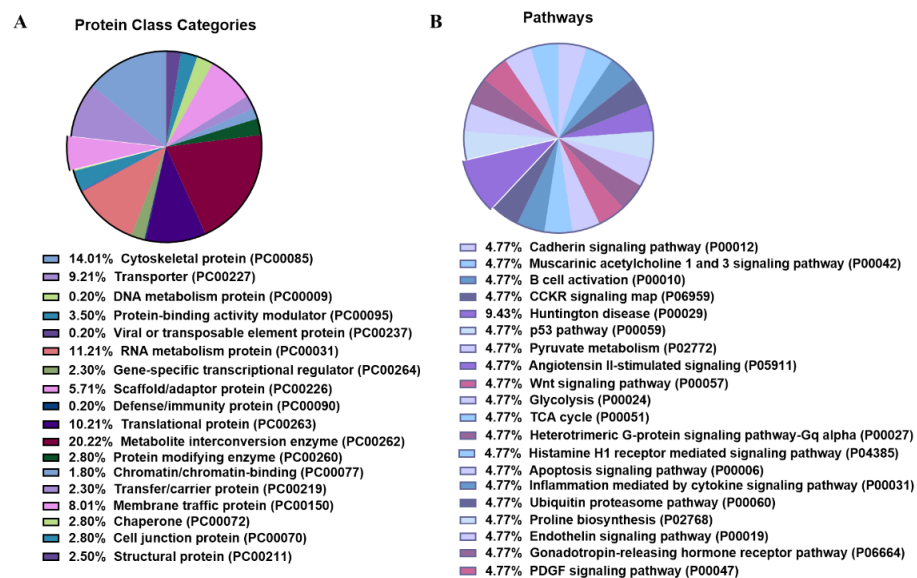


Figure 130. Pie charts showing the proteome distribution on protein class categories and pathways. All dysregulated proteins identified in IGROV-1^{CisR} and IGROV-1^{MK0752R} samples were annotated with the PANTHER Classification system (<http://www.pantherdb.org/>, accessed on 19 October 2022) according to their (A) protein class categories and (B) pathways.

Dysregulated proteins were then applied to Gene Mania through Cytoscape (<https://genemania.org>, accessed on 19 October 2022) to map probable network among them. There were 24 dysregulated proteins with addition of 5-10 possible correlated proteins and their predicted functional associations were networked for IGROV-1^{CisR} cells. Intracellular transport regulatory, cellular protein localization, cell metabolism, cell-cell junction, mitochondrial transport functions were the top enrichments made for IGROV-1^{CisR} cells (Figure 131). IGROV-1^{MK0752R} cell's 20 dysregulated proteins with the addition of 5-10 possible correlated proteins and their predicted functional associations were networked. Apoptotic signalling pathway, endoplasmic reticulum

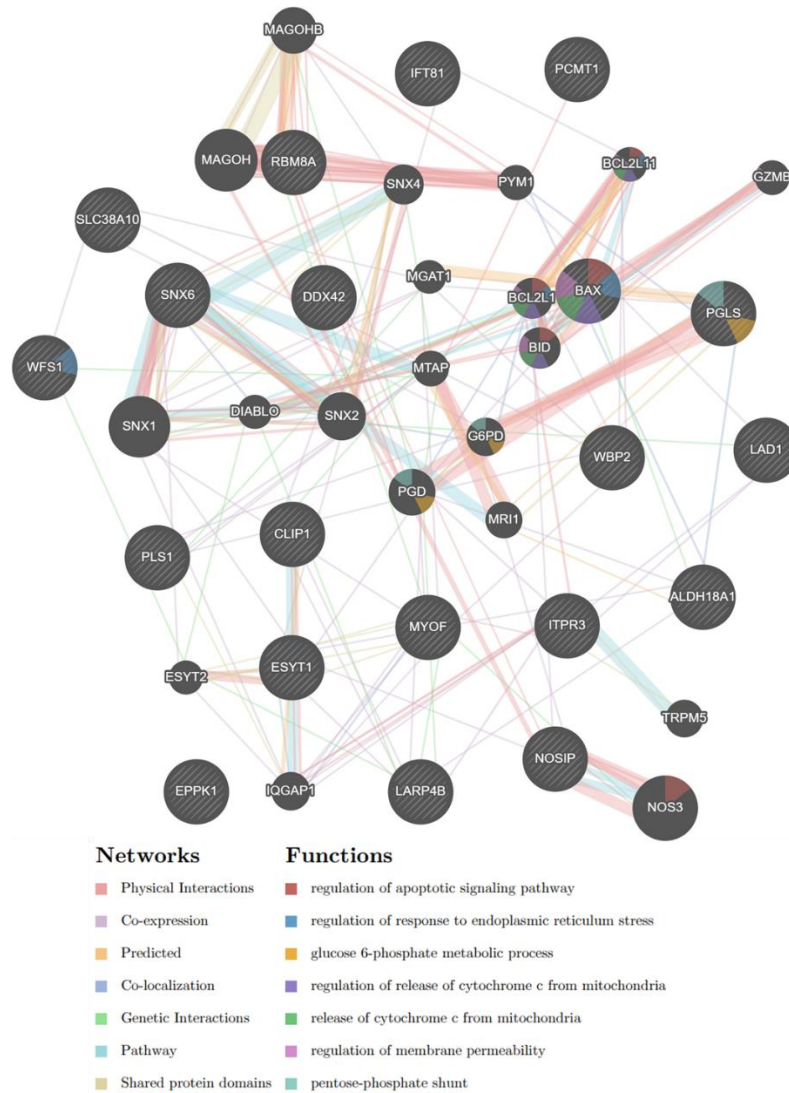


Figure 132. Functional gene network analysis of genes dysregulated in IGROV-1^{MK0752R} cells. Significant enrichment in the functional networks was identified and presented by GeneMania tool. Bold dots without interlines represent further interactions based on the database.

Dysregulated proteins were then categorized based on their cellular functional role and differential log₂ LFQ intensities for IGROV-1, IGROV-1CisR and IGROV-1MK0752R cells. Seven proteins, Dynein cytoplasmic 1 heavy chain 1 (DYNC1H1), solute carrier family 25 member 5 (SLC25A5), PHD finger protein 5A (PHF5A), LRR binding FLII interacting protein 1 (LRRFIP1), zinc finger CCCH-type containing (ZC3H), DEAD-box helicase 42 (DDX42), heterogeneous nuclear ribonucleoprotein D (HNNRPD) were found to be taking role in cell proliferation. DYNC1H1 and PHF5A showed significant 1.5-fold decrease for IGROV-1^{MK0752R} cells compared to IGROV-1

cells. LRRFIP1 resulted in 1.2-fold decrease for IGROV-1^{CisR} cells compared to IGROV-1 cells. ZC3H were 0.7-fold decreased in IGROV-1^{MK0752R} cells and 0.4-fold increase in IGROV-1^{CisR} cells when compared to control group. SLC25A5, DDX42, HNNRPD represented no significant change for abundance comparisons (Figure 134).

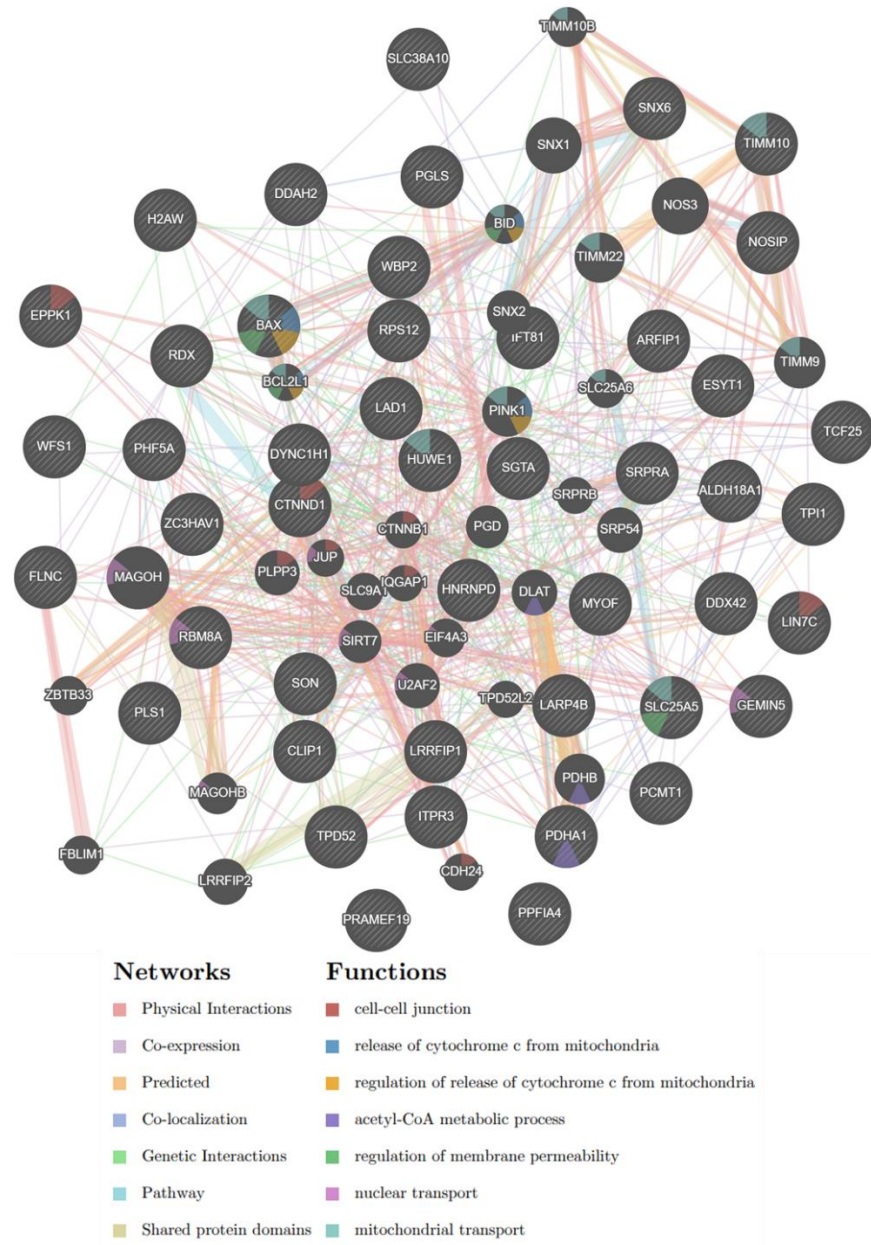


Figure 133. Collective functional gene network analysis of genes dysregulated in IGROV-1^{CisR} and IGROV-1^{MK0752R} cells. Significant enrichment in the functional networks was identified and presented by GeneMania tool. Bold dots without interlines represent further interactions based on the database.

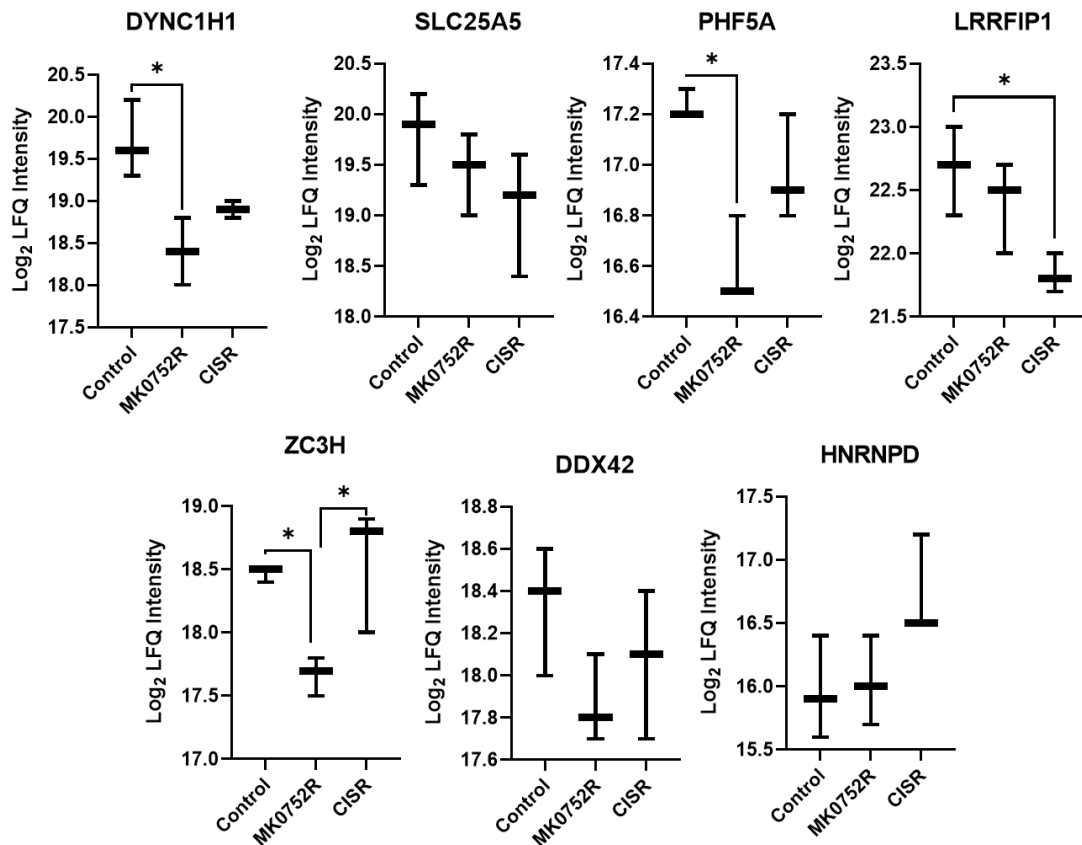


Figure 134. Proteomic signatures of IGROV-1, IGROV-1^{MK0752R} and IGROV-1^{CisR} cells in cell proliferation. Box plots represent dysregulated proteins based on the LFQ intensity. *p<0.05.

Six proteins, ADP ribosylation factor interacting protein 1 (ARFIP1), pyruvate dehydrogenase E1 subunit alpha 1 (PDHA1), wolframin ER transmembrane glycoprotein (WFS1), 6-phosphogluconolactonase (PGLS), RNA binding motif protein 8A (RBM8A), aldehyde dehydrogenase 18 family member A1 (ALDH18A1) were found to be taking role in cell metabolism. ARFIP1 abundance was 0.6-fold decreased in IGROV-1^{MK0752R} cells when compared to nontreated control cells. WFS1 showed increased LFQ intensity by 0.8-fold for IGROV-1^{MK0752R} and by 1.1-fold for IGROV-1^{CisR} cells. PGLS abundance was decreased by 0.4-fold for both IGROV-1^{MK0752R} and IGROV-1^{CisR} cells. PDHA1, RBM8A and ALDH18A1 represented no significant change for abundance comparisons (Figure 135).

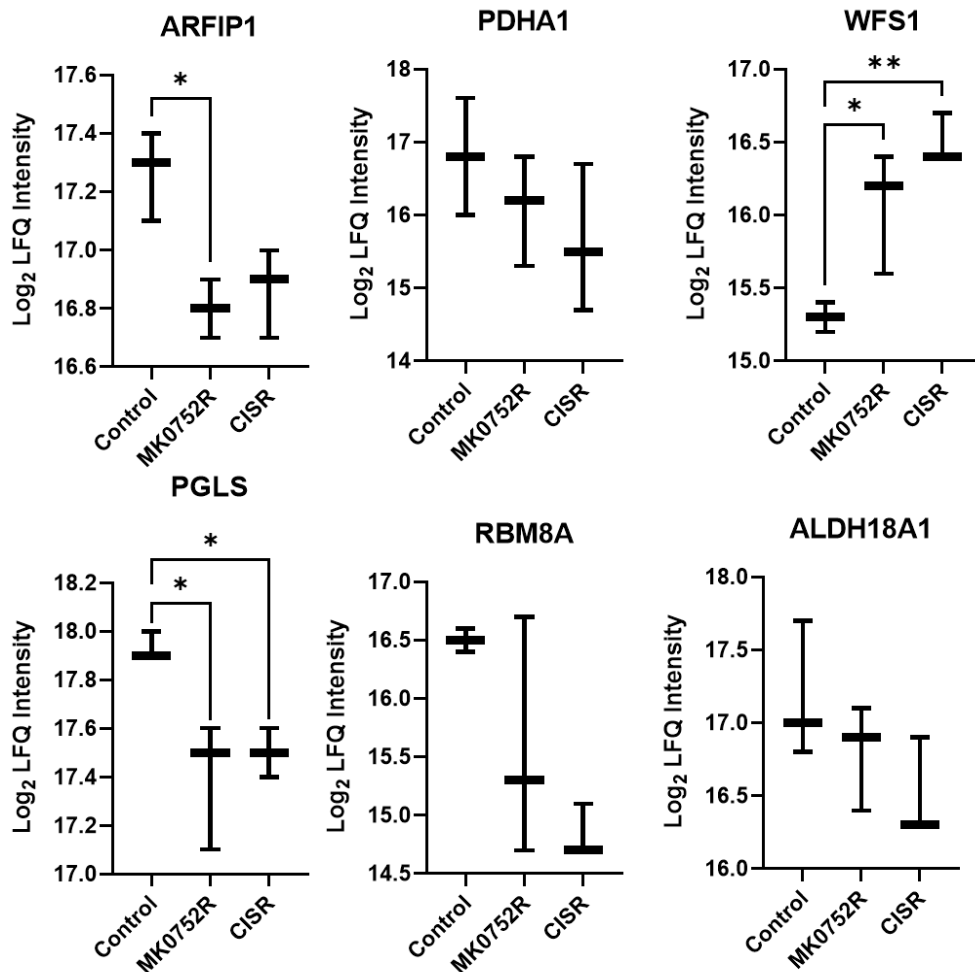


Figure 135. Proteomic signatures of IGROV-1, IGROV-1^{MK0752R} and IGROV-1^{CisR} cells in cell metabolism. Box plots represent dysregulated proteins based on the LFQ intensity. * $p < 0.05$, ** $p < 0.01$.

Four proteins were found taking role in cell growth transcription factor 25 (TCF25), W domain binding protein 2 (WBP2), gem nuclear organelle associated protein 5 (GEMIN5) and La-related protein 4B (LARP4B). LARP4B abundance was decreased significantly by 0.4-fold for IGROV-1^{MK0752R} cells. WBP2 LFQ intensity was also decreased 0.38-fold for IGROV-1^{CisR} cells. 0.41-fold change was observed when IGROV-1^{MK0752R} and IGROV-1^{CisR} cells were compared for WBP2 abundance. TCF25 and GEMIN5 represented no significant change for abundance comparisons (Figure 136).

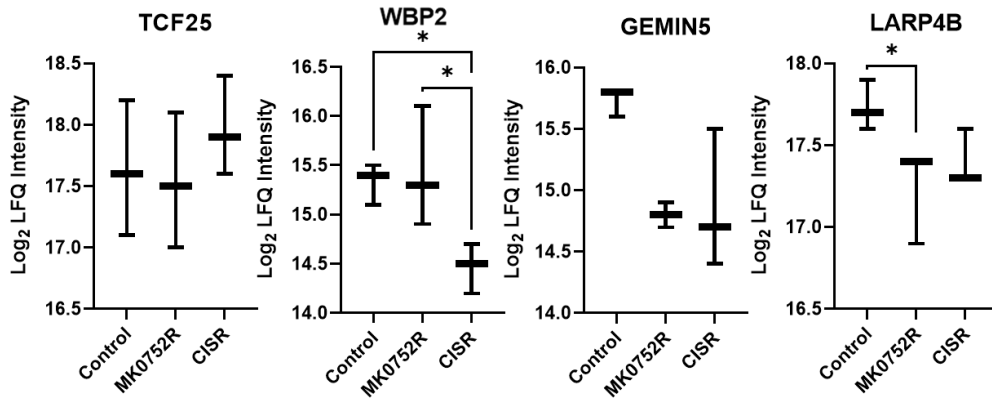


Figure 136. Proteomic signatures of IGROV-1, IGROV-1^{MK0752R} and IGROV-1^{CisR} cells in cell growth. Box plots represent dysregulated proteins based on the LFQ intensity. *p<0.05.

Six proteins, small glutamine rich tetratricopeptide repeat containing alpha (SGTA), translocase of inner mitochondrial membrane 10 (TIMM10), SRP receptor subunit alpha (SPRRA), solute carrier family 38 member 10 (SLC38A10), sorting nexin 6 (SNX6), and extended synaptotagmin 1 (ESYT1) were found taking role in membrane transport. Only SNX6 IGROV-1^{CisR} abundance was increased significantly by 0.6-fold when compared to IGROV-1 cells (Figure 137). Lin-7 homolog C, crumbs cell polarity complex component (LIN7C) and inositol 1,4,5-trisphosphate receptor type 3 (ITPR3) were observed taking role in exocytosis. LIN7C showed no significant changes yet, ITPR3 resulted in 1.1-fold increase for IGROV-1^{MK0752R} cells and 0.3-fold decrease for IGROV-1^{CisR} cells when compared to IGROV-1 cells (Figure 138). Eight proteins were found taking role in the cell cytoskeleton, filamin C (FLNC), pyruvate dehydrogenase E1 subunit alpha 1 (PDHA1), radixin (RDX), intraflagellar transport 88 (IFT81), laminin 1 (LAD1), CAP-Gly domain-containing linker protein 1 (CLIP1), nitric oxide synthase interacting protein (NOSIP) and plastin 1 (PLS1). RDX showed a 0.7-fold increase for IGROV-1^{CisR} cells and PLS1 abundance decreased by 0.6-fold for IGROV-1^{MK0752R} cells and 1.2-fold for IGROV-1^{CisR} cells. LAD1 represented a 0.7-fold decrease in IGROV-1^{CisR} cells. CLIP1 abundance was decreased by 0.8-fold in IGROV-1^{MK0752R} cells and by 0.3-fold for IGROV-1^{CisR} cells when compared to IGROV-1. FLNC, PDHA1, IFT81, and NOSIP showed no significant changes based on abundance values. (Figure 139).

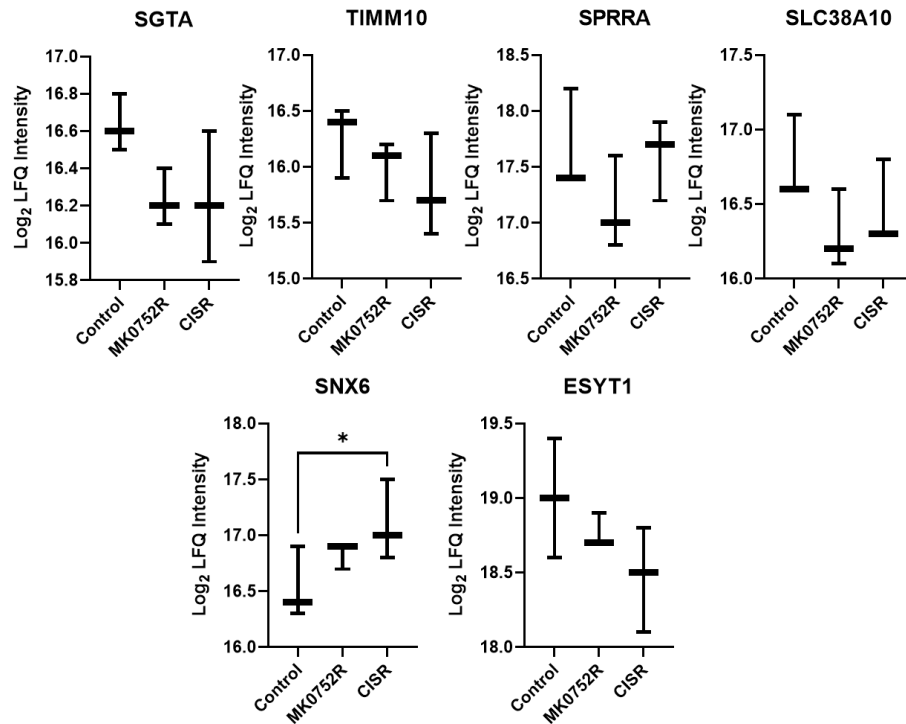


Figure 137. Proteomic signatures of IGROV-1, IGROV-1^{MK0752R} and IGROV-1^{CisR} cells in membrane transport. Box plots represent dysregulated proteins based on the LFQ intensity. *p<0.05.

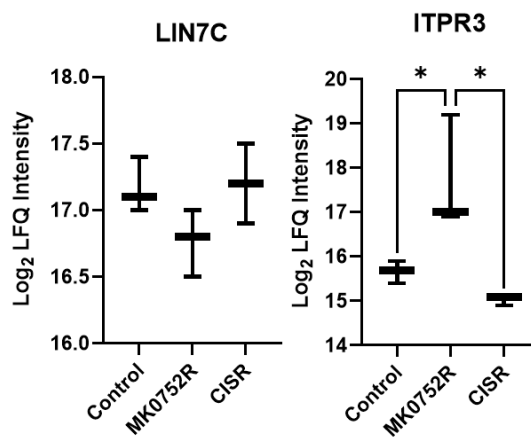


Figure 138. Proteomic signatures of IGROV-1, IGROV-1^{MK0752R} and IGROV-1^{CisR} cells in exocytosis. Box plots represent dysregulated proteins based on the LFQ intensity. *p<0.05.

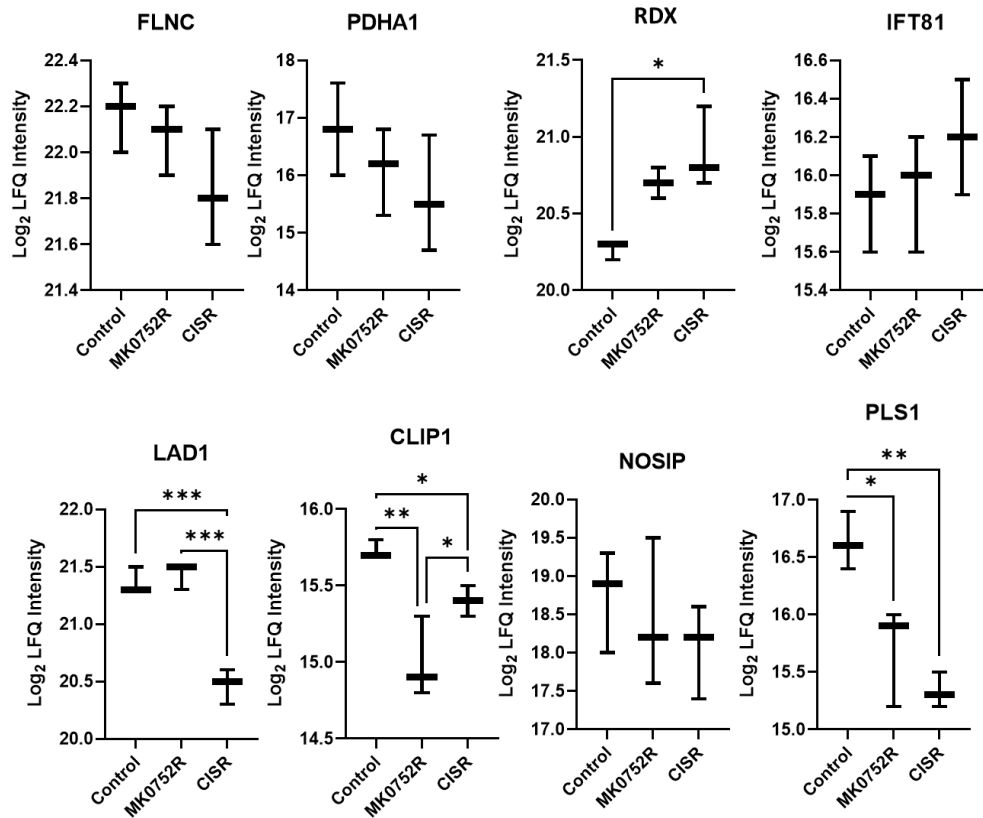


Figure 139. Proteomic signatures of IGROV-1, IGROV-1^{MK0752R} and IGROV-1^{CisR} cells in the cell cytoskeleton. Box plots represent dysregulated proteins based on the LFQ intensity. *p<0.05, **p<0.01, ***p<0.001.

Nine proteins were found to take a role in carcinogenesis, tumour protein D52 (TPD52), epiplakin 1 (EPPK1), H2AW histone (H2AW), myoferlin (MYOF), dimethylarginine dimethylaminohydrolase 2 (DDAH2), protein-L-isoaspartate (D-aspartate) O-methyltransferase (PCMT1), BCL2 associated X, apoptosis regulator (BAX), HECT, UBA and WWE domain containing E3 ubiquitin protein ligase 1 (HUWE1) and catenin delta 1 (CTNND1). TPD52 showed a 0.3-fold change among IGROV-1^{MK0752R} and IGROV-1^{CisR}. DDAH2 LCQ intensity was decreased by 0.4-fold for IGROV-1^{MK0752R} cells and by 0.2-fold for IGROV-1^{CisR} cells. PCMT showed a 0.2fold change for IGROV-1^{MK0752R} cells when compared to IGROV-1 cells. BAX abundance decreased by 0.6-fold for IGROV-1^{MK0752R} and 1-fold for IGROV-1^{CisR} cells. TPD52, EPPK1, H2AW, MYOF, HUWE1 and CTNND1 showed no significant abundance changes when compared (Figure 140). Dysregulated proteins were taking a role in cell proliferation, metabolism, growth, membrane transport, exocytosis, cell

cytoskeleton and carcinogenesis that associates with Notch's essential roles in cell fate homeostasis. Once Notch is constantly inhibited through MK0752, cells' escape routes might be through these aberrant proteins to overcome drug toxicity and develop resistance.

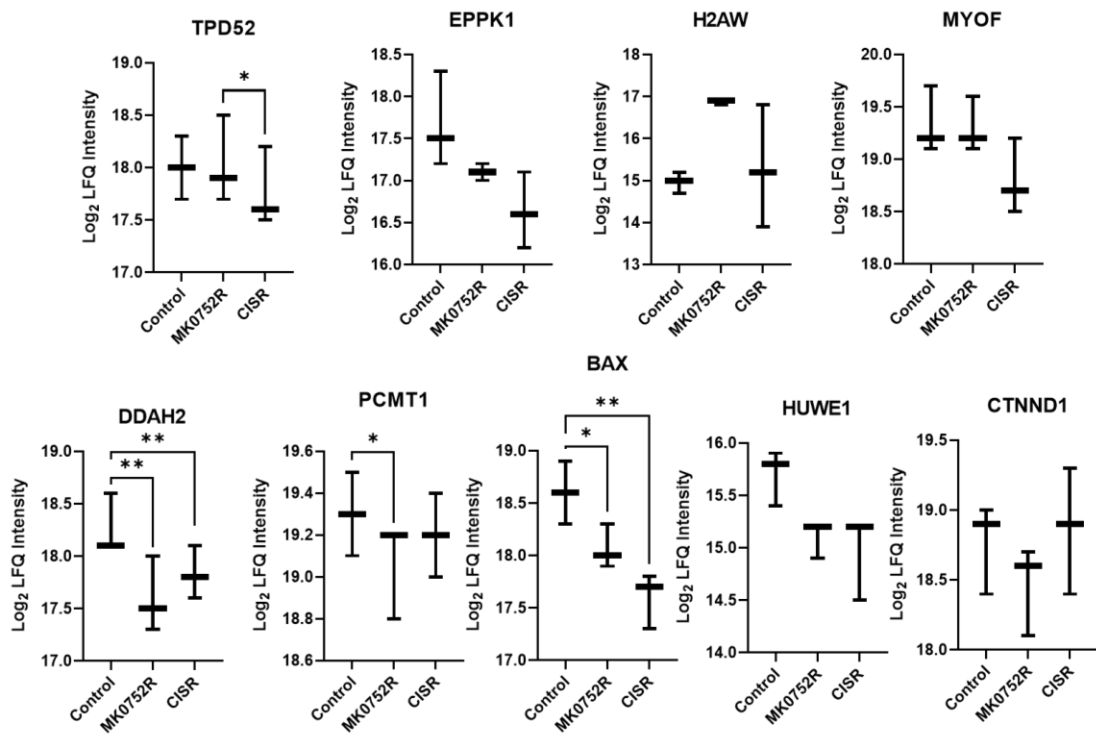


Figure 140. Proteomic signatures of IGROV-1, IGROV-1^{MK0752R} and IGROV-1^{CisR} cells in carcinogenesis. Box plots represent dysregulated proteins based on the LFQ intensity. *p<0.05, **p<0.01.

CHAPTER 5

DISCUSSION AND CONCLUSIONS

5.1. GSI Resistance in Breast Cancer

Notch signalling pathway regulates cell fate through the activation of gamma secretase complex for further cleavage of Notch ligand-receptor complex to regulate the transcription of its downstream target genes (Bray, 2006 and Zlobin and Olsauskas Kuprys, 2013). DAPT, R04929097 and MK0752 were used to inhibit gamma-secretase complex and downregulate aberrant Notch signalling activity along with effectiveness as an anti-neoplastic drug to treat various cancers including breast and ovarian (Feng et al., 2019 and Moore et al., 2020).

Although, DAPT, R04929097 and MK0752 is categorized as GSI, their structures and Notch receptor inhibition capacities differ. R04929097 is transition state analog whereas DAPT and MK0752 is non-transition state analogs. Transition state analogs competitively binds to Presenilin complex's catalytic core (PEN2), and they form more stable inhibition. DAPT and MK0752 binds to interface of PEN1/PEN2 dimers. IC₅₀ dose calculations among various cell lines revealed that DAPT requires IC₅₀<5nM for Notch1 inhibition, IC₅₀<100nM for Notch2 and Notch4, IC₅₀>100nM for Notch3 receptor's suppression. R04929097 requires IC₅₀<5nM for all Notch receptors and MK0752 requires IC₅₀<100nM for Notch1 and Notch2 yet IC₅₀>100nM for Notch3 and Notch4 inhibitions (Tetering and Vooijs, 2011; Osipo et al., 2013; McCaw et al., 2021).

Through Notch receptor inhibitions, DAPT, R04929097 and MK0752's cytotoxic potential adheres vulnerable to possible resistance phenomenon which remains unknown. GSI therapies, including DAPT, R04929097 and MK0752, increased the success of chemotherapies overall (Doyle et al., 1998; Devarajan et al., 2002; Wang et al., 2014 and Edwards and Brennan, 2021). In this study, we focus on two main aspects of GSI treatments. First, we reveal the synergistic effects of co-treatments of

GSI with two common chemotherapeutic drugs Cisplatin and Docetaxel. Second, we investigate possible routes to GSI resistance in MDA-MB-231 and MCF-7 breast cancer cells.

The IC_{50} values for each drug allowed the classification of the cell lines as intrinsically resistant ($IC_{50} > 50 \mu M$) or sensitive ($IC_{50} < 50 \mu M$). MDA-MB-231 cell line was intrinsically sensitive for both DAPT and R04929097 however resistant to MK0752 treatments. MCF-7 cell line was intrinsically resistant to DAPT and MK0752 however sensitive to R04929097. Various strategies to obtain resistance against anti-neoplastic drugs were previously investigated and a gradual increase in the doses starting with IC_{50} showed the most successful outcome (Brennan and Clarke, 2012; McDermott et al., 2014). Here, we obtained MDA-MB-231-R and MCF-7-R cells, which survives in IC_{200} of DAPT or R04929097 treatments. This value (IC_{200}) exceeds the two-fold increase from IC_{50} , that is accepted as the minimum dose the cells should survive to be considered as resistant (McDermott et al., 2014). Successfully generating DAPT or R04929097 resistance for both cell lines were conducted in approximately six months of continuous treatment schedules. Cell's ability to grow and maintain proliferative abilities after continuous DAPT and R04929097 treatments were marked as a hallmark of drug resistance (Nussinov et al., 2021). Changes in the growth rates of parental and DAPT or R04929097 resistant MDA-MB-231 and MCF-7 cells were analysed via MTT cell viability assay. DAPT resistance increased growth rate in MDA-MB-231 and MCF-7 cells by 0.41- and 0.43-fold, respectively, compared to their parental controls. In contrast, R04929097-resistant MDA-MB-231 and MCF-7 cells endured no change in growth rate. This indicates DAPT resistance might have a direct effect on cell proliferation unlike R04929097.

Cancer cells endure constant morphological and molecular changes to tolerate anti-neoplastic drug treatments. Phenotypical changes of cancer cells escalate migration and invasion which are known as hallmarks of cancer drug resistance (Wang et al., 2010). DAPT or R04929097 resistant MDA-MB-231 cells and R04929097 resistant MCF-7 cells showed no significant changes in morphological analysis. On the other hand, DAPT-resistant MCF-7 cells exhibited a more mesenchymal phenotype than the parental cells. Accordingly, the most striking observation in the DAPT-resistant MDA-MB-231-R and MCF-7-R cells was the increase in the migratory behaviour whereas R04929097 resistance did not affect migratory phenotype for both cell lines.

Alterations in the strictly balanced metabolism, urges cells to undergo morphological and behavioural changes via epithelial-mesenchymal transition (EMT) (Wang et al., 2016). Thus, we investigated whether the changes in DAPT or R04929097 resistant MDA-MB-231 and MCF-7 cells might be explained by EMT. In DAPT-resistant MCF-7 cells, consistent with the activation of an EMT program, we observed an increase in EMT regulator Snail2 and mesenchymal marker N-Cadherin, while an epithelial marker ZO1 was decreased. ZO1 downregulation reflects metastatic behaviours and drug resistance (Polette et al., 2007 and Kalluri and Weinberg, 2009). In addition to its role in EMT, Snail2 also regulates diverse functions in development and disease including cancer and is regulated by Notch signalling (Alejandro et al., 2005 and Esmeralda et al., 2011). The two other markers, epithelial marker E-Cadherin and EMT regulator Snail1, were not changed in MCF-7-R cells, which could be explained by partial EMT or the existence of transitional states during EMT. In DAPT resistant MDA-MB-231 cells, although an increase in E-Cadherin and decrease in N-Cadherin suggest a mesenchymal phenotype, the cellular morphology was not affected and the expression pattern of EMT effectors Snail1 and Snail2 were not consistently supporting EMT transition. Although, the migration rate was higher in DAPT resistant MDA-MB-231 cells, this could not be explained by a change in EMT process. All mesenchymal markers were reduced in R04929097 resistant MDA MB 231 cells, which correlates with reduced migration rate. However, the morphology of the cells was not changed towards a more epithelial phenotype. The differences between the EMT markers' expression and cells' morphology could be explained by the degree of EMT shift, which is cell- and context-dependent, and rarely exhibits a fully differentiated mesenchymal character (Singh and Settleman, 2010 and Loh et al., 2019).

Collectively, our results support the literature in which EMT-like transitions are potential targets of multiple drug resistance outcome with metastatic behaviours to multiple anti-neoplastic drugs. Potential DAPT resistance mechanism in MCF-7 cells could rely on EMT, which has pleiotropic functions in cancer, such as favouring the migratory and invasive behaviour, acquisition of stem-cell like characteristics, immune suppression in addition to drug-resistance (Liao and Yang 2017). R04929097 resistance might not depend on increased growth rate, or EMT phenotype including increased migration. Thus, these data suggest alternative paths for R04929097 resistance in MDA-MB-231 cells. DAPT- and R04929097- resistant MDA MB 231 cells showed reduced expression of Notch pathway components indicating that there was no upregulation of

the receptors to compensate for GSI treatment suggesting a Notch-independent resistance mechanisms. MCF-7 cells on the other hand, had increased expression of Notch3 receptor and Hes5 downstream target, which suggests a Notch3-induced compensation mechanism to restore Notch signalling activity.

DAPT or MK0752 GSI's were combined with Docetaxel or Cisplatin and resulted in successful therapeutic outcome by expunging the drug resistance hallmarks for both breast and ovarian cancer (Dai et al., 2018; Kato et al., 2018; Soni et al., 2018). In this study, DAPT and MK0752's intrinsic synergistic activities were tested with both Docetaxel and Cisplatin by MTT cell viability assay. Cell lines were treated with their gradual setup of determined IC₅₀ values for each combinational drug tested. DAPT combined with Docetaxel or Cisplatin showed highly synergistic activity for both MDA-MB-231 and MCF-7 cell lines. MK0752 combinations with Docetaxel or Cisplatin resulted in additive synergy for MDA-MB-231 cells. MCF-7 cells treated with MK0752, and Docetaxel combinations displayed highly synergistic activity and when combined with Cisplatin, additive effects were observed. Synergy matrix calculations also determined the optimum combinative concentration to be used for further studies. Clinical studies also test pre-treatment strategies of GSI's with Docetaxel or Cisplatin treatments as sequential treatments found to be successful to overcome multidrug resistance profiles (Wang et al., 2017). Both MDA-MB-231 and MCF-7 were intrinsically highly sensitive to Docetaxel and Cisplatin. In MDA-MB-231 and MCF-7 cells combined with Docetaxel or Cisplatin, DAPT resulted in greater cell viability decrease when compared to single drug treatments. Initial Docetaxel or Cisplatin treatments followed by DAPT resulted in higher toxicity than the DAPT initial treatment followed by Docetaxel or Cisplatin sequential treatments for MDA-MB-231 cells. The data is in correlation with the literature showing that chemo-therapy resistant cells could be targeted by GSIs. Thus, in sequential treatments, the cells that survive Cisplatin or docetaxel were targeted by DAPT. However, the observation was cell-type specific that in MCF-7 cells sequential treatments of DAPT with Docetaxel or Cisplatin showed greater decrease in cell viability independent of the order of the treatment. In MDA MB 231 cells, co-treatment with MK0752 and Docetaxel or Cisplatin resulted in lowermost cell viability when the drugs were applied sequentially independent of the order of the drugs, compared to simultaneous treatment. In MCF-7 cells, MK0752 combined with Docetaxel or Cisplatin exhibited higher toxicity than the single agent treatments and Docetaxel or Cisplatin initial treatments followed by MK0752 resulted in greater

viability decrease like DAPT. Overall, these findings support both the preclinical studies and clinical outcomes of GSI usages for both single agent and combinational treatments. Thus, could be explained by cells receiving initial anti-cancer treatments either with MK0752, Docetaxel or Cisplatin applications results in the enrichment of a population more vulnerable to the second drug treatments whereas co-treatment targets the intrinsically sensitive population enrichments. This might induce initial decrease in the viability yet not significantly different as cells that are less vulnerable would take over and stabilize/increase the viability. LeVasseur and Chia explains this phenomenon for sequential treatments as cumulative toxicity which implies to exceeded toxic dose limit does not initiate additional efficacy yet induces cumulative toxicity (2017).

Spheroid experiments were set to compare both 2D and 3D response differences and to test how acidosis effects the drug resistance and sensitivity. DAPT, Docetaxel and Cisplatin single agent treatments showed significant decrease in spheroid area for MDA-MB-231 cells, while the had no effect. On the other hand, viability measurements of the spheres showed that despite the indifference in the sphere size, combination therapies are more successful to induce toxicity compared to single therapies. Combinational treatments might be the solution to overcome acidosis-based resistance to toxicity (Khacho et al., 2014). However, in MCF-7 cells response was different in 3D that viability was not reduced in combination therapies. MK0752, Docetaxel and Cisplatin single agent treated MDA-MB-231 cells showed significant decrease in the spheroid area. They are successful as a single agent and both combinational, but combinations resulted in no significant difference with MK0752 when compared to single agent treatments. APA's of MK0752, Docetaxel or Cisplatin resulted in decreased cell viability. MK0752 combinations with Docetaxel or Cisplatin showed higher toxicity when combined for MDA-MB-231 cells. MCF-7 cells showed higher decrease in spheroid area when compared to the nontreated cells. Docetaxel treatments resulted in higher toxicity than the Cisplatin single agent treatments. However, Docetaxel or Cisplatin treatments their combinations with MK0752 showed equal toxicity. Yet, Cisplatin combinations were higher than their single treatments. Oppositely from the spheroid area measurements, MK0752 single agent treatments showed no significant difference when compared to the nontreated control group based on APA's. Docetaxel and Cisplatin single agent treatments showed high decrease and their combinations with MK0752 resulted in even more less APA activity. Collectively, 2D cultures of both MDA-MB-231 and MCF-7 showed significantly decreased cell

viability when treated with either single agent or combinational treatments of DAPT/MK0752, Docetaxel and Cisplatin. Doses were set as IC_{100} for both 2D and 3D cultures to avoid dose dependent toxicity which is not the main aim of the clinical study models. Yet, due to acidic accumulation of the environment, sphere cell's resistant predisposition, sphere layering's (proliferating, quiescent and necrotic cores), increase in the cell volume and medium might require increase of IC_{100} (Wrzesinski and Fey, 2012). Moreover, sphere sizes images showed less shrinking when images were analysed. Supportingly, APA is specifically used for sphere cell viability and showed slight reduction in the cell viability than the 2D cultures. Thus, mutually shows the limitation of a single position imaging in addition to additional dose need which could be solved by sphere size optimizations, IC_{50} determinations of spheroids as a separate start-up, different treatment application design. DAPT, R04929097, MK0752 treatments, resistance and their Docetaxel, Cisplatin combination's differential expression profiles, morphological outcomes, and viability changes in both 2D and 3D cell cultures were compared. Results portrayed both GSI and cell type specific response in breast cancer which can be improved by using differential combinational treatments and strategies to expand the knowledge.

5.2. GSI Resistance in Ovarian Cancer

MK0752's cytotoxic potentiality adheres vulnerable to possible resistance phenomenon which remains unknown for ovarian cancer. Ovarian cancer cell lines were selected through the literature studies based on their potential treatment sensitivity or resistance profiles. IGROV-1 cell line studies were also compared to its Cisplatin resistance clone. BG-1 and SKOV-3 were intrinsically highly sensitive to Cisplatin, Docetaxel and MK0752. IGROV-1 and A2780 were intrinsically resistant to MK0752 treatments and sensitive to Docetaxel and Cisplatin treatments. Including both intrinsically sensitive and resistant cell lines for MK0752 treatments induces a wide spectrum in the study. IGROV-1, IGROV-1^{CisR}, A2780, BG-1 and SKOV-3 cell lines reacted additively when MK0752 was combined with the Docetaxel or Cisplatin.

In general, resistant cells (IGROV-1 and A2780) did not show a significant reduction in viability when MK0752 and the chemotherapeutic drugs were applied simultaneously. However, sequentially treatment of these cells with combinational

treatments resulted in a higher reduction in viability. Interestingly, treating the cells with MK0752 after an initial chemotherapeutic agent treatment, resulted in the strongest effect in both cell lines. Highly sensitive cells (BG-1 and SKOV-3) reduced cell death in response to drug combinations independent of whether they are applied simultaneously or sequentially. However, the best outcome was observed when MK0752 was applied following a chemotherapeutic agent treatment for ovarian cancer and breast cancer cell lines possibly due to cumulative toxicity. Moreover, MK0752 proved to be useful in Cisplatin-resistant IGROV-1 cell lines, which had no Cisplatin-induced death but had almost a 50% reduction in viability in response to MK0752 treatment. Furthermore, MK0752 treatment followed by Cisplatin treatment reduced viability further to almost 20%. These observations suggest that Cisplatin resistance could be overcome by MK0752 treatment. Its potential to not only treat but overcome drug resistance in addition to MK0752 resistant cell's MK0752 re-treatment sensitivity presents a tolerable anti-cancer treatment strategy which can be promising for further trials.

MK0752 is a commonly used GSI for clinical studies and it increased the success of chemotherapies overall (Wang et al., 2014 and Edwards and Brennan, 2021). Through Notch receptor inhibitions, MK0752's cytotoxic potential adheres vulnerable to possible resistance phenomenon which remains unknown. In this study, we aimed to explore potential intrinsic and acquired resistance mechanisms against MK0752 to uncover such problem for further long-term successful treatments. We focused on two main aspects of GSI treatments. First, we revealed the synergistic effects of co-treatments of MK0752 with two common chemotherapeutic drugs Cisplatin and Docetaxel. Second, we investigate possible routes to MK0752 resistance in IGROV-1, A2780, BG-1 and SKOV-3 ovarian cancer cell lines. To assess this phenomenon we generated MK0752-resistant ovarian cancer cell lines (IGROV-1, A2780, BG-1 and SKOV-3). Intrinsically MK0752 sensitive cell lines (SKOV-3 and BG-1) were the quickest to induce resistance and cells showed no morphological changes when compared to the parental cell lines. However, A2780 cells displayed a more mesenchymal-like shape than the parental A2780. Although mesenchymal transitions were not quantified, it was observed that they acquired a more elongated shape. Cells proliferation rates were observed higher under cell maintenance routines, and this was confirmed for IGROV-1^{CisR}, A2780^{MK0752R}, BG-1^{MK0752R} and SKOV-3^{MK0752R} resistant cells reached higher numbers each time than their corresponding parental cell lines. The

mechanism behind this could be investigated further to explain whether it is due to higher proliferation or lower spontaneous cell death rates.

We investigated the behaviour and drug response of the cell lines in spheroid assays to model 3D conditions of the in vivo tumours. 3D studies showed that resistant cells showed no different spheroid size when compared to parental IGROV-1 or IGROV-1^{CisR}. MK0752 treatments showed no significant difference when compared among IGROV-1, IGROV-1^{MK0752R} and IGROV-1^{CisR} cells. Docetaxel treatments were successfully decreasing the spheroid area for IGROV-1, IGROV-1^{MK0752R} and IGROV-1^{CisR} cells. Cisplatin treatments only affected IGROV-1 cells based on spheroid size. MK0752 combinations with Docetaxel and Cisplatin were only decreasing spheroid area for IGROV-1 parental cells whereas IGROV-1^{MK0752R} and IGROV-1^{CisR} cells resulted in nonresponsive to treatments-among day 0,1,2 and 3 and among day 3 comparisons. MK0752 and Cisplatin resistant cells can tolerate IC₁₀₀ of each drug combined which explains the reason why sphere sizes were not differing on day 3. IGROV-1 is responsive to all treatments which remain promising for its treatments and overcoming intrinsic resistance profiles. IGROV-1^{MK0752R} spheres responded to MK0752 but not the other treatments which can be explained by cumulative toxicity as well. IGROV-1^{CisR} responded to MK0752 treatments yet its Cisplatin combinations resulted in no change as it can tolerate Cisplatin's toxicity. Overall, MK0752 represents a successful treatment profile both as a single and combinational treatment with Docetaxel and Cisplatin in ovarian cancer cells.

MK0752-treated BG-1 and BG-1^{MK0752R} cells showed a significant decrease in spheroid size when compared to their parental lines. Docetaxel treatments were only effective to BG-1^{MK0752R} cells and its combinations with MK0752 showed no significant change when compared within growth days. Both Cisplatin and Cisplatin's combinations with MK0752 resulted in decreased spheroid size for all 3 days for both parental and MK0752 resistant BG-1 cells and day 3. SKOV-3 and SKOV-3^{MK0752R} treated with MK0752 resulted in no significant difference from the parental cell lines. Docetaxel combinational treatments with MK0752 resulted in less spheroid size when compared to Docetaxel single treatments. Both Cisplatin single agent and MK0752 combinations resulted in a successful decrease in spheroid size among day123. Day 3 comparisons for Docetaxel and Cisplatin treatments with MK0752 treatments resulted in no significant changes. A2780 and A2780^{MK0752R} spheroid size were decreased when treated with MK0752. A2780^{MK0752R} cells showed no difference when compared within

the 1-2-3 days. Docetaxel and Cisplatin combinations showed an additional decrease in spheroid size for A2780 cells and A2780^{MK0752R} cells were nonresponsive to MK0752 combinational treatments as much as A2780 parental cell line which associates with MK0752 resistance. APA's for MK0752 retreatments showed no significant changes for A2780, A2780^{MK0752R}, BG-1 and BG-1^{MK0752R} cells. Docetaxel or Cisplatin combinations showed similarly reduced APA for both A2780 and A2780^{MK0752R} when compared to single-agent treatments. BG-1 and BG-1^{MK0752R} cells APA showed no changes between the single agent or combinational treatments. SKOV-3 cells showed reduced APA for MK0752, Docetaxel and Cisplatin single agent and combinational treatments when compared to SKOV-3^{MK0752R}. Cisplatin combinations decrease APA higher than Docetaxel combinational treatment for both SKOV-3 and SKOV-3^{MK0752R} cells. IGROV-1, IGROV-1^{MK0752R} and IGROV-1^{CisR} cells showed no difference in APA for all MK0752, Docetaxel, Cisplatin and combinational treatments when compared within the group. Cisplatin combinations with MK0752 responded successfully even under Cisplatin resistance for IGROV-1 cells. In general, MK0752 treatments both as a single agent or combinationally treated with Docetaxel or Cisplatin resulted in successful anti-neoplastic outcomes for all ovarian cancer cell lines tested.

C-Myc, one of the main and direct targets of Notch signalling, induces metabolic activities, proliferation, and tumorigenesis through further networks. Dysregulated C-Myc expression is correlated with drug resistance and cancer recurrence (Singh et al., 2009; Hoffman et al., 2002; Masui et al., 2013 and Sheth et al., 2014). Due to its main role in the pathway, GSI resistance was assessed through C-Myc expression changes. In MK7502 sensitive cell lines (BG-1 and SKOV-3) intrinsic c-Myc levels were not different between MK7502-resistant or control groups neither in 2D nor in 3D, indicating that acquired resistance does not affect c-Myc protein expression. However, c-Myc levels were affected by drug treatments in MK7502-resistant BG-1 and SKOV-3 cells. All single treatments, except for Docetaxel in BG-1, increased c-Myc levels in the resistant cells. However, co-treatment with MK0752 and Docetaxel or Cisplatin reduced c-Myc expression suggesting that the advantage of using drug combinations might stem from the regulation of c-Myc in MK7502 cells. On the other hand, like MK7502-resistant BG-1 and SKOV-3 cells, c-Myc levels were reduced in A2780 cells in response to co-treatment with MK0752 and Docetaxel or Cisplatin. A few of the western blot's total protein levels were not high in the analysis, the level of decrease might not represent the actual situation which requires further repetitions and

confirmations of blots. In contrast to other cell lines, in IGROV-1 cells, MK7502 resistance induced a significant increase c-Myc levels, both in 2D and 3D conditions, which suggests c-Myc as a resistance mechanism against MK0752. Cisplatin-resistant IGROV-1 cells also have increased c-Myc levels indicating a global c-Myc-mediated resistance independent of the drug. Like all other ovarian cancer cell lines, co-treatment with MK0752 and Docetaxel or Cisplatin significantly reduced c-Myc levels. Altogether the data suggest that c-Myc might be involved in drug resistance mechanisms yet co-treatment strategies could be the way to overcome such resistance in ovarian cancer cells.

Migrating to the nearest efficient blood supply for both nutrition, growth factors and oxygen support becomes vital for pre-metastatic cancer cells. This results in overall cancer treatment failure with resistant and relapsed cellular phenotype. Studies provide proximity difference in cancer cells to the oxygen supply induces acidic varieties in the tumor microenvironment (Feron and Corbet, 2017). This phenomenon refers as the Warburg effect and it explains cancer cell's ability to use glucose as the main energy supply with aerobic conditioning, normal cells on the other hand, produces lactate under anaerobic conditions via glycolysis (Gillies et al., 2011). Increased Warburg effect is responsible for or stimulated by the oxidative stress markers imbalance which is associated with the therapy failure and drug resistance in cancers (Keatley et al., 2019; Lo Dico et al., 2019 and Nylund et al., 2021).

To assess resistance outcome, Oxidative stress marker's (Catalase, Smooth muscle actin (SMA), Superoxide Dismutase 1 (SOD1) and Thioredoxin) mRNA expression levels were investigated. Catalase is crucial for ROS activity homeostasis, SMA is used as an equal loading control, SOD1 stimulates lipids, proteins, and nucleic acids oxidation and Thioredoxin takes place in regulating redox signalling processes (Stancill et al., 2021 and Huntosova et al., 2021). Ovarian cancer cell line, BG-1 cells expressed higher Catalase, SOD1 and Thioredoxin than BG-1^{MK0752R} cells. SKOV-3 cells upregulated Catalase activity with no SOD1 expressions and no significant expression changes for Thioredoxin when compared with the SKOV-3^{MK0752R}. A2780^{MK0752R} expressed higher oxidative stress markers. IGROV-1^{MK0752R} cells expressed higher Catalase when compared to IGROV-1 and IGROV-1^{CisR} controls. 2D and 3D comparisons for Oxidative stress markers showed no significant changes between IGROV-1 and A2780 cells and their MK0752-resistant lines. SKOV-3^{MK0752R} cells for 2D conditions showed an increase in thioredoxin whereas decreased in 3D

setup. BG-1^{MK0752R} cells showed overexpression of Thioredoxin for 3D background. However a few of the western blot's total protein levels were not high in the analysis, the level of decrease might not represent the actual situation which requires further repetitions and confirmations of blots. Collectively, ROS imbalance through Catalase, oxidation dyscontrol by SOD1 and increased redox stimulations by dysregulated Thioredoxin protein expressions might reflect another hallmark in ovarian cancers' potential drug resistance response pathways.

Proteomic analysis was carried out with IGROV-1 control, IGROV-1^{CisR}, and IGROV-1^{MK0752R} cells for comprehensive characterization of key molecules and biological processes taking role in resistance response. Among 1477 protein hits, evaluated differential expression of 46 proteins then were selected based on the significance ratios for further analysis. Dysregulated proteins were associated with cell signalling, metabolic regulations and cellular processes as well as taking role in transcription regulator activity and transporter activities. Cellular component enrichment showed that about 79.7% of selected proteins were cytoplasmic due to whole cell lysate sampling. Protein class categories showed stress response regulations for IGROV-1^{CisR} and IGROV-1^{MK0752R} cells. Apoptotic signalling pathway, endoplasmic reticulum stress response, cell junction, cell metabolism, cytochrome c release and membrane permeability showed as the top for biological processes of dysregulated protein's functional enrichments. These pathways were found dysregulated in various cancers and responsible for drug resistance and cancer recurrence (Cree and Charlton 2017 and Wang et al., 2019). Among these hits, dysregulated proteins were categorized as their role in cell proliferation, cell growth, cell metabolism, exocytosis, cell cytoskeleton, carcinogenesis, and membrane transport based on the ovarian cancer drug resistance signatures (Pokhriyal et al., 2019; Khan et al., 2021; Ortiz et al., 2022 and Yang et al., 2022). DYNC1H1 found downregulated for IGROV-1^{MK0752R} cells and its dysregulation of DYNC1H1 was associated with EMT, cell proliferation and growth. Its downregulation represents increased metastasis in various cancers (Pan et al., 2021 and Wang et al., 2022). Chromatin associated protein and oncoprotein PHF5A was also found downregulated for IGROV-1^{MK0752R} cells. Main role of PHF5A signifies migration inhibition and decreasing invasiveness in cancers (Zeng et al., 2018; Yang et al., 2018; Yang et al., 2019 and Begum et al., 2021). Moreover, ZC3H known to be responsible for protein unfolding and EMT response (Ly et al., 2022) Downregulation of ZC3H in IGROV-1^{MK0752R} cells and upregulation in

IGROV-1^{CisR} cells might imply different mechanisms of resistance background. Malignancy biomarker, LRRFIP1 was found downregulated in IGROV-1^{CisR} cells and its role in migration, EMT and cell adhesion proposes potential focus for resistance mechanisms. It indirectly is connected to Notch signalling pathway through WNT signalling pathway which when dysregulated induces cancer drug resistance and recurrence (Li et al., 2014; Takimoto, 2019 and Ma et al., 2022). ARFIP1 was observed downregulated and WFS1 was upregulated in IGROV-1^{MK0752R} cells. Both ARFIP1 and WFS1 takes place in intracellular transport, protein secretion and stress response (Gehart et al., 2012 and Zhu et al., 2021). PGLS was found downregulated based on abundance ratios for both IGROV-1^{CisR} and IGROV-1^{MK0752R} cells. PGLS is involved in pentose-phosphate shift which is important for cellular homeostasis through its role in regulation of 6-phosphogluconolactonase activity and utilize glycolysis (Zuzow et al., 2018). PGLS takes place in pentose phosphate pathway to regulate energy homeostasis and expected to be upregulated in cancers. Downregulation of PGLS might induce sensitivity against anti-cancer therapies which explains how IGROV-1^{MK0752R} and IGROV-1^{CisR} cells remained responsive to MK0752 and Docetaxel or Cisplatin combinations. LARPB4 was found downregulated in IGROV-1^{MK0752R} cells and it is taking role in cell cycle regulation. It also emerges as tumour suppressor in gliomas and liver cancer (Zhang et al., 2015 and Li et al., 2019). An oncogene, WBP2 was analysed as downregulated in IGROV-1^{CisR} cells. WBP2 is responsible for migration and invasion in triple negative breast cancer and associated with transtuzumab resistance (Li et al., 2018; Kang et al., 2019; Tabatabaeian et al., 2020 Lim et al., 2022). IGROV-1^{CisR} cells showed upregulation of SNX6 which is crucial for intracellular trafficking and EMT transition in pancreatic cancer cells (Hu et al., 2018). ITPR3 exocytosis marker similarly was upregulated for IGROV-1^{MK0752R} cells, and it takes place in stress response regulations (Wei et al., 2016). Cell cytoskeleton biomarkers PLS1 and CLIP1 was downregulated for both IGROV-1^{CisR} and IGROV-1^{MK0752R} cells. CLIP1 is associated with taxane resistance and cancer cell migration (Zaoui et al., 2019 and Thakkar et al., 2021) whereas PLS1 is responsible for metastasis in colorectal cancer and promotes breast cancer invasion through PI3K pathway (Zhang et al., 2020 and Machado et al., 2021). Migratory and metastatic outcomes of IGROV-1^{CisR} and IGROV-1^{MK0752R} was not tested however the expectation would be PLS1 and CLIP1's upregulation. However, cells showed no morphological changes which could be explained by PLS1 and CLIP1's downregulation. RDX was upregulated in IGROV-1^{CisR}, and it is known for inducing

metastatic behaviour and cell growth in gastric cancers as well as pancreatic cancers (Chen et al., 2012; Qin et al., 2014 and Tsai et al., 2014). LAD1, candidate for docetaxel resistance in prostate cancers and is a biomarker for aggressiveness in breast cancers was also downregulated in IGROV-1^{CisR} cells yet not in IGROV-1^{MK0752R} cells which might propose differential routes for resistance (Roth et al., 2018 and Li et al., 2021). PCMT1 is inducing ovarian cancer metastasis and glioblastoma migration and it was observed dysregulated in IGROV-1^{MK0752R} cells (Guo et al., 2022 and Zhang et al., 2022). DDAH2 found dysregulated in both IGROV-1^{CisR} and IGROV-1^{MK0752R} cells, it takes place in TRAIL induced apoptosis and increases angiogenic behaviour of lung adenocarcinomas (Lumicisi et al., 2015 and Shiozawa et al., 2015). BAX protein was downregulated for both IGROV-1^{CisR} and IGROV-1^{MK0752R} cells. Crucial role of BAX in apoptosis leads to p53 dependent cell death, drug resistance. Its activation overcomes drug resistance and currently used as novel therapeutic target. It induces release of cytochrome C to initiate caspase dependent cell death. BAX expression induces therapy sensitivity against platinum and Taxol based treatments in ovarian cancer cells (Izabela et al., 2009; Bhavya et al., 2010 and Lopez et al., 2022). All these dysregulated proteins are matching puzzle pieces in the drug resistance classification for MK0752 and its potential trademark for hallmark pathways. (Figure 141) In conclusion, this study enlightens potential resistance response against DAPT, R04929097 and MK0752 with their combinational or pre-treatments with Docetaxel or Cisplatin for both breast and ovarian cancer cell lines. Including morphological, proliferation rates, migration alterations, RNA expressions of EMT markers, 3D set ups for acidosis responses and mRNA expressions for c-myc and Oxidative stress markers followed by proteomic analysis data showed GSI's successful anti-neoplastic and drug resistance profiles which can lead breast and ovarian cancer molecular studies. Although this study reflects wide spectrums in drug resistance against GSI's, in vivo animal models should be tested for further comprehensive interpretation.

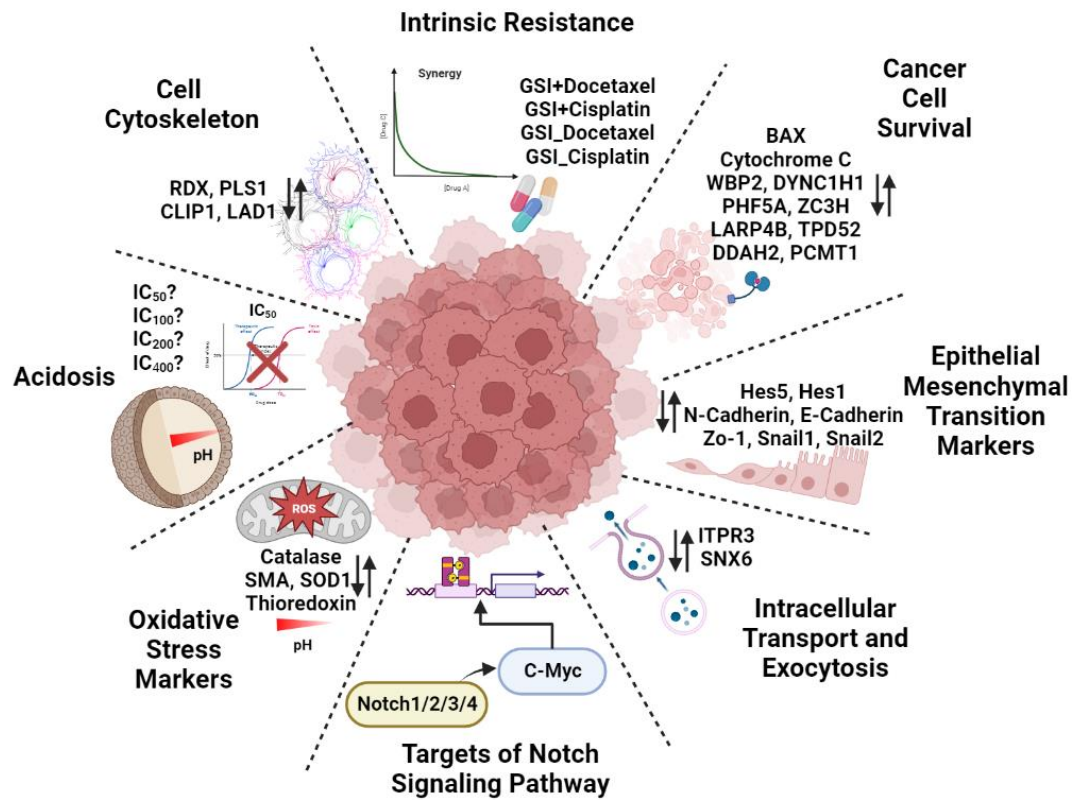




Figure 141. Overall illustration of GSI drug resistance hallmarks for GSI treatments in breast and ovarian cancer cells. Intrinsic resistance, cancer cell survival, EMT markers, intracellular transport and exocytosis, targets of Notch signaling pathway, oxidative stress markers, acidosis, and cell cytoskeleton acts as the potential targets for GSI resistance (BioRender, 2022).


Supplementary Figures (Conclusive)

DAPT/R04929097 Resistance					
MDA-MB-231			MCF-7		
	DAPT	R04929097	DAPT	R04929097	
Intrinsic Sensitivity	Sensitive	Sensitive	Resistant	Sensitive	Sensitive
Growth Rate		NC		NC	NC
Morphology	NC	NC	Mesenchymal	NC	NC
Notch Components					
Epithelial Markers					
Mesenchymal Markers					
Migration Capacity					NC

Increased Decreased Dysregulated Not Changed

Figure 142. Summary of DAPT or R04929097 resistant MDA-MB-231 and MCF-7 breast cancer cell line's results obtained from this project.

		DAPT				MK0752			
		MDA-MB-231		MCF-7		MDA-MB-231		MCF-7	
		Cisplatin	Docetaxel	Cisplatin	Docetaxel	Cisplatin	Docetaxel	Cisplatin	Docetaxel
	BLISS Analysis	✓	✓	✓	✓	✚	✚	✚	✓
	Cell Viability	✓ Cisplatin ¹	✓ Docetaxel ¹	✓ Cisplatin ¹	✓ Docetaxel ¹	✓ Sequentials	✓ Sequentials	✓ Cisplatin ¹	✓ Docetaxel ¹
	Sphere Size	●	●	●	✓	●	●	✓	●
	Spheroid Viability	✓	✓	✘	●	●	●	✓	✓












Synergistic: 
 Additive: 
 Antagonistic: 
 No Effect: 

Figure 143. Summary of DAPT or MK0752's Docetaxel and Cisplatin combination results for MDA-MB-231 and MCF-7 breast cancer cell lines.

MK0752														
IGROV-1			IGROV-1 ^{CisR}			A2780			SKOV-3			BG-1		
	Cisplatin	Docetaxel	Cisplatin	Docetaxel	Cisplatin	Docetaxel	Cisplatin	Docetaxel	Cisplatin	Docetaxel	Cisplatin	Docetaxel		
 2D	+	+	+	+	+	+	+	+	+	+	+	+		
BLISS Analysis	+	+	+	+	+	+	+	+	+	+	+	+		
Cell Viability	✓	✓	✓	✓	✓	✓	✓	✓	✓	✓	✓	✓		
C-Myc Expression	↑	○	↓	↓	↓	↓	↓	↓	○	○	↑	↑		
OXPHOS Expression	↔	↔	↔	↔	↔	↔	↔	↔	↔	↔	↔	↔		
Sphere Size	✓	✓	○	○	✓	✓	✓	✓	✓	✓	✓	✓		
Spheroid Viability	✓	✓	✓	○	✓	✓	✓	✓	✓	✓	✓	✓		

	Increased		Decreased		Dysregulated		NC	Not Changed
---	-----------	---	-----------	---	--------------	---	----	-------------















	Synergistic		Additive		Antagonistic		No Effect
---	-------------	---	----------	---	--------------	---	-----------

Figure 144. Summary of MK0752's Docetaxel and Cisplatin combination results for IGROV-1, IGROV-1^{CisR}, A2780, SKOV-3 and BG-1 ovarian cancer cell lines.

	IGROV-1			IGROV-1 ^{CisR}			A2780		
	Cisplatin	Docetaxel	MK0752	Cisplatin	Docetaxel	MK0752	Cisplatin	Docetaxel	MK0752
 Cell Viability	↓	↓	↓	↓	↓	↓	↓	↓	↓
 C-Myc Expression	↓	↑	NC	↑	↑	↓	↑	↑	↑
 OXPPOS Expression	↔	↔	↔	↔	↔	↔	↔	↔	↔
 Sphere Size	↓	↓	↓	↓	↓	↓	↓	↓	↓
 Spheroid Viability	↓	↓	NC	↓	↓	↓	↓	↓	↓

	SKOV-3			BG-1		
	Cisplatin	Docetaxel	MK0752	Cisplatin	Docetaxel	MK0752
 Cell Viability	↓	↓	↓	↓	↓	↓
 C-Myc Expression	NC	NC	NC	NC	NC	↑
 OXPPOS Expression	↔	↔	↔	↔	↔	↔
 Sphere Size	↓	↓	↓	↓	↓	↓
 Spheroid Viability	↓	↓	↓	↓	↓	NC







 Increased	 Decreased	 Dysregulated	 Not Changed
---	---	--	---

Figure 145. Summary of MK0752, Docetaxel and Cisplatin single agent treatment results for IGROV-1, IGROV-1^{CisR}, A2780, SKOV-3 and BG-1 ovarian cancer cell lines.

		MK0752 Resistance				
		IGROV-1	IGROV-1 ^{CisR}	A2780	BG-1	SKOV-3
 	Intrinsic Sensitivity	Resistant	—	Resistant	Sensitive	Sensitive
	Morphology	NC	NC	Mesenchymal	NC	NC
	Growth Rate	NC	↑	↑	↑	↑
	C-Myc Expression	↑	↑	↓	NC	NC
	OXPHOS Expression	↕	↕	↕	↕	↕
	Sphere Size	↓	↑	↓	↓	NC
	Spheroid Viability	NC	↑	NC	NC	↑
	C-Myc Expression	↑	NC	NC	NC	NC
OXPHOS Expression	NC	NC	↕	NC	NC	

	Increased		Decreased		Dysregulated		Not Changed
--	-----------	--	-----------	--	--------------	--	-------------

Figure 146. Summary of MK0752 resistance results for IGROV-1, IGROV-1^{CisR}, A2780, SKOV-3 and BG-1 ovarian cancer cell lines.

REFERENCES

- A chick homologue of Serrate and its relationship with Notch and Delta homologues during central. (1996). 20894. <https://doi.org/10.1006/dbio.1996.0069>.
- A presenilin-1-dependent gamma-secretase-like protease mediates release of Notch intracellular. (1999). 20894. <https://doi.org/10.1038/19083>.
- Ab, Z., Ms, P., Ga, M., Nguyen, F., Montesano, R., & Maciag, T. (1996). An antisense oligonucleotide to the Notch ligand jagged enhances fibroblast growth factor- induced angiogenesis in vitro. 20894. <https://doi.org/10.1074/jbc.271.51.32499>.
- Acar, A., Simões, B. M., Clarke, R. B., & Brennan, K. (2016). A Role for Notch Signalling in Breast Cancer and Endocrine Resistance. 2016. <https://doi.org/10.1155/2016/2498764>
- Ak, A., Fechtel, K., Cc, K., Sb, S., Pj, K., & Ma, M. (1989). Molecular genetics of Delta, a locus required for ectodermal differentiation in *Drosophila*. 20894. <https://doi.org/10.1002/dvg.1020100315>
- Aktas, C., Zeybek, N. and Piskin, A. (2015). In vitro effects of phenytoin and DAPT on MDA- MB-231 breast cancer cells. *Acta Biochimica et Biophysica Sinica*, 47(9), pp.680-686.
- Albain, K., Czerlanis, C., Rajan, P., Zlobin, A., Godellas, C., & Bova, D. et al. (2010). Abstract PD05-12: Combination of Notch Inhibitor MK-0752 and Endocrine Therapy for Early Stage ER α + Breast Cancer in a Presurgical Window Pilot Study. Poster Discussion Abstracts. doi: 10.1158/0008-5472.sabcs10-pd05-12

Alejandro Barrallo-Gimeno, M. Angela Nieto; The Snail genes as inducers of cell movement and survival: implications in development and cancer.

Development 15 July 2005; 132 (14): 3151–3161. doi:

<https://doi.org/10.1242/dev.01907>

Alfarouk, K., Stock, C., Taylor, S., Walsh, M., Muddathir, A., Verduzco, D., Bashir, A., Mohammed, O., Elhassan, G., Harguindey, S., Reshkin, S., Ibrahim, M. and Rauch, C. (2015). Resistance to cancer chemotherapy: failure in drug response from ADME to P-gp. *Cancer Cell International*, 15(1).

Al-Hussaini, H., Subramanyam, D., Reedijk, M. and Sridhar, S. (2010). Notch Signaling Pathway as a Therapeutic Target in Breast Cancer. *Molecular Cancer Therapeutics*, 10(1), pp.9-15.

Alshaer, W., Alqudah, D. A., Wehaibi, S., Abuarqoub, D., & Zihlif, M. (2019). Downregulation of STAT3, β -Catenin, and Notch-1 by Single and Combinations of siRNA Treatment Enhance Chemosensitivity of Wild Type and Doxorubicin Resistant MCF7 Breast Cancer Cells to Doxorubicin.

Anouk K.M. Claessens, Khava I.E. Ibragimova, Sandra M.E. Geurts, Monique E.M.M. Bos, Frans L.G. Erdkamp, Vivianne C.G. Tjan-Heijnen, The role of chemotherapy in treatment of advanced breast cancer: an overview for clinical practice, *Critical Reviews in Oncology/Hematology*, Volume 153, 2020, 102988, ISSN 1040-8428, <https://doi.org/10.1016/j.critrevonc.2020.102988>.

António Carlos Ferreira, Gianpaolo Suriano, Nuno Mendes, Bárbara Gomes, Xiaogang Wen, Fátima Carneiro, Raquel Seruca, José Carlos Machado, E-cadherin impairment increases cell survival through Notch-dependent

upregulation of Bcl-2, *Human Molecular Genetics*, Volume 21, Issue 2, 15 January 2012, Pages 334–343, <https://doi.org/10.1093/hmg/ddr469>.

Arruga, F., Vaisitti, T., & Deaglio, S. (2018). The NOTCH Pathway and Its Mutations in Mature B Cell Malignancies. *Frontiers in Oncology*, Vol. 8, p. 550. Retrieved from <https://www.frontiersin.org/article/10.3389/fonc.2018.00550>.

Artavanis-tsakonas, S., & Yedvobnick, B. (1983). Molecular cloning of Notch, *80*(April), 1977–1981.

Ayaz, F., & Osborne, B. A. (2014). Non-canonical Notch signaling in cancer and immunity. *4* (2014), 1–6. <https://doi.org/10.3389/fonc.2014.00345>

Aziz MH, Ahmad A. Epigenetic basis of cancer drug resistance. *Cancer Drug Resist* 2020; 3:113-6. <http://dx.doi.org/10.20517/cdr.2020.06>.

Babcock, B., Bw, A., Papayannopoulos, I., Castilleja, A., JI, M., Stifani, S., ... Cg, I. (1998). Ovarian and breast cytotoxic T lymphocytes can recognize peptides from the amino enhancer of split protein of the Notch complex. 20894. [https://doi.org/10.1016/s0161-5890\(98\)00100-x](https://doi.org/10.1016/s0161-5890(98)00100-x)

Bailón-Moscoso N, Romero-Benavides JC, Ostrosky-Wegman P. Development of anticancer drugs based on the hallmarks of tumor cells. *Tumour Biol*. 2014 May;35(5):3981-95. doi: 10.1007/s13277-014-1649-y. Epub 2014 Jan 29. PMID: 24470139.

- Bajaj J, Maliekal TT, Vivien E, Pattabiraman C, Srivastava S, et al. (2011) Notch signaling in CD66+ cells drive the progression of human cervical cancers. *Cancer Res* 71: 4888–4897.
- Baker, R., & Schubiger, G. (1996). Autonomous and nonautonomous Notch functions for embryonic muscle and epidermis development in *Drosophila*. 20894.
- Barr, M., Gray, S., Hoffmann, A., Hilger, R., Thomale, J., & O’Flaherty, J. et al. (2013). Generation and Characterisation of Cisplatin-Resistant Non-Small Cell Lung Cancer Cell Lines Displaying a Stem-Like Signature. *Plos ONE*, 8(1), e54193. doi: 10.1371/journal.pone.0054193
- Basis, G., Two, F. O. R., & Lethality, R. (1971). Genetic Basis for Two Types Of Recessive Lethality. (1), 259–268.
- Bauer, L., Takacs, A., Slotta-Huspenina, J., Langer, R., Becker, K., Novotny, A., ... Keller, G. (2015). Clinical Significance of NOTCH1 and NOTCH2 Expression in Gastric Carcinomas: An Immunohistochemical Study. *Frontiers in Oncology*, 5. <https://doi.org/10.3389/fonc.2015.00094>.
- Bazzoni, R.; Bentivegna, A. Role of Notch Signaling Pathway in Glioblastoma Pathogenesis. *Cancers* 2019, 11, 292.
- Be, B., Thinakaran, G., Pc, W., Ss, S., & Js, N. (1999). Lack of requirement for presenilin1 in Notch1 signaling. 20894. [https://doi.org/10.1016/s0960-9822\(00\)80121-9](https://doi.org/10.1016/s0960-9822(00)80121-9)
- Begum NA, Haque F, Stanlie A, Husain A, Mondal S, Nakata M, Taniguchi T, Taniguchi H, Honjo T. Phf5a regulates DNA repair in class switch recombination via p400 and histone H2A variant deposition. *EMBO J*.

2021 Jun 15;40(12):e106393. doi: 10.15252/emj.2020106393. Epub 2021 May 3. PMID: 33938017; PMCID: PMC8204862.

Benko A, Medina-Cruz D, Vernet-Crua A, O'Connell CP, Świętek M, Barabadi H, Saravanan M, Webster TJ. Nanocarrier drug resistant tumor interactions: novel approaches to fight drug resistance in cancer. *Cancer Drug Resist.* 2021 Jun 19;4(2):264-297. doi: 10.20517/cdr.2020.81. PMID: 35582024; PMCID: PMC9019274.

Bertucci, F., Finetti, P., & Birnbaum, D. (2012). Basal breast cancer: a complex and deadly molecular subtype. *Current molecular medicine*, 12(1), 96–110. <https://doi.org/10.2174/156652412798376134>.

Bhavya Balan Chandrika, Sathish Kumar Maney, Swathi U. Lekshmi, Jeena Joseph, Mahendra Seervi, Praveen K.S., Santhoshkumar T.R., Bax deficiency mediated drug resistance can be reversed by endoplasmic reticulum stress induced death signaling, *Biochemical Pharmacology*, Volume 79, Issue 11, 2010, Pages 1589-1599, ISSN 0006-2952, (<https://doi.org/10.1016/j.bcp.2010.01.032>).

Bierkamp, C., & Ja, C. (1993). A zebrafish homologue of the Drosophila neurogenic gene Notch and its pattern of transcription during early embryogenesis. 20894. [https://doi.org/10.1016/0925-4773\(93\)90027-u](https://doi.org/10.1016/0925-4773(93)90027-u)

Bizzarri, M., Cucina, A. and Proietti, S. (2014). The tumor microenvironment as a target for anticancer treatment. *Oncobiology and Targets*, 1(1), p.3.

Blagosklonny, M. (2007). Mitotic Arrest and Cell Fate: Why and How Mitotic Inhibition of Transcription Drives Mutually Exclusive Events. *Cell Cycle*, 6(1), 70-74. doi: 10.4161/cc.6.1.3682.

- Boelens, M. C., Wu, T. J., Nabet, B. Y., Xu, B., Qiu, Y., Brugge, P. J., Minn, A. J. (2015). NIH Public Access. 159(3), 499–513.
<https://doi.org/10.1016/j.cell.2014.09.051.Exosome>
- Bolós, V., Mira, E., Martínez-Poveda, B., Luxán, G., Cañamero, M., Martínez-A, C., Mañes, S. and de la Pompa, J. (2013). Notch activation stimulates migration of breast cancer cells and promotes tumor growth. *Breast Cancer Research*, 15(4).
- Braune, E., & Seshire, A. (2018). Notch and Wnt Dysregulation and Its Relevance for Breast Cancer and Tumor Initiation. 1–17.
<https://doi.org/10.3390/biomedicines6040101>.
- Bray, S. Notch signalling: a simple pathway becomes complex. *Nat Rev Mol Cell Biol* 7, 678–689 (2006). <https://doi.org/10.1038/nrm2009>.
- Breeden, L., Nasmyth, K., & Breeden, L. (2020). Similarity between cell-cycle genes of budding yeast and fission yeast and the Notch gene of *Drosophila*.
Access options Rent or Buy Author information.
- Brennan, K. and Clarke, R. (2012). Combining Notch inhibition with current therapies for breast cancer treatment. *Therapeutic Advances in Medical Oncology*, 5(1), pp.17-24.
- Callahan, R. (1998). Somatic mutations that contribute to breast cancer. 20894.
- Capulli, M., Hristova, D., Valbret, Z. et al. Notch2 pathway mediates breast cancer cellular dormancy and mobilisation in bone and contributes to haematopoietic stem cell mimicry. *Br J Cancer* 121, 157–171 (2019).
<https://doi.org/10.1038/s41416-019-0501-y>.
- Ce, L., Boulter, J., Gossler, A., & Weinmaster, G. (1996). Expression patterns of Jagged, Delta1, Notch1, Notch2, and Notch3 genes identify ligand-

receptor pairs that may function in neural development . 20894.
<https://doi.org/10.1006/mcne.1996.0040>

Ce, L., Cj, S., Boulter, J., & Weinmaster, G. (1995). Jagged: a mammalian ligand that activates Notch1. 20894. [https://doi.org/10.1016/0092-8674\(95\)90294-5](https://doi.org/10.1016/0092-8674(95)90294-5).

Cerón-Carrasco, J. and Jacquemin, D. (2015). Photoactivatable platinum (II) compounds: in search of novel anticancer drugs. *Theoretical Chemistry Accounts*, 134(12).

Ceroni, M., Te, P., Toniatti, S., Fabozzi, D., Uggetti, C., Frediani, F., ... Carrera, P. (2000). Migraine with aura and white matter abnormalities: Notch3 mutation. 20894. <https://doi.org/10.1212/wnl.54.9.1869>

Challagundla KB, Wise PM, Neviani P, Chava H, Murtadha M, et al. Exosome-mediated transfer of microRNAs within the tumor microenvironment and neuroblastoma resistance to chemotherapy. *J Natl Cancer Inst* 2015;107:djv135.

Chan, S., & Wang, L. (2015). Regulation of cancer metastasis by microRNAs. *Journal Of Biomedical Science*, 22(1). doi: 10.1186/s12929-015-0113-7.

Chandy, T. (2010). 11 - Biocompatibility of materials and its relevance to drug delivery and tissue engineering. In C. P. Sharma (Ed.), *Biointegration of Medical Implant Materials* (pp. 301–325).
<https://doi.org/https://doi.org/10.1533/9781845699802.3.301>.

Chang, H., Zou, Z. Targeting autophagy to overcome drug resistance: further developments. *J Hematol Oncol* 13, 159 (2020).
<https://doi.org/10.1186/s13045-020-01000-2>.

- Chemoresistance in Cancer Stem Cells and Strategies to Overcome Resistance. (2014). *Chemotherapy: Open Access*, 03(01).
- Chen SD, Song MM, Zhong ZQ, Li N, Wang PL, Cheng S, Bai RX, Yuan HS. Knockdown of radixin by RNA interference suppresses the growth of human pancreatic cancer cells in vitro and in vivo. *Asian Pac J Cancer Prev*. 2012;13(3):753-9. doi: 10.7314/apjcp.2012.13.3.753. PMID: 22631643.
- Chen, X., Gong, L., Ou, R., Zheng, Z., Chen, J., & Xie, F. et al. (2016). Sequential combination therapy of ovarian cancer with cisplatin and γ -secretase inhibitor MK-0752. *Gynecologic Oncology*, 140(3), 537-544. doi: 10.1016/j.ygyno.2015.12.011.
- Chillakuri, C. R., Sheppard, D., Lea, S. M., & Handford, P. A. (2012). *Seminars in Cell & Developmental Biology* Notch receptor – ligand binding and activation: Insights from molecular studies. <https://doi.org/10.1016/j.semcdb.2012.01.009>
- Cloning, characterization, and the complete 56.8-kilobase DNA sequence of the human NOTCH4. (1998). 20894. <https://doi.org/10.1006/geno.1998.5330>
- Coffman, C., Harris, W., & Kintner, C. (1990). Xotch, the *Xenopus* homolog of *Drosophila* Notch. 20894. <https://doi.org/10.1126/science.2402639>
- Crabtree JS, Singleton CS and Miele L (2016) Notch Signaling in Neuroendocrine Tumors. *Front. Oncol.* 6:94. doi: 10.3389/fonc.2016.00094.
- Craig, S., & Brady-Kalnay, S. (2010). Cancer Cells Cut Homophilic Cell Adhesion Molecules and Run. *Cancer Research*, 71(2), 303-309. doi: 10.1158/0008-5472.can-10-2301.

- Cree, I., & Charlton, P. (2017). Molecular chess? Hallmarks of anti-cancer drug resistance. *BMC Cancer*, 17(1). doi: 10.1186/s12885-016-2999-1.
- Cytogenetics, T. H. E., Recessive, O. F. A., Mutant, V., & To, D. A. (1985). The Cytogenetics of A Recessive Visible Mutant. 497–506.
- D'Souza, B., Meloty-Kapella, L., & Weinmaster, G. (2010). Canonical and Non-Canonical Notch Ligands. *Current Topics in Developmental Biology*, 73-129. doi: 10.1016/s0070-2153(10)92003-6
- Da, H., & Ta, X. (1987). The embryonic expression of the Notch locus of *Drosophila melanogaster* and the implications of point mutations in the extracellular EGF-like domain of the predicted protein. 20894.
- Dai, G., Deng, S., Guo, W., Yu, L., Yang, J., Zhou, S., & Gao, T. (2018). Notch pathway inhibition using DAPT, a γ -secretase inhibitor (GSI), enhances the antitumor effect of cisplatin in resistant osteosarcoma. *Molecular Carcinogenesis*, 58(1), 3-18. doi: 10.1002/mc.22873.
- Dasari, S., & Bernard Tchounwou, P. (2014). Cisplatin in cancer therapy: Molecular mechanisms of action. *European Journal of Pharmacology*, 740, 364-378. doi: 10.1016/j.ejphar.2014.07.025
- De Bruin, E., & Medema, J. (2008). Apoptosis and non-apoptotic deaths in cancer development and treatment response. *Cancer Treatment Reviews*, 34(8), 737-749. doi: 10.1016/j.ctrv.2008.07.001.
- Deangelo DJ, Stone RM, Silverman LB, et al: (2006). A phase I clinical trial of the Notch inhibitor MK-0752 in patients with T-cell acute lymphoblastic leukemia/ lymphoma (T-ALL) and other leukemias. *J Clin Oncol*.

- Deep G, Agarwal R. Antimetastatic efficacy of silibinin: 17. molecular mechanisms and therapeutic potential against cancer. *Cancer Metastasis Rev* 2010; 29:447-63.).
- Devarajan E, Chen J, Multani AS, Pathak S, Sahin AA, Mehta K. Human breast cancer MCF-7 cell line contains inherently drug-resistant subclones with distinct genotypic and phenotypic features. *Int J Oncol.* 2002 May;20(5):913-20. PMID: 11956583.
- Dexter, J. S. (1914). THE ANALYSIS OF A CASE OF CONTINUOUS.
- Ding L, Ley TJ, Larson DE, Miller CA, Koboldt DC, et al. Clonal evolution in relapsed acute myeloid leukaemia revealed by whole genome sequencing. *Nature* 2012; 481:506-10.
- Dong, B., Li, S., Zhu, S., Yi, M., Luo, S., & Wu, K. (2021). MiRNA-mediated EMT and CSCs in cancer chemoresistance. *Experimental Hematology & Oncology*, 10(1). doi: 10.1186/s40164-021-00206-5.
- Dong, Y., Liao, H., Yu, J. et al. Incorporation of drug efflux inhibitor and chemotherapeutic agent into an inorganic/organic platform for the effective treatment of multidrug resistant breast cancer. *J Nanobiotechnol* 17, 125 (2019). <https://doi.org/10.1186/s12951-019-0559->
- Doyle, L. A., Yang, W., Abruzzo, L. V., Krogmann, T., Gao, Y., Rishi, A. K., & Ross, D. D. (1998). A multidrug resistance transporter from human MCF-7 breast cancer cells. *Proceedings of the National Academy of Sciences of the United States of America*, 95(26), 15665–15670. <https://doi.org/10.1073/pnas.95.26.15665>.

- Edwards, A., & Brennan, K. (2021). Notch Signalling in Breast Development and Cancer. *Frontiers in Cell and Developmental Biology*, Vol.9. Retrieved from <https://www.frontiersin.org/article/10.3389/fcell.2021.692173>.
- Ellis, T.H.N., Hofer, J.M.I., Swain, M.T. et al. Mendel's pea crosses: varieties, traits and statistics. *Hereditas* 156, 33 (2019). <https://doi.org/10.1186/s41065-019-0111-y>
- Embryonic, T. H. E., Of, D., & Melanogaster, D. (1937). Chromosomal deficiencies and the embryonic. 23.
- Esmeralda Casas, Jihoon Kim, Andrés Bendesky, Lucila Ohno-Machado, Cecily J. Wolfe, Jing Yang; Snail2 is an Essential Mediator of Twist1-Induced Epithelial Mesenchymal Transition and Metastasis. *Cancer Res* 1 January 2011; 71 (1): 245–64. <https://doi.org/10.1158/0008-5472.CAN-10-2330>.
- Facilitation of lin-12-mediated signalling by sel-12 , a *Caenorhabditis elegans* S182 Alzheimer ' s disease gene . (1995). 20894. <https://doi.org/10.1038/377351a0>
- Fender, A., Nutter, J., Fitzgerald, T., Bertrand, F., & Sigounas, G. (2015). Notch-1 Promotes Stemness and Epithelial to Mesenchymal Transition in Colorectal Cancer. *Journal Of Cellular Biochemistry*, 116(11), 2517-2527. doi: 10.1002/jcb.25196.
- Feng, J., Wang, J., Liu, Q., Li, J., Zhang, Q., Zhuang, Z., Gao, H. (2019). DAPT, a γ -Secretase Inhibitor, Suppresses Tumorigenesis, and Progression of Growth Hormone-Producing Adenomas by Targeting Notch Signaling. *Frontiers in Oncology*, Vol. 9. Retrieved from <https://www.frontiersin.org/article/10.3389/fonc.2019.00809>.

- Ff, D. A., De, S., Pj, S., Rj, G., Ap, M., & Gridley, T. (1992). Expression pattern of Motch , a mouse homolog of Drosophila Notch , suggests an important role in early postimplantation mouse development . 20894.
- Flaum, N., Crosbie, E. J., Edmondson, R. J., Smith, M. J., & Evans, D. G. (2020). Epithelial ovarian cancer risk: A review of the current genetic landscape. *Clinical genetics*, 97(1), 54–63. <https://doi.org/10.1111/cge.13566>.
- Fm, L., & Se, L. (1996). Constitutively active human Notch1 binds to the transcription factor CBF1 and stimulates transcription through a promoter containing a CBF1-responsive element. 20894. <https://doi.org/10.1073/pnas.93.11.5663>
- Fostert, G. G., & Suzuki, D. T. (1970). Temperature- Sensitive Mutations in Drosophila Melanogaster, IV. A Mutation Affecting Eye Facet Arrangement in a Polarized Manner *, t. 67(2), 738–745.
- Francesco, E. M. De, & Maggiolini, M. (2018). Crosstalk between Notch, HIF-1 α and GPER in Breast Cancer EMT. 1–28. <https://doi.org/10.3390/ijms19072011>
- Garzon S, Laganà AS, Casarin J, et al. Secondary and tertiary ovarian cancer recurrence: what is the best management? *Gland Surg*. 2020;9(4):1118-1129. doi:10.21037/gs-20-325
- Gatti L, Zunino F. Overview of tumour cell chemoresistance mechanisms. *Methods Mol Med*. 2005; 111:127-48. doi: 10.1385/1-59259-889-7:127. PMID: 15911977.
- Gavert N, Ben-Ze'ev A. Epithelial-mesenchymal transition, and the invasive potential of tumors. *Trends Mol Med*. 2008 May;14(5):199-209. doi: 10.1016/j.molmed.2008.03.004. Epub 2008 Apr 10. PMID: 18406208.
- Gehart H, Goginashvili A, Beck R, Morvan J, Erbs E, Formentini I, De Matteis MA, Schwab Y, Wieland FT, Ricci R. The BAR domain protein Arfaptin-1

controls secretory granule biogenesis at the trans-Golgi network. *Dev Cell*. 2012 Oct 16;23(4):756-68. doi: 10.1016/j.devcel.2012.07.019. Epub 2012 Sep 13. PMID: 22981988. Gioli, M. V, Giuliani, E., Screpanti, I., Bellavia, D., & Checquolo, S. (2019). Notch Signaling Activation as a Hallmark for Triple-Negative Breast Cancer Subtype. 2019(Im). <https://doi.org/10.1155/2019/8707053>.

Goodsell, D. (2006). The Molecular Perspective: Cisplatin. *Stem Cells*, 24(3), pp.514-515.

Groeneweg, J., Foster, R., Growdon, W., Verheijen, R., & Rueda, B. (2014). Notch signaling in serous ovarian cancer. *Journal Of Ovarian Research*, 7(1). doi: 10.1186/s13048-014-0091.

Guo J, Du X, Li C. PCMT1 Is a Potential Prognostic Biomarker and Is Correlated with Immune Infiltrates in Breast Cancer. *Biomed Res Int*. 2022 Apr 30; 2022:4434887. doi: 10.1155/2022/4434887. PMID: 35535040; PMCID: PMC9078795.

Guo T, Dong X, Xie S, Zhang L, Zeng P, Zhang L. Cellular Mechanism of Gene Mutations and Potential Therapeutic Targets in Ovarian Cancer. *Cancer Manag Res*. 2021; 13:3081-3100. Guo, S., Liu, M. and Gonzalez-Perez, R. (2010). Role of Notch and its oncogenic signalling crosstalk in breast cancer. *Biochimica et Biophysica Acta (BBA) - Reviews on Cancer*, 1815(2), pp.197-213.

Guo, S., Liu, M. and Gonzalez-Perez, R. (2011). Role of Notch and its oncogenic signaling crosstalk in breast cancer. *Biochimica et Biophysica Acta (BBA) - Reviews on Cancer*, 1815(2), pp.197-213.

- Gupta N, Xu Z, El-Sehemy A, Steed H, Fu Y: Notch3 induces epithelial-mesenchymal transition and attenuates carboplatin-induced apoptosis in ovarian cancer cells. *Gynecol Oncol* 2013, 130:200–206.
- Gupta, P., Pastushenko, I., Skibinski, A., Blanpain, C., & Kuperwasser, C. (2019). Phenotypic Plasticity: Driver of Cancer Initiation, Progression, and Therapy Resistance. *Cell Stem Cell*, 24(1), 65-78. doi: 10.1016/j.stem.2018.11.011.
- Hafen, E., & Basler, K. (1991). Specification of cell fate in the developing eye of *Drosophila*. 20894.
- Han, J., Ma, I., Hendzel, M. and Allalunis-Turner, J. (2011). The cytotoxicity of γ -secretase inhibitor I to breast cancer cells is mediated by proteasome inhibition, not by γ -secretase inhibition. *Breast Cancer Research*, 11.
- Han, S.J., Kwon, S. & Kim, K.S. Challenges of applying multicellular tumor spheroids in preclinical phase. *Cancer Cell Int* 21, 152 (2021). <https://doi.org/10.1186/s12935-021-01853>.
- Hansen, S., Ehlers, N., Zhu, S., Thomsen, M., Nielsen, R., & Liu, D. et al. (2016). The stepwise evolution of the exome during acquisition of docetaxel resistance in breast cancer cells. *BMC Genomics*, 17(1). doi: 10.1186/s12864-016-2749-4.
- Harbeck, N., Penault-Llorca, F., Cortes, J., Gnant, M., Houssami, N., & Poortmans, P. et al. (2019). Breast cancer. *Nature Reviews Disease Primers*, 5(1). doi: 10.1038/s41572-019-0111-2
- Harrison, H., Farnie, G., Howell, S., Rock, R., Stylianou, S., Brennan, K., Bundred, N. and Clarke, R. (2010). Regulation of Breast Cancer Stem Cell Activity by

Signaling through the Notch4 Receptor. *Cancer Research*, 70(2), pp.709-718.

Henrique, D., & Schweisguth, F. (2019). Mechanisms of Notch signaling : a simple logic deployed in time and space. <https://doi.org/10.1242/dev.172148>

Henrique, D., Adam, J., Myat, A., Chitnis, A., & Lewis, J. (1995). Expression of a Delta homologue in prospective neurons in the chick. 20894. <https://doi.org/10.1038/375787a0>.

Hirst, J., Crow, J., Godwin, A., 2018, 'Ovarian Cancer Genetics: Subtypes and Risk Factors', in O. Devaja, A. Papadopoulos (eds.), *Ovarian Cancer - From Pathogenesis to Treatment*, IntechOpen, London. 10.5772/intechopen.72705.

Hk, K., & Siu, G. (1998). The Notch pathway intermediate HES-1 silences CD4 gene expression. 20894. <https://doi.org/10.1128/mcb.18.12.7166>

Hoffman B, Amanullah A, Shafarenko M, Liebermann DA (2002) The protooncogene c-myc in hematopoietic development and leukemogenesis. *Oncogene* 21: 3414–3421.

Hopfer, O., Zwahlen, D., Fey, M. F. & Aebi, S. The Notch pathway in ovarian carcinomas and adenomas. *Br. J. Cancer* 93, 709–718 (2005).

Hoppe, P. E., & Greenspan, R. J. (2020). Local function of the Notch gene for embryonic ectodermal pathway choice in drosophila. 2020.

Hossain, F., Sorrentino, C., Ucar, D. A., Peng, Y., Matossian, M., Wyczechowska, D. Miele, L. (2018). Notch Signaling Regulates Mitochondrial Metabolism and NF- κ B Activity in Triple-Negative Breast Cancer Cells via IKK α -

Dependent Non-canonical Pathways. 8(December), 1–16.
<https://doi.org/10.3389/fonc.2018.00575>.

Housman G, Byler S, Heerboth S, et al. Drug resistance in cancer: an overview. *Cancers (Basel)*. 2014;6(3):1769-1792. Published 2014 Sep 5.
doi:10.3390/cancers6031769.

Hu P, Liang Y, Hu Q, Wang H, Cai Z, He J, Cai J, Liu M, Qin Y, Yu X, Jiang C, Zhang B, Wang W. SNX6 predicts poor prognosis and contributes to the metastasis of pancreatic cancer cells via activating epithelial-mesenchymal transition. *Acta Biochim Biophys Sin (Shanghai)*. 2018 Nov 1;50(11):1075-1084. doi: 10.1093/abbs/gmy110. PMID: 30307473.

Huang D, Duan H, Huang H, Tong X, Han Y, et al. Cisplatin resistance in gastric cancer cells is associated with HER2 upregulation- induced epithelial-mesenchymal transition. *Sci Rep* 2016; 6:20502.

Huntosova V et al. Influence of Oxidative Stress on Time-Resolved Oxygen Detection by [Ru (Phen)₃]²⁺ In Vivo and In Vitro. *Molecules* 26: N/A (2021).

Ianevski, A., Giri, K. A., Aittokallio, T., 2020. SynergyFinder 2.0: visual analytics of multi-drug combination synergies. *Nucleic Acids Research*.,
<https://doi.org/10.1093/nar/gkaa216>.

Izabela Ziółkowska-Seta, Radosław Mądry, Ewa Kraszewska, Teresa Szymańska, Agnieszka Timorek, Alina Rembiszewska, Jolanta Kupryjańczyk, TP53, BCL-2 and BAX analysis in 199 ovarian cancer patients treated with taxane-platinum regimens, *Gynecologic Oncology*, Volume 112, Issue 1,

2009, Pages 179-184, ISSN 0090-8258,
(<https://doi.org/10.1016/j.ygyno.2008.09.008>).

Ja, C. (1996). Numb diverts Notch pathway off the tramtrack. 20894.

[https://doi.org/10.1016/s0896-6273\(00\)80274-3](https://doi.org/10.1016/s0896-6273(00)80274-3)

JAGGED2: a putative Notch ligand expressed in the apical ectodermal ridge and in sites of. (1997). 20894. [https://doi.org/10.1016/s0925-4773\(97\)00146-9](https://doi.org/10.1016/s0925-4773(97)00146-9).

Jamdade, V. S., Sethi, N., Mundhe, N. A., Kumar, P., Lahkar, M., & Sinha, N. (2015).

Therapeutic targets of triple-negative breast cancer: a review Tables of Links. <https://doi.org/10.1111/bph.13211>.

Jarriault, S., Brou, C., Logeat, F., Eh, S., Kopan, R., & Israel, A. (1995). Signalling downstream of activated mammalian Notch. 20894.

<https://doi.org/10.1038/377355a0>.

Jj, H., Henkel, T., Salmon, P., Robey, E., Mg, P., & Sd, H. (1996). Truncated mammalian Notch1 activates CBF1 / RBPJk-repressed genes by a mechanism resembling that of Epstein-Barr virus EBNA2. 20894.

<https://doi.org/10.1128/mcb.16.3.952>.

Jl, R., As, L., Ml, L., & Overbaugh, J. (1996). Transduction of Notch2 in feline leukemia virus-induced thymic lymphoma. 20894.

Jm, K., Jd, G., Dubnick, M., Mh, P., Xiao, H., Cr, M., ... Rf, M. (1991).

Complementary DNA sequencing: expressed sequence tags and human genome project. 20894. <https://doi.org/10.1126/science.2047873>

- Johanna, V., & Port, P. (2020). Fine structure of flight muscles in different Notch mutants of *Drosophila melanogaster* reared at different temperatures. (January 1987), 2020.
- Joutel, A., Corpechot, C., Ducros, A., Vahedi, K., Chabriat, H., Mouton, P., ... Cruaud, C. (1996). Notch3 mutations in CADASIL, a hereditary adult-onset condition causing stroke and dementia. 20894.
<https://doi.org/10.1038/383707a0>
- Jv, S., Uyttendaele, H., Kitajewski, J., & Montesano, R. (2000). Expression of an activated Notch4 (int-3) oncoprotein disrupts morphogenesis and induces an invasive phenotype in mammary epithelial cells in vitro.
[https://doi.org/10.1002/\(sici\)1097-0215\(20000601\)86](https://doi.org/10.1002/(sici)1097-0215(20000601)86).
- Kalluri R, Weinberg RA. The basics of epithelial-mesenchymal transition. *J Clin Invest*. 2009 Jun;119(6):1420-8. doi: 10.1172/JCI39104. Erratum in: *J Clin Invest*. 2010 May 3;120(5):1786. PMID: 19487818; PMCID: PMC2689101.
- Kamatar A, Gunay G, Acar H. Natural and Synthetic Biomaterials for Engineering Multicellular Tumor Spheroids. *Polymers*. 2020; 12(11):2506.
<https://doi.org/10.3390/polym12112506>.
- Kang SA, Guan JS, Tan HJ, Chu T, Thike AA, Bernadó C, Arribas J, Wong CY, Tan PH, Gudi M, Putti TC, Sohn J, Lim SH, Lee SC, Lim YP. Elevated WBP2 Expression in HER2-positive Breast Cancers Correlates with Sensitivity to Trastuzumab-based Neoadjuvant Therapy: A Retrospective and

Multicentric Study. *Clin Cancer Res.* 2019 Apr 15;25(8):2588-2600. doi: 10.1158/1078-0432.CCR-18-3228. Epub 2018 Dec 28. PMID: 30593516.

Kar R, Jha NK, Jha SK, et al. A "NOTCH" Deeper into the Epithelial-To-Mesenchymal Transition (EMT) Program in Breast Cancer. *Genes (Basel)*. 2019;10(12):961. Published 2019 Nov 22. doi:10.3390/genes10120961.

Kato, R., Iwamuro, M., Shiraha, H., Horiguchi, S., Tanaka, E., & Matsumoto, K. et al. (2018). Dipeptide γ -secretase inhibitor treatment enhances the anti-tumor effects of cisplatin against gastric cancer by suppressing cancer stem cell properties. *Oncology Letters*. doi: 10.3892/ol.2018.9301.

Katoh, M. (2020). Precision medicine for human cancers with Notch signaling dysregulation. (4), 279–297. <https://doi.org/10.3892/ijmm.2019.4418>

Keatley K et al. Integrated Approach Reveals Role of Mitochondrial Germ-Line Mutation F18L in Respiratory Chain, Oxidative Alterations, Drug Sensitivity, and Patient Prognosis in Glioblastoma. *Int J Mol Sci* 20: N/A (2019).

Khazaei, M., Kia, N., Rashidi, B., Saeidi, H., Tahergorabi, Z., Dana, N. and Kalantari, E. (2013). Effect of DAPT, a gamma secretase inhibitor, on tumor angiogenesis in control mice. *Advanced Biomedical Research*, 2(1), p.83.

Kidd, S., Kelley, M. R., & Young, M. W. (1986). Sequence of the Notch Locus of *Drosophila melanogaster*: Relationship of the Encoded Protein to Mammalian Clotting and Growth Factors. 6(9), 3094–3108.

- Kidd, S., Mk, B., Gp, G., & Mw, Y. (1989). Structure and distribution of the Notch protein in developing *Drosophila*. 20894.
<https://doi.org/10.1101/gad.3.8.1113>
- Kidd, S., Wa, D., & Mw, Y. (1987). Mutations altering the structure of epidermal growth factor-like coding sequences at the *Drosophila* Notch locus. 20894.
[https://doi.org/10.1016/0092-8674\(87\)90123-1](https://doi.org/10.1016/0092-8674(87)90123-1)
- Kim, B., Stephen, S., Hanby, A., Horgan, K., Perry, S., Richardson, J., Roundhill, E., Valleley, E., Verghese, E., Williams, B., Thorne, J. and Hughes, T. (2015). Chemotherapy induces Notch1-dependent MRP1 up-regulation, inhibition of which sensitizes breast cancer cells to chemotherapy. *BMC Cancer*, 15(1).
- Kl, W., Rw, J., & Pj, B. (1994). *Drosophila* in cancer research: the first fifty tumor suppressor genes. 20894. <https://doi.org/10.1242/jcs.1994.supplement>
- Knust, E., Dietrich, U., Tepass, U., Bremer, K. A., Weigel, D., Vässin, H., & Ortega, J. A. C. (2020). EGF homologous sequences encoded in the genome of *Drosophila melanogaster*, and their relation to neurogenic genes. 2020.
- Knust, E., Ja, C., & Biol, A. D. (1989). The molecular genetics of early neurogenesis in *Drosophila melanogaster*. 20894.
<https://doi.org/10.1002/bies.950110405>
- Kontomanolis, E. N., Kalagasidou, S., Pouliliou, S., Anthoulaki, X., Georgiou, N., Papamanolis, V., & Fasoulakis, Z. N. (2018). The Notch Pathway in Breast Cancer Progression. 2018. <https://doi.org/10.1155/2018/2415489>
- Kopan, R., & Ilagan, M. X. G. (2009). The Canonical Notch Signaling Pathway: Unfolding the Activation Mechanism. *Cell*.
<https://doi.org/10.1016/j.cell.2009.03.045>

- Kopan, R., & Ilagan, M. X. G. (2010). Cell Notch signaling pathway. *137*(2), 216–233. <https://doi.org/10.1016/j.cell.2009.03.045>.
- Krop, I., Demuth, T., Guthrie, T., Wen, P., Mason, W., Chinnaiyan, P., Butowski, N., Groves, M., Kesari, S., Freedman, S., Blackman, S., Watters, J., Loboda, A., Podtelezhnikov, A., Lunceford, J., Chen, C., Giannotti, M., Hing, J., Beckman, R. and LoRusso, P. (2012). Phase I Pharmacologic and Pharmacodynamic Study of the Gamma Secretase (Notch) Inhibitor MK-0752 in Adult Patients with Advanced Solid Tumors. *Journal of Clinical Oncology*, *30*(19), pp.2307-2313.
- Kumar, S., Kumar, R., David, S., Taylor, W. W., Sabrina, R., Jules, K., Chakrabarti, R. (2019). Estrogen-dependent DLL1-mediated Notch signaling promotes luminal breast cancer. *Oncogene*, 2092–2107. <https://doi.org/10.1038/s41388-018-0562-z>
- Lamy, M., Ferreira, A., Dias, J., Braga, S., Silva, G., & Barbas, A. (2017). Notch-out for breast cancer therapies. *New Biotechnology*, *39*, 215-221. doi: 10.1016/j.nbt.2017.08.004.
- Lardelli, M., Dahlstrand, J., & Lendahl, U. (1994). The novel Notch homologue mouse Notch 3 lacks specific epidermal growth factor-repeats and is expressed in proliferating neuroepithelium. 20894. [https://doi.org/10.1016/0925-4773\(94\)90081-7](https://doi.org/10.1016/0925-4773(94)90081-7)
- Lefevre, G. (1953). Frequency of Notch mutations induced in normal, duplicated and inverted x-chromosomes of *Drosophila melanogaster*. (July).
- Leontovich, A.A., Jalalirad, M., Salisbury, J.L. et al. NOTCH3 expression is linked to breast cancer seeding and distant metastasis. *Breast Cancer Res* *20*, 105 (2018). <https://doi.org/10.1186/s13058-018-1020-0>.

- LeVasseur, N., Chia, S. Sequential versus concurrent chemotherapy for adjuvant breast cancer: does dose intensity matter? *Br J Cancer* 117, 157–158 (2017). <https://doi.org/10.1038/bjc.2017.176>
- Li J, Wang Z, Tie C. High expression of ladinin-1 (LAD1) predicts adverse outcomes: a new candidate docetaxel resistance gene for prostatic cancer (PCa). *Bioengineered*. 2021 Dec;12(1):5749-5759. doi: 10.1080/21655979.2021.1968647. PMID: 34516317; PMCID: PMC8806705.
- Li JP, Cao NX, Jiang RT, He SJ, Huang TM, Wu B, Chen DF, Ma P, Chen L, Zhou SF, Xie XX, Luo GR. Knockdown of GCF2/LRRFIP1 by RNAi causes cell growth inhibition and increased apoptosis in human hepatoma HepG2 cells. *Asian Pac J Cancer Prev*. 2014;15(6):2753-8. doi: 10.7314/apjcp.2014.15.6.2753. PMID: 24761896.
- Li L, Zhao F, Lu J, Li T, Yang H, Wu C, et al. (2014) Notch-1 Signaling Promotes the Malignant Features of Human Breast Cancer through NF- κ B Activation. *PLoS ONE* 9(4): e95912. <https://doi.org/10.1371/journal.pone.0095912>.
- Li Y, Jiao Y, Li Y, Liu Y. Expression of La Ribonucleoprotein Domain Family Member 4B (LARP4B) in Liver Cancer and Their Clinical and Prognostic Significance. *Dis Markers*. 2019 Oct 22; 2019:1569049. doi: 10.1155/2019/1569049. PMID: 31772683; PMCID: PMC6854232.
- Li Z, Lim SK, Liang X, Lim YP. The transcriptional coactivator WBP2 primes triple-negative breast cancer cells for responses to Wnt signaling via the JNK/Jun kinase pathway. *J Biol Chem*. 2018 Dec 28;293(52):20014-20028. doi: 10.1074/jbc.RA118.005796. Epub 2018 Nov 15. PMID: 30442712; PMCID: PMC6311518.

- Li, L., Guan, Y., Chen, X., Yang, J., & Cheng, Y. (2021). DNA Repair Pathways in Cancer Therapy and Resistance. *Frontiers In Pharmacology*, 11. doi: 10.3389/fphar.2020.629266.
- Li, L., Id, K., Deng, Y., Genin, A., Ab, B., Cc, C., ... Hood, L. (1997). Alagille syndrome is caused by mutations in human Jagged1, which encodes a ligand for Notch1. 20894. <https://doi.org/10.1038/ng0797-243>
- Liao, T., & Yang, M. (2017). Revisiting epithelial-mesenchymal transition in cancer metastasis: the connection between epithelial plasticity and stemness. *Molecular Oncology*, 11(7), 792-804. doi: 10.1002/1878-0261.12096.
- Lieber, T., Kidd, S., Alcamo, E., Corbin, V., & Mw, Y. (1993). Antineurogenic phenotypes induced by truncated Notch proteins indicate a role in signal transduction and may point to a novel function for Notch in nuclei. 20894. <https://doi.org/10.1101/gad.7.10.1949>
- Lippert, T., Ruoff, H., & Volm, M. (2011). Intrinsic and Acquired Drug Resistance in Malignant Tumors. *Arzneimittelforschung*, 58(06), 261-264. doi: 10.1055/s-0031-1296504.
- Lisa Choy, Thijs J. Hagenbeek, Margaret Solon, Dorothy French, David Finkle, Amy Shelton, Rayna Venook, Matthew J. Brauer, Christian W. Siebel; Constitutive NOTCH3 Signaling Promotes the Growth of Basal Breast Cancers. *Cancer Res* 15 March 2017; 77 (6): 1439–1452. <https://doi.org/10.1158/0008-5472.CAN-16-1022>Liu, Y., Li, Q., Zhou, L., Xie, N., Nice, E. C., Zhang, H., Huang, C., & Lei, Y. (2016). Cancer drug resistance: redox resetting renders a way. *Oncotarget*, 7(27), 42740–42761. <https://doi.org/10.18632/oncotarget.8600>.

- Lo Dico A et al. Intracellular Redox-Balance Involvement in Temozolomide Resistance-Related Molecular Mechanisms in Glioblastoma. *Cells* 8: N/A (2019).
- Locatelli, M., & Cur, G. (2017). Notch Inhibitors and Their Role in the Treatment of Triple Negative Breast Cancer: Promises and Failures National Center for Biotechnology Information. 19.
<https://doi.org/10.1097/CCO.0000000000000406>.
- Locatelli, M., Aftimos, P., Dees, E., LoRusso, P., Pegram, M., & Awada, A. et al. (2016). Phase I study of the gamma secretase inhibitor PF-03084014 in combination with docetaxel in patients with advanced triple-negative breast cancer. *Oncotarget*, 8(2). doi: 10.18632/oncotarget.13727.
- Loh, C. Y., Chai, J. Y., Tang, T. F., Wong, W. F., Sethi, G., Shanmugam, M. K., Chong, P. P., & Looi, C. Y. (2019). The E-Cadherin and N-Cadherin Switch in Epithelial-to-Mesenchymal Transition: Signaling, Therapeutic Implications, and Challenges. *Cells*, 8(10), 1118.
<https://doi.org/10.3390/cells8101118>.
- Lopez, A., Reyna, D.E., Gitego, N. et al. Co-targeting of BAX and BCL-XL proteins broadly overcomes resistance to apoptosis in cancer. *Nat Commun* 13, 1199 (2022). (<https://doi.org/10.1038/s41467-022-28741-7>).
- Lu, K. H. et al. Selection of potential markers for epithelial ovarian cancer with gene expression arrays and recursive descent partition analysis. *Clin. Cancer Res.* 10, 3291–3300 (2004).
- Luiken, S., Fraas, A., Bieg, M. et al. NOTCH target gene HES5 mediates oncogenic and tumor suppressive functions in hepatocarcinogenesis. *Oncogene* 39, 3128–3144 (2020). <https://doi.org/10.1038/s41388-020-1198-3>.

- Lukyanova NY1, Rusetskya NV, Tregubova NA, Chekhun VF. Molecular profile and cell cycle in MCF-7 cells resistant to cisplatin and doxorubicin. *Exp Oncol.* 2009 Jun;31(2):87-91.
- Lumicisi BA, Cartwright JE, Leslie K, Wallace AE, Whitley GS. Inhibition of DDAH1, but not DDAH2, results in apoptosis of a human trophoblast cell line in response to TRAIL. *Hum Reprod.* 2015 Aug;30(8):1813-9. doi: 10.1093/humrep/dev138. Epub 2015 Jun 16. PMID: 26082478; PMCID: PMC4507332.
- Luqmani, Y. (2008). Mechanisms of Drug Resistance in Cancer Chemotherapy. *Medical Principles and Practice*, 14(1), pp.35-48.
- Lw, E., Bird, J., Dc, W., Al, S., Tc, R., Sd, S., & Sklar, J. (1991). TAN-1 , the human homolog of the Drosophila Notch gene , is broken by chromosomal translocations in T lymphoblastic neoplasms . 20894. [https://doi.org/10.1016/0092-8674\(91\)90111-b](https://doi.org/10.1016/0092-8674(91)90111-b)
- Ly PT, Xu S, Wirawan M, Luo D, Roca X. ZAP isoforms regulate unfolded protein response and epithelial- mesenchymal transition. *Proc Natl Acad Sci U S A.* 2022 Aug 2;119(31): e2121453119. doi: 10.1073/pnas.2121453119. Epub 2022 Jul 26. PMID: 35881805; PMCID: PMC9351355.
- Ma W, Bao Z, Qian Z, Zhang K, Fan W, Xu J, Ren C, Zhang Y, Jiang T. LRRFIP1, an epigenetically regulated gene, is a prognostic biomarker and predicts malignant phenotypes of glioma. *CNS Neurosci Ther.* 2022 Jun;28(6):873-883. doi: 10.1111/cns.13817. Epub 2022 Mar 26. PMID: 35338570; PMCID: PMC9062568.
- Machado RAC, Stojevski D, De Landtsheer S, Lucarelli P, Baron A, Sauter T, Schaffner-Reckinger E. L-plastin Ser5 phosphorylation is modulated by the PI3K/SGK pathway and promotes breast cancer cell invasiveness. *Cell*

Commun Signal. 2021 Feb 22;19(1):22. doi: 10.1186/s12964-021-00710-5. PMID: 33618712; PMCID: PMC7898450.

- Magadoux, I., Isambard, N., Planchette, S., Jeannine, J., and Laurens, V. (2014). Emerging targets to monitor and overcome docetaxel resistance in castration resistant prostate cancer (Review). *International Journal of Oncology*, 45(3), 919-928. doi: 10.3892/ijo.2014.2517.
- Markopoulou, K. (1989). The expression of the neurogenic locus Notch during the postembryonic development of *Drosophila melanogaster* and its relationship to mitotic activity. 20894. <https://doi.org/10.3109/01677068909107097>
- Martina, M.; et al. In vitro development of chemotherapy and targeted therapy drug-resistant cancer cell lines: a practical guide with case studies. *Front Oncol.* 2014, 4: 40.
- Mas, J., & Andersson, E. R. (2017). The developmental biology of genetic Notch disorders. 1743–1763. <https://doi.org/10.1242/dev.148007>
- Masui K, Tanaka K, Akhavan D, Babic I, Gini B, et al. (2013) mTOR complex 2 controls glycolytic metabolism in glioblastoma through FoxO acetylation and upregulation of c-Myc. *Cell Metab* 18: 726–739. 10.
- Matulonis, U., Sood, A., Fallowfield, L. et al. Ovarian cancer. *Nat Rev Dis Primers* 2, 16061 (2016). <https://doi.org/10.1038/nrdp.2016.61>.
- Mc, R., Sj, P., Da, A., & Jw, S. (1988). Precise determination of the molecular limits of a polytene chromosome band: regulatory sequences for the Notch gene are in the interband. 20894. [https://doi.org/10.1016/0092-8674\(88\)90067-0](https://doi.org/10.1016/0092-8674(88)90067-0)
- McDermott M, Eustace AJ, Busschots S, Breen L, Crown J, Clynes M, et al. In vitro Development of Chemotherapy and Targeted Therapy Drug-Resistant

Cancer Cell Lines: A Practical Guide with Case Studies. *Front Oncol.* 2014; 4:40.

McGranahan, N., & Swanton, C. (2017). Clonal Heterogeneity and Tumor Evolution: Past, Present, and the Future. *Cell*, 168(4), 613-628. doi: 10.1016/j.cell.2017.01.018.

Me, F., Rebay, I., & La, C. (1993). An activated Notch receptor blocks cell-fate commitment in the developing *Drosophila* eye. 20894. <https://doi.org/10.1038/365555a0>

Mk, L., Hh, S., Lj, M., Thinakaran, G., Kim, G., Se, G., ... Ss, S. (1996). Expression of presenilin 1 and 2 (PS1 and PS2) in human and murine tissues. 20894.

Mohammad Aslam Khan, Kunwar Somesh Vikramdeo, Sarabjeet Kour Sudan, Seema Singh, Annelise Wilhite, Santanu Dasgupta, Rodney Paul Rocconi, Ajay Pratap Singh, Platinum-resistant ovarian cancer: From drug resistance mechanisms to liquid biopsy-based biomarkers for disease management, *Seminars in Cancer Biology*, Volume 77, 2021, Pages 99-109, ISSN 1044-579X, (<https://doi.org/10.1016/j.semcancer.2021.08.005>).

Mohr, O. L. (1919). 7, 1918. 275–282.

Molecular bases of early neural development in *Xenopus* embryos. (1992). 20894. <https://doi.org/10.1146/annurev.ne.15.030192.001343>

Molecular interaction between TLE1 and the carboxyl-terminal domain of HES-1 containing the WRPW motif. *Hes factors in development*. (1996). 20894. <https://doi.org/10.1006/bbrc.1996.0959>.

- Mollen, E. W. J., Ient, J., & Tjan-heijnen, V. C. G. (2018). Moving Breast Cancer Therapy up a Notch. 8(November).
<https://doi.org/10.3389/fonc.2018.00518>.
- Moo TA, Sanford R, Dang C, Morrow M. Overview of Breast Cancer Therapy. *PET Clin.* 2018;13(3):339-354. doi: 10.1016/j.cpet.2018.02.006.
- Moore, G.; Annett, S.; McClements, L.; Robson, T. Top Notch Targeting Strategies in Cancer: A Detailed Overview of Recent Insights and Current Perspectives. *Cells* 2020, 9, 1503. <https://doi.org/10.3390/cells9061503>.
- Moulder, S. (2010). Intrinsic Resistance to Chemotherapy in Breast Cancer. *Women's Health*, 6(6), 821-830. doi: 10.2217/whe.10.60.
- Mouse mammary tumor gene int-3: a member of the Notch gene family transforms mammary. (1992). 20894.
- Mrozik, K.M., Blaschuk, O.W., Cheong, C.M. et al. N-cadherin in cancer metastasis, its emerging role in haematological malignancies and potential as a therapeutic target in cancer. *BMC Cancer* 18, 939 (2018).
<https://doi.org/10.1186/s12885-018-4845-0>.
- Muggia, F., Bonetti, A., Hoeschele, J., Rozencweig, M. and Howell, S. (2015). Platinum Antitumor Complexes: 50 Years Since Barnett Rosenberg's Discovery. *Journal of Clinical Oncology*, 33(35), pp.4219-4226.
- Nami, B., & Wang, Z. (2017). HER2 in Breast Cancer Stemness: A Negative Feedback Loop towards Trastuzumab Resistance. 2(i).
<https://doi.org/10.3390/cancers9050040>

- Neophytou CM, Trougakos IP, Erin N, Papageorgis P. Apoptosis Deregulation, and the Development of Cancer Multi-Drug Resistance. *Cancers*. 2021; 13(17):4363. <https://doi.org/10.3390/cancers13174363>.
- Nikolaou, M., Pavlopoulou, A., Georgakilas, A.G. et al. The challenge of drug resistance in cancer treatment: a current overview. *Clin Exp Metastasis* 35, 309–318 (2018). <https://doi.org/10.1007/s10585-018-9903-0>.
- Novel association of a diverse range of genes with renal cell carcinoma as identified by differential. (2000). 20894. [https://doi.org/10.1002/1097-0215\(20001201\)88](https://doi.org/10.1002/1097-0215(20001201)88)
- Nylund P et al. A distinct metabolic response characterizes sensitivity to EZH2 inhibition in multiple myeloma. *Cell Death Dis* 12:167 (2021).
- Ohtsuka, T., Ishibashi, M., Gradwohl, G., Nakanishi, S., Guillemot, F., & Kageyama, R. (1999). Hes1 and Hes5 as Notch effectors in mammalian neuronal differentiation. *Hes factors in development*. 20894. <https://doi.org/10.1093/emboj/18.8.2196>
- O'Neill, A., Prencipe, M., Dowling, C., Fan, Y., Mulrane, L., & Gallagher, W. et al. (2011). Characterisation and manipulation of docetaxel resistant prostate cancer cell lines. *Molecular Cancer*, 10(1), 126. doi: 10.1186/1476-4598-10-126
- Organ, P. R. T. H. M. (1917). *Electronic Scholarly Publishing* <http://www.esp.org>.
- Ortiz M, Wabel E, Mitchell K, Horibata S. Mechanisms of chemotherapy resistance in ovarian cancer. *Cancer Drug Resist* 2022; 5:304-16. <http://dx.doi.org/10.20517/cdr.2021.147>.

- Osipo, C., Zlobin and Olsauskas-Kuprys (2013). Gamma secretase inhibitors of Notch signaling. *OncoTargets and Therapy*, p.943.
- P., Baker, A., Wyatt, D., Jun, L., & Aleksandra, F. (2018). Notch-1-PTEN-ERK1 / 2 Signaling Axis Promotes HER2 + Breast Cancer Cell Proliferation and Stem Cell Survival National Center for Biotechnology Information. 19. <https://doi.org/10.1038/s41388-018-0251-y>.
- Pan H, Chai W, Liu X, Yu T, Sun L, Yan M. DYNC1H1 regulates NSCLC cell growth and metastasis by IFN- γ -JAK-STAT signaling and is associated with an aberrant immune response. *Exp Cell Res*. 2021 Dec 1;409(1):112897. doi: 1.1016/j.yexcr.2021.112897. Epub 2021 Oct 27. PMID: 34717919.
- Pancewicz, J., & Nicot, C. (2011). Current views on the role of Notch signaling and the pathogenesis of human leukemia. *BMC Cancer*, 11(1). doi: 10.1186/1471-2407-11-502
- Pandya, K., Wyatt, D., Gallagher, B., Shah, D., & Baker, A. (2016). PKC α Attenuates Jagged-1-Mediated Notch Signaling in ErbB-2-Positive Breast Cancer to Reverse Trastuzumab Resistance National Center for Biotechnology Information. 19. <https://doi.org/10.1158/1078-0432.CCR-15-0179>
- Panelos, J., Batistatou, A., Paglierani, M. et al. Expression of Notch-1 and alteration of the E-cadherin/ β -catenin cell adhesion complex are observed in primary cutaneous neuroendocrine carcinoma (Merkel cell carcinoma). *Mod Pathol* 22, 959–968 (2009). <https://doi.org/10.1038/modpathol.2009.55>.
- Park, J. T. et al. Notch3 gene amplification in ovarian cancer. *Cancer Res*. 66, 6312–6318 (2006).

- Pe, H., & Rj, G. (1990). The Notch locus of *Drosophila* is required in epidermal cells for epidermal development. 20894.
- Perche F, Torchilin VP. Cancer cell spheroids as a model to evaluate chemotherapy protocols. *Cancer Biol Ther.* 2012;13(12):1205-1213.
doi:10.4161/cbt.21353.
- Physical interaction between a novel domain of the receptor Notch and the transcription factor RBP-J kappa / Su (H). (1995). 20894.
[https://doi.org/10.1016/s0960-9822\(95\)00279](https://doi.org/10.1016/s0960-9822(95)00279).
- Pogribny, I., Filkowski, J., Tryndyak, V., Golubov, A., Shpileva, S., & Kovalchuk, O. (2010). Alterations of microRNAs and their targets are associated with acquired resistance of MCF-7 breast cancer cells to cisplatin. *International Journal Of Cancer*, 127(8), 1785-1794. doi: 10.1002/ijc.25191
- Pokhriyal R, Hariprasad R, Kumar L, Hariprasad G. Chemotherapy Resistance in Advanced Ovarian Cancer Patients. *Biomark Cancer.* 2019 Jul 5; 11:1179299X19860815. doi: 10.1177/1179299X19860815. PMID: 31308780; PMCID: PMC6613062.
- Polette M, Mestdagt M, Bindels S, Nawrocki-Raby B, Hunziker W, Foidart JM, Birembaut P, Gilles C. Beta-catenin and ZO1: shuttle molecules involved in tumor invasion-associated epithelial-mesenchymal transition processes. *Cells Tissues Organs.* 2007;185(1-3):61-5. doi: 10.1159/000101304. PMID: 17587809.
- Presenilins are required for gamma-secretase cleavage of beta-APP and transmembrane cleavage. (2000). 20894. <https://doi.org/10.1038/35017108>
- Prica, A., Chan, K. and Cheung, M. (2014). Combined modality therapy versus chemotherapy alone as an induction regimen for primary central nervous

system lymphoma: a cost-effectiveness analysis. *Neuro-Oncology*, 16(10), pp.1384-1391.

Purow BW, Haque RM, Noel MW, Su Q, Burdick MJ, et al. (2005) Expression of Notch-1 and its ligands, Delta-like-1 and Jagged-1, is critical for glioma cell survival and proliferation. *Cancer Res* 65: 2353–2363.

Puspita, N., & Bedford, A. (2017). Morphological Changes of Cisplatin-resistant Human Breast Cancer MCF-7 Cell Line. *International Journal of Integrated Health Sciences*, 5(1), 8-14. doi: 10.15850/ijihhs. v5n1.960.

Qin JJ, Wang JM, Du J, Zeng C, Han W, Li ZD, Xie J, Li GL. Radixin knockdown by RNA interference suppresses human glioblastoma cell growth in vitro and in vivo. *Asian Pac J Cancer Prev*. 2014;15(22):9805-12. doi: 10.7314/apjcp.2014.15.22.9805. PMID: 25520109.

Rasul, S., Balasubramanian, R., Filipović, A., Slade, M., Yagüe, E. and Coombes, R. (2009). Inhibition of γ -secretase induces G2/M arrest and triggers apoptosis in breast cancer cells. *British Journal of Cancer*, 100(12), pp.1879-1888.

Rathore, R., McCallum, J.E., Varghese, E. et al. Overcoming chemotherapy drug resistance by targeting inhibitors of apoptosis proteins (IAPs). *Apoptosis* 22, 898–919 (2017). <https://doi.org/10.1007/s10495-017-1375-1>.

Repair of UV-induced pyrimidine dimers in the individual genes *Gart*, *Notch* and *white* from *Drosophila melanogaster* cell lines. (1991). 20894. <https://doi.org/10.1093/nar/19.12.3289>

Riggio, A.I., Varley, K.E. & Welm, A.L. The lingering mysteries of metastatic recurrence in breast cancer. *Br J Cancer* 124, 13–26 (2021). <https://doi.org/10.1038/s41416-020-01161-4>.

Rizzo S, Hersey JM, Mellor P, Dai W, Santos-Silva A, Liber D, Luk L, Titley I, Carden CP, Box G, Hudson DL, Kaye SB, Brown R: Ovarian cancer stem

cell-like side populations are enriched following chemotherapy and overexpress EZH2. *Mol Cancer Ther* 2011, 10:325–335.

Rj, F., Tn, S., & Rj, D. (1990). The gene *Serrate* encodes a putative EGF-like transmembrane protein essential for proper ectodermal development in *Drosophila melanogaster*. 20894. <https://doi.org/10.1101/gad.4.12a.2188>

Rl, C., & Df, R. (1989). Notch is required for successive cell decisions in the developing *Drosophila* retina. 20894. <https://doi.org/10.1101/gad.3.8.1099>

Rocha, C., Silva, M., Quinet, A., Cabral-Neto, J., & Menck, C. (2018). DNA repair pathways and cisplatin resistance: an intimate relationship. *Clinics*, 73(Suppl 1). doi: 10.6061/clinics/2018/e478s.

Rodriguez, D., Ramkairsingh, M., Lin, X., & Kapoor, A. (2019). The Central Contributions of Breast Cancer Stem Cells in Developing Resistance to Endocrine Therapy.

Rose SL, Kunnimalaiyaan M, Drenzek J, Seiler N. Notch 1 signalling is active in ovarian cancer. *Gynecol Oncol*. 2010 Apr;117(1):130-3. doi: 10.1016/j.ygyno.2009.12.003. Epub 2010 Jan 8. PMID: 20060575.

Roth L, Srivastava S, Lindzen M, Sas-Chen A, Sheffer M, Lauriola M, Euka Y, Noronha A, Mancini M, Lavi S, Tarcic G, Pines G, Nevo N, Heyman O, Ziv T, Rueda OM, Gnocchi D, Pikarsky E, Admon A, Caldas C, Yarden Y. SILAC identifies LAD1 as a filamin-binding regulator of actin dynamics in response to EGF and a marker of aggressive breast tumors. *Sci Signal*. 2018 Jan 30;11(515): ean0949. doi: 10.1126/scisignal. ean0949. PMID: 29382783.

Ruth Nussinov, Chung-Jung Tsai, Hyunbum Jang, Anticancer drug resistance: An update and perspective, *Drug Resistance Updates*, Volume

59,2021,100796, ISSN 1368-7646,
<https://doi.org/10.1016/j.drug.2021.100796>.

Sarkar, S., Horn, G., Moulton, K., Oza, A., Byler, S., Kokolus, S., & Longacre, M. (2013). Cancer Development, Progression, and Therapy: An Epigenetic Overview. *International Journal of Molecular Sciences*, 14(10), 21087-21113. doi: 10.3390/ijms141021087.

Sb, S., Sa, B., & Ma, M. (1989). A tripartite interaction among alleles of Notch, Delta, and Enhancer of split during imaginal development of *Drosophila melanogaster*. 20894.

Schott, A., Landis, M., Dontu, G., Griffith, K., Layman, R., & Krop, I. et al. (2013). Preclinical and Clinical Studies of Gamma Secretase Inhibitors with Docetaxel on Human Breast Tumors. *Clinical Cancer Research*, 19(6), 1512-1524. doi: 10.1158/1078-0432.ccr-11-3326.

Sh, S., Kyungeun, K., Hwa-ryeon, K., Ylaya, K., Do, S., & Stephen, M. (2019). Deubiquitylation and stabilization of Notch1 intracellular domain by ubiquitin-specific protease 8 enhance tumorigenesis in breast cancer.

Shao, S., Zhao, X., Zhang, X., Luo, M., Zuo, X., Huang, S., & Wang, Y. (2015). Notch1 signaling regulates the epithelial – mesenchymal transition and invasion of breast cancer in a Slug-dependent manner. 1–17.
<https://doi.org/10.1186/s12943-015-0295-3>.

Shawber, C., Boulter, J., Ce, L., & Weinmaster, G. (1996). Jagged2: a serrate-like gene expressed during rat embryogenesis. 20894.
<https://doi.org/10.1006/dbio.1996.0310>.

- Shawber, C., Nofziger, D., Jj, H., Lindsell, C., Bögler, O., Hayward, D., & Weinmaster, G. (1996). Notch signaling inhibits muscle cell differentiation through a CBF1-independent pathway. 20894.
- Shellenbargerls, D. L., & Mohler, J. D. (1975). Temperature-sensitive mutations of the Notch locus. 1974.
- Sheth A, Escobar-Alvarez S, Gardner J, Ran L, Heaney ML, et al. (2014) Inhibition of human mitochondrial peptide deformylase causes apoptosis in cmyc-overexpressing hematopoietic cancers. *Cell Death Dis* 5: e1152.
- Shibue, T., Weinberg, R. EMT, CSCs, and drug resistance: the mechanistic link and clinical implications. *Nat.Rev.Clin.Oncol.* 14, 611–629 (2017).
<https://doi.org/10.1038/nrclinonc.2017.44>
- Shimizu, K., Chiba, S., Hosoya, N., Kumano, K., Saito, T., Kurokawa, M., ... Hirai, H. (2000). Binding of Delta1, Jagged1 , and Jagged2 to Notch2 rapidly induces cleavage , nuclear translocation , and hyperphosphorylation of Notch2 . 20894. <https://doi.org/10.1128/mcb.20.18.6913-6922.2000>
- Shiozawa T, Iyama S, Toshima S, Sakata A, Usui S, Minami Y, Sato Y, Hizawa N, Noguchi M. Dimethylarginine dimethylaminohydrolase 2 promotes tumor angiogenesis in lung adenocarcinoma. *Virchows Arch.* 2016 Feb;468(2):179-90. doi: 10.1007/s00428-015-1863-z. Epub 2015 Oct 29. PMID: 26515557; PMCID: PMC4778151.
- Siddik, Z. (2003). Cisplatin: mode of cytotoxic action and molecular basis of resistance. *Oncogene*, 22(47), pp.7265-7279.
- Simmons, M., Serra, R., Hermance, N., & Kelliher, M. (2012). NOTCH1 inhibition in vivo results in mammary tumor regression and reduced mammary

tumorsphere-forming activity in vitro. *Breast Cancer Research*, 14(5). doi: 10.1186/bcr3321.

Singh AM, Dalton S (2009) The cell cycle and Myc intersect with mechanisms that regulate pluripotency and reprogramming. *Cell Stem Cell* 5: 141–149. 13.

Singh, A., & Settleman, J. (2010). EMT, cancer stem cells and drug resistance: an emerging axis of evil in the war on cancer. *Oncogene*, 29(34), 4741-4751. doi: 10.1038/onc.2010.215.

Sirén, M., & Portin, P. (1989). Interaction of hairless, delta, enhancer of split and Notch genes of *Drosophila melanogaster* as expressed in adult morphology. 20894. <https://doi.org/10.1017/s0016672300028330>

Soni, H., Matthews, A., Pallikkuth, S., Gangaraju, R., & Adebisi, A. (2018). γ -secretase inhibitor DAPT mitigates cisplatin-induced acute kidney injury by suppressing Notch1 signaling. *Journal Of Cellular and Molecular Medicine*, 23(1), 260-270. doi: 10.1111/jcmm.13926.

Stancill JS, Corbett JA. The Role of Thioredoxin/Peroxiredoxin in the β -Cell Defense Against Oxidative Damage. *Front Endocrinol (Lausanne)*. 2021 Sep 7; 12:718235. doi: 10.3389/fendo.2021.718235.

Stephen J. Fey, Krzysztof Wrzesinski, Determination of Drug Toxicity Using 3D Spheroids Constructed From an Immortal Human Hepatocyte Cell Line, *Toxicological Sciences*, Volume 127, Issue 2, June 2012, Pages 403–411, <https://doi.org/10.1093/toxsci/kfs122>.

Steg AD, Bevis KS, Katre AA, Ziebarth A, Dobbin ZC, Alvarez RD, Zhang K, Conner M, Landen CN: Stem cell pathways contribute to clinical chemoresistance in ovarian cancer. *Clin Cancer Res* 2012, 18:869–881.

- Steinbuck, M. P., Winandy, S., & Osborne, B. A. (2018). A Review of Notch Processing with New Insights into Ligand- Independent Notch Signaling in T-Cells. 9(June), 1–11. <https://doi.org/10.3389/fimmu.2018.01230>
- Street, D. (1984). Chemical inhomogeneity of mantle above 670 km transition.
- Struhl, G., Fitzgerald, K., & Greenwald, I. (1993). Intrinsic activity of the Lin-12 and Notch intracellular domains in vivo. 20894. [https://doi.org/10.1016/0092-8674\(93\)90424](https://doi.org/10.1016/0092-8674(93)90424).
- Sun, Y., Zhao, Z., Yang, Z., Xu, F., Lu, H., Zhu, Z., & Shi, W. (2017). Risk Factors and Preventions of Breast Cancer. 13. <https://doi.org/10.7150/ijbs.21635>.
- Sung, H., Ferlay, J., Siegel, R., Laversanne, M., Soerjomataram, I., Jemal, A., & Bray, F. (2021). Global cancer statistics 2020: GLOBOCAN estimates of incidence and mortality worldwide for 36 cancers in 185 countries. *CA: A Cancer Journal for Clinicians*. doi: 10.3322/caac.21660.
- Susan Dalrymple, Lizamma Antony, Yi Xu, Aarti R. Uzgare, Julia T. Arnold, Jurga Savaugeot, Lori J. Sokoll, Angelo M. De Marzo, John T. Isaacs; Role of Notch-1 and E-Cadherin in the Differential Response to Calcium in Culturing Normal versus Malignant Prostate Cells. *Cancer Res* 15 October 2005; 65 (20): 9269–9279. <https://doi.org/10.1158/0008-5472.CAN-04-3989>.
- Sw, S., Cf, A., & Ch, L. (1988). Restriction-map variation in the Notch region of *Drosophila melanogaster*. 20894. <https://doi.org/10.1093/oxfordjournals.molbev.a040475>
- Ta, M., Henrique, D., Thesleff, I., & Lendahl, U. (1997). Mouse Serrate-1 (Jagged-1): expression in the developing tooth is regulated by epithelial- mesenchymal interactions and fibroblast growth factor-4. 20894.

Ta, M., Lardelli, M., Lendahl, U., & Thesleff, I. (1995). Expression of Notch 1, 2 and 3 is regulated by epithelial-mesenchymal interactions and retinoic acid in the developing mouse tooth and associated with determination of ameloblast cell fate. 20894. <https://doi.org/10.1083/jcb.130.2.407>

Tabatabaeian H, Rao A, Ramos A, Chu T, Sudol M, Lim YP. The emerging roles of WBP2 oncogene in human cancers. *Oncogene*. 2020 Jun;39(24):4621-4635. doi: 10.1038/s41388-020-1318-0. Epub 2020 May 11. PMID: 32393834; PMCID: PMC7286818.

Takebe, N., Nguyen, D. and Yang, S. (2014). Targeting Notch signaling pathway in cancer: Clinical development advances and challenges. *Pharmacology & Therapeutics*, 141(2), pp.140- 149.

Takimoto M. Multidisciplinary Roles of LRRFIP1/GCF2 in Human Biological Systems and Diseases. *Cells*. 2019 Jan 31;8(2):108. doi: 10.3390/cells8020108. PMID: 30709060; PMCID: PMC6406849.

Talora, C., Campese, A. F., Bellavia, D., Pia, M., Vacca, A., Gulino, A., & Screpanti, I. (2008). *Biochimica et Biophysica Acta* Notch signaling and diseases: An evolutionary journey from a simple beginning to complex outcomes. 1782, 489–497. <https://doi.org/10.1016/j.bbadis.2008.06.008>

Tamagnone, L., Zacchigna, S., & Rehman, M. (2018). Taming the Notch Transcriptional Regulator for Cancer Therapy. *Molecules*, 23(2), 431. doi: 10.3390/molecules23020431.

Tetering, G. Van, Diest, P. Van, Verlaan, I., Wall, E. Van Der, Kopan, R., & Vooijs, M. (2009). Metalloprotease ADAM10 Is Required for Notch1. <https://doi.org/10.1074/jbc.M109.006775>.

Thakkar PV, Kita K, Castillo UD, Galletti G, Madhukar N, Navarro EV, Barasoain I, Goodson HV, Sackett D, Díaz JF, Lu Y, RoyChoudhury A, Molina H, Elemento O, Shah MA, Giannakakou P. CLIP-170S is a microtubule +TIP

variant that confers resistance to taxanes by impairing drug-target engagement. *Dev Cell*. 2021 Dec 6;56(23):3264-3275.e7. doi: 10.1016/j.devcel.2021.09.023. Epub 2021 Oct 20. PMID: 34672971; PMCID: PMC8665049.

The human NOTCH1, 2, and 3 genes are located at chromosome positions 9q34, 1p13-p11, and 19p13.2-p13.1 in regions of neoplasia-associated translocation. (1994). 20894. <https://doi.org/10.1006/geno.1994.1613>

The mammalian transcriptional repressor RBP (CBF1) targets TFIID and TFIIA to prevent activated. (1998). 20894. <https://doi.org/10.1101/gad.12.11.1621>

The molecular genetics of Enhancer of split, a gene required for embryonic neural development in. (1988). 20894.

The, I. S., Locus, N., Repeat, A. T., Of, C., & Genetic, T. H. E. (1973). IS THE NOTCH LOCUS OF DROSOPHILA. (6051).

Thör, G. E. W., He, P. W. H., Ru, B. L. A. De, & Scharloo, W. (2020). The effects of recessive lethal Notch mutations of *Drosophila melanogaster* on flavoprotein enzyme activities whose inhibitions cause Notch -like phenocopies. (February 1987), 2020.

Tp, D., Af, G., Ak, V., Sepetavec, T., Kr, H., Jd, M., ... Dp, C. (2000). Chromosome 19 translocation, overexpression of Notch3, and human lung cancer. 20894. <https://doi.org/10.1093/jnci/92.16.1355>.

Tsai MM, Wang CS, Tsai CY, Chen CY, Chi HC, Tseng YH, Chung PJ, Lin YH, Chung IH, Chen CY, Lin KH. MicroRNA-196a/-196b promote cell metastasis via negative regulation of radixin in human gastric cancer. *Cancer Lett*. 2014 Sep 1;351(2):222-31. doi: 10.1016/j.canlet.2014.06.004.

Epub 2014 Jun 13. Erratum in: *Cancer Lett.* 2017 May 1; 393:129. PMID: 24933454.

Tyler R. McCaw, Evelyn Inga, Herbert Chen, Renata Jaskula-Sztul, Vikas Dudeja, James A. Bibb, Bin Ren, J. Bart Rose, Gamma Secretase Inhibitors in Cancer: A Current Perspective on Clinical Performance, *The Oncologist*, Volume 26, Issue 4, April 2021, Pages e608–e621, <https://doi.org/10.1002/onco.13627>.

Ughachukwu, P., & Unekwe, P. (2012). Efflux pump-mediated resistance in chemotherapy. *Annals of medical and health sciences research*, 2(2), 191–198. <https://doi.org/10.4103/2141-9248.105671>.

US National Library of Medicine, Clinical Trials, (<https://clinicaltrials.gov/ct2/result/4929097>).

Ute Koch, Freddy Radtke; A third Notch in colorectal cancer progression and metastasis. *J Exp Med* 5 October 2020; 217 (10): e20201017. doi: <https://doi.org/10.1084/jem.20201017>

Uyttendaele, H., Marazzi, G., Wu, G., Yan, Q., Sassoon, D., & Kitajewski, J. (1996). Notch4/int-3, a mammary proto-oncogene, is an endothelial cell-specific mammalian Notch gene. 20894.

Vasan, N., Baselga, J. & Hyman, D.M. A view on drug resistance in cancer. *Nature* 575, 299–309 (2019). <https://doi.org/10.1038/s41586-019-1730-1>.

Venkatesh V, Nataraj R, Thangaraj GS, Karthikeyan M, Gnanasekaran A, Kaginelli SB, Kuppanna G, Kallappa CG, Basalingappa KM. Targeting Notch signalling pathway of cancer stem cells. *Stem Cell Investing*. 2018 Mar

12;5:5. doi: 10.21037/sci.2018.02.02. PMID: 29682512; PMCID: PMC5897708.

Waks AG, Winer EP. Breast Cancer Treatment: A Review. *JAMA*. 2019;321(3):288–300. doi:10.1001/jama.2018.19323.

Wang X, Zhang H, Chen X. Drug resistance and combating drug resistance in cancer. *Cancer Drug Resist* 2019; 2:141-60.
<http://dx.doi.org/10.20517/cdr.2019.10>.

Wang Y, Han J, Zhou H, Ai S, Wan D. A Prognosis Marker Dynein Cytoplasmic 1 Heavy Chain 1 Correlates with EMT and Immune Signature in Liver Hepatocellular Carcinoma by Bioinformatics and Experimental Analysis. *Dis Markers*. 2022 May 11; 2022:6304859. doi: 10.1155/2022/6304859. PMID: 35601740; PMCID: PMC9117040.

Wang Z, Banerjee S, Li Y, Rahman KM, Zhang Y, et al. (2006) Down- regulation of Notch-1 inhibits invasion by inactivation of nuclear factor-kappaB, vascular endothelial growth factor, and matrix metalloproteinase-9 in pancreatic cancer cells. *Cancer Res* 66: 2778–2784.

Wang, A., Lin, W., Liu, D., & He, C. (2013). Application of liposomal technologies for delivery of platinum analogs in oncology. *International Journal Of Nanomedicine*, 3309. doi: 10.2147/ijn. s38354.

Wang, G., & Guo, S. (2013). Regulation of Angiogenesis via Notch Signaling in Breast Cancer and Cancer Stem Cells National Center for Biotechnology Information. 19. <https://doi.org/10.1016/j.bbcan.2013.10.003>.

Wang, H., Vo, T., Hajar, A. et al. Multiple mechanisms underlying acquired resistance to taxanes in selected docetaxel-resistant MCF-7 breast cancer cells. *BMC Cancer* 14, 37 (2014). <https://doi.org/10.1186/1471-2407-14-37>.

- Wang, J., Wei, Q., Wang, X., Tang, S., Liu, H., Zhang, F., ... Luu, H. H. (2016). Transition to resistance: An unexpected role of the EMT in cancer chemoresistance. *Genes & Diseases*, 3(1), 3–6.
<https://doi.org/https://doi.org/10.1016/j.gendis.2016.01.002>.
- Wang, L., Wu, Q., Li, Z., Sun, S., Yuan, J., Li, J., & Zhang, Y. (2019). Delta / Notch-like epidermal growth factor-related receptor promotes stemness to facilitate breast cancer progression.
- Wang, M., MA, X., Wang, J., Wang, L. and Wang, Y. (2014). Pretreatment with the γ -secretase inhibitor DAPT sensitizes drug-resistant ovarian cancer cells to cisplatin by downregulation of Notch signaling. *International Journal of Oncology*, 44(4), pp.1401-1409.
- Wang, S. C., Lin, X. L., Wang, H. Y., Qin, Y. J., Chen, L., Li, J., Jia, J. S., Shen, H. F., Yang, S., Xie, R. Y., Wei, F., Gao, F., Rong, X. X., Yang, J., Zhao, W. T., Zhang, T. T., Shi, J. W., Yao, K. T., Luo, W. R., Sun, Y., ... Xiao, D. (2015). Hes1 triggers epithelial-mesenchymal transition (EMT)-like cellular marker alterations and promotes invasion and metastasis of nasopharyngeal carcinoma by activating the PTEN/AKT pathway. *Oncotarget*, 6(34), 36713–36730.
<https://doi.org/10.18632/oncotarget.5457>.
- Wang, W., Wang, L., Mizokami, A. et al. Down-regulation of E-cadherin enhances prostate cancer chemoresistance via Notch signaling. *Chin J Cancer* 36, 35 (2017). <https://doi.org/10.1186/s40880-017-0203-x>.
- Wang, X., Zhang, H., & Chen, X. (2019). Drug resistance and combating drug resistance in cancer. *Cancer Drug Resistance*. doi: 10.20517/cdr.2019.10.
- Wang, X., Zhang, H., & Chen, X. (2021). Drug resistance and combating drug resistance in cancer. Retrieved 24 April 2021.

- Wang, Z., Li, Y., Ahmad, A., Banerjee, S., Azmi, A., Kong, D., Wojewoda, C., Miele, L. and Sarkar, F. (2010). Down-regulation of Notch-1 is associated with Akt and FoxM1 in inducing cell growth inhibition and apoptosis in prostate cancer cells. *Journal of Cellular Biochemistry*, 112(1), pp.78-88.
- Wang, Z., Li, Y., Ahmad, A., Banerjee, S., Azmi, A., Kong, D., Wojewoda, C., Miele, L. and Sarkar, F. (2010). Down-regulation of Notch-1 is associated with Akt and FoxM1 in inducing cell growth inhibition and apoptosis in prostate cancer cells. *Journal of Cellular Biochemistry*, 112(1), pp.78-88.
- Wei W, Huang W, Yue J. Requirement of IP3 receptor 3 (IP3R3) in nitric oxide induced cardiomyocyte differentiation of mouse embryonic stem cells. *Exp Cell Res*. 2016 Aug 1;346(1):9-16. doi: 10.1016/j.yexcr.2016.06.016. Epub 2016 Jun 24. PMID: 27349290.
- Weinmaster, G., Vj, R., & Lemke, G. (1992). Notch2: a second mammalian Notch gene. 20894.
- Welshons, W. J. (1985). The cytogenetic analysis of a fractured gene in *Drosophila*. (5), 775–794.
- Wharton, K. A., & Johansen, K. M. (1985). Nucleotide Sequence from the Neumgenic Locus Notch Implies a Gene Product That Shares Homology with Proteins Containing EGFLike Repeats. 43 (December 1965).
- Ws, P., Jc, A., Ml, S., Rp, H., Soffer, B., Sklar, J., & Baltimore, D. (1996). Exclusive development of T cell neoplasms in mice transplanted with bone marrow expressing activated Notch alleles. 20894.
<https://doi.org/10.1084/jem.183.5.2283>
- Xie, J., Lin, L. S., Huang, X. Y., Gan, R. H., Ding, L. C., Su, B. H., Zhao, Y., Lu, Y. G., & Zheng, D. L. (2020). The NOTCH1-HEY1 pathway regulates self-renewal and epithelial-mesenchymal transition of salivary adenoid cystic

carcinoma cells. *International journal of biological sciences*, 16(4), 598–610. <https://doi.org/10.7150/ijbs.36407>.

Xiu, M., Wang, Y., Li, B., Wang, X., Xiao, F., Chen, S., ... Hua, F. (2021). The Role of Notch3 Signaling in Cancer Stemness and Chemoresistance: Molecular Mechanisms and Targeting Strategies. *Frontiers in Molecular Biosciences*, 8. <https://doi.org/10.3389/fmolb.2021.694141>

Xu, T., La, C., & Rg, F. (1992). The involvement of the Notch locus in *Drosophila* oogenesis. 20894.

Yan, Y., Liu, F., Han, L., Zhao, L., Chen, J., Olopade, O. I., & He, M. (2018). HIF-2 α promotes conversion to a stem cell phenotype and induces chemoresistance in breast cancer cells by activating Wnt and Notch pathways. 1–14.

Yang Q, Zhang J, Xu S, Jia C, Meng W, Tang H, Zhang X, Zhang Y, Fu B. Knockdown of PHF5A Inhibits Migration and Invasion of HCC Cells via Downregulating NF- κ B Signaling. *Biomed Res Int*. 2019 Jan 15; 2019:1621854. doi: 10.1155/2019/1621854. PMID: 30766880; PMCID: PMC6350539.

Yang Y, Zhu J, Zhang T, Liu J, Li Y, Zhu Y, Xu L, Wang R, Su F, Ou Y, Wu Q. PHD-finger domain protein 5A functions as a novel oncoprotein in lung adenocarcinoma. *J Exp Clin Cancer Res*. 2018 Mar 22;37(1):65. doi: 10.1186/s13046-018-0736-0. PMID: 29566713; PMCID: PMC5863814.

Yang, L., Xie, H., Li, Y., Wang, X., Liu, X., & Mai, J. (2022). Molecular mechanisms of platinum-based chemotherapy resistance in ovarian cancer (Review). *Oncology Reports*, 47, 82. <https://doi.org/10.3892/or.2022.8293>.

Yao, J., Qian, C., Shu, T., Zhang, X., Zhao, Z. and Liang, Y. (2013). Combination treatment of PD98059 and DAPT in gastric cancer through induction of

apoptosis and downregulation of WNT/ β -catenin. *Cancer Biology & Therapy*, 14(9), pp.833-839.

Yates LR, Knappskog S, Wedge D, Farmery JHR, Gonzalez S, Martincorena I, et al. Genomic evolution of breast cancer metastasis and relapse. *Cancer Cell*. (2017) 32:169–84 e7. doi: 10.1016/j.ccell.2017.07.005.

Yochem, J., Weston, K., & Greenwald, I. (1988). The *Caenorhabditis elegans* lin-12 gene encodes a transmembrane protein with overall similarity to *Drosophila* Notch. 20894. <https://doi.org/10.1038/335547a0>.

Yuan, X., Wu, H., Xu, H., Xiong, H., Chu, Q., Yu, S., Wu, G. and Wu, K. (2015). Notch signaling: An emerging therapeutic target for cancer treatment. *Cancer Letters*, 369(1), pp.20.

Zagouras, P., Stifani, S., Cm, B., & Ml, C. (1995). Alterations in Notch signaling in neoplastic lesions of the human cervix. 20894. <https://doi.org/10.1073/pnas.92.14.6414>

Zahreddine, H., & Borden, K. (2013). Mechanisms and insights into drug resistance in cancer. *Frontiers In Pharmacology*, 4. doi: 10.3389/fphar.2013.00028.

Zaoui K, Duhamel S, Parachoniak CA, Park M. CLIP-170 spatially modulates receptor tyrosine kinase recycling to coordinate cell migration. *Traffic*. 2019 Mar;20(3):187-201. doi: 10.1111/tra.12629. Epub 2019 Jan 15. PMID: 30537020; PMCID: PMC6519375.

Zeller, C., & Brown, R. (2010). Therapeutic modulation of epigenetic drivers of drug resistance in ovarian cancer. *Therapeutic advances in medical oncology*, 2(5), 319–329. <https://doi.org/10.1177/1758834010375759>.

Zhang J, Li Y, Liu H, Zhang J, Wang J, Xia J, Zhang Y, Yu X, Ma J, Huang M, Wang J, Wang L, Li Q, Cui R, Yang W, Xu Y, Feng W. Genome-wide CRISPR/Cas9 library screen identifies PCMT1 as a critical driver of

ovarian cancer metastasis. *J Exp Clin Cancer Res.* 2022 Jan 15;41(1):24. doi: 10.1186/s13046-022-02242-3. PMID: 35033172; PMCID: PMC8760697.

Zhang T, Wang Z, Liu Y, Huo Y, Liu H, Xu C, Mao R, Zhu Y, Liu L, Wei D, Liu G, Pan B, Tang Y, Zhou Z, Yang C, Guo Y. Plastin 1 drives metastasis of colorectal cancer through the IQGAP1/Rac1/ERK pathway. *Cancer Sci.* 2020 Aug;111(8):2861-2871. doi: 10.1111/cas.14438. Epub 2020 Jul 5. PMID: 32350953; PMCID: PMC7419044.

Zhang Y, Peng L, Hu T, Wan Y, Ren Y, Zhang J, Wang X, Zhou Y, Yuan W, Wang Q, Cheng T, Zhu X. La-related protein 4B maintains murine MLL-AF9 leukemia stem cell self-renewal by regulating cell cycle progression. *Exp Hematol.* 2015 Apr;43(4):309-18.e2. doi:10.1016/j.exphem.2014.12.003.

Lim YX, Lin H, Chu T, Lim YP. WBP2 promotes BTRC mRNA stability to drive migration and invasion in triple-negative breast cancer via NF- κ B activation. *Mol Oncol.* 2022 Jan;16(2):422-446. doi: 10.1002/1878-0261.13048. Epub 2021 Aug 12. PMID: 34197030; PMCID: PMC8763649.

Zhang, C., Yan, Z., Zong, Q., Fang, D., Painter, C., & Zhang, Q. et al. (2013). Synergistic Effect of the γ -Secretase Inhibitor PF-03084014 and Docetaxel in Breast Cancer Models. *STEM CELLS Translational Medicine*, 2(3), 233-242. doi: 10.5966/sctm.2012-0096.

Zhang, X., Li, Y., Xu, H., & Zhang, Y. (2014). The γ -secretase complex: from structure to function, 1–10. <https://doi.org/10.3389/fncel.2014.00427>.

Zhang, Y. U., Xie, Z. I. Y. A. N., Guo, X. T., Xiao, X. H. U. A., & Xiong, L. I. X. I. A. (2019). Notch and breast cancer metastasis: Current knowledge, new

sights and targeted therapy (Review). 2743–2755.

<https://doi.org/10.3892/ol.2019.10653>

Zhang, YQ., Liang, YK., Wu, Y. et al. Notch3 inhibits cell proliferation and tumorigenesis and predicts better prognosis in breast cancer through transactivating PTEN. *Cell Death Dis* 12, 502 (2021).

<https://doi.org/10.1038/s41419-021-03735-3>.

Zhang, Z., Zhou, Z., Zhang, M., Gross, N., Gong, L., & Zhang, S. et al. (2019). High Notch1 expression affects chemosensitivity of head and neck squamous cell carcinoma to paclitaxel and cisplatin treatment. *Biomedicine & Pharmacotherapy*, 118, 109306. doi: 10.1016/j.biopha.2019.109306.

Zhao, Z., Zhang, L., Huang, C., Ma, S., Bu, L., & Liu, J. et al. (2016). NOTCH1 inhibition enhances the efficacy of conventional chemotherapeutic agents by targeting head neck cancer stem cell. *Scientific Reports*, 6(1). doi: 10.1038/srep24704.

Zheng YZ, Xue MZ, Shen HJ, Li XG, Ma D, Gong Y, Liu YR, Qiao F, Xie HY, Lian B, Sun WL, Zhao HY, Yao L, Zuo WJ, Li DQ, Wang P, Hu X, Shao ZM. PHF5A Epigenetically Inhibits Apoptosis to Promote Breast Cancer Progression. *Cancer Res*. 2018 Jun 15;78(12):3190-3206. doi: 10.1158/0008-5472.CAN-17-3514. Epub 2018 Apr 26. PMID: 29700004.

Zhong, W., Feder, J.N., Jiang, M.-M., Jan, L.Y., and Jan, Y.N. (1996). *Neuron* 17.

Zhou, B., Lin, W., Long, Y. et al. Notch signalling pathway: architecture, disease, and therapeutics. *Sig Transduct Target Ther* 7, 95 (2022).

<https://doi.org/10.1038/s41392-022-00934-y>.

Zhu M, Li Y, Dong G, Chen X, Huang K, Wu W, Dai Y, Zhang L, Lin H, Wang S, Polychronakos C, Fu J. Prevalence, and phenotypic features of diabetes

due to recessive, non-syndromic WFS1 mutations. *Eur J Endocrinol.* 2021 Dec 10;186(2):163-170. doi: 10.1530/EJE-21-0097. PMID: 34792487.

Zi-Hao Liu, Xiao-Meng Dai & Bin Du (2015) Hes1: a key role in stemness, metastasis and multidrug resistance, *Cancer Biology & Therapy*, 16:3, 353-359, DOI: 10.1080/15384047.2015.1016662.

Zou, Y., Fang, F., Ding, Y., Dai, M., Yi, X., Chen, C. ... Chen, S. (2016). Notch 2 signaling contributes to cell growth, anti-apoptosis, and metastasis in laryngeal squamous cell carcinoma. *Molecular Medicine Reports*, 14, 3517-3524. <https://doi.org/10.3892/mmr.2016.5688>.

Zuzow N, Ghosh A, Leonard M, Liao J, Yang B, Bennett EJ. Mapping the mammalian ribosome quality control complex interactome using proximity labeling approaches. *Mol Biol Cell.* 2018 May 15;29(10):1258-1269. doi: 10.1091/mbc.E17-12-0714. Epub 2018 Mar 22. PMID: 29540532; PMCID: PMC5935074.

Zz, B., & Cl, C. (1997). The expression and function of Notch pathway genes in the developing rat eye. *abrogates transforming growth.* 20894.

VITA

Kübra Telli received honours in bachelor's degree in Molecular Biology and Genetics from Istanbul Arel University, in 2015. Throughout her undergraduate internship studies in Aalto University, she took part in 'Hyperthermostable Thermotoga maritima xylanase XYN10B shows high activity at high temperatures in the presence of biomass-dissolving hydrophilic ionic liquids' paper. She has attended to 11th Carbohydrate Bioengineering Meeting in Espoo with a poster presentation. She then established her Master of Science degree in Cancer Cell and Molecular Biology from Leicester University with a merit, in 2018. During the same year, she has started her Doctor of Philosophy research in Molecular Biology and Genetics at İzmir Institute of Technology and received the title in 2022. During her MSc and PhD journey, she has learnt about cancer drug resistance in yeast and human cell culture experimental setup's. She has been awarded by TÜBİTAK 2214A scholarship for one year in Linköping University, Sweden. 'Epithelial-mesenchymal transition as a potential route for DAPT resistance in breast cancer cells' paper was accepted by Turkish Journal of Biochemistry, in 2022.